VOL.107 NO.GT12. DEC. 1981

JOURNAL OF THE GEOTECHNICAL ENGINEERING DIVISION

PROCEEDINGS OF
THE AMERICAN SOCIETY
OF CIVIL ENGINEERS

VOL.107 NO.GT12. DEC. 1981

JOURNAL OF THE GEOTECHNICAL ENGINEERING DIVISION

PROCEEDINGS OF
THE AMERICAN SOCIETY
OF CIVIL ENGINEERS

ISSN 0093-6405

William F. Marcuson III, Editor
U.S. Army Engineers

AMERICAN SOCIETY OF CIVIL ENGINEERS

CONTENTS

Modeling the Liquefaction Process
by Takaaki Kagawa and Leland M. Kraft, Jr. 1593

Ground Movement Analysis of Earth Support System
by C. K. Shen, S. Bang, and L. R. Herrmann 1609

Field Measurements of an Earth Support System
by C. K. Shen, S. Bang, K. M. Romstad, L. Kulchin, and J. S. DeNatale 1625

Cellular Cofferdam for Trident Drydock: Design
by Max D. Sorota and Edward B. Kinner 1643

Cellular Cofferdam for Trident Drydock: Performance
by Max D. Sorota, Edward B. Kinner, and Mark X. Haley 1657

Compressibility and Bearing Capacity
by Nabil F. Ismael and Aleksandar S. Vesic 1677

The Journal of the Geotechnical Engineering Division (ISSN 0093-6405) is published monthly by the American Society of Civil Engineers. Publications office is at 345 East 47th Street, New York, N.Y. 10017. Address all ASCE correspondence to the Editorial and General Offices at 345 East 47th Street, New York, N.Y. 10017. Allow six weeks for change of address to become effective. Subscription price to members is $16.00. Nonmember subscriptions available; prices obtainable on request. Second-class postage paid at New York, N.Y. and at additional mailing offices. GT.

POSTMASTER: Send address changes to American Society of Civil Engineers, 345 East 47th Street, New York, NY 10017.

Probabilistic Soil Exploration: Case History
by Tien H. Wu and Kinfun Wong 1693

Lateral Pile Response During Earthquakes
by Takaaki Kagawa and Leland M. Kraft 1713

TECHNICAL NOTES

Proc. Paper 16688

Seismic Displacement Analysis of Earth Dams
by Sarada K. Sarma 1735

DISCUSSION

Proc. Paper 16683

Seismic Response of Cohesive Marine Soils,* by Chan-Feng Tsai, Ignatius Lam, and Geoffrey R. Martin (Sept., 1980).
by Tam J. Larkin 1743

Ground Control for Shallow Tunnels by Soil Grouting,* by David Y. Tan and G. Wayne Clough (Sept., 1980).
by Kurt M. Borchert and Herbert Klapperich 1745

End of Year Index 1747

INFORMATION RETRIEVAL

The key words, abstract, and reference "cards" for each article in this Journal represent part of the ASCE participation in the EJC information retrieval plan. The retrieval data are placed herein so that each can be cut out, placed on a 3 × 5 card and given an accession number for the user's file. The accession number is then entered on key word cards so that the user can subsequently match key words to choose the articles he wishes. Details of this program were given in an August, 1962 article in CIVIL ENGINEERING, reprints of which are available on request to ASCE headquarters.

*Discussion period closed for this paper. Any other discussion received during this discussion period will be published in subsequent Journals.

16709 MODELING THE LIQUEFACTION PROCESS

KEY WORDS: Earthquakes; **Liquefaction;** Models; **Pore water pressure;** Predictions; **Sands; Shear stress;** Simulation models

ABSTRACT: The liquefaction model presented in based solely on observed pore pressure responses of sands and was constructed employing some simplifying assumptions. Pore pressure generation of sands under uniform as well as irregular loadings can be simulated by this model. The model requires only a limited number of laboratory tests and a few model parameters. All model parameters can be determined from results of conventional undrained cyclic tests employing uniform stress cycles. Assumptions and performance of this liquefaction model were examined through case studies. This liquefaction model predicted with good accuracy the pore pressure response for both uniform and earthquake-type irregular stress loadings. The model can be incorporated into nonlinear site response methods and soil-structures response methods, and it may be used as a simple alternative to other equally effective, but sophisticated liquefaction models currently available.

REFERENCE: Kagawa, Takaaki (Engrg. Consultant, McClelland Engrs., Inc., Houston, Tex.), and Kraft, Leland M., Jr., "Modeling the Liquefaction Process," *Journal of the Geotechnical Engineering Division,* ASCE, Vol. 107, No. GT12, **Proc. Paper 16709**, December, 1981, pp. 1593-1607

16732 GROUND MOVEMENT ANALYSIS

KEY WORDS: **Excavation;** Finite element method; Foundation design; **Lateral displacement effect; Reinforced earth;** Soil mechanics; **Vertical alinement**

ABSTRACT: Ground movements associated with a new insitu earth reinforcement lateral support system are analyzed using a two-dimensional plane strain finite element technique specially developed for reinforced soil and soil-structure interaction problems. Incremental construction and nonlinear soil characterization are included. The calculated ground movements are represented in terms of angular and lateral distortions. These were selected as indications of potential building damage ajacent to an open excavation. Typical design charts of angular and lateral distortions in relation to the depth of excavation and reinforcement length are presented. The system described in this paper is unique and in many instances offers a better choice over the conventional temporary earth support systems currently being used. The working stress analysis when coupled with the limit analysis calculation provide not only an adequate design of the system, but also information concerning ground movements critical to building damage adjacent to open cuts.

REFERENCE: Shen, C. K. (Prof., Dept. of Civ. Engrg., Univ. of California, Davis, Calif. 95616), Bang, S., and Herrmann, L. R., "Ground Movement Analysis of Earth Support System," *Journal of the Geotechnical Engineering Division,* ASCE, Vol. 107, No. GT12, **Proc. Paper 16732**, December, 1981, pp. 1609-1624

16734 FIELD MEASUREMENTS OF AN EARTH SUPPORT SYSTEM

KEY WORDS: Analysis; **Case reports;** Construction; **Excavation;** Finite element method; Foundation design; **Ground motion; Reinforced earth;** Soil mechanics

ABSTRACT: Two case studies of lateral earth support system are presented. This system uses the insitu earth reinforcement technique, which is different from the conventional systems that serve to retain soils behind a vertical cut, to strengthen the native soil. The field results were compared with predictions obtained from a finite element method of analysis. In general, the predictions agree well with the field measurement demonstrating that the analytical procedures developed can correctly predict the field behavior. Furthermore, it has shown that ground movements adjacent to an open excavation can be determined and controlled if a properly designed system is installed. Hence, the insitu earth reinforcement lateral support system has shown to offer a viable alternative for providing lateral support in deep excavation.

REFERENCE: Shen, C. K. (Prof., Dept. of Civ. Engrg., Univ. of California, Davis, Calif. 95616), Bang, S., Romstad, K. M., Kulchin, L., and DeNatale, J. S., "Field Measurements of an Earth Support System," *Journal of the Geotechnical Engineering Division,* ASCE, Vol. 107, No. GT12, **Proc. Paper 16734**, December, 1981, pp. 1625-1642

16758 CELLULAR COFFERDAM FOR TRIDENT DRYDOCK: DESIGN

KEY WORDS: Aquifers; Artesian pressure; **Cellular cofferdams;** Compaction (soils); Corrosion prevention; Dewatering; Dredging; Drydocks; **Steel sheet piles; Structural design; Wye branches**

ABSTRACT: A description is provided of the design of a steel sheet pile cellular cofferdam required for construction of a graving drydock. The cofferdam was constructed approximately 550 ft (168 m) offshore within the Hood Canal of Washington State and was required to retain 79 ft (24 m) of water after basin unwatering. Interlock tensions associated with the required cell diameter in this deep water location resulted in one of the first United States cofferdam applications of high strength steel sheet piling and extruded wye connections. Much of the cofferdam was designed to be permanent to provide in-service laydown areas adjacent to the completed drylock. Items discussed include the need for two pumped dewatering systems, the need for vibratory probe compaction of the cell and are fill, site soil conditions, dredging and steel sheet pile corrosion protection.

REFERENCE: Sorota, Max D. (Vice. Pres., Fay, Spofford & Thorndike, Inc., Boston, Mass), and Kinner, Edward B., "Cellular Cofferdam for Trident Drydock: Design," *Journal of the Geotechnical Engineering Division,* ASCE, Vol. 107, No. GT12, **Proc. Paper 16758**, December, 1981, pp. 1643-1655

16733 CELLULAR COFFERDAM FOR TRIDENT DRYLOCK

KEY WORDS: **Cellular cofferdams; Compaction (soils);** Dewatering; Dredging; Drydocks; Instrumentation; **Steel sheet piles**

ABSTRACT: The construction and performance of a permanent steel sheet pile cellular cofferdam designed to accommodate a maximum water depth of 79 ft (24 m) is described. The cofferdam is among the first to be constructed in the United States which, because of expected interlock tensions, required the use of high strength steel sheet piles and extruded wye connections. Vibratory probe compaction of the cell and connecting are fill was performed to prohibit earthquake liquefaction, to minimize settlements and to obtain necessary weight for cofferdam stability. A pumped cell fill dewatering system was used to limit interlock tensions during and following cofferdam basin unwatering.

REFERENCE: Sorota, Max D. (Sr. Vice Pres., Fay, Spofford & Thorndike, Inc., Boston, Mass.), Kinner, Edward B., and Haley, Mark X., "Cellular Cofferdam for Trident Drydock: Performance," *Journal of the Geotechnical Engineering Division,* ASCE, Vol. 107, No. GT12, **Proc. Paper 16733**, December, 1981, pp. 1657-1676

16718 COMPRESSIBILITY AND BEARING CAPACITY

KEY WORDS: **Bearing capacity; Compressibility (soils);** Compressible soils; **Foundations; Model tests;** Overburden; Pressure; **Sands**

ABSTRACT: Small-scale model footing tests were carried out on two frictional soils having identical strength characteristics and different deformation characteristics. The results emphasized the importance of soil compressibility. Test results are compared with existing analyical methods dealing with the bearing capacity of compressible soils. The suitability of these methods is examined in light of the test results.

REFERENCE: Ismael, Nabil F. (Assoc. Prof., Coll. of Engrg. and Petroleum, Kuwait Univ., Kuwait), and Vesic, Aleksandar S., "Compressibility and Bearing Capacity," *Journal of the Geotechnical Engineering Division,* ASCE, Vol. 107, No. GT12, **Proc. Paper 16718**, December, 1981, pp. 1677-1691

16764 PROBABILISTIC SOIL EXPLORATION: CASE HISTORY

KEY WORDS: **Clays;** Clay structure; **Shear strength (soils);** Soft soils; **Soil investigations; Soil stratification;** Two layer soil system

ABSTRACT: Probability concepts are applied to the interpretation of soil exploration data at a site where failure in a weak layer is considered probable. The subsoil is modeled as a two-class material with soft clay layer as included within a stiff clay. A hypothetical case history is constructed to illustrate the interpretation of data obtained at different stages of the soil exploration program. The analysis of the soil exploration program considers detection and recognition of the soft material and inference that the soft material exists at unexplored locations, given that it has been detected at explored locations. The judgment of practicing engineers regarding the site conditions are presented as subjective probabilities.

REFERENCE: Wu, Tien H. (Prof. of Civ. Engrg., Ohio State Univ., Columbus, Ohio. 43210), and Wong, Kinfun, "Probabilistic Soil Exploration: Case History," *Journal of the Geotechnical Engineering Division,* ASCE, Vol. 107, No. GT12, **Proc. Paper 16764**, December, 1981, pp. 1693-1711

16735 LATERAL PILE RESPONSE DURING EARTHQUAKES

KEY WORDS: Earthquake loads; **Earthquakes; Liquefaction;** Nonlinear systems; **Offshore structures;** Pile structures; **Pore water pressure; Sands**

ABSTRACT: A nonlinear method for seismic soil-pile-structure interaction is presented. Primary features of the proposed method include a consistent approach to determine seismic p-y relationships and a liquefaction model that is suited to pore pressure evaluation for earthquake-type irregular loadings. The seismic- p-y relationships are determined from nonlinear stress-strain relations of soils, and include soil nonlinearity as well as pore pressure buildup effects around a pile. The performance and validity of the method were evaluated through an analysis of shaking table test on model soil-pile-structure systems. Using the proposed method, seismic response characteristics of an idealized offshore pile-supported structure at a sand site were analyzed. Results indicated that liquefaction as well as pore pressure bulidup around a pile can have a large impact on the response of pile-supported structures.

REFERENCE: Kagawa, Takaaki (Engrg. Consultant, McClelland Engrs., Inc., Houston, Tex.), and Kraft, Leland M., Jr., "Lateral Pile Response During Earthquakes," *Journal of the Geotechnical Engineering Division,* ASCE, Vol. 107, No. GT12, **Proc. Paper 16735**, December, 1981, pp. 1713-1731

U.S. Customary-SI Conversion Factors

In accordance with the October, 1970 action of the ASCE Board of Direction, which stated that all publications of the Society should list all measurements in both U.S. Customary and SI (International System) units, the following list contains conversion factors to enable readers to compute the SI unit values of measurements. A complete guide to the SI system and its use has been published by the American Society for Testing and Materials. Copies of this publication (ASTM E-380) can be purchased from ASCE at a price of $3.00 each; orders must be prepaid.

All authors of *Journal* papers are being asked to prepare their papers in this dual-unit format. To provide preliminary assistance to authors, the following list of conversion factors and guides are recommended by the ASCE Committee on Metrication.

To convert	To	Multiply by
inches (in.)	millimeters (mm)	25.4
feet (ft)	meters (m)	0.305
yards (yd)	meters (m)	0.914
miles (miles)	kilometers (km)	1.61
square inches (sq in.)	square millimeters (mm^2)	645
square feet (sq ft)	square meters (m^2)	0.093
square yards (sq yd)	square meters (m^2)	0.836
square miles (sq miles)	square kilometers (km^2)	2.59
acres (acre)	hectares (ha)	0.405
cubic inches (cu in.)	cubic millimeters (mm^3)	16,400
cubic feet (cu ft)	cubic meters (m^3)	0.028
cubic yards (cu yd)	cubic meters (m^3)	0.765
pounds (lb) mass	kilograms (kg)	0.453
tons (ton) mass	kilograms (kg)	907
pound force (lbf)	newtons (N)	4.45
kilogram force (kgf)	newtons (N)	9.81
pounds per square foot (psf)	pascals (Pa)	47.9
pounds per square inch (psi)	kilopascals (kPa)	6.89
U.S. gallons (gal)	liters (L)	3.79
acre-feet (acre-ft)	cubic meters (m^3)	1,233

MODELING THE LIQUEFACTION PROCESS

By Takaaki Kagawa[1] and Leland M. Kraft, Jr.,[2] Members, ASCE

INTRODUCTION

Liquefaction of cohesionless soils has contributed to the failure of soil structure systems during earthquakes. The mechanisms of liquefaction have, in recent years, been studied extensively, and many liquefaction models have been proposed.

Available liquefaction models are based on either: (1) Experimentally observed undrained stress paths during pore pressure buildup (5,6); (2) a correlation between pore pressure response and volume change tendency of dry soils (2,9); (3) the formulation of pore pressure response directly from observed data (3,12,13,14); (4) a plasticity theory in which the plastic volume change is related to pore pressure build-up (10,18); or (5) treatment of the soil as a two-phase medium (1,8). Except for the models that formulate pore pressure response directly from observed data, all the other models explicitly or implicitly include the correspondence between the volume change tendency of soil and the pore pressure increase. Use of a volume change-pore pressure relationship sometimes, however, complicates the model and requires a relatively large number of model parameters that must be obtained from several types of laboratory tests. On the other hand, the available models that formulate the pore pressure response directly from observed data on undrained tests require less effort to determine model parameters. The capabilities of most models have been confirmed primarily for uniform loading cases.

A pore pressure generation model, based solely on observed pore pressure responses, is presented in this paper. The model is conceptually simple and requires only a limited number of laboratory tests and a few model parameters. All model parameters can be determined from conventional stress-controlled, undrained tests employing uniform stress cycles. The model also works well for earthquake-type stress variations.

An important feature of the model is that it can be used with any nonlinear dynamic response method that accounts for the time-dependent stiffness degrading effect due to the pore pressure build-up in the soil, and it provides a convenient

[1]Engrg. Consultant, McClelland Engrs., Inc., Houston, Tex.
[2]Mgr., McClelland Engrs., Inc., Houston, Tex.

Note.—Discussion open until May 1, 1982. To extend the closing date one month, a written request must be filed with the Manager of Technical and Professional Publications, ASCE. Manuscript was submitted for review for possible publication on June 4, 1980. This paper is part of the Journal of the Geotechnical Engineering Division, Proceedings of the American Society of Civil Engineers, ©ASCE, Vol. 107, No. GT12, December, 1981. ISSN 0093-6405/81/0012-1593/$01.00.

alternative to sophisticated liquefaction models to evaluate the effects of pore pressure generation within soil media. Due to its simplicity, the model is numerically efficient.

Liquefaction Model

Background.—During drained cyclic loading, loose soils densify and dense soils dilate. Similar phenomena also are observed during undrained cyclic loading. This volume change tendency is a key influence on the liquefaction of cohesionless soils.

When an element of relatively loose soil is subjected to cyclic stress reversals in undrained simple shear condition, pore pressure develops in the soil. In an early stage of loading when the pore pressure ratio is low, the effective stress system in the soil is nearly identical to that before loading. Therefore, the pore pressure increment during an undrained stress cycle may be adequately predicted using the potential for a drained volume change corresponding to the initial stress system. As the cyclic straining proceeds to generate large pore pressures in the soil, the effective confining pressure reduces and the soil may exhibit a tendency to dilate. The pore pressure response at this stage can no longer be predicted from the volume change tendency of the soil under the initial stress system.

Pore pressure generation can be related to the drained volume change characteristics of the soil, which are affected by the cyclic shear strain and the change in effective confining pressure based on the effective stress point of view (2,9). This approach, however, requires experimental data on cyclic stress-strain behavior for the soil, a relationship between the cyclic strain and the volume change behavior of dry soil, and a relationship between the volumetric expansion and the effective stress reduction for the soil.

A simple alternative to the effective stress method may be obtained by empirically relating the observed pore pressure responses to the drained volume change of the soil (11,16) by assuming that the volume change tendency of the soil during undrained cyclic loading can be described by the volume change of the dry soil under the initial stress system. The stress ratio is chosen as a key parameter in these methods. Due to the simplifying assumptions involved in these methods, predicted pore pressure responses may not be adequate for any type of loading and soil conditions. A major advantage of this approach, however, is simplicity.

In this study, the writers constructed a liquefaction model based on the observed pore pressure responses in laboratory undrained cyclic tests employing uniform stress cycles. The liquefaction process is viewed as a result of two distinct phenomena: (1) In early stages of loading, pore pressure generation is dominated by the tendency of the soil to decrease in volume under the initial effective stress system; and (2) the pore pressure generation capability of the soil also is affected by the change in effective confining pressure during cyclic loading. The former is characterized using the drained volume decrease behavior of sands, and the latter is represented by an empirical "pore pressure function." Although the key model parameter is the stress ratio, the "pore pressure function" implicitly accounts for the strain dependent nature of the liquefaction process, as analysed below.

Assumptions.—Three fundamental assumptions were made to construct this liquefaction model:

1. Pore pressure generation is due to volume change characteristics, and this is influenced by; (1) The magnitude of applied shear stress for a given confining pressure and relative density of the soil; (2) the stress history (repeated loading); and (3) the effective increase of the applied shear stress relative to the shear strength, as effective stresses decrease with an increase in pore pressure.

The pore pressure generation of a sand depends on the magnitude of applied shear stress (3,11,13,14,16). Previous studies also have shown that pore pressure generation of a sand is related to the volume decrease tendency of the soil under repeated loading. Under drained conditions, volume during a uniform stress cycle decreases rather quickly with an increasing number of cycles. If this volume decrease of a sand were directly converted to the pore pressure

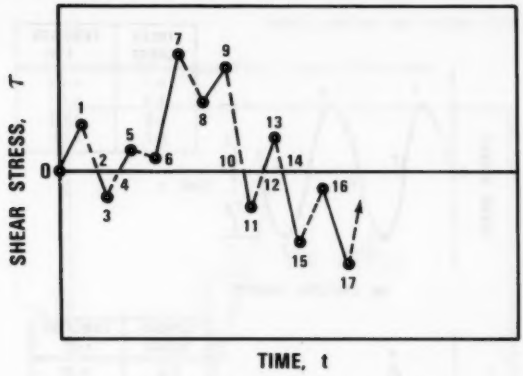

FIG. 1.—Pore Pressure Computation Scheme

increase of the sand in an undrained condition, the amount of pore pressure build-up in a stress cycle would decrease with an increase in the number of cycles. Large pore pressures, however, are generally developed at high pore pressure ratios near liquefaction. This phenomenon may be a consequence of an increase in cyclic shear strain amplitude near liquefaction, or can be attributed to the third influence previously mentioned.

2. Soil exhibits an identical pore pressure generation in both positive and negative shear stress applications only when the stress histories are the same in both directions and the pore pressures before the stress application are the same. The soil remembers the stress histories independently for the positive and negative shear stresses.

3. Pore pressure is assumed to develop only in the loading and reloading process. An earthquake-type irregular stress-time history is shown in Fig. 1. The portions in which irrecoverable pore pressure develops are represented by solid lines. For example, the stress changes from 0–1, 4–5, 6–7, 8–9, and 12–13 correspond to loading or reloading in the positive shear stress. Thus,

pore pressure develops during these stress changes. On the other hand, the stress changes from 1–2, 5–6, 7–8, 9–10, and 13–14 are unloading processes in the positive shear stress. Thus, no pore pressure, according to the assumption, develops during these stress changes. Similarly, pore pressure develops also during loading and reloading processes in the negative shear stress (from 2–3, 10–11, 14–15, and 16–17).

Model Description.—When a "potential function" for pore pressure build-up, ψ, exists, we can compute the pore pressure increase due to a shear stress change from τ_1 to τ_2 as

$$\frac{\Delta u}{\bar{\sigma}_v} = \int_{|\tau_1/\bar{\sigma}_v|}^{|\tau_2/\bar{\sigma}_v|} \psi \, d\left(\frac{\tau}{\bar{\sigma}_v}\right); \quad |\tau_1| \leq |\tau_2| \quad \ldots\ldots\ldots\ldots\ldots\ldots\ldots\ldots (1)$$

in which Δu = pore pressure increase; $\bar{\sigma}_v$ = initial effective overburden stress;

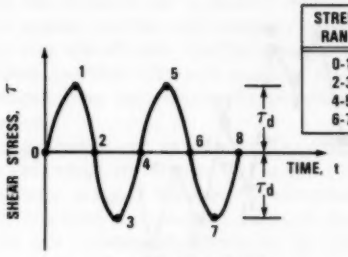

STRESS RANGE	FUNCTION n(N)
0-1	n (1)
2-3	n (1)
4-5	n (2)
6-7	n (2)

(a) UNIFORM LOADING

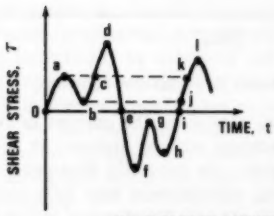

STRESS RANGE	FUNCTION n(N)
0-a	n (1)
b-c	n (2)
c-d	n (1)
e-f	n (1)
g-h	n (2)
i-j	n (2)
j-k	n (3)
k-l	n (2)

(b) IRREGULAR LOADING

FIG. 2.—Pore Pressure Evaluation and Memory Function, $n(N)$

and τ = shear stress. ψ is considered uniquely determined for a given soil density and a confining pressure following the first assumption, and is expressed as

$$\psi = \bar{A}\left[n(N) + f\left(\frac{u}{\bar{\sigma}_v}\right)\right]\left|\frac{\tau}{\bar{\sigma}_v}\right|^{\beta} \quad \ldots\ldots\ldots\ldots\ldots\ldots\ldots\ldots (2)$$

in which $\bar{A}$ and β = model parameters; $n(N)$ = "memory function" that depends

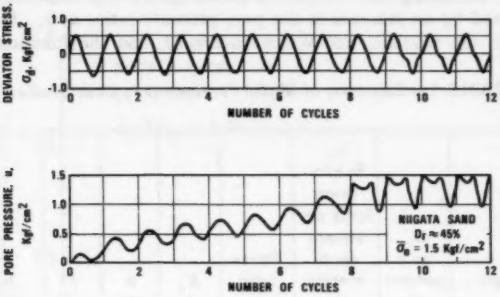

(AFTER ISHIHARA AND YASUDA, 1972)

FIG. 3.—Typical Pore Pressure Response

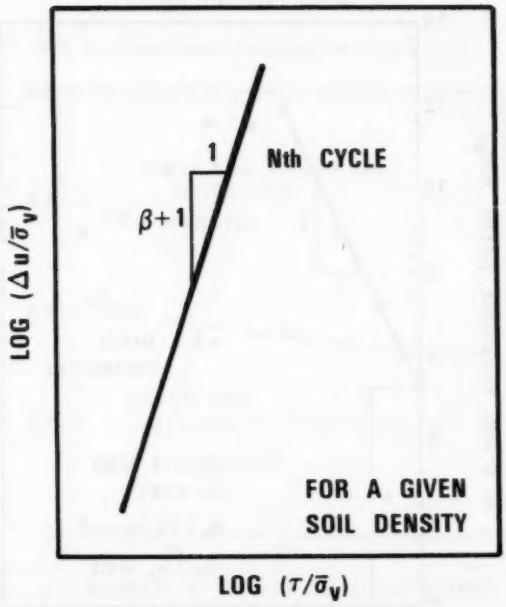

FIG. 4.—Determination of Parameter β

on the number of the times a soil element is sheared; and $f(u/\bar{\sigma}_v)$ = a function representing the change in the pore pressure generation capability of a soil element caused by an increase in the pore pressure ratio, $u/\bar{\sigma}_v$. The function $n(N)$ reflects the tendency for volume decrease, and the function, $f(u/\bar{\sigma}_v)$,

TABLE 1.—Summary of Model Parameters in Case Studies

Sand sample (1)	D_r, as a percent (2)	$\hat{\sigma}_v$, in kilogram force per square centimeters (3)	Stress ratio (4)	K_0 (5)	a (6)	b (7)	β (8)	$\bar{A}$ (9)
Niigata sand	45	1.5	0.20	1.0	3.14	2.06	2	187.5
Fuji River sand	55	1.0	0.27	1.5	5.85	1.94	2	76.2
	55	1.0	0.155	0.5	6.98	1.72	2	402.8

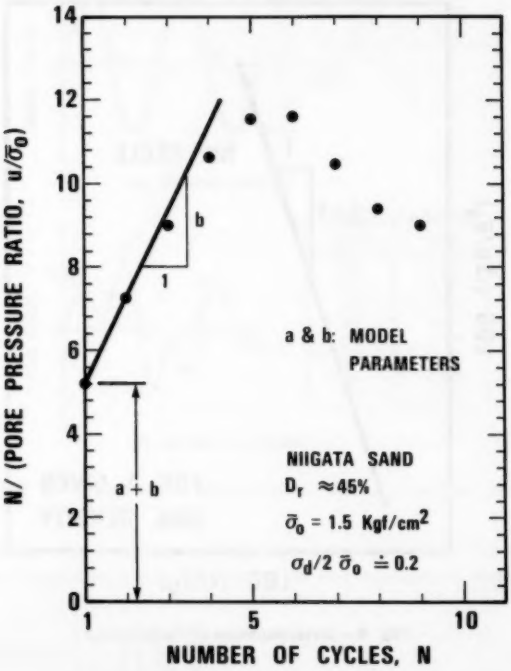

FIG. 5.—Model Parameter Determination Procedure

accounts for the effective increase in the applied shear stress as a result of a decrease in confining pressure during the liquefaction process. Alternatively,

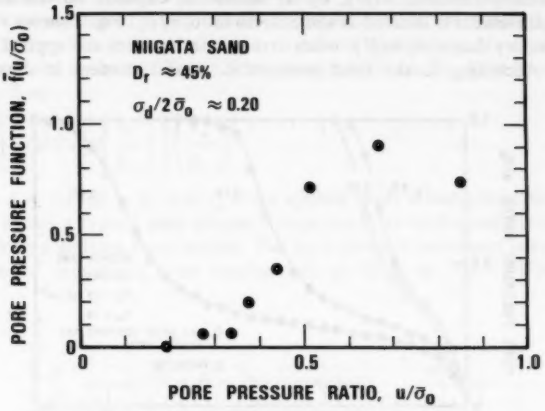

FIG. 6.—Pore Pressure Function $\bar{f}$ for Niigata Sand

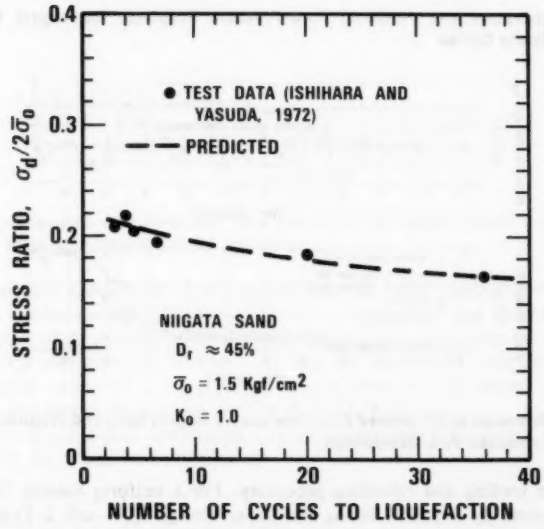

FIG. 7.—Measured and Predicted Stress Ratio at Liquefaction for Niigata Sand

$f(u/\bar{\sigma}_v)$ may be considered as an empirical function that represents the effects of an increase in cyclic shear strain near liquefaction and of the volume expansion

tendency of the soil due to the reduction of effective confining pressure on the pore pressure generation capability of a sand.

The memory function, $n(N)$, by its definition, depends on the number of times a soil element is sheared at some stress ratio, $\tau/\bar{\sigma}_v$. Fig. 2 shows variations of the memory function, $n(N)$, when stress-time histories are applied to a soil element. According to the third assumption, a soil element is sheared only

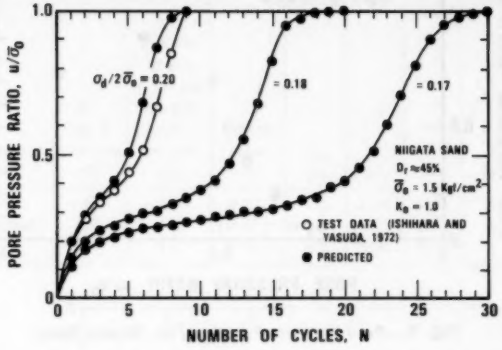

FIG. 8.—Measured and Predicted Pore Pressure Response for Niigata Sand and Uniform Stress Cycles

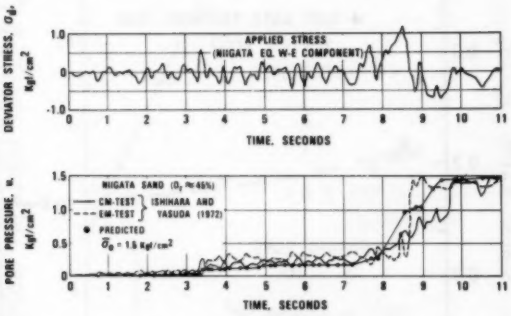

FIG. 9.—Measured and Predicted Pore Pressure for Niigata Sand and Irregular Loading, Niigata Earthquake W-E Component

during the loading and reloading processes. For a uniform loading case, Fig. 2(*a*), the memory function during the stress changes (0–1 and 2–3) is $n(1)$ as the soil element is sheared for the first time. The memory function for the stress changes (4–5 and 6–7), however, is $n(2)$ as the soil element is sheared for the second time in these stress ranges. Variation of $n(N)$ for an irregular stress history also will be defined in a similar manner (Fig. 2(*b*)). On the other hand, the function $f(u/\bar{\sigma}_v)$ will be considered independent of the stress history

and is uniquely related to the pore pressure ratio, $u/\bar{\sigma}_v$, for a given soil density and confining pressure.

Determination of Model Parameters.—Most pore pressure data have been obtained from undrained cyclic tests employing uniform stress cycles. Therefore, it is convenient for us to construct a model the parameters of which can be determined from such tests. For uniform stress conditions, Eq. 1 can be integrated using Eq. 2 as

$$\frac{\Delta u}{\bar{\sigma}_v} = A\left[n(N) + f\left(\frac{u}{\bar{\sigma}_v}\right)\right]\left(\frac{\tau_d}{\bar{\sigma}_v}\right)^{\beta+1} \quad \ldots\ldots\ldots\ldots\ldots\ldots\ldots\ldots (3)$$

in which $A = 2\bar{A}/(\beta + 1)$; and τ_d = the applied shear stress amplitude.

Fig. 3 shows a typical pore pressure response in an undrained cyclic triaxial test employing uniform stress cycles. The pore pressure increment in each stress cycle can be determined from results such as those in Fig. 3. When cyclic

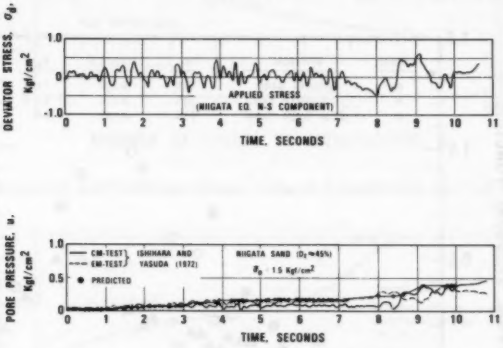

FIG. 10.—Measured and Predicted Pore Pressures for Niigata Sand and Irregular Loading, Niigata Earthquake N-S Component

undrained tests are performed on samples with the same density and confining pressure but for several different stress ratios, the parameter β can be obtained as a function of the number of stress cycles. A method to determine the parameter β is shown schematically in Fig. 4. β may be considered independent of N for practical values of N. β typically ranges from 0.0–3.0, based on data in our files and results of previous studies (3,11,13,14,16,17).

With the β value thus determined, and an appropriate shear stress amplitude, τ_d (Fig. 3), Eq. 3 can be simplified as

$$\frac{\Delta u}{\bar{\sigma}_v} = n(N) + f\left(\frac{u}{\bar{\sigma}_v}\right); \quad A = \frac{1}{\left(\frac{\tau_d}{\bar{\sigma}_v}\right)^{\beta+1}} \quad \ldots\ldots\ldots\ldots\ldots\ldots\ldots\ldots (4)$$

Functions $n(N)$ and $f(u/\bar{\sigma}_v)$ can be determined from a pore pressure response such as that in Fig. 3. To determine these functions using test results with

several stress ratios, we must employ the results with a stress ratio that is representative of the field loading condition. The pore pressure response in Fig. 3 is shown in Fig. 5 in terms of $N/(u/\bar{\sigma}_v)$. To determine the function $n(N)$, we recall: (1) That the function $n(N)$ dominates for small N values, as this function represents the pore pressure increase due to the potential for a volume decrease of a sand under the initial effective stress system; and (2) the drained volume decrease of a sand can be approximated by a hyperbolic function for practical values of N (2,9,11,16). Thus, the initial straight line portion of the curve in Fig. 5 must represent the pore pressure increase due to the volume decrease potential of the sand under the initial effective stress system that is given as

$$\bar{n}(N) = \frac{N}{(a + bN)} \quad \ldots\ldots\ldots\ldots\ldots\ldots\ldots\ldots\ldots\ldots\ldots\ldots\ldots\ldots (5)$$

in which parameters a and b can be determined from Fig. 5. Therefore, the

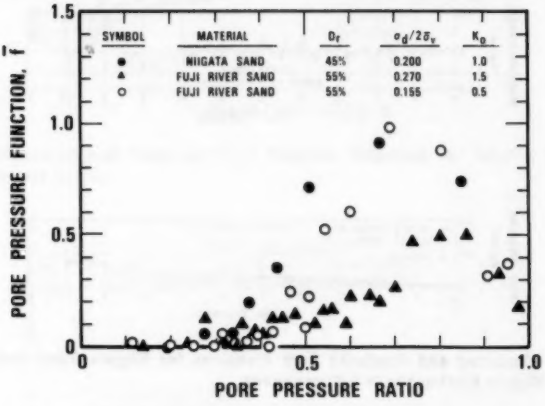

FIG. 11.—Summary of Pore Pressure Function $\bar{f}$ in Case Studies

pore pressure increase during the Nth cycle, due to the volume decrease potential of sand, is derived as

$$n(N) = \bar{n}(N) - \bar{n}(N-1) = \frac{a}{(a + bN)(a - b + bN)} \quad \ldots\ldots\ldots\ldots\ldots (6)$$

The observed pore pressure increase in the Nth cycle in Fig. 5, in excess of that in Eq. 6, is due to the function, $f(u/\bar{\sigma}_v)$.

$$f\left(\frac{u}{\bar{\sigma}_v}\right) = (\text{Pore Pressure Increase during the } N\text{th cycle}) - n(N) \quad \ldots\ldots (7)$$

The function, $f(u/\bar{\sigma}_v)$, obtained for the pore pressure response in Fig. 3, is normalized by $n(1)$ and shown in Fig. 6—$\bar{f}(u/\bar{\sigma}_v) = f(u/\bar{\sigma}_v)/n(1)$.

Case Studies

Assumptions and performance of the liquefaction model were examined by analyzing pore pressure responses obtained in laboratory tests for both uniform and earthquake-type loading conditions.

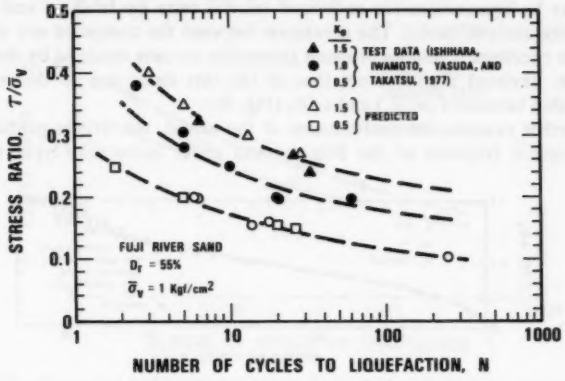

FIG. 12.—Measured and Predicted Stress Ratio at Liquefaction for Fuji River Sand

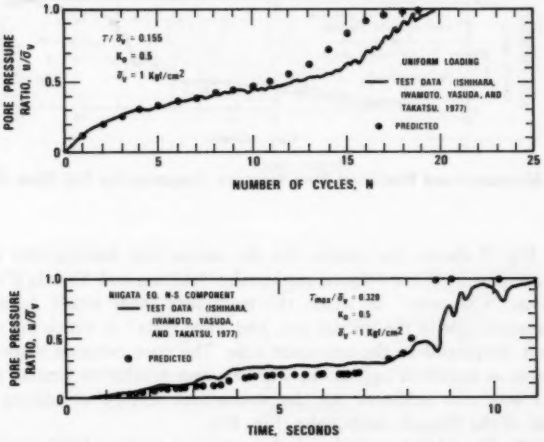

FIG. 13.—Measured and Predicted Pore Pressure Response for Fuji River Sand with $K_o = 0.5$

Case Study I.—Ishihara and Yasuda (7) performed undrained triaxial tests on Niigata sand employing as input both uniform and earthquake-type irregular

stress histories. All the parameters and the functions, $n(N)$ and $f(u/\bar{\sigma}_0)$ for the liquefaction model except β were determined using their test data for uniform stress loading (Table 1). Available data were not sufficient to determine the parameter, β. Therefore, β was assumed, and a value of 2.0 was used in the analysis. The function, $\bar{f}(u/\bar{\sigma}_0)$, was determined, as shown in Fig. 6.

Fig. 7 shows the relationship obtained between the stress ratio and the number of cycles to liquefaction for undrained triaxial tests by Ishihara and Yasuda (7) and the analytic model. The agreement between the computed and observed results is excellent. The pore pressure generation process obtained by the model, however, deviated slightly from that of the test data, due to the nonlinear relationship between $f(u/\bar{\sigma}_0)$ and $u/\bar{\sigma}_0$ (Fig. 8).

To further examine the performance of the model, the writers predicted the pore pressure response of the Niigata sand under earthquake-type, irregular

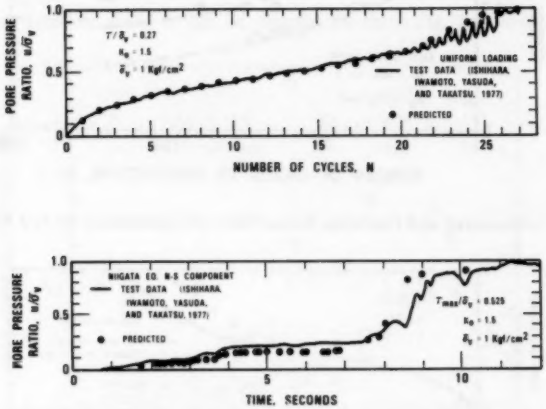

FIG. 14.—Measured and Predicted Pore Pressure Response for Fuji River Sand with $K_0 = 1.5$

loadings. Fig. 9 shows the results for the stress-time history that simulates the W-E component of the Niigata earthquake. Ishihara and Yasuda (7) reported results from "CM tests" in which the maximum shear stress developed on the compression side of the triaxial test, and "EM tests" in which the maximum shear stress developed on the extension side. The pore pressure response from the model is in excellent agreement with the test results. A similar degree of agreement was also achieved for the stress-time history simulating the N-S component of the Niigata earthquake (Fig. 10).

Case Study II.—Using a torsional shear testing device, Ishihara, Iwamoto, Yasuda, and Takatsu (4) studied the effect of the earth pressure coefficient at rest, K_0, on the liquefaction potential of Fuji River sand. Their tests included both uniform and irregular stress loadings.

The parameters and the functions $n(N)$ and $\bar{f}(u/\bar{\sigma}_v)$ were determined using the test results in the same way as in Case Study I, but for K_0 equal to 0.5

and 1.5 (Table 1 and Fig. 11). The value of β was assumed to be 2.0.

The relationships between the stress ratio and the number of cycles to liquefaction from the test data and the model, are summarized in Fig. 12. Figs. 13 and 14 compare computed and measured pore pressure histories. Again,

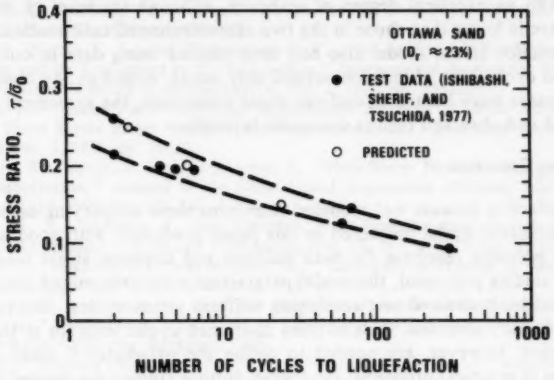

FIG. 15.—Measured and Predicted Stress Ratio at Liquefaction for Ottawa Sand

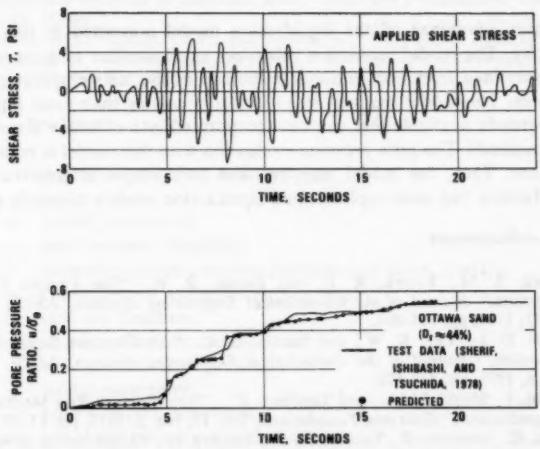

FIG. 16.—Measured and Predicted Pore Pressure Response for Ottawa Sand and Irregular Loading

the model satisfactorily predicted the pore pressure response for both uniform and irregular loading conditions.

Other Case Studies.—Beside the case studies described above, performance

of the model was examined using the test results reported by Ishibashi, Sherif, and Tsuchiya (3), and Sherif, Ishibashi, and Tsuchiya (13). As their data were not sufficient to determine all the model parameters and functions, we assumed appropriate values. The results for uniform stress conditions and earthquake-type irregular loading are shown in Figs. 15 and 16. We could reproduce their test results with an excellent degree of accuracy, although the level of simulation in this case is lower than those in the two aforementioned case studies.

Performance of the model also has been studied using data in our files on undrained cyclic triaxial tests on several silty sands. Although the comparisons in these cases were limited to uniform stress conditions, the agreement between computed and observed results was quite favorable.

Concluding Comments

A liquefaction process was modeled employing some simplifying assumptions. The liquefaction model presented in this paper predicted, with good accuracy, the pore pressure response for both uniform and irregular stress loadings. In the case studies presented, the model parameters were determined using results from a single, undrained test employing uniform stress cycles. The parameter β was tactically assumed. Results from undrained cyclic tests for at least three stress ratios, however, are needed to define the parameter β when applying the model in practical problems. Of course, further studies are needed to define the system parameters in more detail and to relate the system parameters to the status of soil, especially to the relative density of soil and initial confining pressure.

The major advantage of the liquefaction model presented in this paper is its simplicity. The model requires a relatively small number of parameters that can be determined from conventional undrained cyclic tests employing uniform stress cycles. The model requires less laboratory testing than most liquefaction models currently available that can be incorporated into effective stress seismic response methods. The pore pressure evaluation with this model is computationally efficient. Thus, the model may be used as a simple alternative to other equally effective, but more sophisticated liquefaction models currently available.

Appendix I.—References

1. Blazquez, R. M., Krizek, R. J., and Bazant, Z. P., "Site Factors Controlling Liquefaction," *Journal of the Geotechnical Engineering Division*, ASCE, Vol. 106, No. GT7, 1980, pp. 785–801.
2. Finn, W. D. L., Lee, K. W., and Martin, G. R., "An Effective Stress Model for Liquefaction," *Journal of the Geotechnical Engineering Division*, ASCE, Vol. 103, No. GT6, 1977, pp. 517–533.
3. Ishibashi, I., Sherif, M. A., and Tsuchiya, C., "Pore-Pressure Rise Mechanism and Soil Liquefaction," *Soils and Foundations*, Vol. 17, No. 2, 1977, pp. 17–27.
4. Ishihara, K., Iwamoto, S., Yasuda, S., and Takatsu, H., "Liquefaction of Anisotropically Consolidated Sand," *Proceedings, 9th International Conference on Soil Mechanics and Foundation Engineering*, Vol. 2, 1977, pp. 261–264.
5. Ishihara, K., Lysmer, J., Yasuda, S., and Hirao, H., "Prediction of Liquefaction in Sand Deposits during Earthquakes," *Soils and Foundations*, Vol. 16, No. 1, 1976, pp. 1–16.
6. Ishihara, K., Tatsuoka, F., and Yasuda, S., "Undrained Deformation and Liquefaction of Sand under Cyclic Stresses," *Soils and Foundations*, Vol. 15, No. 1, 1975, pp. 29–44.

7. Ishihara, K. and Yasuda, S., "Sand Liquefaction due to Irregular Excitation," *Soils and Foundations*, Vol. 12, No. 4, 1972, pp. 65–77.
8. Liou, C. P., Streeter, V. L., and Richart, F. E., Jr., "Numerical Model for Liquefaction," *Journal of the Geotechnical Engineering Division*, ASCE, Vol. 103, No. GT6, 1977, pp. 589–606.
9. Martin, G. R., Finn, W. D. L., and Seed, H. B., "Fundamentals of Liquefaction under Cyclic Loading," *Journal of the Geotechnical Engineering Division*, ASCE, Vol. 101, No. GT5, 1975, pp. 423–438.
10. Mroz, Z., Norris, V. A., and Zienkiewicz, O. C., "An Anisotropic Hardening Model for Soils and its Application to Cyclic Loading," *International Journal for Numerical and Analytical Methods in Geomechanics*, Vol. 2, 1978, pp. 203–221.
11. Oh-oka, H., "Drained and Undrained Stress-Strain Behavior of Sands Subjected to Cyclic Shear Stress under Nearly Plane Strain Condition," *Soils and Foundations*, Vol. 16, No. 3, 1976, pp. 19–31.
12. Seed, H. B., Martin, P. P., and Lysmer, J., "Pore-Water Pressure Changes during Soil Liquefaction," *Journal of the Geotechnical Engineering Division*, ASCE, Vol. 102, No. GT4, 1976, pp. 323–346.
13. Sherif, M. A., Ishibashi, I., and Tsuchiya, C., "Pore-Pressure Prediction during Earthquake Loading," *Soils and Foundation*, Vol. 18, No. 4, 1978, pp. 19–30.
14. Shibata, T., Yukitomo, H., and Miyoshi, M., "Liquefaction Process of Sand during Cyclic Loading," *Soils and Foundations*, Vol. 12, No. 1, 1972, pp. 1–16.
15. Silver, M. L. and Seed, H. B., "The Behavior of Sands under Seismic Loading Conditions," *Report No. EERC 69-16*, Earthquake Engineering Research Center, University of California, Berkeley, Calif.
16. Yagi, N., "Volume Change and Excess Pore Pressure in Sands under Repeated Shear Stress," *Proceedings* of the Japan Society of Civil Engineers, Vol. No. 275, 1978, pp. 79–90. (in Japanese).
17. Yoshimi, Y. and Oh-oka, H., "Influence of Degree of Shear Stress Reversal on the Liquefaction Potential of Saturated Sand," *Soils and Foundations*, Vol. 15, No. 3, 1975, pp. 27–40.
18. Zienkiewicz, O. C., Chang, C. T., and Hinton, E., "Non-Linear Seismic Response and Liquefaction," *International Journal for Numerical and Analytical Methods in Geomechanics*, Vol. 2, 1978, pp. 381–404.

Appendix II.—Notation

The following symbols are used in this paper:

A = model parameter;
$f(u/\bar{\sigma}_v)$ = pore pressure function;
$\bar{f}(u/\bar{\sigma}_v)$ = normalized pore pressure function $(=f(u/\sigma_v)/n(1))$;
K_0 = coefficient of earth pressure at rest;
$n(N)$ = memory function;
N = number of stress cycles;
u = excess pore-water pressure;
β = model parameter;
Δu = pore pressure increment;
$\bar{\sigma}_v$ = initial effective overburden stress;
$\bar{\sigma}_0$ = initial effective ambient stress;
τ = shear stress; and
ψ = potential function for pore pressure generation.

GROUND MOVEMENT ANALYSIS OF EARTH SUPPORT SYSTEM

By C. K. Shen,[1] M. ASCE, S. Bang,[2] A. M. ASCE, and L. R. Herrman,[3] M. ASCE

INTRODUCTION

In recent years, a relatively new in situ earth reinforcement lateral support system for deep excavation has been introduced. Unlike the conventional systems that serve to retain soil behind a vertical cut, this procedure is based on the concept of soil reinforcement, i.e., the native soil adjacent to the excavation is strengthened so that it can stand unsupported at depths which would normally require the installation of sheet pilings or soldier piles and bracings. Briefly, this system is composed of an array of reinforcing members that are grouted into the soil mass, a wire-mesh reinforced shotcrete panel facing, and rows of re-bars which form horizontal wales at each reinforcement level. The various components of this system are shown in Fig. 1.

Excavation begins from the ground level. After each layer of excavation, reinforcement is immediately applied to both the native soil and the exposed cut. This system provides a unique means of temporary earth support with the advantages that it: (1) Requires no pile driving; (2) prevents any loosening or sloughing of the soil; (3) provides an obstruction-free site for subsequent foundation work; and (4) significantly reduces construction time. The system has so far been successfully used for thousands of square meters of excavation, to depths of up to approx 18 m. A more detailed description of it can be found elsewhere (10).

GROUND MOVEMENTS AND OPEN EXCAVATION

Ground movements associated with deep open excavation have often been observed in the field. Unless a permanent type of often costly lateral earth support system (such as slurry walls) is used, ground movement adjacent to

[1]Prof., Dept. of Civ. Engrg., University of California, Davis, Calif. 95616.
[2]Asst. Prof., Dept. of Civ. Engrg., Univ. of Notre Dame, Notre Dame, Ind.
[3]Prof., Dept. of Civ. Engrg., Univ. of California, Davis, Calif. 95616.

Note.—Discussion open until May 1, 1982. Separate discussions should be submitted for the individual papers in this symposium. To extend the closing date one month, a written request must be filed with the Manager of Technical and Professional Publications, ASCE. Manuscript was submitted for review for possible publication on March 12, 1981. This paper is part of the Journal of the Geotechnical Engineering Division, Proceedings of the American Society of Civil Engineers, ©ASCE, Vol. 107, No. GT12, December, 1981. ISSN 0093-6405/81/0012-1609/$01.00.

an open excavation is almost unavoidable. At the present time, however, there is no rational method capable of accurately predicting the extent as well as the magnitude of both the horizontal and vertical movements. This is due largely to the fact that construction practice of temporary lateral earth support systems varies from place to place, and, frequently, its execution is entirely at the discretion of the contractor. The lack of standardized construction procedures together with other local influences make it difficult, if not impossible, to quantify ground movements associated with deep excavation. Consequently, only limited field information is available pertaining to this subject. For instance, Peck (9)

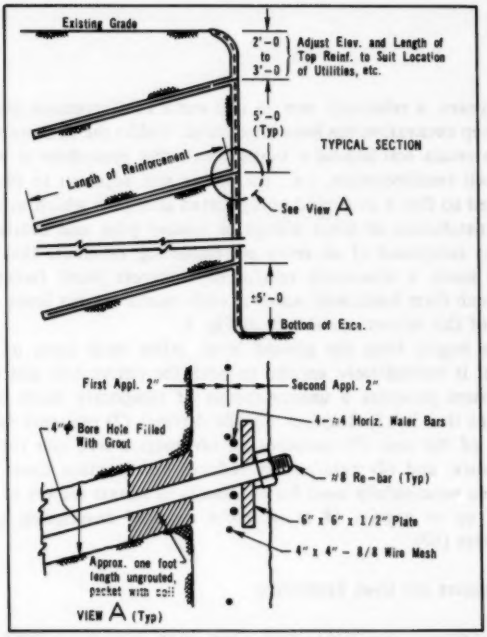

FIG. 1.—Construction Detail—Earth Reinforcement Lateral Support System (1 ft = 0.305 m; 1 in. = 25.4 mm)

studied the field records of many excavation sites using soldier piles or sheet piles that were braced and classified the field performance of open excavation systems into three categories as in Fig. 2. Zone I, which gives the best performance, refers to well-braced systems with slurry walls or substantial amount of berms left permanently in place. Zone II, describing intermediate performance, indicates systems with temporary berms and raker support. Zone III includes systems with ground loss from caisson construction or insufficient support. Similar information gathered at Chicago and Washington D.C. areas were reported by O'Rourke, et al. (8). These records have clearly indicated that the amount and

distribution of ground movements depends heavily upon the soil type, the method and sequential procedure of construction, and the depth of excavation. Since control of these factors is extremely difficult using the current excavation methodology, it is unlikely that accurate prediction of ground movements can be made possible. Ground movements, however, could bear grave consequences to the stability of adjacent buildings, the operation of utilities, and the use of nearby streets. In adopting a particular temporary lateral earth support system, one should ideally be able to judge or estimate the magnitude and distribution of ground movements to appraise the potential for damage and to evaluate the need for proper design or protective measures or both. Unless the procedures of construction practice can be controlled and standardized, the question of ground movement prediction will remain unresolved.

On the other hand, if the construction procedures of a lateral earth support system can be standardized and systematically carried out in the field and if a physical model can be devised to properly describe the system behavior and

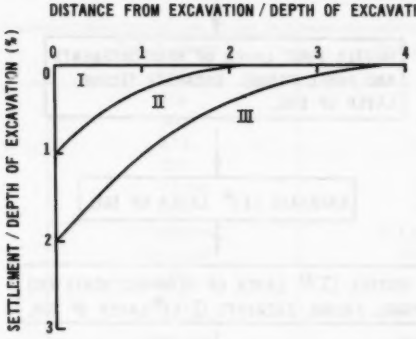

FIG. 2.—Field Performance of Open Excavation System (Ref. 9)

its construction sequence, it is possible that an analytical procedure may be formulated to predict the ground movements more accurately. The system described in this paper has a unique and well-defined construction procedure such that it can be expected to achieve a better and more uniform control of field practice than any currently employed temporary system. For this reason, it appears that a more rigorous analytical treatment can be applied in order to determine the magnitude and distribution of ground movements associated with deep excavation. Such analyses and the interpretation of the analytical results form the remaining parts of this paper.

Finite Element Study

Computer Program.—Analyses were performed using the finite element computer program for general two-dimensional soil and soil reinforcement problems developed by Herrmann (5). The program assumes that plane strain conditions exist. Because of the finite width and the horizontal spacing of

reinforcement of the system studied, it did not exactly satisfy the plane strain criterion. However, it could be reasonably assumed that deviation from plane strain conditions was not substantial for most practical purposes (6). Several elements were incorporated into the analyses to simulate the special features of the system properly; these include the interface bond layer, the sequential procedure of construction, and the composite reinforced soil model. A more detailed description is given in the following sections.

Bond Layer.—Slippage between the reinforcing members and the surrounding soil was accounted for in the analyses (5). The maximum bond stress was assumed

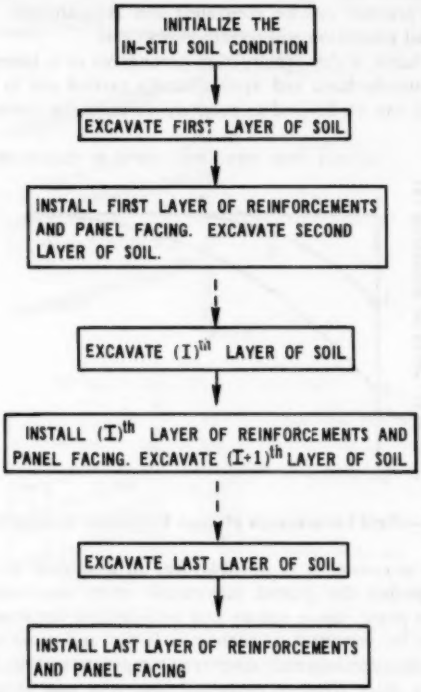

FIG. 3.—Construction Steps Used in Finite Element Analysis

to be governed by the Coulomb's failure criterion, $\tau_{max} = c + \sigma_v \tan \phi$. It was assumed that adhesion was fully maintained even though slippage might have taken place. No yielding of re-bars relative to the grout was considered.

Construction Sequence.—The analyses were carried out as a sequence of incremental steps with iterations conducted in each increment. The incremental procedure simulated the sequential excavation steps and the installation of the reinforcing members. The number of increments required was determined in

such a way that the excavation and the stress history of the soil were adequately represented. Generally, the greater the number of increments, the better is the accuracy of the analysis. A flow chart of the computational steps of the analysis is shown in Fig. 3.

Composite Model.—A composite model was used to describe the reinforced soil system. The composite representation adopted for this analysis was different from the conventional composite approach expressing simply the orthotropic composite material properties as functions of the properties of each of the constituent materials and their geometric arrangement. The procedure used in this study accounted for the composite nature of the reinforced soil system by combining the element stiffness matrices of the constituent materials (i.e. soil, reinforcing members, and the bond behavior) directly to produce the composite element matrices. The approximate solution was then selected by minimizing the incremental potential energy of the system. Detailed description

TABLE 1.—Properties of Soils Used in Analysis

(1)	Soil number 1 (2)	Soil number 2 (3)
K	100	280
K_{ur}	300	840
n	0.84	0.6
ϕ	27°	18°
c	7.5 psi	12.64 psi
R_f	0.77	0.93
ν	0.3 (assumed)	0.3 (assumed)
γ_t	121.3 pcf	124.6 pcf
LL	19	25
PI	1	12
D_{10}	0.013 mm	—
D_{30}	0.045 mm	0.002 mm
D_{60}	0.070 mm	0.04 mm

Note: 1 psi = 6.9 KN/m^2; and 1 pcf = 157 N/m^3.

of the development can be found in Ref. 7. The soil model employed in the analysis was the nonlinear, and the inelastic model was proposed by Duncan and Chang (4). This characterization assumed that the soil behavior can always be described by the instantaneous values of modulus, i.e., the soil does not experience stress or strain induced anisotropy. A hyperbola was assumed to represent the stress-strain relationship for primary loading and a straight line for unloading and reloading. Duncan and Chang also proposed a similar expression for the Poisson's ratio. They, however, failed to include the effects of unloading-reloading on Poisson's ratio. It was found during this study that the expression for Poisson's ratio did not represent the proper behavior of soil during excavation, particularly in the prediction of ground surface movements. A constant Poisson's ratio value of 0.3 was, therefore, used in the analyses.

Analysis.—Based on a previous parametric study (1), it was concluded that the construction sequence; the depth of excavation, H; the soil type; the length

L; the size, D, and the spacing of the reinforcing members were important parameters to be considered in design. It was also indicated that the reinforcing members were best oriented at a horizontal inclination between 15–25°. To examine the effects of these parameters on ground movements further, the following analyses were performed.

The depths of excavation studied were in range of approx 0.5–1.5 times the length of the reinforcing members of 15–40 ft (4.5–12 m) in length. An angle

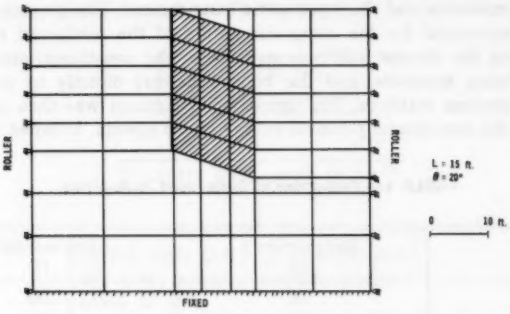

FIG. 4.—Typical Finite Element Grid (1 ft = 0.305 m)

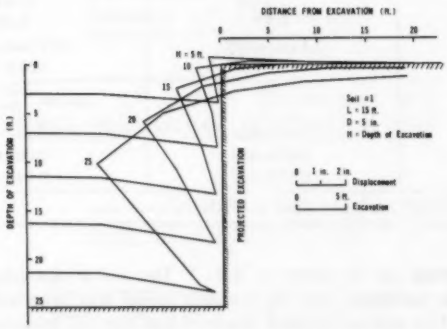

FIG. 5.—Deformed Shapes of the System Due to Excavations (1 ft = 0.305 m; 1 in. = 25.4 mm)

of inclination of 20° was selected, and a spacing of 5 × 5 ft (1.5 × 1.5 m) was used for the reinforcement grid pattern. The diameters of the reinforcing members were 3.33 in. (85 mm) and 5 in. (127 mm), corresponding to 0.24 and 0.54% of the total cross-sectional area of the reinforced soil mass, respectively. In the plane strain analysis, equivalent reinforcing members that had a tensile strength equal to that of steel and a contact area of $\pi LD/H_z$ per unit width of wall were used, where D is the diameter of the grout hole; H_z = the horizontal

spacing of reinforcement; and L = the length of reinforcement. Two different soils, a sandy-silt (soil #1) and a sandy clay (soil #2) were chosen. Their physical properties and the hyperbolic parameters were obtained from Wong and Duncan (11) as in Table 1.

Fig. 4 shows a typical finite element mesh and its boundaries for a system having a 15-ft (4.5-m) reinforcement length and a maximum depth of excavation of 25 ft (7.5 m). The shaded portion of the mesh represents the reinforced soil forming the in situ lateral earth support system. In the analyses, the reinforced soil mass was modeled by composite elements, and the facing was represented by one-dimensional elements. Six increments were required to simulate the excavation to a depth of 25 ft (7.5 m) and the installation of reinforcement; one more increment was added to generate the initial geostatic stresses in the soil mass.

The successive displacement profiles of the ground surface adjacent to the excavation for soil #1 (for the case of D = 5 in. (127 mm) and L = 15 ft

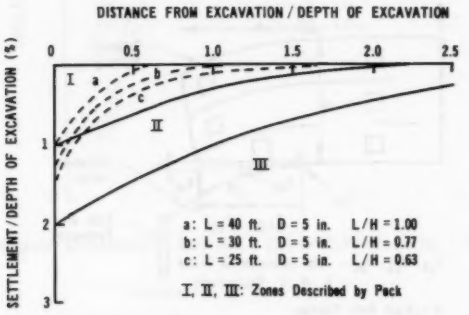

FIG. 6.—Ground Surface Settlement of Soil No. 1 (H = 40 ft; 1 ft = 0.305 m; 1 in. = 25.4 mm)

(4.5 m)) are shown in Fig. 5. It can be seen that a small amount of rebound of the ground surface near the edge occurs during the first 5 ft (1.5 m) of excavation. The maximum amount of rebound is approx 0.3 in. (7.5 mm) which corresponds to approx 0.5% of the depth of excavation. The deformed shape of the facing is approximately linear. However, as excavation proceeds, the pattern of ground movement is generally concave downward with the maximum movements occuring along the edge of the ground surface. The maximum horizontal displacement increases rapidly with increasing depth of excavation. For instance, a maximum horizontal displacement of 0.5 in. (12.7 mm) (0.75% of the depth of excavation) is recorded at 5 ft (1.5 m) excavation, and, at 25 ft (7.5 m) excavation, the displacement is 5.1 in. (13 mm) (1.7% of the depth of excavation). This indicates that the effectiveness of reinforcement decreases with decreasing ratio of reinforcement length to the depth of excavation, L/H. Furthermore, results of ground surface settlement for soil #1 are plotted in Fig. 6. Curves a, b, and c represent the settlement profiles with reinforcement lengths of 40, 30, and 25 ft (12, 9, and 7.5 m), respectively. The depth of

excavation is 40 ft (12 m), and the diameter of the reinforcing members is 5 in. (127 mm) in all cases. The ratios of L/H for curves a, b, and c are 1.0, 0.77, and 0.63, respectively. These results show again that the effectiveness of reinforcement decreases with decreasing ratio of L/H. Comparing Figs. 2 and 6 as suggested by Peck, it can be seen that, if properly designed, the anticipated ground movements associated with this system appear to be well within the movements normally identified with currently used temporary lateral earth support systems in construction practice.

Discussion

Conventionally, the safety evaluation of an earth retaining structure is based on a stability calculation performed against failure. This limit analysis approach of design methodology does not provide any information concerning the movement or displacement of the ground adjacent to an open excavation. As a result,

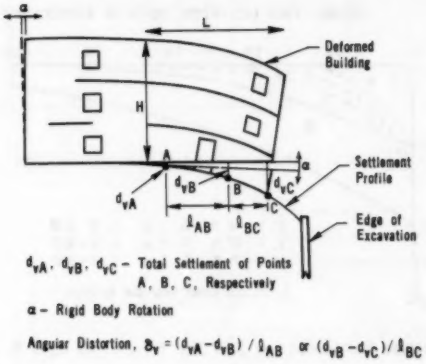

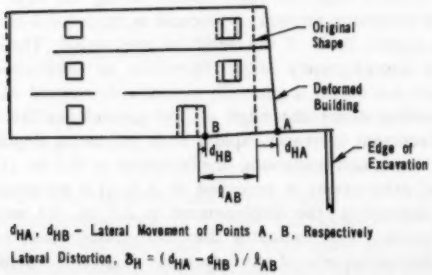

FIG. 7.—Angular and Lateral Distortions of Ground Surface Adjacent to Open Cut (Ref. 8)

different values of safety factors are imposed to indirectly limit the movement of the structure by maintaining the shear stresses everywhere within the soil-structure system well below its shear strength. Unfortunately, the margin

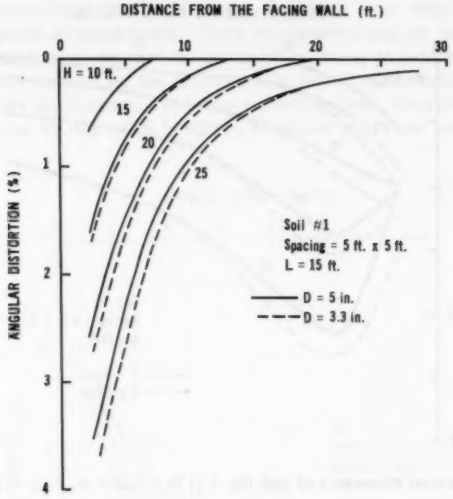

FIG. 8.—Angular Distortion of Soil No. 1 (1 ft = 0.305 m; 1 in. = 25.4 mm)

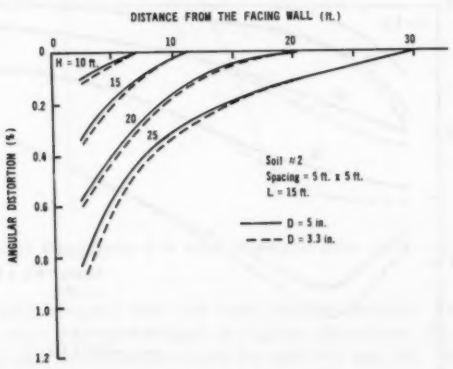

FIG. 9.—Angular Distortion of Soil No. 2 (1 ft = 0.305 m; 1 in. = 25.4 mm)

of safety against failure alone is not sufficient in judging the damage potential to surrounding buildings or other installations. An additional design criterion is needed, therefore, to relate, at the working stress level, the ground movements

to excavation depth and reinforcement. These movements can then be translated to damage potential to surrounding structures so that the appropriateness of the design can be properly evaluated.

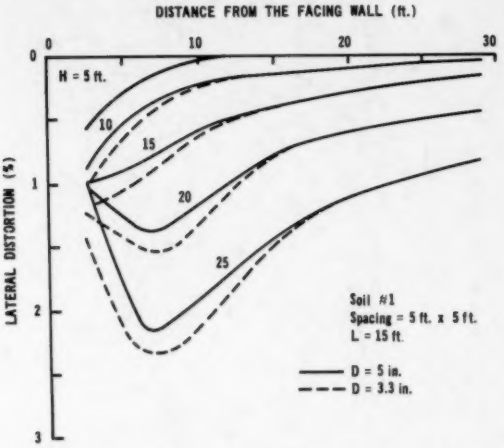

FIG. 10.—Lateral Distortion of Soil No. 1 (1 ft = 0.305 m; 1 in. = 25.4 mm)

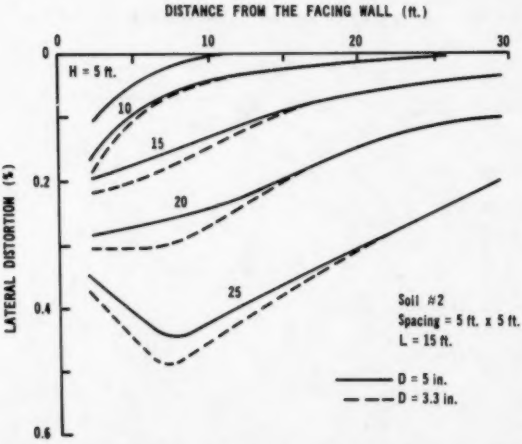

FIG. 11.—Lateral Distortion of Soil No. 2 (1 ft = 0.305 m; 1 in. = 25.4 mm)

Ground movements expressed as angular and lateral distortions have been correlated to building damages as reported recently by O'Rourke, Cording, and

Boscardin (8). The definitions of angular and lateral distortions are shown in Fig. 7. The angular distortion, δ_v, is the differential settlement between two points divided by the horizontal distance separating them. The term angular distortion has often been related to architectural and structural damages of buildings due to settlement (3). However, buildings near open cuts are also affected by lateral displacements. These movements can be significant, and can cause a substantial amount of strain to adjacent structures. The lateral distortion, δ_H, is defined as the difference in lateral movement between two points divided by the horizontal distance separating them. Correlations between damages suffered by old brick buildings to lateral distortion can be found in Ref. 8.

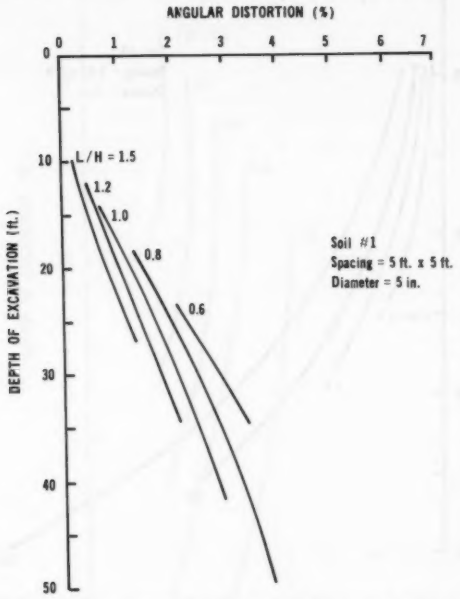

FIG. 12.—Angular Distortions 5 ft from the Excavation (1 ft = 0.305 m; 1 in. = 25.4 mm)

Using the data obtained from the finite element analysis, Figs. 8 and 9 are presented to show the distribution of angular distortions for various depths of excavation and reinforcement sizes for soils #1 and #2. The length of the reinforcement is 15 ft (4.5 m) for all cases shown. The angular distortion between two surface node points is first calculated and then plotted at the midpoint between the two nodes. It is noted that the further the distance from the edge of excavation, the smaller is the magnitude of angular distortion. The rate of decrease of angular distortion with respect to the distance from the edge of excavation is substantial; only a negligible amount of distortion is recorded

when that distance equals the depth of excavation as in Fig. 8 for soil #1. Soil #2 experiences even smaller amounts of angular distortion. The effect of reinforcement size on the ground movement is relatively insignificant in comparison to the L/H ratio. This is because the prime source of resisting force of this system is derived from friction and adhesion between the reinforcing members and the soil. It can be shown that for the same amount of reinforcement in terms of volume per unit width the increase in frictional resistance per unit length of reinforcement can be achieved more readily by increasing the contact

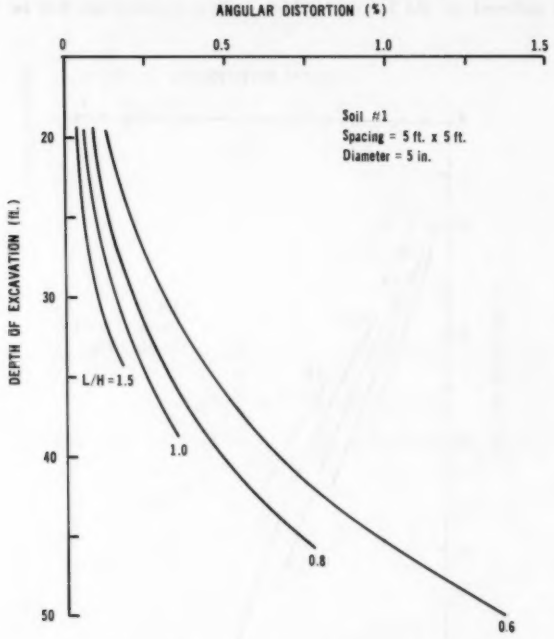

FIG. 13.—Angular Distortions 20 ft from the Excavation (1 ft = 0.305 m; 1 in. = 25.4 mm)

area; i.e., instead of increasing the size of reinforcing members, it is more beneficial to reduce their spacings in the soil mass.

The lateral distortions, which are measurements of surface tensile strains for the same excavation system, are plotted in Figs. 10 and 11 for soils #1 and #2, respectively. For relatively shallow depths of excavation, the maximum lateral distortion occurs near the edge, but the pattern changes as the depth increases. The maximum lateral distortion, for instance, is located at a distance approx 6.7 ft (2 m) from the edge when the excavation reaches a depth of 20 ft (6 m) for soil #1 and 25 ft (7.5 m) for soil #2. This indicates that the

largest tensile strain at the ground surface does not always develop along the edge of excavation but rather at some distance away from it. This distance, however, is determined largely by the soil type, the characteristics of the reinforcement, and the depth of excavation. The locations of maximum lateral

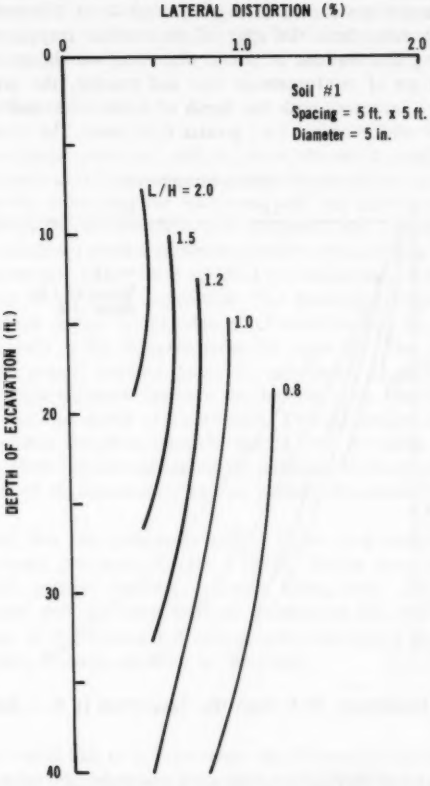

Figure 14. Lateral Distortions 5 ft. From the Excavation
(1 ft. = 0.305 m, 1 in. = 2.54 cm)

FIG. 14.—Lateral Distortions 5 ft from the Excavation (1 ft = 0.305 m; 1 in. = 25.4 mm)

distortion predicted in the analyses seem to agree with field measurements of a braced wall system reported by O'Rourke, et al. (8). According to their measurements of an open excavation system having five rows of struts, the maximum lateral distortion occurred near the edge of excavation when it was 20 ft (6 m) deep; and approx 15 ft (4.5 m) from the edge when the excavation

was 60 ft (18 m) deep. The predicted maximum lateral distortion appears to relate to tension cracks often observed around open cuts.

Useful design information concerning both the angular and lateral distortions of the ground surface can be derived from Figs. 8 and 10 for soil #1. The distribution of angular distortion with respect to the depth of excavation and reinforcement length are shown in Figs. 12 and 13 at distances 5 ft (1.5 m) and 20 ft (6 m) away from the edge of excavation, respectively. Likewise, the corresponding distributions of lateral distortion are shown in Figs. 14 and 15. For a given set of reinforcement size and spacing, the magnitude of the angular distortion increases with the depth of excavation, and decreases with the length of the reinforcement, i.e., greater L/H ratio. The variation of lateral

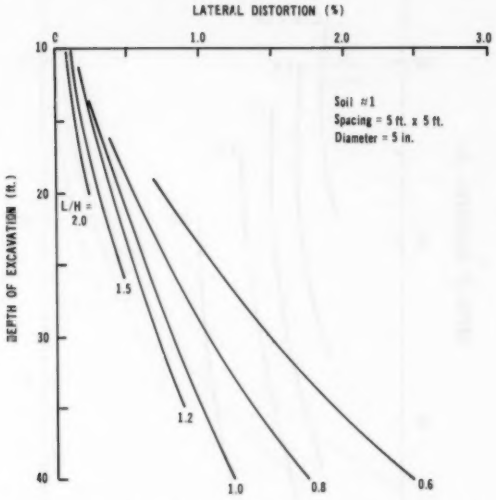

FIG. 15.—Lateral Distortions 20 ft from the Excavation (1 ft = 0.305 m; 1 in. = 25.4 mm)

distortion of the ground surface is not always a monotonically decreasing function as is the case for angular distortion. It decreases monotonically for relatively shallow depths of excavation, but, as excavation becomes deeper, the maximum distortion occurs at some distance away from the edge. This indicates that the lateral distortion near the edge decreases as the depth of excavation increases as shown by the curves in Fig. 14. This pattern, however, does not hold at distances further away from the excavation as in Fig. 15.

Having constructed the design charts and knowing the constraints in terms of permissible ground distortions to possible building damage adjacent to an open cut, one may determine first, if the proposed system is a suitable choice for a particular job; or, second, the required reinforcement spacing and length for a given depth of excavation so that ground distortion can be limited within

its tolerance. This design methodology is unique in its approach, and applies only to the in situ lateral earth support system described above. It may be noted that the illustrations given here have not included any form of surface loading (such as building, fill, etc.) in the analysis. However, provisions are available in the computer program to approximate such loading conditions. The tolerance of ground distortion in buildings and other structures is a subject of great importance to foundation engineering; however, its formulation is beyond the scope of this paper.

Summary and Conclusion

Ground movements associated with a new in situ earth reinforcement lateral support system were analyzed using a two-dimensional plane strain finite element technique specially developed for reinforced soil and soil-structure interaction problems. Incremental construction and nonlinear soil characterization were included. The calculated ground movements were represented in terms of angular and lateral distortions. These were selected as indications of potential building damage adjacent to an open excavation. The maximum angular distortion at the ground surface occurs at the edge of excavation, and its value decreases rapidly with respect to the distance from the open cut. The maximum lateral distortion of the ground surface, however, may occur at some distance away from the edge; this distance depends on the soil type, the characteristics of reinforcement and the depth of excavation. Typical design charts of angular distortion and lateral distortion were developed from the finite element analysis results. Similar plots can be established for different types of soils, for different size and length of reinforcement, and at various distances from the edge of excavation.

It is believed that the system described above is a unique and attractive one, and, in many instances, offers a better choice over the conventional temporary earth support systems currently being used. The working stress analysis, coupled with the limit analysis calculation (2), provide not only an adequate design of the system but information concerning ground movements critical to building damage adjacent to open cuts.

Acknowledgments

The authors would like to acknowledge the National Science Foundation for its support of this research under Grant No. APR77-03944.

Appendix.—References

1. Bang, S., "Analysis and Design of Lateral Earth Support System," thesis presented to the University of California, at Davis, Calif., in 1979, in partial fulfillment of the requirements for the degree of Doctor of Philosophy.
2. Bang, S., Shen, C. K., and Romstad, K. M., "Analysis of an Earth-Reinforcing System for Deep Excavation," *Transportation Research Record*, No. 749, 1980.
3. Burland, J. B., Broms, B. B., and DeMello, V. F. B., "Behavior of Foundations and Structures," Proceedings 9th International Conference for Soil Mechanics and Foundation Engineering, Vol. 2, Tokyo, Japan, 1977.
4. Duncan, J. M., and Chang, C. K., "Nonlinear Analysis of Stress and Strain in Soils,"

Journal of the Soil Mechanics and Foundations Division, ASCE, Vol. 96, No. SM5, Proc. Paper 7513, Sept., 1970, pp. 1629–1653.
5. Herrmann, L. R., *User's Manual for Reinforced Earth Analysis*, Univ. of California, Davis, Calif., Jan., 1978.
6. Herrmann, L. R., *Mechanics and Analysis of Reinforced Earth*, Dept. of Civil Engineering Report, Univ. of California, Davis, Calif., Sept., 1978.
7. Herrmann, L. R., and Alyassin, Z., "Numerical Analysis of Reinforced Soil Systems," *Proceedings of the Symposium on Earth Reinforcement*, ASCE, Apr., 1978, p. 428.
8. O'Rourke, T. K., Cording, E. J., and Boscardin, M., "The Ground Movements Related to Braced Excavation and Their Influence on Adjacent Buildings," Report No. DOT-TST-76T-23, Aug., 1976.
9. Peck, R. B., "Deep Excavations and Tunneling in Soft Ground," Proceedings 7th International Conference for Soil Mechanics and Foundation Engineering, Mexico, 1969.
10. Shen, C. K., Bang, S., Herrmann, L. R., and Romstad, K. M., "A Reinforced Lateral Earth Support System," *Proceedings of the Symposium on Earth Reinforcement*, ASCE, Apr., 1978, p. 764.
11. Wong, K. S., and Duncan, J. M., "Hyperbolic Stress-Strain Parameters for Nonlinear Finite Element Analyses of Stresses and Movements in Soil Masses," Report No. TE-74-3, University of California, Berkeley, Calif., 1974.

FIELD MEASUREMENTS OF AN EARTH SUPPORT SYSTEM

By C. K. Shen,[1] M. ASCE, S. Bang,[2] A. M. ASCE, K. M. Romstad,[3] M. ASCE, L. Kulchin,[4] M. ASCE, and J. S. DeNatale[5]

INTRODUCTION

The lateral earth support system using the in situ earth reinforcement technique has been described in an accompanying paper (8). For this system to be recognized and accepted by the geotechnical and construction profession, it is necessary that documented field performance records are made available. This paper presents the field measurement records of two sites—the Portland study and the Davis study—and their comparison with results obtained from the finite element method of analysis.

The first application of this system in the United States was on the foundation excavation site for the expansion of the Good Samaritan Hospital and Medical Center in Portland, Oregon, in the summer of 1976. Since the system was relatively new and unfamiliar to the local engineers and contractors, a limited amount of field instrumentation was installed to monitor its performance and safety. This instrumentation was not meant, however, to provide a complete set of data for field evaluation and analysis. The Davis study was carried out in the summer of 1979. This was a field investigation with extensive instrumentation and data collection. The field work was a part of a comprehensive study of the in situ earth reinforcement lateral support system funded by the National Science Foundation. Descriptions and comparisons of the field measurements together with analyses of the two sites are reported herein.

[1]Prof., Dept. of Civ. Engrg., Univ. of California, Davis, Calif. 95616.
[2]Asst. Prof., Dept. of Civ. Engrg., Notre Dame Univ., Notre Dame, Ind.
[3]Prof., Dept. of Civ. Engrg., Univ. of California, Davis, Calif. 95616.
[4]Pres., Kulchin and Associates Inc.
[5]Research Asst., Dept. of Civ. Engrg., Univ. of California, Davis, Calif. 95616.

Note.—Discussion open until May 1, 1982. Separate discussions should be submitted for the individual papers in this symposium. To extend the closing date one month, a written request must be filed with the Manager of Technical and Professional Publications, ASCE. Manuscript was submitted for review for possible publication on March 12, 1981. This paper is part of the Journal of the Geotechnical Engineering Division, Proceedings of the American Society of Civil Engineers, ©ASCE, Vol. 107, No. GT12, December, 1981. ISSN 0093-6405/81/0012-1625/$01.00.

PORTLAND STUDY

General.—The construction site was located immediately west of the existing hospital as shown on the plot plan in Fig. 1. The general street level elevation around the site was about 110 ft (33.6 m). A basement with a finished floor grade established at elevation 70 ft (21.4 m), extended under the entire new addition. The earth reinforcement lateral support system was installed along the north (Marshall Street), the west (NW 23rd Avenue), and the south (NW Lovejoy Street) boundaries to depths varying from 35–45 ft (10.7–13.7 m). A total of 683 reinforcing members were installed and a lateral surface area of about 23,000 sq ft (2,140 m^2) was covered by a 4-in. (100-mm) thick wire-mesh

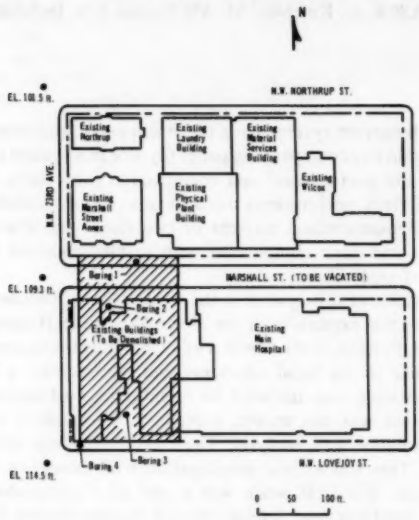

FIG. 1.—Foundation Excavation Good Samaritan Hospital, Portland, Oregon (1 ft = 0.305 m)

reinforced shotcrete facing. The westerly boundary along NW 23rd Avenue was the longest, approx 250 ft (76.3 m), with depths of excavation ranging from 42 ft (12.8 m) at the southern end to approx 35 ft (10.7 m) near the north. The deepest cut (45 ft) was along Marshall Street, where the boundary of excavation was parallel to and about 5 ft away from a four-story brick building (the Marshall Street Annex). Fig. 2 shows a general view of the excavation site near its completion; the brick building and its proximity to the edge of excavation is shown in Fig. 3.

Subsurface Conditions.—Based on the record of a nearby well log, it was indicated that the general area of the site was underlain by a 70–90 ft (21.4–27.5 m) thick formation of silty, sandy lacustrine soil. Below this was a layer of

gravel, cobble, and boulder formation approx 90 ft (27.5 m) thick. The basaltic bedrock was found at elevations between −55–−60 ft (−16.8–−18.3 m). A subsurface soil investigation (4) for this site was carried out by drilling four

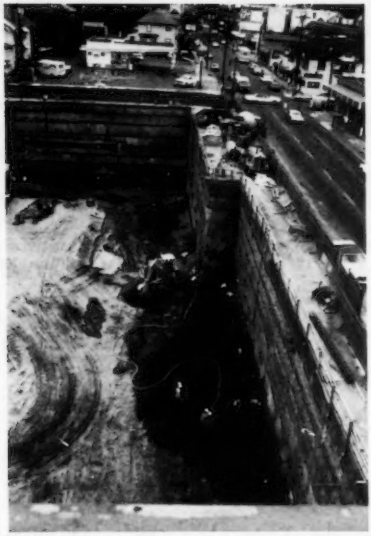

FIG. 2.—General View of Portland Site

FIG. 3.—Marshall Street Annex

boreholes to depths of about 95 ft (29 m). A typical borehole log is shown in Fig. 4: the top 10 ft (3 m) was a brownish fine sandy silt which was followed by a silty fine sand with randomly interbedded layers of fine sand and silt

to a depth of about 30 ft (10 m). Below that depth was a layer of predominantly fine sands with occasional thin layers of silt. The transition zone between the lacustrine soil formation and the underlying gravel formation was observed at

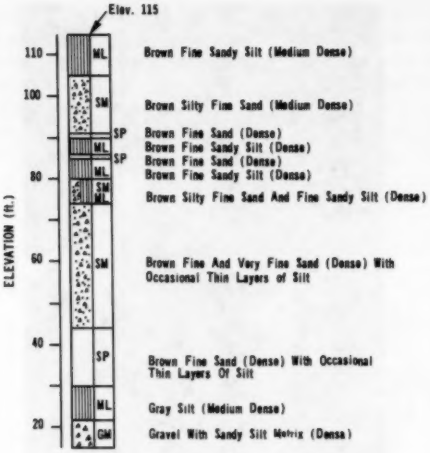

FIG. 4.—Typical Boring Log—Portland Site (1 ft = 0.305 m)

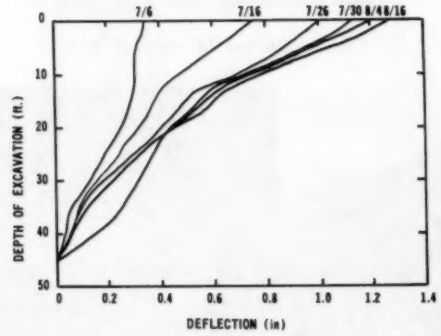

FIG. 5.—Horizontal Deflection Profiles From Inclinometer Readings (1 ft = 0.305 m; 1 in. = 25.4 mm)

elevation 22 ft (6.7 m). No ground water table was encountered within the depth explored.

Field Instrumentation and Measurements.—This being the first job using the in situ earth reinforcement lateral support system for deep excavation in the United States, a limited field instrumentation program was initiated to monitor

and safeguard the stability of the excavation during construction. Among the measurements obtained, two sets of information were selected for comparison with analytical results: the lateral ground movement profiles from a borehole inclinometer readings and the surface tension cracks on the ground floor slab of the Marshall Street Annex.

The casing-lined borehole for inclinometer readings was 45 ft (13.7 m) deep located 10 ft (3 m) from and approximately halfway along the length of the westerly boundary. The depth of excavation at that location was about 37 ft (11.3 m). A continuous record of the ground movements was taken during and right after the completion of excavation as in Fig. 5; however, no detailed information relating depth of excavation to movement is available. The maximum lateral movement at the ground surface was 1.3 in. (33 mm), which was only about 0.3% of the maximum depth of excavation.

The Marshall Street Annex, a four-story brick building, being so close to the excavation, experienced severe tensile cracks on the ground floor concrete slab. This building had an additional half-story basement below the street level.

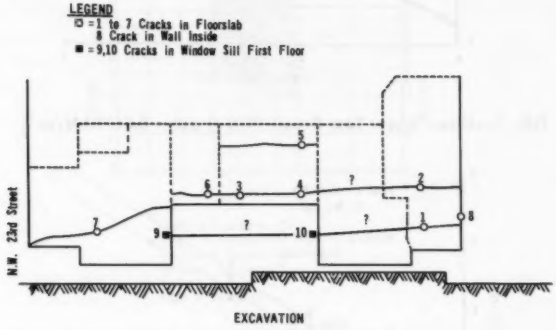

FIG. 6.—Crack Survey—Marshall Street Annex

The "surcharge loading" on top of the northerly lateral support system was, therefore, quite substantial. This was the most critical area of the excavation, insofar as safety was concerned. The depth of excavation along the northerly boundary was approx 37 ft (11.3 m); however, a large footing to be placed below the general floor level required the deepening of the excavation along the vicinity of a portion of that boundary to a total depth of 45 ft (13.7 m) from the street level. Since the half basement and the concrete floor slab extended about 9 ft (2.75 m) below the ground surface, the actual depth of excavation at the deepest area was about 37 ft (11.3 m). During the period of excavation, tensile cracks were noticed to develop. The first set of major cracks developed parallel to, and at a distance of approx 9 ft (2.75 m) from the edge of excavation. Subsequently, the second and third sets of major cracks were noticed at distances of approx 17 and 25 ft (5.2 and 7.6 m) from the edge of excavation, respectively. The widths of those crack openings at the completion of excavation were measured 10/32, 8/32, and 2/32 in. (8.0, 6.4, and 1.6 mm), respectively. A schematic

plot indicating the cracking pattern is shown in Fig. 6.

Finite Element Analysis and Comparison.—The two records described above were analyzed using the finite element method discussed in the accompanying paper (8). Since the depth of excavation was in general no deeper than 40 ft (12.2 m), [except the 45-ft (13.7-m) depth near the Marshall Street Annex], it was deemed appropriate that the soil strata to be considered in the analyses

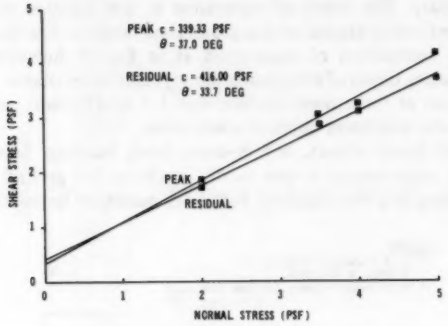

FIG. 7.—Direct Shear Test Result (ML) (1 psf = 0.0479 kN/m^2)

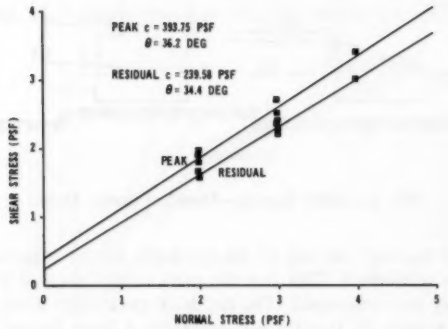

FIG. 8.—Direct Shear Test Result (SM) (1 psf = 0.0479 kN/m^2)

be confined to the top formation consisting primarily an approx 80-ft (24.4-m) thick layer of fine silts and silty sands as in Fig. 4.

To obtain the strength characteristics of the soils on the site, direct shear tests were performed on undisturbed samples under normal pressures equal to the magnitudes of the existing overburden. The strength test results of typical silty and sandy soils were plotted as in Figs. 7 and 8, respectively, for both the peak and residual values. The values of cohesion and friction angle shown in the figures were obtained from a linear regression analysis. It can be noted

TABLE 1.—Properties of Soils

Soil Type (1)	SM (2)	ML (3)	SM (4)
elevation	86 ft	91 ft	—
cohesion	peak 393.8 psf	339.3 psf	380 psf
—	residual 239.6 psf	416.0 psf	—
friction angle	peak 36.2°	37°	31°
—	residual 34.4°	33.7°	—
D_{10}	0.06 mm	0.06 mm	0.013 mm
D_{60}	0.08 mm	0.1 mm	0.07 mm
γ_t	103 pcf	101.5 pcf	104 pcf

Note: 1 psf = 6.9 kN/m^2; 1 pcf = 157 N/m^3.

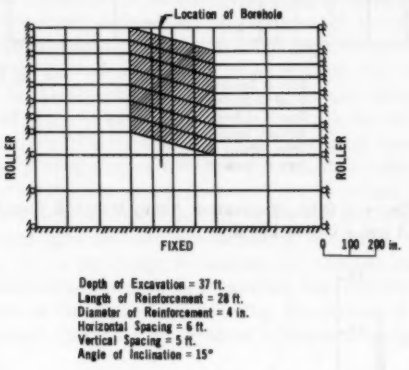

FIG. 9.—Finite Element Grid—Excavation Along 23rd Avenue (1 ft = 0.305 m; 1 in. = 25.4 mm)

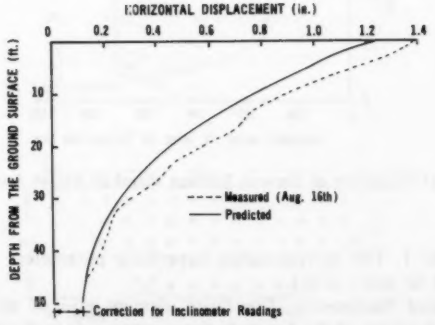

FIG. 10.—Comparison of Horizontal Movement—23rd Avenue (1 ft = 0.305 m; 1 in. = 25.4 mm)

that the two soil groups have similar strength parameters, and, because of the lack of available triaxial test data to determine the hyperbolic parameters, a single representative soil was chosen from Ref. 10 to reflect the average physical properties and the hyperbolic parameters of the entire soil formation at the

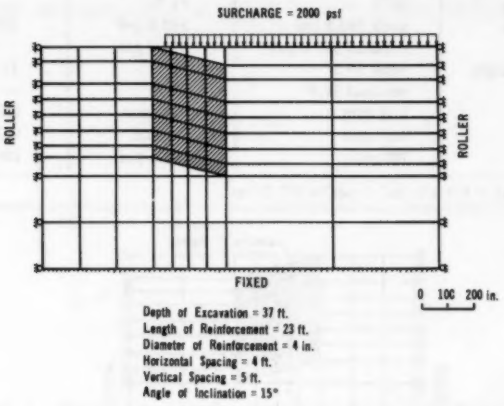

FIG. 11.—Finite Element Grid—Excavation Along Marshall Street (1 ft = 0.305 m; 1 in. = 25.4 mm; 1 psf = 0.0479 kN/m^2)

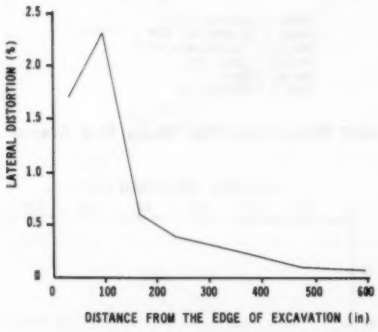

FIG. 12.—Lateral Distortion of Ground Surface Marshall Street Annex (1 in. = 25.4 mm)

site as in Table 1. The corresponding hyperbolic parameters are $k = 270$; $n = 0.38$; $R_f = 0.82$; and $\nu = 0.3$.

Lateral Ground Movement.—The finite element grid of the cross section containing the location of the borehole for measuring lateral ground movement is shown in Fig. 9; other pertinent information necessary to complete the computer input are also listed. A comparison of the predicted and measured horizontal

movements along the length of the borehole is in Fig. 10. The predicted values were interpolated from movements of the adjacent nodes. Because the inclinometer measures the ground movement relative to the bottom of the borehole, the actual ground movement can only be obtained if the reference point is immobile. The actual lateral ground movement could, therefore, be larger than those in Fig. 5 since the bottom of the hole was only about 10 ft (3 m) deeper than the depth of excavation. At that level, ground movement as a result of nearby open excavation was likely to take place. In Fig. 10, a correction has been made by shifting the measured curve to the right so that the reading at the bottom of the hole matches the movement predicted by the finite element analysis at that depth. As can be seen, both the shape and the magnitude of the predicted soil movement profiles agree with the measured values. In all cases, the maximum movement is less than 0.32% of the depth of excavation.

Tensile Cracks.—The distribution and magnitude of lateral distortion of the ground surface was chosen as the basis for predicting the development of tensile cracks. Lateral distortion, defined as the differential horizontal movement between two reference points divided by the length separating them, is a measure of tensile strain of the ground surface near an excavation. Due to the limitations of the employed soil characterization in describing the near-failure soil behavior, and the absence of realistic knowledge in dealing with the frictional behavior at the soil-slab interface, it is beyond the present analytical capability to predict the generation and propagation of tensile cracks in slabs adjacent to an open excavation. Consequently, the interpretation of the analytical results and their comparison with the field behavior can only be viewed in a qualitative manner.

The finite element grid and other information related to the analysis are presented in Fig. 11. A surcharge simulating the existing building load was applied to the ground surface prior to the excavation. Fig. 12 shows the distribution of lateral distortion of the ground surface after completion of the excavation. The maximum lateral distortion occurred at a distance of approx 9 ft (2.75

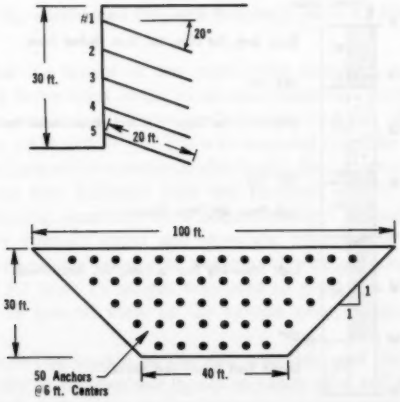

FIG. 13.—Orientation of Reinforcing Members (1 ft = 0.305 m)

m) from the edge of excavation; this agrees well with the location of the first set of major tensile cracks recorded. The computer solution, however, is not capable of predicting the locations of all the tensile cracks, simultaneously.

The foundation excavation and the construction of the expansion facility of the hospital were successfully completed. The movements of the ground were relatively small. While tensile cracks did develop in the Marshall Street Annex, the building was fully occupied and functional throughout the construction period. According to the master plan, the brick building was to be demolished, making room for a parking facility. Though the field measurement records and the soil data were relatively incomplete, the study has shown that the analytical methodology employed can adequately capture the field behavior of the lateral earth support system.

FIG. 14.—General View of Davis Excavation Site

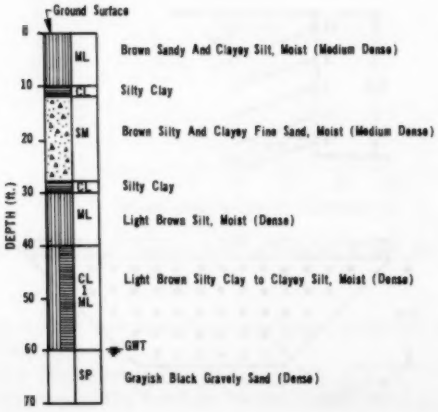

FIG. 15.—Typical Boring Log—Davis Site (1 ft = 0.305 m)

DAVIS STUDY

General.—This was a field prototype study conducted as a part of the comprehensive investigation of the in situ earth reinforcement lateral support system. During the last three years, an analytical procedure for evaluating the stability of the system was formulated (3) and later verified by means of centrifuge model studies (7). In addition, a method for predicting the field behavior at the working stress level was also completed as reported in the accompanying paper (8) and in Ref. 2. Due to the lack of available field measurements of prototype behavior, it was concluded that an instrumented field study would be beneficial to further substantiate the capability of the analytical solutions for the prediction of field system behavior. The construction and instrumentation of this sytem were carried out in the summer of 1979. The study site was located at the northwest corner of the sanitary landfill facility on the Davis campus of the University of California. The 30-ft (9.2-m) deep excavation was constructed in five lifts with each lift approx 6 ft (1.83 m) thick. The geometry

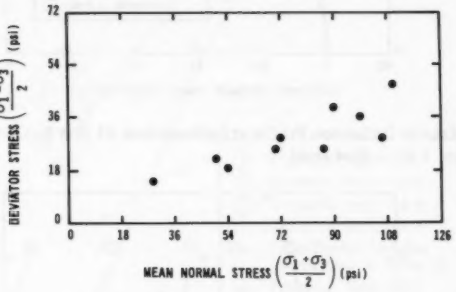

FIG. 16.—Undrained Strength Results (1 psi = 6.9 kN/m^2)

of the system and the layout of the reinforcing members are shown in Fig. 13. The remaining three sides of the excavation were left untreated with slopes of about 45°. The vertical cut had a surface area of 2,100 sq ft (195 m^2) and a total of 5,500 cu yd (4,215 m^3) of soil was removed from the open excavation. As this was a small job with limited available funds, the construction methodology applied to this site was different from the Portland site (9). The drilling and grouting of reinforcing members were done manually. Instead of using special fast setting, early strength grout and shotcrete mixtures, a concrete mixture of water-cement-aggregate (sand and pea gravel with a maximum size of 3/8 in.) having a 1:2.5:8 ratio by weight was used to grout the holes and gunnnite the vertical cut. A general view of the system near completion is shown in Fig. 14.

Site Conditions.—The terrain at the site was flat, and the soil deposit was composed primarily of interbedded layers of sandy silts and silty clays. Boring logs were recorded at the time the inclinometer casings were installed. A total of four boreholes were drilled along the center line perpendicular to the vertical

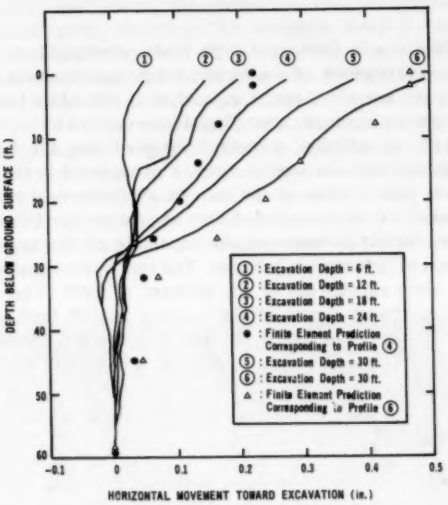

FIG. 17.—Horizontal Deflection Profile at Inclinometer #1 (5 ft Behind the Excavation) (1 ft = 0.305 m; 1 in. = 25.4 mm)

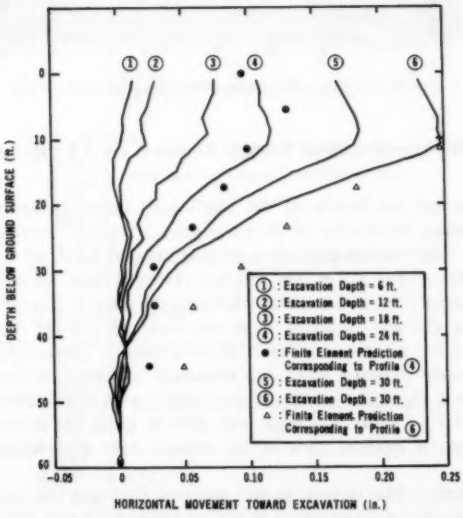

FIG. 18.—Horizontal Deflection Profile at Inclinometer #2 (15 ft Behind the Excavation) (1 ft = 0.305 m; 1 in. = 25.4 mm)

cut. These holes were spaced at distances of 5, 15, 30, and 45 ft (1.5, 4.6, 9.2, and 13.7 m) from the edge of excavation. The two holes closest to the excavation were each 60 ft (18.3 m) deep, while the remaining two holes were each 45 ft (13.7) deep. Undisturbed cylindrical samples were taken at appropriate depths using a pitcher sample tube. A typical soil profile extending to a depth of 60 ft (18.3 m) is shown in Fig. 15. A gravelly sand layer and the ground-water table were encountered at this depth. Later during the excavation, it was

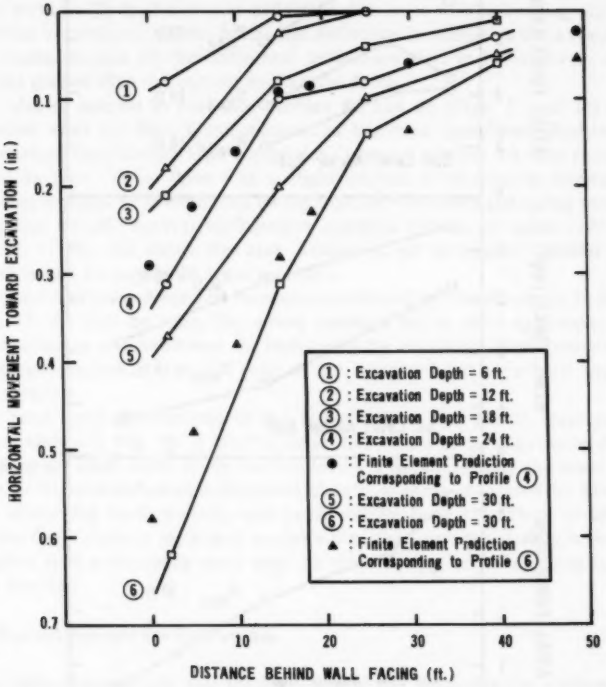

FIG. 19.—Horizontal Movement of Ground Surface at Excavation Centerline (By Field Transit Survey) (1 ft = 0.305 m; 1 in. = 25.4 mm)

discovered that the soil deposit at the site was extremely variable in both the vertical and horizontal directions, typical of the Putah Creek deposits of this region.

Undrained triaxial compression tests were performed in order to determine the shear strengths of the various soil types encountered. The undrained strength associated with these test results are plotted in Fig. 16. Further discussion of the test results will be given later.

Field Instrumentation and Measurements.—Extensive instrumentation was

installed at the site so that the field performance of the system could be monitored and evaluated. Four boreholes with special casings for inclinometer readings were installed along the center line of the excavation in order to obtain a set of horizontal displacement profiles. A network of surface movement markers

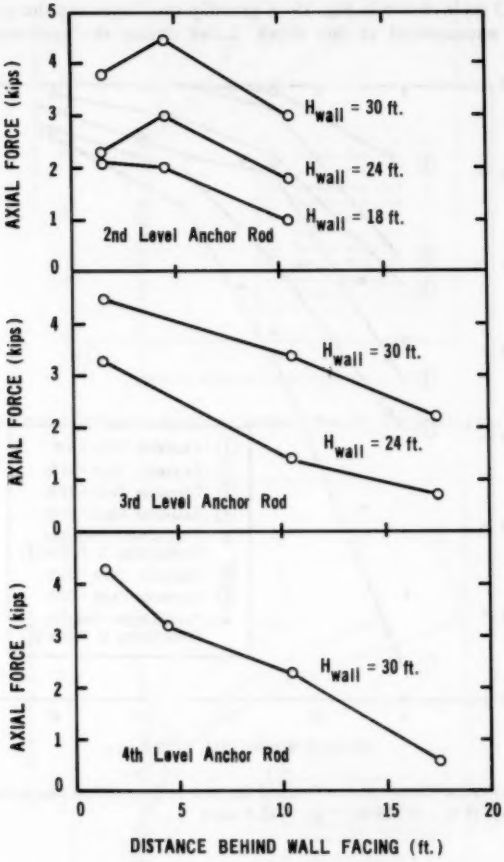

FIG. 20.—Measured Axial Force Distribution in Second-, Third-, and Fourth-Level Anchor Rods (1 ft = 0.305 m; 1 kip = 4.45 kN)

was installed prior to the start of excavation so that the horizontal and vertical displacements of the ground surface could be monitored by transit survey. Finally, the centermost column of reinforcing members were mounted with resistance-type strain gages. Four sets of gages were spot welded to each anchor rod (#8

re-bar) so that the magnitude and the distribution of the axial force in each member could be measured. A complete set of borehole inclinometer and survey readings were taken before and after each lift of excavation. Strain gage readings were made after each anchor rod had been grouted into place, and after the completion of each subsequent lift.

The horizontal deflection profiles yielded by inclinometers #1 and #2 are shown in Figs. 17 and 18, respectively. It may be observed from these records that: (1) The horizontal deflection decreases with increasing depth from the ground surface; (2) the horizontal deflection decreases with increasing distance behind the vertical cut; (3) the horizontal deflection increases as the excavation depth increases; and (4) the horizontal deflections tend to be relatively small at depths greater than the current excavation depth.

It is also of interest to note that profiles #5 and #6 (Figs. 17 and 18) were both taken after the final lift of excavation had been completed. Profiles #5 were obtained immediately after completion, whereas profiles #6 were recorded two weeks later. Thus, there was a slight amount of short-term movement. Additional readings were continued throughout the wet winter and spring months. During this period, several earthquakes centered approx 75 miles (120 km) southeast of the site shook the area. However, no movements greater than those reflected by profile #6 were recorded.

The record of ground surface movements obtained by transit survey is shown in Fig. 19. As may be seen, the survey readings are in close agreement with the inclinometer measurements. In both cases the maximum displacements are quite small—approx 0.8 in. (20 mm) at the center of the uppermost edge of the excavation.

The axial force distributions in the second, third, and fourth level anchor rods are shown in Fig. 20. It may be noted that, for a given excavation depth, the maximum axial force at the various levels is approximately the same. The shapes of force distribution correspond closely to those measured by Mitchell (5) in reinforced earth models, and predicted by Bang (1), Shen, et al. (6), using the finite element method of analysis, i.e., the force distribution is roughly triangular, with a maximum at or near the panel facing, and decreasing to zero at the free end.

Finite Element Analysis and Comparisons

The finite element grid and the locations of the boreholes for inclinometer readings are shown in Fig. 21. Also listed are the dimensions and spacings of the reinforcement. As stated previously, the soil condition at the site was extremely variable, and it would be impossible and impractical to delineate its variations with depth in accordance with the boring log information. Furthermore, there were not enough undisturbed samples to determine the hyperbolic parameters for each sublayer of the soil deposit encountered. An average set of soil parameter was, therefore, used for analytical purposes. In choosing the parameters, considerations were given to the possible sample disturbance and strength loss due to sampling, handling, and testing. Consequently, more weight was placed on samples which exhibit stiffer soil properties. The hyperbolic soil parameters were determined to be $k = 548$; $n = 0.05$; $R_f = 0.79$; and $\nu = 0.3$.

The predicted horizontal deflection profiles of inclinometers #1 and #2 (5 and 15 ft behind the vertical cut, respectively) are shown as dots in Figs. 17

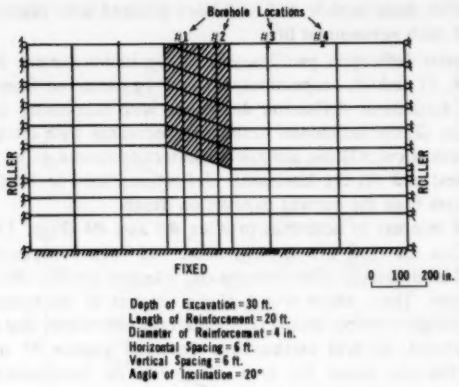

FIG. 21.—Finite Element Grid—Excavation Davis Site (1 ft = 0.305 m; 1 in. = 25.4 mm)

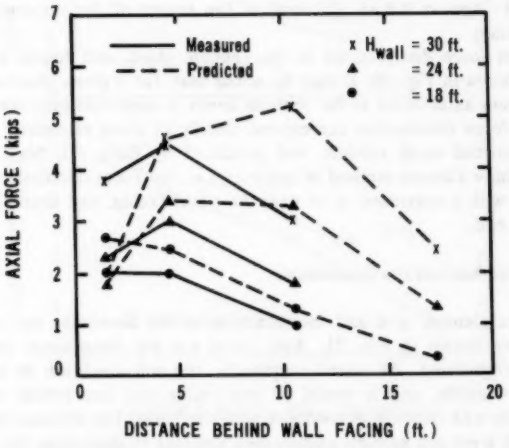

FIG. 22.—Axial Force Comparison—Second Level Anchor Rod (1 ft = 0.305 m; 1 kip = 4.45 kN)

and 18, respectively. For each of these locations, the predicted profiles corresponding to excavation depths of both 24 and 30 ft (7.3 and 9.2 m) are presented. In all instances, the agreement between the measured and the predicted movements

is good. As may be seen, for depths of less than about 20 ft (6 m) the agreement is remarkably close. However, for greater depths the finite element predictions tend to exceed the actual measured ground movements. One possible explanation is that the actual soil may have been stiffer than indicated by the strength tests and modeled by the selected parameters.

As may be observed in Fig. 19, the predicted surface movements are likewise in excellent agreement with the results of the field transit surveys. The predicted axial forces in the second level anchor rod are shown in Fig. 22. In general, the predicted values are about twice as large as the measured; however, the shapes of force distribution are similar. The sources of discrepancy between the measured and the predicted axial forces in the reinforcing members cannot be positively identified. Three possible sources, however, can be listed as follows:

1. The strain gages might have been damaged during the installation of the re-bars and grouting of the holes.
2. Strain gage measurements might be in error caused by the drifting of reference readings under extremely hot weather conditions.
3. The bond behavior between the reinforcing members and the surrounding soil might not be fully captured by a simplified soil profile assumed in the analysis.

Summary and Conclusion

This paper presents two field performance records of a lateral earth support system. This system uses the in situ earth reinforcement technique to strengthen the native soil, and is different from the conventional systems that serve to retain soils behind a vertical cut. The field results were compared with predictions obtained from a finite element method of analysis. In general, the predictions agree with the field measurement demonstrating that the analytical procedures developed can correctly predict the field behavior. Furthermore, it has shown that ground movements adjacent to an open excavation can be predicted and controlled if a properly designed in situ earth reinforcement lateral support system is installed. The system is also economical in saving time (30% less time than the conventional soldier piling and bracing system for the Portland job) and money (the cost is approx \$10/sq ft in the summer of 1979 for the Davis job, and 15% below the low bid for a conventional system for the Portland job). Although the system is intended to serve as a temporary support only, the fact that no additional movements at the Davis site were recorded during a 12-month period following the completion of construction—a period which included a wet winter and spring, and several earthquakes—indicates that the system also has a great deal of long-term stability. Thus, the in situ earth reinforcement lateral support system has shown to offer a viable alternative for providing temporary support in deep excavations.

Acknowledgments

The research presented in this paper was partially sponsored by the National Science Foundation, under grant number NSF-APR77-03944. The authors are extremely grateful for this support. The authors would also like to express

their appreciation to Albert Lueng, Ken Robbin, Ted Mason, and Del Dees for providing field information about the Portland project; to Dennis Long for his assistance during the installation of the inclinometer casings; to James F. Mitchell for the construction of the Davis project; to Siamak Jafroudi, Ken Lo, and Norm Fries for their help on the Davis project.

Appendix.—References

1. Bang, S., "Analysis of A Lateral Earth Support System," thesis presented to the University of California, at Davis, Calif., in 1978, in partial fulfillment of the requirements for the degree of Master of Science.
2. Bang, S., "Analysis and Design of Lateral Earth Support System," thesis presented to the University of California, at Davis, Calif., in 1979, in partial fulfillment of the requirements for the degree of Doctor of Philosophy.
3. Bang, S., Shen, C. K., and Romstad, K. M., "Analysis of An Earth Reinforcing System for Deep Excavation," *Transportation Research Record 749*, 1980.
4. Dames and Moore, "Foundation Investigation—Proposed Phase I New Construction, Good Samaritan Hospital," Portland, Oregon, 1974.
5. Mitchell, J. F., "Investigation of Friction in Reinforced Earth," thesis presented to the University of California, at Davis, Calif., in 1978, in partial fulfillment of the requirements for the degree of Master of Science.
6. Shen, C. K., Bang, S., Herrmann, L. R., and Romstad, K. M., "A Reinforced Lateral Earth Support System," *Proceedings of Symposium on Earth Reinforcement*, ASCE, 1978.
7. Shen, C. K., Kim, Y. S., Bang, S., and Mitchell, J. F., "Centrifuge Modeling of A Lateral Earth Support," *Proceedings of Symposium on Centrifuge Modeling of Geotechnical Problems*, ASCE, Oct. 1979.
8. Shen, C. K., Bang, S., and Herrmann, L. R., "Ground Movement Analysis of An Earth Support System," *Journal of the Geotechnical Engineering Division*, ASCE, Vol. 107, No. GT12, Dec., 1981.
9. "Sprayed Concrete Wall Cuts Overall Cost by 30% on Underpinning, Shoring," *Engineering News Record*, Aug., 1976.
10. Wong, K. S., and Duncan, J. M., "Hyperbolic Stress—Strain Parameters for Non-linear Finite Element Analysis of Stresses and Movements in Soil Masses," *Report No. TE-74-3*, University of California, Berkeley, Calif., 1974.

CELLULAR COFFERDAM FOR TRIDENT DRYDOCK: DESIGN

By Max D. Sorota,[1] F. ASCE, and Edward B. Kinner,[2] M. ASCE

INTRODUCTION

Extensive waterfront and shore-based facilities are being constructed at the Naval Submarine Base, Bangor, Bremerton, Washington in connection with the development of a new submarine refit and crew training facility for support of the Trident class submarine. The submarine base is located on Hood Canal, in the state of Washington, at the location shown in Fig. 1. The base development includes a graving drydock which involved the deep water, offshore construction of a steel sheet pile cellular cofferdam. At extreme high water (EHW), the cofferdam retained 79 ft (24 m) of water. Interlock tensions associated with the size of cells needed to resist this water depth resulted in the use of one of the first United States cellular cofferdam applications of high strength steel sheet piling and extruded wye connections. To the writers' knowledge, it is one of the deepest cellular cofferdams which has been successfully unwatered without the use of internal earth stability berms.

The purpose of this paper is to describe the cofferdam and to summarize important design considerations, many of which are unique and represent an advancement in the state-of-the-art for cofferdam design and construction. Included are descriptions of the cofferdam geometry, site constraints which influenced the design, foundation soil conditions, cell fill dewatering used to limit interlock tensions, seismic design, cell fill densification, and artesian pressure relief systems. Additional information concerning cofferdam construction and performance are provided in Ref. 5.

DESIGN CONSTRAINTS AND DRYDOCK CONCEPTS

The facility was located offshore in order to permit the continued shallow water migration of salmon fingerlings. The drydock centerline is located in the Hood Canal, approximately 550 ft (168 m) offshore from the mean higher high

[1]Sr. Vice Pres., Fay, Spofford & Thorndike, Inc., Boston, Mass.
[2]Sr. Vice Pres., Haley & Aldrich, Inc., Cambridge, Mass.

Note.—Discussion open until May 1, 1982. Separate discussions should be submitted for the individual papers in this symposium. To extend the closing date one month, a written request must be filed with the Manager of Technical and Professional Publications, ASCE. Manuscript was submitted for review for possible publication on October 31, 1980. This paper is part of the Journal of the Geotechnical Engineering Division, Proceedings of the American Society of Civil Engineers, ©ASCE, Vol. 107, No. GT12, December, 1981. ISSN 0093-6405/81/0012-1643/$01.00.

water (MHHW) shoreline, as shown in Fig. 2. The drydock and two immediately adjacent, pile supported piers form the three-sided Trident Refit Delta.

Refit Pier No. 1 and the South Trestle were constructed first, and the cofferdam was then constructed concurrently with Refit Pier No. 2. The drydock was constructed immediately following completion of the cofferdam. This scheduling accelerated the construction but imposed severe constraints on the cofferdam design by limiting the area available for positioning the structure relative to the drydock and piers. In addition, the offshore location resulted in very deep cofferdam water depths.

The following is a brief description of the drydock design and construction which provided the basis for the cofferdam geometry and design requirements: The drydock basin is 90 ft (27.4 m) wide by 690 ft (210.3 m) long. Permanent

FIG. 1.—Vicinity Map

laydown areas of a 73 ft (22.3 m) minimum width are required to provide for work areas, roadways, and service buildings. The laydown areas are at El. 20 ft (6.1 m) to provide adequate freeboard above extreme high water (EHW) at El. 14.6 ft (4.5 m). Project datum is El. 0 at mean lower low water (MLLW). The top of the drydock floor is at El. −43 ft (−13.1 m) which is 49.4 ft (15.1 m) below mean tide level (MTL).

Extensive drydock concept studies were performed to evaluate alternate design and construction methods. Drydock designs considered included a fully relieved type, in which granular fill and drains would be used to intercept the seepage flow to relieve hydrostatic pressures on the walls and floor; relieved floor and non-relieved wall type; and a gravity type, in which the walls and floor would be sized to resist the full hydrostatic pressure. Designs considered for the laydown areas included pile-supported slabs, a ballasted precast concrete cofferdam, and

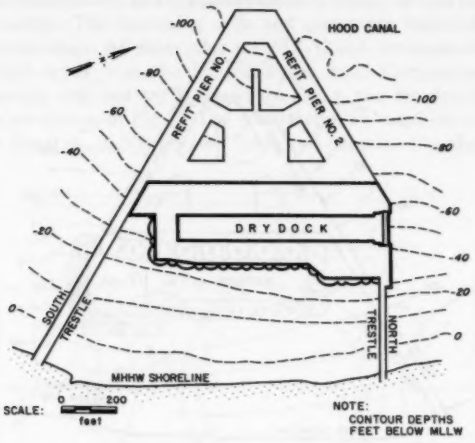

FIG. 2.—Site Plan (1 ft = 0.305 m)

an earth-filled steel sheet pile cellular cofferdam. Drydock construction methods considered ranged from tremie underwater floor and wall construction, to tremie placement of the floor, with subsequent in-the-dry wall construction in an unwatered cofferdam, to both floor and wall construction in-the-dry in an unwatered cofferdam.

Cofferdam Selection and Geometry

The decision was made to construct a full gravity drydock, and to have all construction performed in-the-dry in an earth-filled steel sheet pile cellular cofferdam. It was further established that the cofferdam would be permanent, except at the drydock entrance, to provide major portions of the required drydock laydown areas. The gravity design of the drydock required a floor thickness of from 16 ft (4.9 m) to 19 ft (5.8 m), depending on location. This thickness, when combined with an 18 in. (460 mm) gravel subbase and 6 in. (150 mm) concrete working mat below the floor, resulted in a final excavation subgrade of El. −61 ft (−18.6 m) to El. −64 ft (−19.5 m) and maximum water depth of 78.6 ft (24.0 m) below EHW.

When unwatered during construction, the cellular cofferdam had to retain almost 80 ft (24.4 m) of water. Additionally, it is a part of the permanent laydown area for the completed drydock. A plan of the cofferdam is shown in Fig. 3, and a typical section through the structure and future drydock is shown in Fig. 4. Fig. 5 is a photograph of the cofferdam after its pump down.

The cofferdam basin is approximately 774 ft (236 m) long and has a minimum width of 130 ft (40 m). The cofferdam consists of 24 circular cells, each 75.83 ft (23.11 m) in diameter, and 24 connecting arcs, hereafter termed arcs. The cells are spaced from 83.55 ft (25.47 m) to 93.57 ft (28.52 m) on center, to

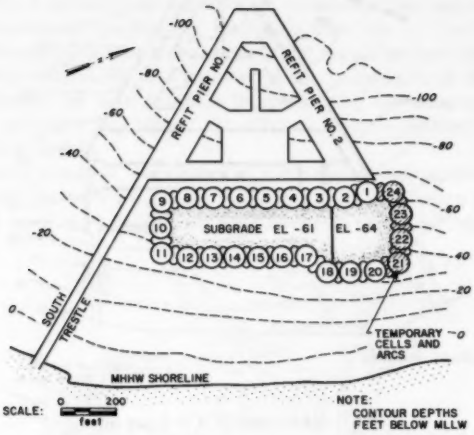

FIG. 3.—Cofferdam Plan (1 ft = 0.305 m)

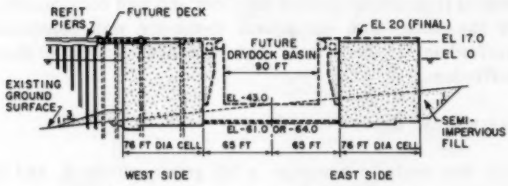

FIG. 4.—Typical Section (1 ft = 0.305 m)

FIG. 5.—Cofferdam After Pump Down

obtain the required geometry and to achieve closure. Cells 1–20 and the in-between arcs are permanent. The remaining cells and arcs were removed at the end of drydock construction. All sheet piles are PSX-32 and the connecting elements are 40° extruded wyes from the United States Steel Corporation. The plan of a representative cell and arc is shown in Fig. 6 and the details at the 40° extruded wye are shown in Fig. 7. The manufacturer's rated interlock strength is 28 kips per lineal in. (4,900 kN/m). Each cell contains 172 sheets and four

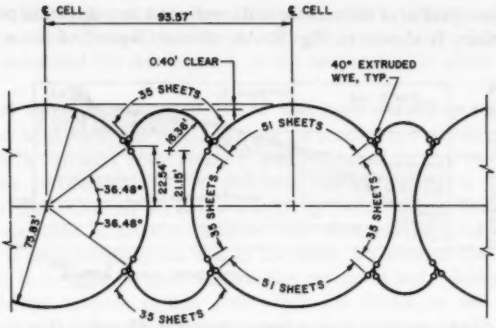

FIG. 6.—Representative Cell and Arc (1 ft = 0.305 m)

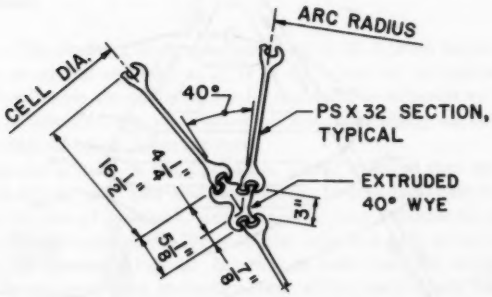

FIG. 7.—40 Degree Extruded Wye (1 in. = 25.4 mm)

wye sections. The arcs each contain from 29 to 35 sheets, depending on the cell location and spacing. The sheet lengths vary from a minimum of 83 ft (25.3 m) at Cell 11 to a maximum of 103 ft (31.4 m) at Cell 1. A maximum of one splice was permitted per sheet, with this splice being in the upper portion of the sheet. During basin unwatering and drydock floor construction the cofferdam fill surface was at El. 17 ft (5.5 m). Thereafter, it was raised as required to achieve the in-service level of El. 20 ft (6.1 m) for the drydock laydown areas.

As shown in Fig. 4, the presence of the adjacent refit piers necessitated

construction of the west side cells immediately adjacent to the future drydock walls and floor slab, thus precluding the use of interior earth berms. Similar constraints were imposed by the South Trestle at the head end of the future drydock. Cost and environmental considerations directed construction of the east side cells immediately adjacent to the future drydock walls.

Subsurface Conditions

A generalized profile of subsurface soil conditions, in a direction perpendicular to the shoreline, is shown in Fig. 8. An alluvial deposit of loose to medium

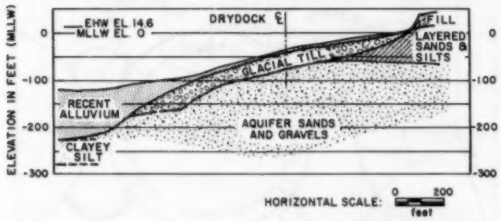

FIG. 8.—Generalized Soil Profile Perpendicular to Shoreline (1 ft = 0.305 m)

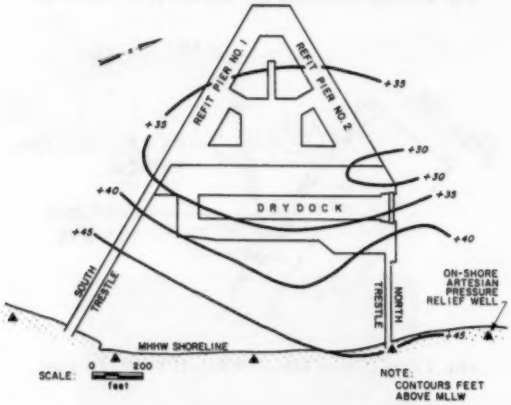

FIG. 9.—Aquifer Piezometric Conditions (1 ft = 0.305 m)

compact sands and gravels forms the uppermost soil stratum underlying the Hood Canal. At the cofferdam site, this deposit averages about 10 ft (3 m) in thickness. A glacial till stratum, consisting principally of a very compact gray, silty, coarse to fine sand to sandy silt, underlies the alluvium. The penetration resistance typically varied from 50 to over 200 blows per ft (0.3 m) using a 300 lb (136 kg) hammer falling 30 in. (762 mm), and a 2.5 in. (64 mm) inside

diameter split spoon sampler. The glacial till varies from about 20 ft (6 m) to 40 ft (12 m) in thickness. The average natural water content, liquid, and plastic limits are 9.0%, 17.5%, and 13.5%, respectively. Underlying the till is a very compact, glacially overconsolidated deposit of interbedded sands and gravels with silt layers, herein termed the aquifer sands and gravels. The penetration resistance ranged from 70 to over 400 blows per ft (0.3 m), and is influenced by the coarse gravel and cobbles present. Available data indicate that the aquifer varies from about 200 to 250 ft (61 to 76 m) in thickness. From five to fifteen percent by weight of the aquifer samples tested pass a No. 200 sieve. Specific information on soils at greater depths is not known. It has been estimated (3) that bedrock in the site area is at about El. −2,000 ft (−610 m).

An unusual site condition encountered was high artesian pressures in the aquifer sands and gravels. Shown in Fig. 9 are the piezometric elevations measured by piezometers installed both onshore and offshore. In the vicinity of the cofferdam the piezometric level ranged from El. 30 ft (9 m) to El. 40 ft (12 m), which is approximately 25 ft (7 m) to 35 ft (10 m) above mean tide level. A dramatic variation in artesian pressure was observed near the apex of the refit delta. At approximately the end of the delta, no artesian conditions were encountered. It is believed that the artesian pressures are "daylighting" into the deep alluvial deposits in this area which are shown on the left side of Fig. 8. An analysis of the effect of these artesian conditions on design is presented later.

Cofferdam Design

Dredging.—The drydock floor subgrade is up to 30 ft (9 m) below the bottom grade of the canal and as much as 25 ft (8 m) below the surface of the dense glacial till. Positioning the cofferdam cells immediately adjacent to the drydock floor subgrade required the installation of the sheet piling on the basin side of the cofferdam to below subgrade level.

Because of the density of the glacial till, it was believed that the sheet piles could not be driven into this layer more than a few feet without danger of driving the piles out of interlock. Accordingly, it was established that dredging would be performed within the limits of the cells and arcs prior to cofferdam construction, as shown in Fig. 10. In order to limit the total dredged volume, the glacial till was excavated in-the-dry from within the drydock floor subgrade area following basin unwatering. The typical relationship between the existing ground surface and the dredged/excavated depth is shown in Fig. 4.

Analysis Methods.—The cofferdam was designed in general accordance with the procedures of Design Manual DM-7 (2), except that the maximum interlock tensions caused by the cell and arc were calculated in accordance with the TVA secant formula (1). Because of the very dense glacial till and the expected minimal sheet pile penetrations, the cofferdam was assumed to act similarly to a cofferdam founded on rock. The point of maximum interlock tension was assumed to occur at one-quarter the cofferdam height (H) above the subgrade level, H/4. Comments on the reasonableness of this assumption are made in Ref. 5.

The 75.83 ft (23.11 m) cell diameter was selected to provide adequate safety

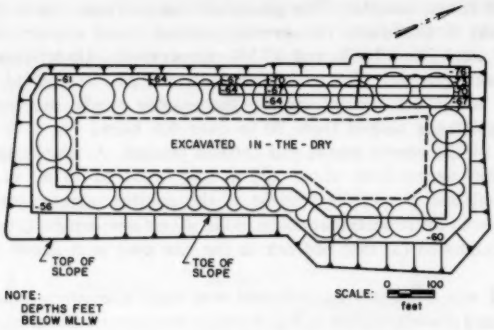

FIG. 10.—Dredging Plan (1 ft = 0.305 m)

against overturning, sliding, and shear in the fill on the cell centerline and between the cell fill and sheet piling. Cell interlock tensions obtained in accordance with DM-7 assume a sloped phreatic surface across the width of the cells resulting from weep hole drainage of the fill during and following cofferdam basin unwatering. Initial calculations indicated that this loading produced excessive interlock tensions.

A major effort was undertaken to develop a method for reducing the estimated tensions to at least the magnitude which would permit use of high-strength sheet piling having a rated strength of 28 kips/in. (4,900 kN/m). Cell diameters required for sliding and overturning, fill unit weights and lateral earth pressure coefficients, were all re-evaluated with little beneficial effect on estimated tensions. The only adjustable factor which was found to have a significant effect on calculated maximum tensions was the water level within the cells and arcs. Calculations disclosed that interlock tensions could be reduced to tolerable levels when the fill water levels were lowered to or below El. −45 ft (−13.7 m) and maintained essentially flat across the full widths of the cells and arcs. El. −45 ft (−13.7 m) is only 16 to 19 ft (4.9 to 5.8 m) above the excavation subgrade level. Thus, in order for the cofferdam to be technically feasible, it was necessary to devise a reliable procedure for obtaining and maintaining extremely low water levels within all cells and arcs. It was also determined that during most of the cofferdam basin unwatering phase, the cell and arc water levels would have to be lowered at rates such that the water levels were maintained at or below the basin level.

Fill Dewatering System.—Cell fill dewatering by pumped wells was considered to be the only method by which water levels could be lowered and maintained at the required elevations. The writers were not aware of any similar previous application of cell dewatering which could be referenced as a guide for estimating leakage rates through the interlocks into the fill. The pumps were sized assuming a leakage rate of 20 gpm (1.3 L/s) into the cells following fill dewatering. Assuming a cell fill specific yield of 0.2 and minimal interlock leakage, a pumping rate of 20 gpm (1.3 L/s) also allowed the cells to be dewatered at a rate of at least 5 ft (1.5 m) per day.

The system for dewatering the cell fill consisted of two wells within each cell (three in corner Cells 9, 11, 21, and 24) and one within each arc, the wells being 6 in. (150 mm) diameter slotted PVC pipe. The wells were located about 7 ft (2.1 m) from the sheet piling, as shown in Fig. 11. Submersible

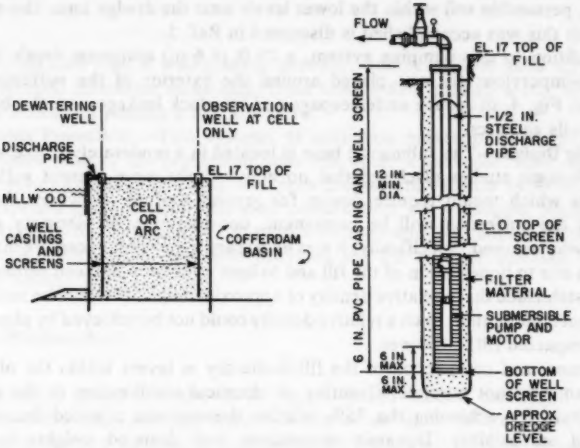

FIG. 11.—Cell Fill Dewatering and Observation Wells (1 in. = 25.4 mm)

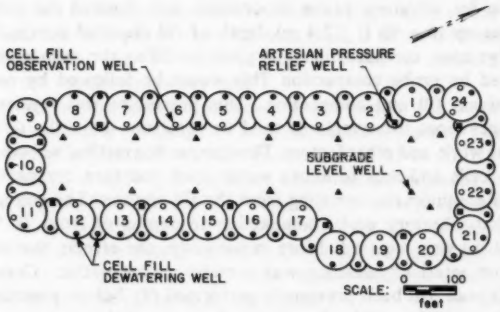

FIG. 12.—Location Plan: Cell Fill Dewatering Wells and Artesian Pressure Relief Wells at Cofferdam (1 ft = 0.305 m)

1.5 hp (1.1 kW) pumps rated 20 gpm (1.3 L/s) at 100 ft (30.5 m) head were installed to within 6 in. (150 mm) of the bottom of each well, as shown in Fig. 11. The pumps were automatically operated by on-off probes in each well. The wells located adjacent to the cofferdam basin were not required to be pumped but were provided to function as observation wells and also as standby

wells in the event of excessive seepage or breakdown of the pumped well (Fig. 12). Weep holes were also provided at and below El. −49 ft (−14.9 m) to monitor the dewatering system and to serve as an additional backup. The well design made it imperative that dredge residue be removed from the cells and arcs prior to filling, and that filling be performed in such a manner as to produce a clean, permeable soil within the lower levels near the dredge line. The method by which this was accomplished is discussed in Ref. 5.

In addition to this pumping system, a 15 ft (4.6 m) minimum depth blanket of semi-impervious fill was placed around the exterior of the cofferdam, as shown in Fig. 4, to reduce underseepage and interlock leakage near the bottoms of the cells and arcs.

Seismic Design.—The submarine base is located in a moderately active seismic area. Geologic studies disclosed that no active faults were present within the site area which would require design for ground rupture. However, because most of the cofferdam will be permanent, consideration of vibratory ground motion was required. Specifically, it was necessary to prohibit excessive interlock tensions due to liquefaction of the fill and to limit cyclically-induced settlements. It was established that a relative density of approximately 75% would be necessary to prevent liquefaction. Such a relative density could not be achieved by placement of uncompacted fill in-the-wet.

Placement and compaction of the fill in-the-dry in layers within the offshore cofferdam was not possible. Grouting or chemical stabilization of the soil as a substitute for achieving the 75% relative density was rejected because of cost and unfeasibility. Dynamic compaction with dropped weights was not possible, due to the danger of damaging the cells. Use of nonliquefiable soil such as peastone was rejected because of construction seepage considerations and cost.

Compaction by vibratory probe procedures was deemed the only feasible method. Since up to a 90 ft (27.4 m) depth of fill required compaction in the deepest dredge area, consideration was given to filling the cells a partial depth to be followed by probe compaction This would be followed by one or more lifts of additional fill and compaction. This procedure was rejected because of interferences from the templates used to construct the cells, difficulties in controlling the work, and other factors. The compaction method selected consisted of filling the cells and arcs to above water level and then compacting the fill full depth, with equipment operating from the fill surface. The compaction was unusual in that vibratory probe compaction to depths of from 70 ft (21.3 m) to 90 ft (27.4 m) was required. More importantly, the effects that compaction would have on interlock tensions was a major consideration. Compaction of a cellular bulkhead had been previously performed (4), but no precedent existed for a cofferdam which would subsequently be unwatered.

Choice of Cell Fill.—Soil for use as fill in the cells and arcs had to meet the following design requirements:

1. High unit weight after compaction to provide stability to sliding and overturning after basin unwatering.
2. High internal friction to minimize lateral earth pressures and interlock tensions.
3. Limited percentage of gravel to permit full depth penetration of the probes

for vibratory probe compaction and to facilitate subsequent augering through the fill for bearing pile installation during drydock construction.

4. Relatively low percentage of fines to facilitate probe compaction and to permit rapid fill dewatering during cofferdam basin unwatering.

5. Adequately low permeability to limit underseepage near the bottoms of the cells and arcs.

The fill specified was a well-graded, gravelly, coarse to fine sand having a 2 in. (50.8 mm) maximum stone size, from 15% to 45% passing a No. 40 sieve and 10% maximum passing a No. 200 sieve.

Corrosion Protection.—Two systems of corrosion protection were provided for the sheet piles of the permanent cells and arcs. A two-coat, shop applied, coal tar epoxy-polyamide coating was provided on the exterior surfaces of all sheets exposed to the Hood Canal after construction. An automatic, impressed-current type, cathodic protection system which became operational at the end of drydock construction, was also provided for the exterior surfaces of the exposed sheets.

Artesian Pressure Relief

The artesian conditions, shown in Fig. 9, posed unique challenges to the project. Studies disclosed that there was risk of an uplift failure of the glacial till during dredging if the aquifer piezometric level were not reduced. In addition, major pressure reduction in the aquifer was required to permit cofferdam basin unwatering. Lastly, a permanent partial reduction in artesian pressure was required for drydock in-service conditions to limit uplift pressures on the drydock and to provide adequate seismic stability of the offshore slope upon which the facility is built. Extensive design phase pumping tests from a 12 in. (305 mm) diameter test well, installed on shore, confirmed that it would be technically feasible to accomplish the required pressure relief.

It was decided to eliminate all excess pressure within the aquifer, relative to tide water levels during dredging. An onshore, artesian pressure relief, pumped well system was provided to lower the piezometric level to El. 0. The system consisted of five 12 in. (305 mm) diameter wells located adjacent to the shore, as shown in Fig. 9. The system was designed for an operating capacity of 2,500 gpm (158 L/s). Seventy-five ft (22.9 m) long well screens were used with the wells installed to depths of up to 200 ft (61 m) below ground surface. Two submersible 25 hp (18.6 kW) pumps, each rated 750 gpm (47 L/s) at 90 ft (27.4 m) head, were provided in each well.

Because of the critical nature of the pressure relief and the extremely rapid rate at which the aquifer would recover if pumping were interrupted, several backup systems were provided. These consisted of two submersible pumps in each well capable of being operated independently or simultaneously, multiple generators with automatic transfer and start-up capability, dual power feeders, high water alarms in each well, and an emergency connection to the Base power system. The system was designed for a capacity approximately double that expected to be required for a condition with some of the pumps inoperable.

An aquifer piezometric level of El. −67 ft (−20.4 m) was required for cofferdam

basin unwatering, subgrade preparation, and drydock floor construction. Studies disclosed that it would be necessary to transfer pressure relief pumping from the onshore system to a second well system at the cofferdam to achieve this drawdown. A series of twelve 12 in. (305 mm) diameter wells with 40 ft (12.2 m) long screens was designed for an operating capacity of 5,300 gpm (334 L/s). The pressure relief wells were installed within alternate arcs in the cofferdam after fill compaction, as shown in Fig. 12. Two submersible 15 hp (11.1 kW) pumps, each rated 300 gpm (18.9 L/s) at 140 ft (42.7 m) head were provided in each well. Redundancy and backup systems similar to those for the onshore wells were also provided. The system was designed for a capacity approximately 50% greater than that expected to be required. After basin unwatering, an additional system of open, stand-pipe, subgrade level wells was installed through the subgrade to provide for controlled venting of aquifer pressure in case of pumping failure. The well locations are shown in Fig. 12.

The cofferdam and subgrade level wells were subsequently incorporated into the drydock system. These provide the permanent level of artesian pressure relief and backup required for drydock service conditions.

Summary

By using high unit weight cell fill, high interlock strength steel sheet piling and extruded wyes, a pumped cell fill dewatering system and pumped artesian pressure relief system, it was possible to design a cellular cofferdam that would permit the in-the-dry construction of a graving drydock at the required deep water location. Since most of the cofferdam will be a permanent part of the completed facility, vibratory probe compaction of the fill was considered necessary to prevent liquefaction and to minimize seismically-induced settlements. The dense glacial till at the site provided an excellent foundation soil for the cofferdam, in terms of both bearing capacity and high strength for providing restraint to the sheet pile tips.

FIG. 13.—Interior of Unwatered Cofferdam

Unwatering of the cofferdam basin was performed without incident. Fig. 13 is a photograph from within the unwatered cofferdam. Drydock floor construction took approximately one year after unwatering. Throughout this period, the cell fill dewatering and artesian pressure relief systems performed satisfactorily and all aspects of the cofferdam performance were well within expected limits.

Acknowledgments

The facility was constructed for the Department of the Navy, Commander, Naval Facilities Engineering Command, through the Officer in Charge of Construction, Naval Facilities Engineering Command Contracts, Trident. The design was by Fay, Spofford & Thorndike, Inc., Boston, Massachusetts. The geoetechnical consultant was Haley & Aldrich, Inc., Cambridge, Massachusetts. The construction contractor was Willamette-General-Manson, a joint venture of Willamette-Western Corporation, Portland, Oregon, General Construction Company, Seattle, Washington, and Manson Construction and Engineering Company, Seattle, Washington. The writers wish to express their appreciation to the engineers on the staff of the Officer in Charge of Construction, Naval Facilities Engineering Command Contracts, Trident, for their contributions to the successful completion of the project.

Appendix.—References

1. "Steel Sheet Piling Cellular Cofferdams on Rock," Tennessee Valley Authority Technical Monograph 75, Tennessee Valley Authority, Knoxville, Tenn., Vol. 1, Dec., 1957.
2. *Design Manual Soil Mechanics, Foundations and Earth Structures*, Dept. of the Navy, Naval Facilities Engineering Command, (DM-7), Mar., 1971, Washington, D.C.
3. Hall, J. B., and Othberg, K. L., "Thickness of Unconsolidated Sediments, Puget Lowland, Washington," State of Washington Division of Geology and Earth Resources, Geologic Map GM-12, 1974.
4. Schroeder, W. L., Marker, D. K., and Khuayjarernpanishk, T., "Performance of a Cellular Wharf," *Journal of the Geotechnical Engineering Division*, ASCE, Vol. 103, No. GT3, Mar., 1977, pp. 153–168.
5. Sorota, M. D., Kinner, E. B., and Haley, M. X., "Cellular Cofferdam for Trident Drydock: Performance," *Journal of the Geoetechnical Engineering Division*, ASCE, Vol. 107, No. GT12, Proc. Paper 16733, Dec., 1981, pp. 1657–1676.

CELLULAR COFFERDAM FOR TRIDENT DRYDOCK: PERFORMANCE

By Max D. Sorota,[1] F. ASCE, Edward B. Kinner,[2] M. ASCE, and Mark X. Haley,[3] A. M. ASCE

INTRODUCTION

The construction of the drydock for Trident class submarines at the Naval Submarine Base, Bangor, Bremerton, Washington included a steel sheet pile cellular cofferdam. In order to build the drydock in-the-dry at the required offshore location, it was necessary that a cofferdam be designed to accommodate a maximum water depth of 79 ft (24 m) and be suitable to be incorporated into the final drydock configuration. The cofferdam is among the first to be constructed in the United States, and because of the expected interlock tensions, the construction required the use of high strength steel sheet piles and extruded wye connections.

The purpose of this paper is to: (1) Provide a summary of the cofferdam construction procedures; (2) provide data on instrumentation that was used to monitor cofferdam performance throughout construction; and (3) compare measured cofferdam performance, specifically cell interlock tensions and deformations, with published design procedures.

COFFERDAM DESCRIPTION AND SITE CONDITIONS

A plan and typical section of the cofferdam are shown in Figs. 1 and 2, respectively. The structure consists of 24 cells, each having a diameter of 75.83 ft (23.11 m) and 24 connecting arcs. Cells 1–20 and their connecting arcs are permanent. The remaining cells and arcs were removed at the end of drydock construction. The subgrade excavation levels within the cofferdam basin required for drydock floor construction are shown in Fig. 1. Project datum, elevation 0, is the mean lower low water (MLLW). Extreme high water (EHW) is at elevation 14.6 ft (4.5 m) and mean tide level at elevation 6.4 ft (1.9 m). Soil

[1]Sr. Vice Pres., Fay, Spofford & Thorndike, Inc., Boston, Mass.
[2]Sr. Vice Pres., Haley & Aldrich, Inc., Cambridge, Mass.
[3]Sr. Engr., Haley & Aldrich, Inc., Cambridge, Mass.

Note.—Discussion open until May 1, 1982. Separate discussions should be submitted for the individual papers in this symposium. To extend the closing date one month, a written request must be filed with the Manager of Technical and Professional Publications, ASCE. Manuscript was submitted for review for possible publication on October 31, 1980. This paper is part of the Journal of the Geotechnical Engineering Division, Proceedings of the American Society of Civil Engineers, ©ASCE, Vol. 107, No. GT12, December 1981. ISSN 0093-6405/81/0012-1657/$01.00.

conditions at the site consisted of loose sand and gravel alluvium overlying very compact glacial till which was underlain by a very dense sand and gravel stratum (10).

Site Preparation

The cofferdam configuration required that the sheet piles be driven to below the drydock floor subgrade on the basin side of the cofferdam. Due to expected

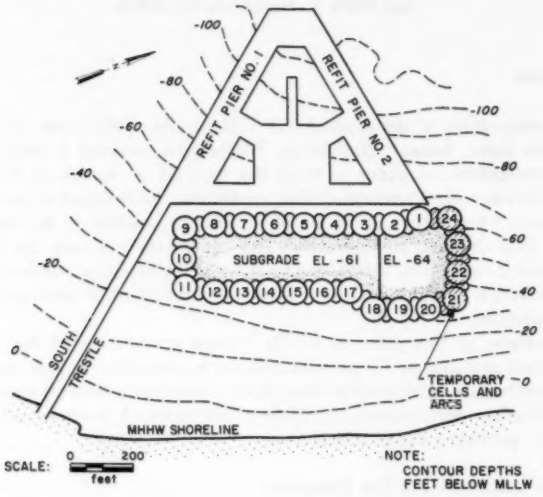

FIG. 1.—Cofferdam Plan (1 ft = 0.305 m)

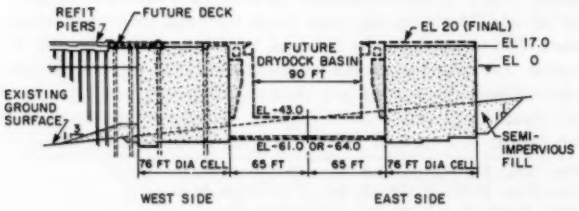

FIG. 2.—Typical Section (1 ft = 0.305 m)

hard driving in the dense glacial till, it was not considered possible to drive the sheets from original bottom grades to the required tip elevations without significant risk of sheet damage or jumped interlocks. Dredging was therefore conducted at the cells prior to cell construction.

Cell Construction.—High strength, PSX-32 sheet piles and 40° extruded

connecting wyes were used, as described in (10). Cell construction began at Cell 9 and initially proceeded toward Cell 2, then continued from Cell 10 toward Cell 20. The remaining cells and arcs were then built with closure being made at Connecting Arc 22–23.

The cell sheets were set around two 10 ft (3.1 m) high rigid, circular steel templates approximately 74.7 ft (22.8 m) in diameter. The templates were positioned by four H-pile studs driven into the foundation soils. The vertical distance between templates varied from 10 ft (3.1 m) to 30 ft (9.3 m), with the greater spacing being used at the deeper cells. The cell design radius was achieved at the upper template by placing wood blocks between the template and the sheets. No attempt was made to block the sheets at the lower template.

Sheet piles were set commencing at each of the four connecting wyes. Four closure points per cell were made in this way, one near the center of each cell segment between wyes. Similarly, closure was made near the central portion of each connecting arc. Two arc sheets were threaded to the wyes prior to driving the wyes or the cell sheets.

Sheets were driven with a MKT 10B3 single acting hammer having a rated energy of 13,100 ft-lb (17.8 kN·m). Driving was terminated when a driving resistance of 10 blows per inch (25.4 mm) was attained for sheets driven in pairs. Alternatively, driving was stopped if the penetration of a pair of sheets exceeded 6 ft (1.8 m) below the dredge level and the driving resistance was equal to 5 blows per inch (25.4 mm). Sheets typically were driven in pairs to a penetration of at least 2 ft (0.6 m) with most sheets being driven about 4 ft (1.2 m). Positioning the cell template sheet pile threading, and driving usually required ten 10-hr shifts per cell.

Filling and Densification of Cells and Arcs

Following completion of sheet pile driving at a cell, the cell was mucked out with a smooth-edged clamshell bucket. A diver inspection was made to verify that the sheets were not damaged nor out of interlock and that an essentially firm, clean bottom existed prior to filling. A second diver inspection of the interlocks was made after filling. Cell fill consisted of a well-graded, gravelly, coarse to fine sand having a 2 in. (51 mm) maximum particle size and not more than 10% by weight passing a No. 200 sieve (Fig. 3). The fill was placed by clamshell bucket in a manner that displaced any remaining dredging sludge away from the locations of the cell fill dewatering and observation wells which were installed later. All fill placed below water was deposited by lowering the bucket to the surface of the previously placed fill before opening. Typically, the cells were filled prior to placement of fill within adjacent connecting arcs. In all cases, however, the soil within the arcs was maintained at or below the fill level in the adjacent cells. In order to prevent tilting or other detrimental movements of individual cells and connecting arcs during filling, the fill surface adjacent to the sheets was maintained approximately level (within a range of 5 ft (1.5 m)).

The fill in all permanent cells and connecting arcs was densified to a minimum 75% relative density to prevent seismically induced liquefaction, minimize settlements, and obtain the necessary effective weight required for cofferdam stability (10). Fill in the temporary cells and arcs was similarly densified to

provide uniformity in soil properties for cofferdam stability. The depth of fill compacted ranged from 70 ft (21.3 m) within portions of the eastern and southern cells, to 90 ft (27.4 m) in portions of Cell 1.

The contractor used a vibratory probe manufactured by Toyomenka (America), Inc. The probe was 22 in. (559 mm) in diameter and approximately 100 ft (31 m) long. Penetration of the probe and compaction was achieved by a combination of vertical and horizontal vibrations generated by a vertically mounted vibratory pile driver, a VM2-25000A (1,450 ft-lb, 1.96 kN·m) at the top of the probe, and a horizontally mounted vibratory pile driver, a VM2-5000A (360 ft-lb, 0.49 kN·m), at the probe tip. Penetration of the probe was aided by jetting with two 2 in. (51 mm) diameter jet pipes which discharged vertically. The probe was vibrated at full depth for 10 min. Subsequent compaction was performed by consecutively raising the probe 6 ft (1.8 m), holding it momentarily, and then reinserting it 3 ft (0.9 m) until the probe was withdrawn to the surface. As compaction proceeded, fill was added by placing additional soil around the

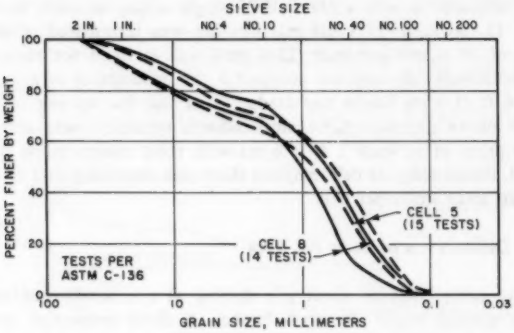

FIG. 3.—Fill Gradation Cells 5 and 8

probe. Penetration of the probe to an 80 ft (24 m) depth typically took 5–15 min. The penetration and compaction cycle at one individual probe location required about one hour.

Various center to center probe spacings were evaluated during a trial compaction program at Cell 8 in order to establish a procedure to compact the remaining cells. The next six cells were compacted using 31 probes located at about a 12 ft (3.7 m) center to center probe spacing. This initial spacing was found to provide a level of compaction in excess of that required. Therefore, nineteen probes were used within the remaining 17 cells, all at about 15 ft (4.6 m) spacings. The sequence of compaction for each pattern is shown in Fig. 4. Compaction results were measured by the standard penetration test, with results correlated to relative density, in accordance with Gibbs and Holtz (4). Typical results are shown in Fig. 5. Near surface, in-place unit weight tests were also performed at each of the cells. Soil moist unit weights after compaction ranged from 118.2 pcf (1,894 kg/m^3) to 139.5 pcf (2,235 kg/m^3) with an average of 130.3 pcf (2,087 kg/m^3).

Compaction in the connecting arcs was conducted following compaction of the adjacent cells. The number of probes within each arc varied depending on the area but typically ranged from four to six.

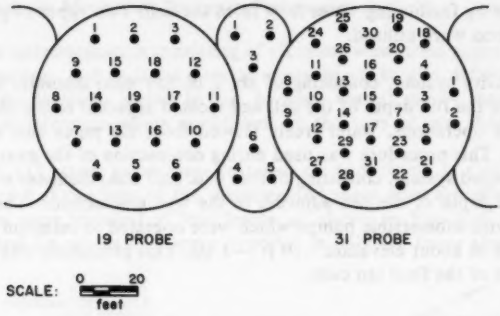

FIG. 4.—Vibratory Probe Patterns (1 ft = 0.305 m)

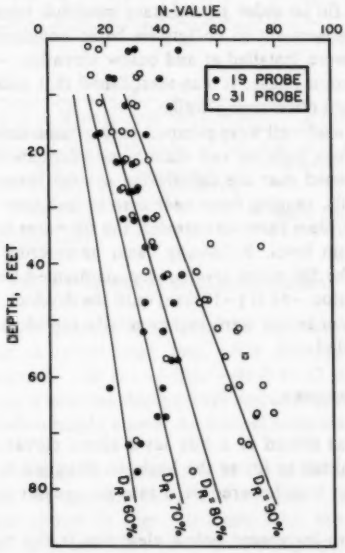

FIG. 5.—Compaction Results (1 ft = 0.305 m)

At the first four cells compacted, high pore water pressures were observed to develop within the fill during probe insertion and compaction. Momentary excess heads of 50 ft (15 m) or more were observed at piezometers located

close to the probe locations. Increases in interlock tension were also observed to be associated with development of the compaction pore pressures.

A pore pressure relief system was designed during the construction phase and installed in the remaining cells to limit excess pore pressures and aid the compaction by facilitating water flow from the soil. Two types of pore pressure relief systems were utilized:

1. A gravity system, consisting of six 2 in. (51 mm) diameter slotted pipes installed for the full depth of the cell and located adjacent to the sheets. During compaction operations, water freely flowed from the pipes and was diverted overboard. This procedure was used during compaction of the next ten cells.
2. A pumped system, consisting of four 8 in. (203 mm) diameter wells installed for the full depth of the cell adjacent to the wye connections. The wells were equipped with submersible pumps which were operated to maintain water levels in the wells at about elevation −10 ft (−3 m). This procedure was used during compaction of the final ten cells.

Cell Fill Dewatering

After fill compaction, wells were installed within each cell and connecting arc to dewater the fill in order to maintain interlock tensions within tolerable limits during and subsequent to cofferdam basin unwatering (10). In addition, drilled weep holes were installed at and below elevation −49 ft (−14.9 m) (10). During the construction phase, it was established that additional pumps should be installed in the cell observation wells.

Both wells within each cell were pumped during basin unwatering. Intermittent pumping from only one well per cell maintained adequate drawdown thereafter. Measurements disclosed that the dewatering system maintained hydraulic gradients across the cells, ranging from near zero to less than 5 ft (1.5 m).

During initial cofferdam basin unwatering, the fill water levels were maintained at or below the basin level. Following basin unwatering below elevations of −45 ft (−13.7 m), the fill water levels were maintained between elevation −46 ft (−14 m) and elevation −61 ft (−18.6 m) until the drydock floor was completed. The cell and arc water levels were incrementally raised as subsequent drydock construction proceeded.

Cofferdam Basin Unwatering

The cofferdam was closed at a tide level about elevation 9 ft (2.7 m). The contractor was permitted to lower the basin to elevation 0 without restrictions. Thereafter, the basin was lowered at a rate no greater than 5 ft (1.5 m) per 24 hr period.

At each 10 ft (3 m) increment below elevation 0, the basin water level was held constant for a day while the cofferdam performance monitoring instrumentation was read, a diver inspection was made of the interior and exterior perimeter of the cofferdam, and the data were reviewed to evaluate cofferdam performance.

The basin level was maintained at elevation −20 ft (−6 m) for a three week period while the cells were proof tested. The proof loading was obtained by temporarily raising the water level in the cells and connecting arcs to elevation

0. Typically, two to three cells and the adjacent connecting arcs were proof tested at one time. The estimated maximum interlock tension under this loading was comparable to that expected during the final unwatering stage.

Instrumentation for Monitoring Cofferdam Performance

Cofferdam instrumentation consisting of vibratory wire strain gages to monitor interlock tensions, and inclinometers to measure sheet pile deflections, was installed at the locations shown in Fig. 6. Also, optical survey measurements were made at reference points established on the tops of two sheets in each cell.

A total of 112 strain gages were installed on two sheets at Cell 8 and six sheets at Cell 5. Locations of the instrumented sheet piles are shown in Fig. 6. The gages were installed at four levels, as shown in Fig. 7(*a*), except for Sheets 5-4 and 5-6 where they were provided at only the lower three and two

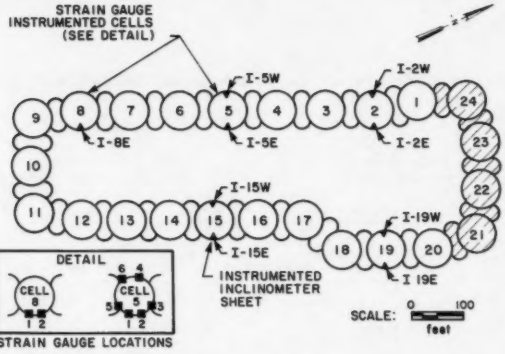

FIG. 6.—Locations of Instrumentation

levels, respectively. The gages were placed on the sheets before sheet pile threading and driving at levels such that, after driving, the gages were at approximately elevation 0, −20 ft (−6 m), −40 ft (−12 m), and −58 ft (−17 m). This placed the gages near the dredge level and at intervals of approximately one-quarter the cofferdam height above. Additional installation details are shown in Fig. 8(*a*).

Inclinometers were installed at the centers of the basin and Hood Canal sides of Cells 2, 5, 15 and 19, and the basin side of Cell 8, as shown in Fig. 6. Installation details are shown in Figs. 7(*b*) and 8(*b*). Horizontal and vertical sheet movements for each cell were monitored using optical survey points at the top of two sheets, one each at the center of the basin and Hood Canal cell segments.

Interlock Tensions During Cell Construction and Compaction

Interlock tensions measured after filling and compaction are shown in Figs.

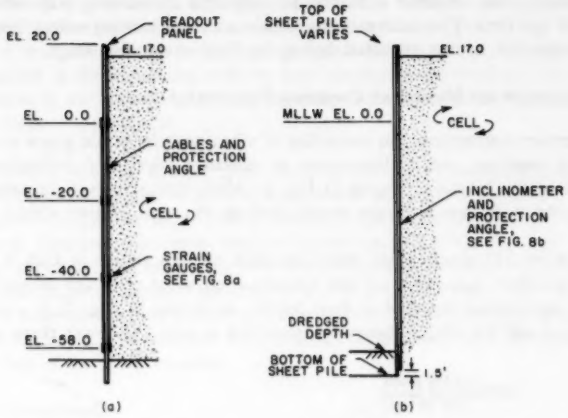

FIG. 7.—Instrumentation—Typical Sections (*a*) Strain Gauge Sheet (*b*) Inclinometer Sheet (1 ft = 0.305 m)

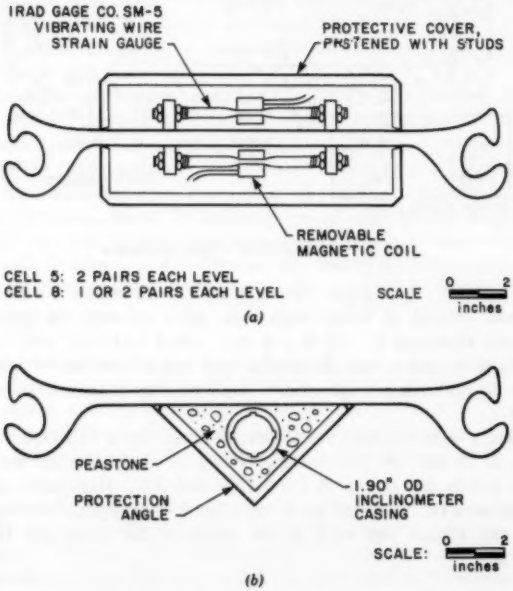

FIG. 8.—Instrumentation Details (*a*) Strain Gauges (*b*) Inclinometers (1 in. = 25.4 mm)

9 and 10 for Cells 8 and 5, respectively. The following comments apply:

1. Cell 8 was the cell at which trial compaction operations to establish production probe spacings took place. As such, the cell compaction was somewhat atypical with a total of 29 probes being made versus the 19 or 31 probe arrays utilized at the other cells.

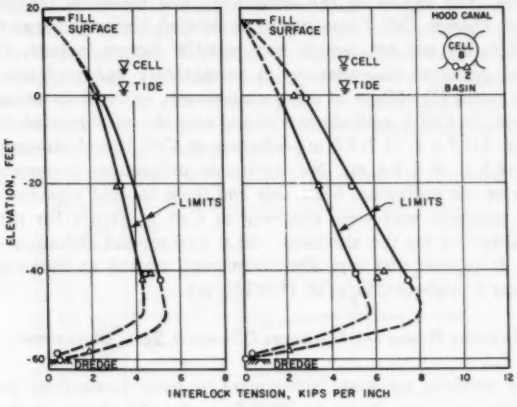

FIG. 9.—Cell 8 Interlock Tensions (*a*) After Filling (*b*) After Compaction (1 ft = 0.305 m) (1 kip/in. = 175 kN/m)

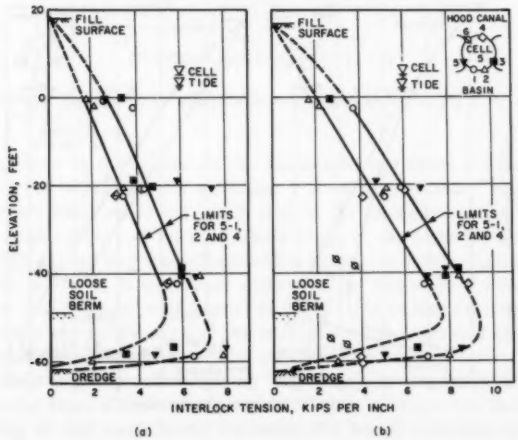

FIG. 10.—Cell 5 Interlock Tensions (*a*) After Filling (*b*) After Compaction (1 ft = 0.305 m) (kip/in. = 175 kN/m)

2. During tide cycles, interlock tensions varied by up to 1 kip/in. (175 kN/m), with the higher tensions occurring at low tide. All data presented herein are for conditions at approximately low tide.

The limit lines shown in Figs. 9 and 10 represent the writers' estimate of the probable total range of interlock tensions on the basin and Hood Canal sides of the cells. The causes of the abnormally low measured tensions at Sheet 5-6 are not known. Cell 5 consistently exhibited higher tensions than Cell 8. Reasons for this are not certain but possible factors include: (1) Differing compaction patterns; (2) variations in permeability and gradation of the cell fill (Fig. 3); and (3) effects of sheet embedment on tensions measured at the dredge level. At Cell 8, embedments at and near the instrumented sheets ranged from about 4.0–7.5 ft (1.7–2.0 m), whereas at Cell 5, embedments were from about 2.5–4.5 ft (0.8–1.4 m). No significant differences in tensions between the sheets on the cofferdam basin side and those located adjacent to the wyes along the common wall were observed at Cell 5, except for the data after filling at sheet 5-5 for the elevation −20 ft (−6 m) and elevation −40 ft (−12 m) levels. It is seen that typically compaction caused an increase in tension of from near 0 to about 2 kips/in. (350 kN/m).

Interlock Tensions During and Following Cofferdam Basin Unwatering

Interlock tensions measured subsequent to basin unwatering are shown in Fig. 11. The limit lines shown for Cell 5 are for the sheets on the basin side (5-1 and 5-2). The limit lines for Cells 5 and 8 indicate a relationship between the two cells similar to that observed prior to basin unwatering, with the tensions continuing to be higher in Cell 5. For example, the post-unwatered limit line

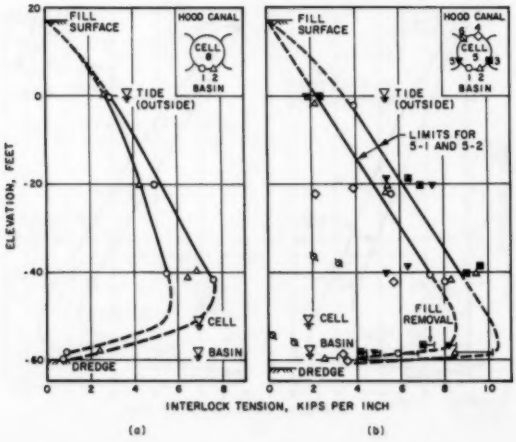

FIG. 11.—Interlock Tensions After Basin Unwatering (*a*) Cell 8 (*b*) Cell 5 (1 ft = 0.305 m) (1 kip/in. = 175 kN/m)

tensions in Cell 5 at elevation −40 ft (−12 m) are 7.2–8.6 kips/in. (1,260–1,500 kN/m), whereas in Cell 8 the range is from 5.5–7.2 kips/in. (960–1,260 kN/m).

Changes in interlock tension which occurred in Cell 5 at elevation −58 ft (−17 m) subsequent to basin lowering are shown in Fig. 11. These changes are attributed to removal of a loose fill berm which had accummulated against the basin side of the cell to elevation −49 ft (−15 m). At Sheet 5-2, the tension at the elevation −60 ft (−18 m) upper level strain gages increased by 1.65 kips/in. (290 kN/m) to a value of 10.2 kips/in. (1,790 kN/m). Other lesser changes occurred as indicated. The relatively small increases observed at Sheets 5-3 and 5-5 suggest that significant resisting frictional forces had developed between the sheets and the cell fill along the common walls near the wyes. The data also indicate that even relatively loosely placed interior soil berms can be beneficial in limiting interlock tensions.

Following unwatering, some differences were observed between the Cell 5

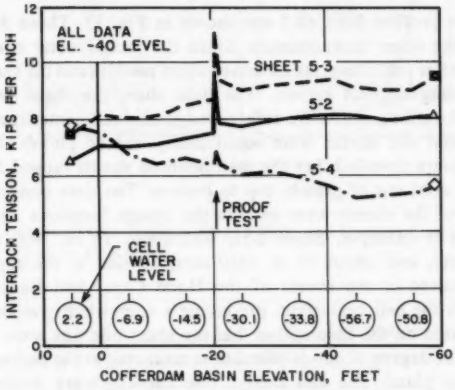

FIG. 12.—Changes in Interlock Tensions During Basin Unwatering (1 ft = 0.305 m) (1 kip/in. = 175 kN/m)

interlock tensions at the sheets on the basin side and those on the common wall side of the wyes. At the elevation 0 level, the common wall tensions were essentially identical to the lower limit of the tensions on the basin side. At the elevation −20 ft (−6 m) level, the average of the common wall tensions was about 20% higher than the average of the basin side sheets. At the elevation −40 ft (−12 m) level, a significant difference in measured tensions existed between the two common wall sheets. However, the average for the common wall sheets was essentially equal to the average for the basin side sheets.

When the cofferdam basin and cell fill water levels were lowered, the measured interlock tensions at the cell sheets on the basin side increased, whereas the tensions on the Hood Canal side decreased. Typical changes are shown in Fig. 12. Lowering of the water levels increased the lateral pressure on the basin side of the cell. However, the lowering of the cell water level decreased the lateral pressure on the Hood Canal side. The direction of the measured changes is compatible with the expected behavior.

Data obtained during cofferdam proof testing are also included in Fig. 12. The spikes in the tensions correspond to the maximum test water level in the cell fill. The tensions after proof testing, when the cell and pool water levels were both at elevation −20 ft (−6.1 m), were somewhat larger than those measured for this condition prior to the test. This is attributed to a slight increase in cell diameter under the maximum test water level in the cell fill and the accompanying small radial expansion of the cell fill. The sheets experienced only partial elastic shortening following removal of the test load because full recovery was prevented by the cell fill which had previously been displaced outwards against the sheets during the proof loading. The data in Fig. 12 indicate that this prestressing effect was essentially overcome by the time the basin water level was at elevation −30 ft (−9 m).

Sheet Pile Profiles and Movements

Inclinometer profiles for Cell 5 are shown in Fig. 13. These data are typical of those for the other inclinometers. Since the inclinometer casings were not installed until after cell filling, the as-driven sheet profiles and the sheet movements during cell filling are not known. The data show the sheet profiles relative to the design locations which are referenced to the cell centerline.

It is seen that the sheets were significantly out of plumb. Data from the nine inclinometers revealed that the instrumented sheets ranged from 12.7–54.5 in. (323–1,380 mm) out of plumb, top to bottom. The data consistently showed that the tops of the sheets were outside the design locations and the bottoms were inside. For example, Sheet I-5E was about 16 in. (400 mm) inside at the dredge level, and about 19 in. (480 mm) outside at the top. Compaction of the fill resulted in movement of the Hood Canal and Basin sides of the cell away from the cell centerline, producing a somewhat oval shape. The data have been plotted on the assumption that the sheet pile tips were fixed.

Because of the degree of out-of-plumbness measured at the inclinometer sheets, extensive diver plumb line and dredge line surveys were made at each cell. These surveys disclosed that at the dredge line, the sheets near the wyes were typically outside the design radius, whereas those midway between the wyes were inside the design radial location. This is believed to be the result of the cell construction procedures wherein blocking was only used at the upper template level. The sheets initially set near the wye were positioned with the bottom outside the radial line; the remaining sheets had to be toed in to complete closure. All inclinometers were located on sheets that were near the closure points where the sheet tips were inside the design radius.

Movements of the Cell 5 inclinometers during unwatering are shown in Fig. 14. The displacements shown are incremental movements for the various stages of unwatering from the sheet pile positions which existed when the basin was at elevation 5.3 ft (1.6 m). Movements resulting from proof testing the cell at a basin level of elevation −20 ft (−6 m) are included. The causes of the movements during proof testing are not fully understood, but are believed to be, at least partially, the result of creep movements which occurred during the three week period that the basin was at elevation −20 ft (−6 m).

Total movements measured at the top of the cell were very small, with the movements of both inclinometers being less than 3 in. (76 mm) during unwatering

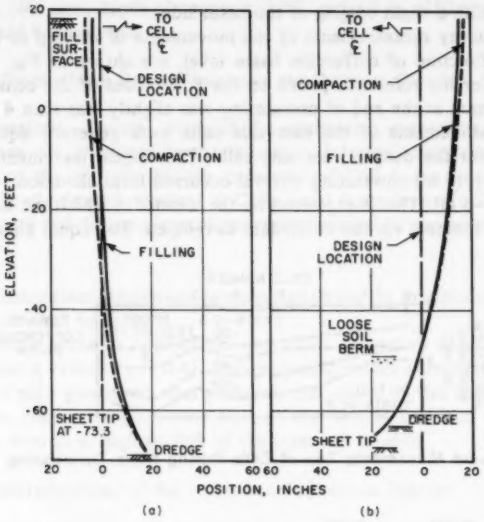

FIG. 13.—Cell 5 Inclinometer Profiles After Filling and Compaction (*a*) I-5W (*b*) I-5E (1 ft = 0.305 m) (1 in. = 25.4 mm)

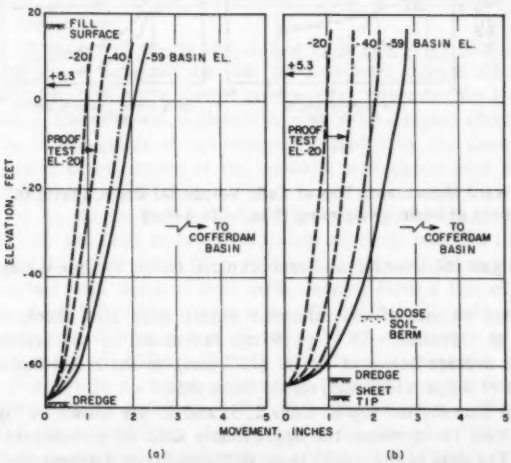

FIG. 14.—Cell 5 Inclinometer Movements During Basin Unwatering (*a*) I-5W (*b*) I-5E (1 ft = 0.305 m) (1 in. = 25.4 mm)

to elevation −59 ft (−18 m). The data indicate a substantially rigid body rotation of the cell with a slight bulging of the basin side.

Optical survey measurements of the movements of the top of the west side cells, as a function of cofferdam basin level, are shown in Fig. 15. The data shown are for the reference points on the basin sides of the cells. The largest total movement at the end of unwatering was slightly less than 4 in. (102 mm) at Cell 2. Movements of the east side cells were generally equal to or less than those for the deeper west side cells. The largest incremental movement for each 20 ft (6 m) unwatering interval occurred from elevation −0.3 to −20.0 ft (−0.1 to −6 m). This is explained by the manner in which the net hydrostatic overturning moment on the cofferdam developed. For equal changes in basin

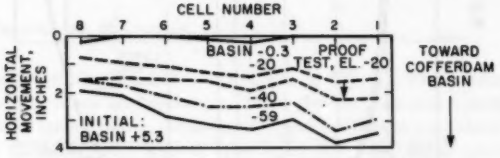

FIG. 15.—Inward Movements Top of Cells During Basin Unwatering (1 in. = 25.4 mm)

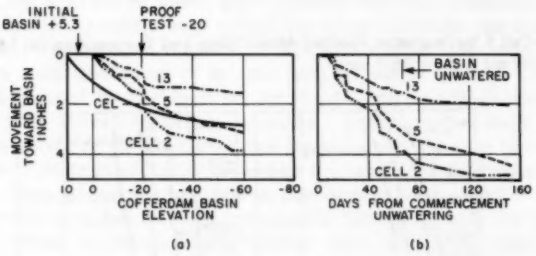

FIG. 16.—Inward Movements Top of Cells Versus (*a*) Basin Levels (*b*) Time Since Commencement of Basin Unwatering (1 in. = 25.4 mm)

level, the largest incremental moments occurred during the initial stages of basin lowering.

Vertical movements of the reference points were also checked. With the basin level at elevation −59 ft (−18 m), movement of the reference points indicated an average heave of 0.5 in. (12.7 mm) on the Hood Canal side, and a settlement of 0.5 in. (12.7 mm) on the basin side.

Movement data for the top of Cells 2, 5, and 13 are shown in Fig. 16. Data for Cells 2 and 13 represent the approximate limit of movements within the cofferdam. The data in Fig. 16(*b*) show that creep type deformations continued after the cofferdam was unwatered. The rate of movement for Cells 2 and 13 decreased with time, whereas the creep rate for Cell 5 remained approximately constant during the observation period. Final excavation for, and preparation

of the drydock floor subgrade occurred during this period. At the end of this time, an 18 in. (460 mm) depth of compacted fill, and a 6 in. (150 mm) concrete working slab had been placed.

Comparison of Recommended Design Procedures and Observed Behavior

Interlock Tensions.—Several methods for estimating maximum sheet pile interlock tension are presented in the literature. Interlock tensions calculated using several of the sources for the geometry of Cell 5 are summarized in Table 1. Measured interlock tensions at Cells 5 and 8 are shown in Table 2.

Soil parameters and design assumptions recommended by the several sources vary as follows:

1. The maximum interlock tension is computed above the dredge line at heights which vary from zero to H/3.
2. Lateral earth pressure coefficients vary from the active condition, $K_h = 0.28$, to a Krynine value, $K_h = 0.45$, with empirical values most often used.
3. For the Cell 5 geometric configuration, the effect of the connecting arc loading on the common wall sheets next to the wye is assumed to increase tensions from zero to as high as 50% of the main cell tension.

The writers' interpretations of the cofferdam data are as follows:

1. For the basin side sheets, the interlock tensions both before basin unwatering, (Figs. 9 and 10) and after (Fig. 11), indicate that maximum tensions occurred at approximately 10 ft (3 m) above the dredge line instead of the commonly used H/4 level, which, for the instrumented cells, is approximately 20 ft (6 m) above the dredge line.
2. For the common wall sheets adjacent to basin side wyes, the after filling and after compaction data indicate that the maximum tension also occurred at approximately 10 ft (3 m) above the dredge level. However, for these sheets after unwatering, the point of maximum tension is at a higher elevation. This is believed to be the result of the restraint provided by the connecting arc fill, which limited deformations of the common wall sheets near the bottom of the cell during basin unwatering.
3. Values of K_h shown in Fig. 17 have been calculated based on in-place soil densities and the limit lines of measured interlock tensions indicated in Figs. 9, 10, and 11. After filling (Fig. 17(*a*)), K_h values for the loose fill were relatively constant with depth in both cells, ranging from a low of about 0.2 to a high of about 0.4. After compaction, (Fig. 17(*b*)), K_h values increased with depth and ranged from a low of about 0.2 at elevation 0 to a high in Cell 5 of 0.46 at the elevation −40 ft (−12 m) level. Conversely, after basin unwatering, (Fig. 17(*c*)), K_h values decreased with depth, ranging from 0.3–0.45 at the elevation 0 level, and from 0.23–0.36 at the elevation −40 ft (−12 m) level. For the three conditions, the K_h values for the after-filling condition are believed to be the most representative values of the "true" lateral earth pressures within the cells, because of the absence of prestress effects in the sheets. The K_h values after compaction are believed to have been affected by residual prestressing of the sheets due to compaction operations. Residual

TABLE 1.—Calculated Interlock Tensions Following Basin Unwatering Using Various Design Procedures

Reference (1)	Assumed point of maximum interlock tension (2)	Lateral earth pressure coefficient, K_h (3)	Calculated Interlock Tension, in kips per inch		Recommended factor of safety (6)
			Cell (4)	At wye connection (5)	
TVA (3)	H/4	active 0.28	6.9[a]	10.4[c]	2.0
Lacroix, et al. (6)	H/4	empirical 0.40	—	12.0[b]	2.0
Navy Design Manual (7)	H/4	Krynine 0.45	—	11.1[a]	—
Swatek (11)	H/4	empirical 0.25–0.35	6.2–8.6[a]	9.3–13.0[c]	—
Terzaghi (12)	H/3–H/4	empirical 0.4	—	8.8–9.9[a]	2.5
Corps of Engineers (13)	dredge level	active 0.28	8.7[a]	13.1[c]	2.0

[a] $t = pr$.
[b] $t = pL/2$.
[c] $t = pL/2$ (sec α).
Note: 1 kip/in. = 175 kN/m; $\bar{\Phi} = 38°$ Assumed.

TABLE 2.—Measured Interlock Tensions Following Basin Unwatering

Location (1)	Point of measured interlock tension (2)	Lateral earth pressure coefficient, K_h (3)	Average Range of Measured Values, in kips per inch		Remarks (6)
			Cell (4)	At wye connection (5)	
Cell 5	H/4	0.29–0.36	7.4–8.8	5.9–9.4	Fig. 11(*b*)
	(a)	—	8.5–10.5 (estimated)	(b)	
Cell 8	H/4	0.23–0.31	5.5–7.6	—	Fig. 11(*a*)
	(a)	—	5.8–7.6 (estimated)	—	

[a] Magnitude of maximum interlock tension based on interpretation of data.
[b] Data insufficient for estimate.
Note: 1 kip/in. = 175 kN/m.

prestresses developed as a result of compaction pore pressures, soil displacements due to probe insertion, and fill densification. The K_h values after unwatering were controlled by the net effect of changes in vertical effective stress and interlock tension. The pumped dewatering of the cell and connecting arc fill resulted in increased vertical effective stress, with the largest increments occurring in the lower levels of the cells and arcs. At the lower levels, the magnitude of the increased effective stress was sufficient to counteract all or most of the prestress effect. The range of K_h values for the after-filling and after-unwatering conditions are almost identical at elevation −20 ft (−6 m) at Cell 5 and at elevation −40 ft (−12 m) at Cells 5 and 8.

4. For the unwatered condition, the back calculated K_h values are within the range of values recommended in the literature. The K_h values in Fig. 17 show that K_h is not constant and varies as a result of construction procedures.

5. The data for Cell 5 show that the interlock tensions at the common wall sheets next to the wyes were from zero to 20% higher than measured on the basin side. Thus, the procedures in Table 1 utilizing the TVA secant formula to account for the arc effect appear conservative. Published field data on the connecting arc effect are available for a cellular bulkhead where a common wall sheet close to a T-pile connection was instrumented, (14). After filling

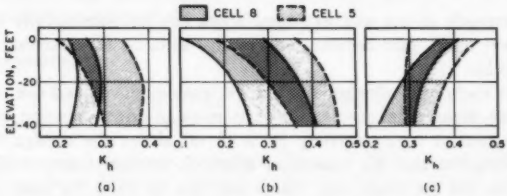

FIG. 17.—Range of Lateral Earth Pressure Coefficients Cells 5 and 8 (*a*) After Filling (*b*) After Compaction (*c*) After Basin Unwatering (1 ft = 0.305 m)

behind the connecting arc was completed, the common wall tensions were generally found to be equal to or less than the tensions on the cell sheets in front of the T-pile connection. Recent studies for another cellular bulkhead (9) showed that the common wall tensions close to the connection were also equal to or less than those on the cell sheets in front of the connecting member.

Cofferdam Movements.—Swatek (11) states that cofferdams commonly move inward toward the basin an amount equal to about 1% of the cofferdam height during unwatering. This would be equal to about 9.5 in. (240 mm) for this cofferdam. Actual movements ranged from 1.5–4.0 in. (38–100 mm), which is 0.16–0.42% of the height. The reduced deflections are considered to be principally the result of the quality of the fill and the compaction operations which increased the fill density and shear modulus. These observations are consistent with those previously reported by Rimstad (8) where movements of model sheet pile cofferdams were measured. The study found that laboratory models having dense soil deflected less than those at which the soil was less dense.

Prior to cofferdam unwatering, a prediction of cell movements was made by Forrest (2) using a computerized procedure patterned after a method proposed

by Brown (1). The shear modulus of the fill with depth was based on an assumed 75% relative density. The predicted movement, labeled "CEL" in Fig. 16(*a*), is within the range of the observed inward movements. The calculation assumed a rigid foundation for the cells, which appears reasonable since the inboard sheets were observed to move only about 0.5 in. (12 mm) vertically during unwatering.

Many investigators, e.g., Swatek (11), Terzaghi (12), and others, report that following unwatering, maximum bulging of the cells occurs at approximately H/4 above the dredge level. From these observations it has been concluded that the point of maximum tension similarly occurred at H/4. The inclinometer data in Figs. 13 and 14, and the interlock tension data, do not support these observations. The profiles show that the cells did not experience the degree of bulging that is common in most cofferdams. It is believed that the high quality of the fill and the densification may have contributed to this occurrence.

Conclusions

The following principal conclusions are made:

1. High strength sheets and extruded wyes can be successfully utilized to construct steel sheet pile cellular cofferdams suitable for resisting 80 ft (24 m) water depths.
2. The data show that substantial interlock tensions developed near the dredge level. For the basin side sheets, the maximum interlock tension is believed to have occurred at approximately 10 ft (3 m) above the dredge level. The common assumption that the maximum interlock tension occurs at H/4 above the dredge line for the basin side sheets may not be valid for deep cofferdam cells having shallow sheet pile embedments.
3. The data indicate that the elevation of maximum tension for the common wall sheets is also at about 10 ft (3 m) above the dredge level prior to basin unwatering. However, it is believed that because of the restraint provided by the connecting arc fill, the maximum tensions after unwatering occurred at a greater distance above the dredge line. Insufficient data exist to establish the specific elevation, and use of the 10 ft (3 m) distance for the common wall tensions in cofferdams of this type is considered prudent.
4. Lateral earth pressure coefficients can be variable with depth, depending on construction procedures. Therefore, empirical values should be used in design rather than coefficients based on highly theoretical considerations. For compacted, well graded sand and gravel fill, K_h values in the range of 0.35–0.40 are considered appropriate for computing sheet pile interlock tensions following basin unwatering.
5. For the 40° extruded wye connection, the data indicate that the common wall tension near the wye is not significantly higher than the tension in the basin side sheet piles. An allowance of 15% for increased tension is considered a reasonable factor.
6. The quality and density of the cell fill have a significant influence on the magnitude of cell movements during cofferdam basin unwatering.
7. In deep, large diameter cells, two or more template levels, including one

at or near the dredge level, should be used to ensure sheet pile plumbness and geometric control.

8. The successful construction of the cofferdam was largely dependent on the high bearing capacity and strength of the glacial till at the site which provided a nearly rigid foundation and large lateral resistance to the embedded sheet piles.

Acknowledgment

The facility was constructed for the Department of the Navy, Commander, Naval Facilities Engineering Command through the Officer in Charge of Construction, Naval Facilities Engineering Command Contracts, Trident. The design was by Fay, Spofford & Thorndike, Inc., Boston, Massachusetts. The geotechnical consultant was Haley & Aldrich, Inc., Cambridge, Massachusetts. The construction contractor was Willamette-General-Manson, a Joint Venture of Willamette-Western Corporation, Portland, Oregon, General Construction Company, Seattle, Washington and Manson Construction and Engineering Company, Seattle, Washington. The authors wish to express their appreciation to the engineers on the staff of the Officer in Charge of Construction, Naval Facilities Engineering Command Contracts, Trident for their contributions to the successful completion of the project.

Appendix.—References

1. Brown, P. P., discussion of "Field Study of a Cellular Bulkhead," *Journal of the Soil Mechanics and Foundations Division,* ASCE, Vol. 88, SM1, Part 1, Feb., 1962, pp. 72–75.
2. Civil Engineering Laboratory, "Analysis of Lateral Deflection of Cofferdam Based Upon Shear Beam Analogy," Naval Construction Battalion Center, Port Hueneme, California, in-house memorandum by J. B. Forrest, Mar., 1978.
3. "Steel Sheet Piling Cellular Cofferdams on Rock," Tennesse Valley Authority, Technical Monograph 75, Knoxville, Tenn., Vol. 1, Dec., 1957, 281 p.
4. Gibbs, H. J., and Holtz, W. G,. "Research on Determining the Density of Sands by Spoon Penetration Testing," *Proceedings of the 4th International Conference Soil Mechanics and Foundation Engineering,* London, England, 1957, pp. 35–39.
5. Krynine, D. P., discussion of "Stability and Stiffness of Cellular Cofferdams," *Transactions,* ASCE, Vol. 110, 1945, pp. 1175–1178.
6. Lacroix, Y., Esrig, M. L., and Luscher, U., "Design Construction and Performance of Cellular Cofferdams," ASCE Specialty Conference Lateral Stresses in the Ground and Design of Earth-Retaining Structures, 1970, pp. 271–328.
7. Dept. of the Navy, Naval Facilities Engineering Command, *Design Manual Soil Mechanics, Foundations and Earth Structures,* (DM-7), Washington, D.C., Mar. 1971.
8. Rimstad, I. A., "Zur Bemessung des doppelten Spundwandbauwerkes," *Ingenieurvidenskabelige Skrifter,* No. 4, Copenhagen, G.E.C. Gad., 1940.
9. Schroeder, W. L., Marker, D. K., and Khuayjarernpanishk, T., "Performance of a Cellular Wharf," *Journal of the Geotechnical Engineering Division,* ASCE, Vol. 103, No. GT3, Mar., 1977, pp. 153–168.
10. Sorota, M. D., and Kinner, E. B., "Cellular Cofferdam for Trident Drydock: Design," *Journal of the Geotechnical Engineering Division,* ASCE, Vol. 107, No. GT12, Proc. Paper 16758, Dec., 1981, pp. 1643–1655.
11. Swatek, E. P., "Summary Cellular Structure Design and Installation," *Design and Installation of Pile Foundations and Cellular Structures,* Envo Publishing Co., Inc., Lehigh Valley, Penn., 1970, pp. 413–424.
12. Terzaghi, K., "Stability and Stiffness of Cellular Cofferdams," *Transactions,* ASCE, Vol. 110, Paper No. 2253, 1945, pp. 1083–1119.

13. U.S. Army Corps of Engineers, "Design of Pile Structures and Foundations," Department of the Army Manual EM 1110-2-2906 (Draft), Washington, D.C., Nov. 1970.
14. White, A., Cheney, J. A., and Duke, C. M., "Field Study of a Cellular Bulkhead," *Journal of the Soil Mechanics and Foundations Division*, ASCE, Vol. 87, No. SM4, Aug., 1961, pp. 89–124.

COMPRESSIBILITY AND BEARING CAPACITY

By Nabil F. Ismael,[1] M. ASCE and Aleksandar S. Vesic,[2] F. ASCE

INTRODUCTION

The analysis of ultimate loads on shallow foundations usually employs the well-known Terzaghi equation (6), in which contributions to the bearing capacity from different soil and loading conditions are summed. This analysis is based on solutions developed for the rigid-plastic solid of the classical theory of plasticity. As presently known, this solid is assumed to exhibit no deformation prior to shear failure and a plastic flow at constant stress after failure. Thus, the capabilities of theoretical predictions of ultimate load are limited to relatively incompressible soils or the general shear failure mode (8). For compressible soils, it is common practice to use the available solutions with possible reduction in the strength parameters for the effects of compressibility.

Compressible soils fail usually in either local or punching shear. These modes are characterized by substantial strain prior to failure and a limited slip surface ending in the soil mass below the footing at failure. The failure mode that can be expected depends on the relative compressibility of the soil in the particular geometrical and loading conditions. Among the principal factors governing the failure mode are the soil compressibility, relative density, the foundation size, and the presence of overburden pressure.

Because of the lack of rational methods for analyzing bearing capacity failures for compressible soils, Terzaghi proposed the use of the bearing capacity equation for the general shear failure mode with reduced strength parameters $\bar{c}$ and $\bar{\phi}$ defined as $\bar{c} = 2/3\ c$ and $\tan \bar{\phi} = 2/3 \tan \phi$. Although this proposal is simple to apply, it is not supported by either documented laboratory model tests or field tests. It also suggests a jump in bearing capacity on transition to general shear failure, a phenomenon which, of course, does not occur. Furthermore, to apply this method, the practicing engineer must have data available on the load-settlement behavior of the soil to judge the probable failure mode. Such data are not always available.

Proposals of this kind may be useful in practice; however, they are based on a doubtful premise that the effects of the relative compressibility of a soil

[1]Assoc. Prof., Coll. of Engrg. and Petroleum, Kuwait Univ., Kuwait.
[2]Prof. and Dean of Engrg., Duke Univ., Durham, N.C.

Note.—Discussion open until May 1, 1982. To extend the closing date one month, a written request must be filed with the Manager of Technical and Professional Publications, ASCE. Manuscript was submitted for review for possible publication on October 31, 1980. This paper is part of the Journal of the Geotechnical Engineering Division, Proceedings of the American Society of Civil Engineers, ©ASCE, Vol. 107, No. GT12, December, 1981. ISSN 0093-6405/81/0012-1677/$01.00.

under different geometrical and loading conditions can be accounted for by adjusting c and ϕ. A different solution proposed recently by Vesic (8) is based on an extension of the cavity expansion solutions (5,7) to include shallow foundations on compressible soils. To apply this solution, the rigidity index, I_r, defined as the inverse of the shear strain of the soil, is first determined; then the compressibility factors are calculated for use in the bearing capacity formula. These are reduction factors which vary with the angle of shearing resistance and the parameter, I_r. The method emphasizes the importance of the deformation parameters of the soil, E, ν, in the calculation of the compressibility factors.

This paper examines the effect of soil compressibility on the ultimate bearing capacity of shallow foundations by means of small-scale model tests (4) carried out on two frictional soils having identical shear strength characteristics, c, ϕ, but different deformation characteristics, E, ν. The tests include surface tests as well as tests with initial overburden pressure varying up to 15 psi (103 kN/m^2) on strip and circular footings.

Experimental results are compared with the available analytical methods. The influence of soil compressibility on the load-settlement behavior, and bearing capacity is assessed in light of test results.

Soil Conditions

The test medium, Chattahoochee sand, is a subangular medium sand containing traces of mica. Mixing it with 10% (by weight) mica gave a homogeneous

TABLE 1.—Classification Properties of the Test Soils

Property (1)	Sand (2)	Sand plus 10 percent mica (3)
Coefficient of uniformity	2.5	2.73
Mean diameter	0.37 mm	0.37 mm
Specific gravity	2.66	2.68
Maximum density	102.5 pcf	95.5 pcf
Void ratio at maximum density	0.615	0.76
Minimum density	79 pcf	73.5 pcf
Void ratio at minimum density	1.10	1.28

TABLE 2.—Specifications of Mica[a] Number 60, "dry ground"

Passing number (1)	Maximum specifications, as a percentage (2)
40	85 max
100	35 max
200	20 max
325	15 max

[a]United States Gypsum Company.
[b]United States Standard Sieve.
Note: Minimum density = 15 pcf.

compressible material. Its physical properties and that of Chattahoochee sand are shown in Table 1. The mica used in a dry roofing grade having the specifications in Table 2.

As in Fig. 1, the two soils have almost identical grain size distribution curves. Triaxial compression tests with volume change measurements were performed on air dry samples of both soils at an initial relative density of 70%. This same relative density was achieved by vibration in the model tests described

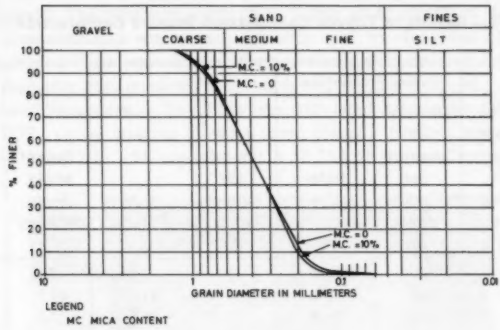

FIG. 1.—Grain Size Distribution Curves

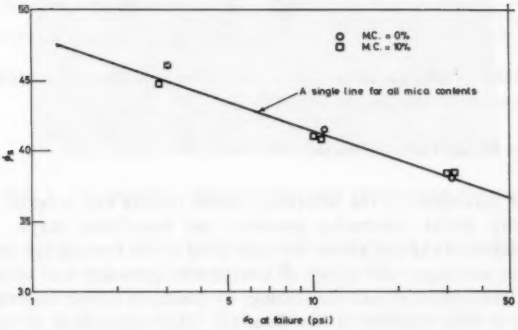

FIG. 2.—σ_o at Failure versus ϕ_s for D_r = 70% (1 psi = 6.9 kN/m²)

in the next section. Because of the curvature of the Mohr envelope, the secant angle of shearing resistance, ϕ_s, varies with the mean normal stress at failure, σ_o. A straight line uniquely determined this variation for the two soils employed herein, as in Fig. 2.

While Fig. 2 shows identical shear strength characteristics for the two cohesionless soils, their deformation characteristics varied considerably with the addition of mica. For example, the initial modulus, E_i, determined from triaxial test, $\sigma_1 - \sigma_3$, versus axial strain, ϵ, plots decreased by nearly half

by adding mica. Table 3 summarizes the strength and initial modulus values determined from the triaxial tests. Values of Poisson's ratio were calculated by means of

$$\nu = \frac{\delta\epsilon - \delta\Delta}{2\delta\epsilon} \quad \text{(1)}$$

in which ν = Poisson's ratio; Δ is the volumetric strain; and δ = incremental

TABLE 3.—Results of Triaxial Consolidated Drained Compression Tests

Test number (1)	Mica content, as a percentage (2)	Initial Properties: Density, in pounds per square foot (3)	Initial Properties: Relative density (4)	σ_3, in pounds per square inch (5)	σ_ϕ at failure (6)	Secant angle, ϕ_s, in degrees[a] (7)	E_i, in pounds per square inch (8)
1	0	94	0.70	1	2.9	47.8	1,210
2	0	94	0.70	5	11.5	41.5	3,013
3	0	93.7	0.69	15	30.9	38.0	5,000
4	10	88	0.71	1	2.8	46.4	585
5	10	87.8	0.71	5	11.3	40.8	1,350
6	10	85.9	0.65	15	31.4	38.4	2,360

[a] $\sin \phi_s = (\sigma_1 - \sigma_3)f/(\sigma_1 + \sigma_3)f$.

change. Values calculated from the initial portion of the stress-strain curves varied in a narrow range of 0.3–0.33.

Description of Model Testing Program

Significant parameters in the laboratory model footing test program were soil compressibility, initial overburden pressure, and foundation shape. Assuming that the influence of the soil above the base level of the footing can be replaced by a uniform surchage, the effect of overburden pressure was simulated by air pressure transmitted around the footings by means of rubber bags in a similar arrangement to that reported by De Beer (3). This assumption is on the safe side and implies that the shearing resistance of the overburden soils above the foundation level is ignored. Three initial overburden pressure equal to 0, 5, and 15 psi (0, 34, 103 kN/m^2) were used, the largest value is equivalent to nearly 20 ft (6.1 m) of overburden soils and represents a transition to deep conditions (Depth/Width > 4) for most foundations. A rectangular strip footing measuring 2.5 × 15 in. (63 × 381 mm) and a 4.3-in. (109-mm) diameter circular footing were employed. Duplicate tests were performed and the average results were taken. A total of 12 tests were completed for each footing at the same relative density of 70%. The footings had rough bases achieved by attaching sand paper to the base.

Test Equipment.—The program used a sand box measuring 45 × 45 × 18

in. depth (1,143 × 1,143 × 457 mm). A rigid frame mounted on the box provided reaction. A manually operated hydraulic jack (20-ton capacity, 5.06-in. stroke) applied the load. Loads were measured by a proving ring connected to the jack and the footing. Figure 3 shows a general view prior to a test with overburden pressure. Restraining steel plates attached to the box enabled application of overburden pressure by inflating rubber bags connected to the steel plates.

A regulator and a test gauge with a pressure range of 0–30 psi (0–207 kN/m^2) supplied air under controlled pressure to the rubber bags through quick fittings in the steel plate. The pressure gauge (Fig. 3) has an accuracy of ±0.25%.

Density measurements were made in each test by the sand cone method. Penetrometer soundings were also performed for density control. A small 0.5-in. (12.5-mm) diameter penetrometer was employed for this purpose.

Experimental Procedure.—To fill the box with sand having the desired relative density of 70%, equal weights of sand were placed, levelled, and vibrated for three min to form 2-in. (51-mm) layers. A V-35A (Syntron Company) vibrator

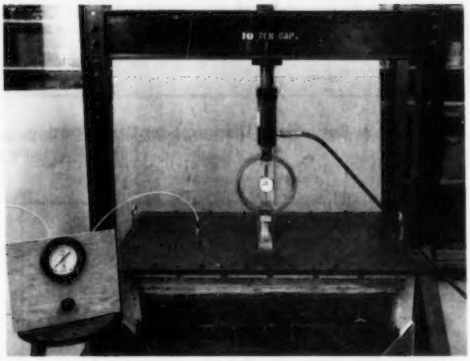

FIG. 3.—General View Prior to Test with Overburden Pressure

mounted on a 0.25-in. (6-mm) thick steel plate achieved the same relative density for both soils by using nearly the same vibrating effort.

In tests with overburden pressure, the steel plate equipped with rubber sheet was tightened to the top of the box, and air pressure applied to the desired level. Slow jacking enabled the footing to touch the soil surface and two dial gages mounted on the footing measured vertical displacements.

Equal increments of stress were applied and maintained for at least 5 min until all movements had ceased based on recorded deflection readings. Each loading increment was approximately equal to 5% of the expected ultimate pressure. Tests with high overburden pressure of 15 psi (103 kN/m^2) required additional jacking to maintain a constant stress.

Analysis and Discussion of Test Results

Ultimate Load Criterion.—Two ultimate load criteria were evaluated. The first

defines the ultimate load as the point at which the slope of the load-settlement curve first reaches zero or a minimum value. Another ultimate load criterion defines the ultimate load at the point of break of the load-settlement curve in a log-log plot (3). Both criteria require that the loading test be carried to

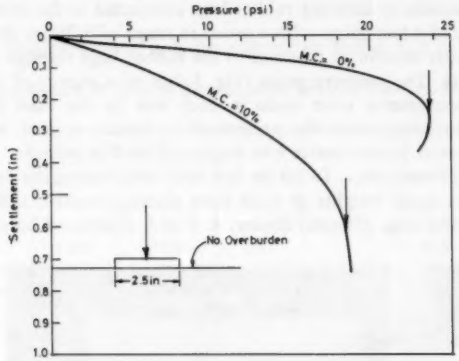

FIG. 4.—Pressure-Settlement Diagrams for Strip Footing, $q = 0$

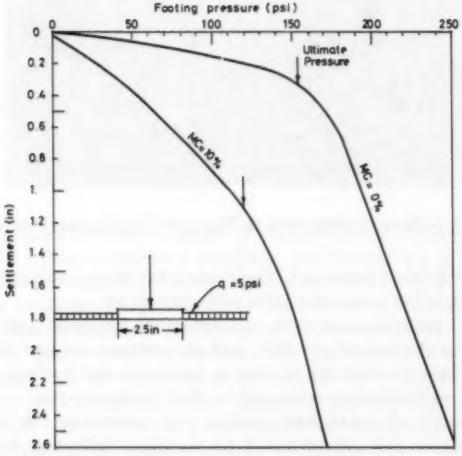

FIG. 5.—Pressure-Settlement Diagrams for Strip Footing, $q = 5$ psi (1 in. = 25.4 mm; 1 psi = 6.9 kN/m^2)

large displacements, exceeding 25% of the foundation size. Because the log-log method is more consistent it was selected to define the ultimate bearing capacity for these model tests.

Angle of Shearing Resistance.—The secant angle, ϕ_s, determined from triaxial tests was used in the analyses irrespective of the shape of the footing. Since this angle varies with the mean normal stress along the shearing surface, the

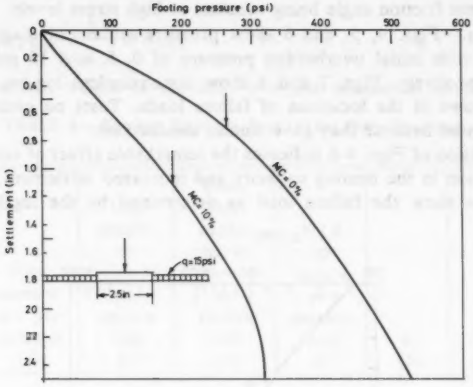

FIG. 6.—Pressure Settlement Diagrams for Strip Footing, q = 15 psi (1 in. = 25.4 mm; 1 psi = 6.9 kN/m^2)

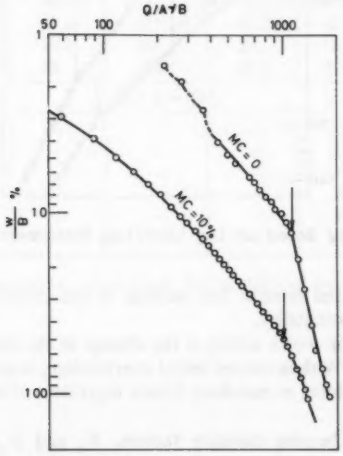

FIG. 7.—Ultimate Load Based on Log Load/Log Settlement Plot—Strip Footing, q = 5 psi

analyses employed De Beer's (2) recommendation that the bearing capacity should be made using strength characteristics corresponding to an average mean normal stress equal to

$$\sigma_o = \frac{1}{4}(q_o + 3q)(1 - \sin\phi) \quad (2)$$

in which q_o = the ultimate pressure; q = the initial overburden pressure; and ϕ = the tangent friction angle being constant at high stress levels.

Test Results.—Figs. 4, 5, and 6 show pressure-settlement diagrams for the strip footing with initial overburden pressure of 0, 5, and 15 psi (0, 34, 103 kN/m^2), respectively. Figs. 7 and 8 show dimensionless log-log plots of the data with arrows at the locations of failure loads. Tests on circular footings are not presented because they gave similar conclusions.

An examination of Figs. 4–6 indicates the remarkable effect of compressibility on the reduction in the bearing capacity and increased settlement. The arrows on the curves show the failure load as determined by the log-log criterion.

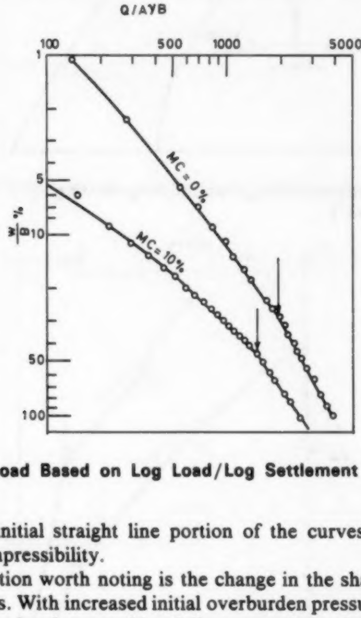

FIG. 8.—Ultimate Load Based on Log Load/Log Settlement Plot—Strip Footing, q = 15 psi

The slope of the initial straight line portion of the curves is greatly reduced with increased compressibility.

Another observation worth noting is the change in the shape of the pressure-settlement diagrams. With increased initial overburden pressure, the failure mode gradually changes to local or punching failure regardless of the relative compressibility of the soil.

To determine the bearing capacity factors, N_q and N_γ, the shape factors determined by De Beer (3) from small-scale laboratory testing were used, thus:

$$\xi_\gamma = 1 - 0.4\frac{B}{L} \quad (3)$$

$$\xi_q = 1 + \frac{B}{L}\tan\phi_s \quad (4)$$

in which ξ_γ, ξ_q are shape factors; B = width of footing; and L = length of footing.

To obtain an approximate value of $N_\gamma \xi_\gamma / 2$ from tests on the surface, the bearing capacity equation is written in the form

$$q_o = \gamma \cdot w \cdot N_q \xi_q \xi_{qd} + \frac{1}{2} \gamma B N_\gamma \xi_\gamma \quad \ldots \ldots \ldots \ldots \ldots \ldots \ldots \ldots \ldots \ldots \ldots \ldots (5)$$

in which γ = unit weight of the soil; w = the settlement of the footing at

TABLE 4.—Bearing Capacity Factors for Strip Footings

q, in pounds per square inch (1)	Mica content, as a percentage (2)	Unit weight, in pounds per square foot (3)	Bearing capacity, in pounds per square inch (4)	W/B, at failure, as a percentage (5)	ϕ_s (6)	N_γ (7)	N_q (8)
			(*a*) $\phi = \phi_s$				
0	0	95.6	24.4	10.2	45.5	336	164
0	10	87.9	18.1	24	47.7	235	107
5	0	95.1	152.1	12.7	40.0	—	23.3
5	10	87.6	121.7	45.2	40.4	—	16.9
15	0	96.1	266.2	28.1	38.2	—	13.0
15	10	88	190.1	45.4	39.0	—	9.4
			(*b*) $\phi = 38°$				
0	0	—	—	—	38	326	206
0	10	—	—	—	38	218	138
5	0	—	—	—	38	—	22.7
5	10	—	—	—	38	—	17.6
15	0	—	—	—	38	—	13.5
15	10	—	—	—	38	—	9.5

the moment of failure; and ξ_{qd} is a depth factor defined by

$$\xi_{qd} = 1 + 0.35 \frac{w}{B} \quad \ldots \ldots \ldots \ldots \ldots \ldots \ldots \ldots \ldots \ldots \ldots \ldots \ldots \ldots (6)$$

Solving for $N_\gamma \xi_\gamma$ yields

$$\frac{N_\gamma \xi_\gamma}{2} = \frac{q_o}{\gamma B} - \frac{w}{B} N_q \xi_q \xi_{qd} \quad \ldots \ldots \ldots \ldots \ldots \ldots \ldots \ldots \ldots \ldots \ldots \ldots (7)$$

Solving for N_q gives

$$N_q = \frac{q_o}{\gamma B \left(\frac{w}{B} \xi_q \xi_{qd} + \frac{N_\gamma}{2 N_q} \xi_\gamma \right)} \quad \ldots \ldots \ldots \ldots \ldots \ldots \ldots \ldots \ldots \ldots \ldots (8)$$

To determine N_q from Eq. 8, Eqs. 3, 4, and 6 are used with assumed factor N_γ in the form

$$N_\gamma = 2(N_q + 1)\tan\phi \quad \ldots\ldots\ldots\ldots\ldots\ldots\ldots\ldots\ldots\ldots\ldots\ldots (9)$$

Introducing the value, N_q, determined in this way into Eq. 7 an approximate value $N'_\gamma \xi'_\gamma/2$ of $N_\gamma \xi_\gamma/2$ is obtained.

To determine an approximate value, $N_q \xi_q$, from tests with overburden pressure, the bearing capacity equation is written

$$q_o = (q + \gamma w)\, N'_q \xi'_q \xi_{qd} + \frac{1}{2}\gamma B\, N'_\gamma \xi'_\gamma \quad \ldots\ldots\ldots\ldots\ldots\ldots\ldots\ldots (10)$$

Introducing into Eq. 10 the values $N'_\gamma \xi'_\gamma$, previously determined an approximate

TABLE 5.—Bearing Capacity Factors for Circular Footings

q, in pounds per square inch (1)	Mica content, as a percentage (2)	Unit weight, in pounds per square foot (3)	Bearing capacity, in pounds per square inch (4)	W/B, at failure, as a percentage (5)	ϕ_s (6)	N_γ (7)	N_q (8)
			(a) $\phi = \phi_s$				
0	0	95.5	14.5	3.7	47	183	85
0	10	88.3	12.9	9.2	47.3	151	69
5	0	95.5	237.9	25.3	38.7	—	22.9
5	10	87.5	178.4	45.8	39.4	—	15.6
15	0	95.7	376.6	20.6	37.3	—	13
15	10	87.7	337	42.8	37.4	—	9.4
			(b) $\phi = 38°$				
0	0	—	—	—	38	180	114
0	10	—	—	—	38	145	92
5	0	—	—	—	38	—	25.2
5	10	—	—	—	38	—	17.7
15	0	—	—	—	38	—	14
15	10	—	—	—	38	—	12.8

value, $N'_q \xi'_q$, for $N_q \xi_q$ was obtained. Values of N'_γ and N'_q were determined from $N'_\gamma \xi'_\gamma$ and $N'_q \xi'_q$ by using expressions 3 and 4 for shape factors. In a similar analysis by De Beer (3), approximate values of the bearing capacity factors were subsequently used to deduce more exact values since improper shape factors were assumed in deriving first approximate values. However, the first values were found sufficiently accurate in this analysis.

The aforementioned analysis employed the secant angle of shearing resistance ϕ_s. The bearing capacity factors were also obtained using the constant tangent friction angle $\phi = 38°$, and the results for both cases are summarized in Tables

4 and 5 for the strip and the circular footings, respectively. A comparison of the theoretical values of N_q with experimental results is shown in Fig. 9. The theoretical values are given by:

$$N_q = e^{\pi \tan\phi} \tan^2\left(\frac{\pi}{4} + \frac{\phi}{2}\right) \quad \ldots\ldots\ldots\ldots\ldots\ldots\ldots\ldots\ldots\ldots\ldots\ldots (11)$$

$$N_q^* = e^{2\pi \tan\phi/3} \tan^2\left|\frac{\pi}{4} + \frac{1}{2}\arctan\left(\frac{2}{3}\phi\right)\right| \quad \ldots\ldots\ldots\ldots\ldots\ldots\ldots\ldots\ldots\ldots (12)$$

Equation 12 represents Terzaghi's proposal (6) to use reduced shear strength parameters for soils failing in local shear.

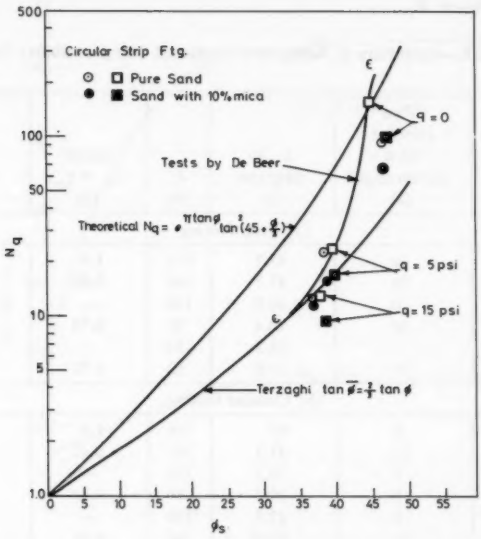

FIG. 9.—Comparison of Experimental and Theoretical Values of N_q

Test results in Fig. 9 indicate that for surface tests on incompressible soil the values of N_q are equal to or less than the theoretical values (Eq. 11). Surface tests on compressible soil with 10% mica give a value of N_q, smaller than the theoretical one, but larger than that suggested by Terzaghi for local shear failure. Thus, a flat reduction of ϕ as proposed by Terzaghi appears to be conservative for surface tests. With increased overburden pressure to 15 psi (103 kN/m^2), the bearing capacity factor, N_q, for relatively compressible soils approaches that for relatively incompressible soils, and both become closer to the Terzaghi values for local shear. This is consistent with the fact that with increased overburden pressure the mode of general shear failure disappears, and failure is of the local or punching mode, regardless of the soil compressibility.

The above data show that the effect of soil compressibility is more pronounced in surface tests as compared to tests with initial overburden pressure. For the latter with moderate overburden pressure, the Terzaghi proposal to use reduced strength parameters is in agreement with the present measurements.

The values of the bearing capacity factor, N_γ, obtained from surface tests are summarized in Tables 4 and 5 for strip and circular footings, respectively. The values for the strip footing on compressible soil are nearly 70% of those for incompressible soils, increasing to 80% in the case of the circular footing. The value of N_γ for the strip footing on incompressible soil compares well with the theoretical value based on Eq. 11 and the analysis made by Caquot and Kerisel (1) leading to Eq. 9. As shown in Tables 4 and 5, N_γ values were not listed for tests with overburden pressure because these tests were used only to determine N_q.

TABLE 6.—Summary of Actual and Predicted Compressibility Factors

q, in pounds per square inch (1)	Mica content, as a percentage (2)	ϕ_s, in degrees (3)	I_r (4)	Actual $\xi_{\gamma c} = \xi_{qc}$ (5)	$\xi_{qc} = \xi_{\gamma c}$ (6)
		(*a*) Strip footing			
0	0	45.5	651	1.0	0.85
0	10	47.7	284	0.69	0.52
5	0	40.0	190	—	—
5	10	40.4	85	0.73	0.47
15	0	38.2	134	—	—
15	10	39.0	62	0.72	0.40
		(*b*) Circular footing			
0	0	47	516	1.0	0.9
0	10	47.3	243	0.82	0.65
5	0	38.7	196	—	—
5	10	39.4	94	0.68	0.70
15	0	37.3	139	—	—
15	10	37.4	64	0.93	0.6

Note: $\phi = \phi_s$.

So far, test results were compared with conventional plasticity theories. Now actual compressibility factors are determined and compared with the analytical factors proposed by Vesic (8). The compressibility factors, $\xi_{qc}, \xi_{\gamma c}$, are introduced in the classical equation to obtain the bearing capacity of compressible soils:

$$q_o = q\, N_q\, \xi_q\, \xi_{qd}\, \xi_{qc} + \frac{1}{2}\gamma\, B\, N_\gamma\, \xi_\gamma\, \xi_{\gamma c} \quad \ldots\ldots\ldots\ldots\ldots\ldots \quad (13)$$

The analytical values of the compressibility factors are determined from

$$\xi_{\gamma c} = \xi_{qc} = \exp\left[\left(-4.4 + 0.6\,\frac{B}{L}\right)\tan\phi + \left|\frac{(3.07\sin\phi)(\log 2\,I_r)}{1+\sin\phi}\right|\right] \quad \ldots \quad (14)$$

in which I_r = the rigidity index defined as:

$$I_r = \frac{G}{c + q \tan \phi} = \frac{E}{2(1 + \nu)(c + q \tan \phi)} \quad \ldots\ldots\ldots\ldots\ldots\ldots \quad (15)$$

This index, appearing in solutions of the problem of expansion of cavities in an infinite solid, is associated with the assumed elastic-ideal plastic behavior of soil. To compute ξ_{qc}, the rigidity index, I_r calculated, then introduced into Eq. 14. To calculate I_r, the average mean normal stress in the expansion zone is taken as the initial mean normal stress at a depth, $B/2$, below the base of the footing, and the modulus, E, corresponding to this mean normal

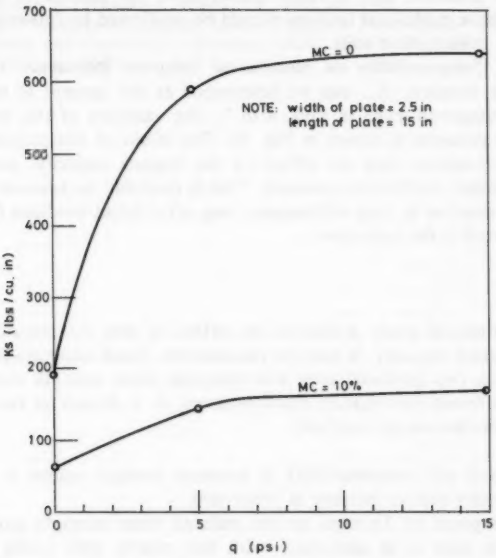

FIG. 10.—Variation of Subgrade Reaction Modulus with Overburden Pressure (1 psi = 6.9 kN/m²)

stress is determined from triaxial compression test results. The measured Poisson ratio of 0.3 was used. Examples of the computation procedure to determine the compressibility factors are given by Vesic (8). Actual compressibility factors were determined by dividing the actual bearing capacity factor for the soil by those of incompressible soil having the same secant angle of shearing resistance, ϕ_s (4). Thus, for the same overburden pressure and footing shape compressibility factors were determined from:

$$\xi_{\gamma c} = \frac{N_\gamma(\text{compressible})}{N_\gamma(\text{incompressible})}; \quad \xi_{qc} = \frac{N_q(\text{compressible})}{N_q(\text{incompressible})} \quad \ldots\ldots\ldots\ldots \quad (16)$$

For the relatively incompressible sand with no mica, the above factors are equal to unity. A summary of the results is shown in Table 6. Examination of Table 6 reveals that agreement resulted between measured and predicted compressibility factors for tests with no overburden pressure. However, tests performed with initial overburden pressure indicate generally much higher compressibility factors than predicted by Vesic's (8) method. This should be expected since this analysis was proposed for surface or near surface footings.

The results indicate that Vesic's method of analysis (8) can successfully determine the compressibility factors for shallow foundations on compressible soils. For footings with substantial overburden pressure, the method underestimates the compressibility factors. Terzaghi's method is suitable for cases with overburden pressure, and is fairly conservative for surface or near surface footings. These model test findings should be confirmed by full-scale field tests in different cohesionless soils.

Effect of Compressibility on Modulus of Subgrade Reaction.—The modulus of subgrade reaction, K_s, can be determined as the tangent to the pressure-settlement diagrams given in Figs. 4 to 7. The variation of this modulus with overburden pressure is shown in Fig. 10. The effect of compressibility on K_s is more pronounced than the effect on the bearing capacity, particularly in tests with initial overburden pressure. This is probably so because the bearing capacity is reached at large settlements, long after initial localized failures have already started in the soil mass.

Conclusions

An experimental study evaluated the effect of soil compressibility on the ultimate bearing capacity of shallow foundations. Small-scale model tests were performed on two frictional soils with identical shear strength characteristics, c, ϕ, but different deformation characteristics, E, ν. Based on test results the following conclusions are reached:

1. Increased soil compressibility at constant strength causes a decrease of bearing capacity and an increase in settlement.
2. The proposal by Terzaghi to use reduced shear strength parameters for compressible soils is in agreement with test results with initial overburden pressure, but, for surface tests, it is conservative.
3. The method proposed by Vesic to use compressibility factors in the bearing capacity formula is satisfactory for surface tests, but too conservative at high overburden stress.
4. With increased overburden pressure, the failure mode changes to local or punching failure, regardless of the soil compressibility.
5. Increased soil compressibility substantially reduces the modulus of subgrade reaction.

Appendix.—References

1. Caquot, A., and Kerisel, J., "Sur le Terme de Surface Dans le Calcul des Fondations en Milieu Pulverulent," *Proceedings*, Third International Conference on Soil Mechanics and Foundation Engineering, Zurich, Switzerland, Vol. 1, 1953, pp. 336–337.
2. De Beer, E. E., "Bearing Capacity and Settlement of Shallow Foundations on Sand,

Bearing Capacity, and Settlement of Foundations," *Proceedings of a Symposium held at Duke University*, 1965, pp. 15–34.

3. De Beer, E. E., "Experimental Determination of the Shape Factors and the Bearing Capacity Factors of Sand," *Geotechnique*, Vol. 20, No. 4, 1970, pp. 387–411.
4. Ismael, N. F., "Effect of Compressibility on the Ultimate Bearing Capacity of Shallow Foundations," thesis presented to Duke University, Durham, N.C., in 1974, in partial fulfillment of the requirement for the degree of Doctor of Philosophy.
5. Skempton, A. W., Yassin, A. A., and Gibson, R. E., "Theorie de la Force Portante des Pieux," *Annales de l'Institut Technique du Batiment et des Travaux Publics No. 63–64*, 1953, pp. 285–290.
6. Terzaghi, K., *Theoretical Soil Mechanics*, John Wiley and Sons, Inc., New York, N.Y., 1943,
7. Vesic, A., "Theoretical Studies of Cratering Mechanisms Affecting the Stability of Cratered Slopes," *Final Report*, Project No. A-655, Engineering Experiment Station, Georgia Institute of Technology, Atlanta, Ga., 1963, pp. 1–67.
8. Vesic, A. S., "Analysis of Ultimate Loads of Shallow Foundations," *Journal of the Soil Mechanics and Foundations Division*, ASCE, Vol. 99, No. SM1, Proc. Paper 9480, Jan., 1973, pp. 45–73.

PROBABILISTIC SOIL EXPLORATION: CASE HISTORY

By Tien H. Wu[1] F. ASCE and Kinfun Wong[2]

INTRODUCTION

Geotechnical engineers are familiar with the uncertainties associated with the evaluation of soil properties and inaccuracies in analytical methods. Casagrande explained the concept of these risks in his classic paper (6). The use of probability theories to assess risk and reliability of designs represents a rational approach, and recent contributions have added to the theoretical basis of reliability assessment. In slope stability analysis, studies have considered spatial variation of soil properties and inaccuracies in analysis and in measurement of soil strength (12,16,18,19). However, it is important to note that most failures in geotechnical construction were initiated by failure modes not anticipated during design (14). Often these failure modes were related to undetected weaknesses in the subsoil. Thus, one major source of uncertainty lies in the interpretation of data from subsoil exploration emphasized by Terzaghi (17) many years ago. Probability methods are helpful in the evaluation of this uncertainty.

A major problem in the interpretation of data from soil exploration is the classification of soils at the observed points and the use of this information to draw inferences about soils at unobserved points (4,5). Baecher (4) has introduced the concept of a probabilistic map, in which we associate probabilities with the materials that may exist at various locations. Such maps would allow us to obtain discrete distributions of significant soil properties such as strength or compressibility, which in turn may be used to estimate risk or reliability.

This paper describes the use of probability methods to interpret information obtained from borehole samples at different stages of a soil exploration program. It addresses the special problem of probable failure caused by the presence of a weak layer. As an illustration, data from the embankment failure at Cleveland (21) is used to construct a hypothetical case history. Opinions of several

[1]Prof. of Civ. Engrg., Ohio State Univ., Columbus, Ohio.
[2]Grad. Research Assoc., Ohio State Univ., Columbus, Ohio.

Note.—Discussion open until May 1, 1982. To extend the closing date one month, a written request must be filed with the Manager of Technical and Professional Publications, ASCE. Manuscript was submitted for review for possible publication on January 7, 1981. This paper is part of the Journal of the Geotechnical Engineering Division, Proceedings of the American Society of Civil Engineers, ©ASCE, Vol. 107, No. GT12, December, 1981. ISSN 0093-6405/81/0012-1693/$01.00.

professional engineers are presented as subjective probability and compared with the results of probability analysis.

Soil Exploration

Fig. 1 shows the plan of the site, and two representative cross-sections are shown in Figs. 2 and 3. Preliminary soil exploration at the site of the embankment began with borings WX7 and WX11, which were made prior to design. Standard penetration tests were made in these boreholes, and the representative samples recovered by the penetration spoon were used for classification and determination of index properties. Limited numbers of 2 in. (51 mm) Shelby tube samples also were taken from these boreholes. These were used largely for unconfined compression tests and consolidation tests. Prior to construction, Borings 2 and 2A were made from which almost continuous 3 in. (76 mm) Shelby tube samples were obtained. Unconfined compression and consolidation tests were performed

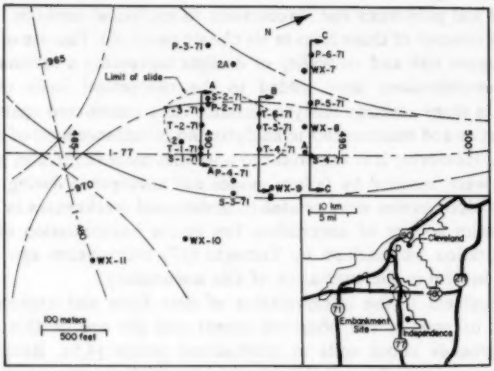

FIG. 1.—Plan of Independence Interchange

on most of these samples. The site is underlain by alternating layers of lacustrine clay and glacial till. The lacustrine clay consists of stratified silt and clay. Where the silt and clay layers are thin, the material may be called a varved clay. However, thicker layers of silt and clay have also been found (21). The data obtained from Boring 2 is shown in Fig. 2 as preliminary information for Section A-A.

In March, 1971, a slide occurred, the extent of which is shown in Fig. 1. Large horizontal displacements were also noted at section C-C. Additional borings were made as part of the investigation into the failure mechanism. Fig. 3 shows the detailed information from all the boreholes at section A-A.

Stability analysis for sections A-A and B-B was made after the failure. For a safety factor of 1, the calculated shear strength along the horizontal portions of the failure surfaces is of the order of 550 psf (26 kN/m^2). For section C-C, the calculated shear strength is of the order of 1,100 psf (53 kN/m^2).

In our hypothetical case history we address the following question: If a stability analysis, made prior to construction, had given the information that a layer with shear strength of 550 psf (26 kN/m^2) would lead to failure at section A-A and B-B, how could the soil exploration data be analyzed to access the risk due to this mode of failure? The approach presented in the subsequent sections allows one to evaluate the uncertainties at different stages of a soil exploration program and to decide at any stage whether additional exploration would be beneficial.

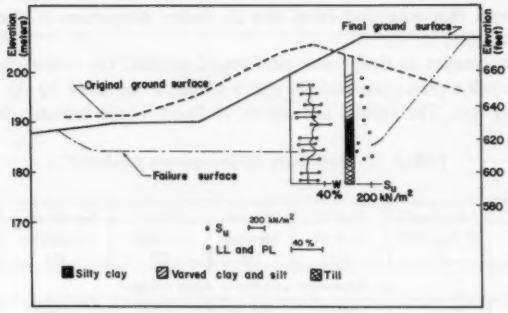

FIG. 2.—Section A-A, Preliminary Information

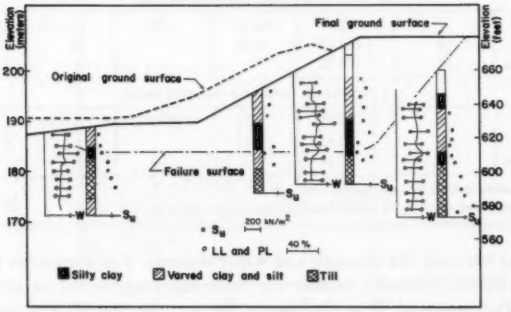

FIG. 3.—Section A-A, Detailed Information

In order to make the probability analysis, certain information about the characteristics of the subsoil must be known. In the present study, the necessary information was derived from borehole records and results of tests on samples from the embankment site and a nearby site, shown as D in Fig. 1. This information is analyzed in the next two sections. Because we have used information available at a much later date, our case history is hypothetical and primarily serves to illustrate how various sources of information can be utilized in planning soil exploration. In a real-life problem some of the information normally would

come from the engineer's previous experience with the soil deposit under consideration or other deposits of similar geologic history, or both.

Correlation with Index Properties

In many cases, including the present one, preliminary investigation emphasizes classification tests and may contain only a few strength tests. Hence, it is often necessary to estimate the strength from the index properties. A large number of unconfined compression tests have been performed on samples obtained from this area and from site D. Index properties of these samples are also available.

Linear regression analysis was performed to find the correlation between the various index properties and the shear strength measured by the unconfined compression test. The results are shown in Table 1 and indicate that the best

TABLE 1.—Summary of Regression Analyses[a]

Source of variation (1)	Degrees of freedom (2)	Sum of squares (3)	Mean squares (4)	*F*-test statistics (5)	Significance probability (6)	Correlation coefficient (7)
(*a*) Dependent variable = water content						
Model	1	903.10	903.10	82.72	0.0001	0.72
Error	80	873.40	10.92			
Corrected total	81	1,776.50				
(*b*) Dependent variable = liquid limit						
Model	1	102.63	102.63	5.59	0.0205	0.26
Error	80	1,469.09	18.36			
Corrected total	81	1,571.72				
(*c*) Dependent variable = liquidity index						
Model	1	3.71	3.71	28.46	0.0001	0.51
Error	80	10.43	0.13			
Corrected total	81	14.14				

[a]Ref. 13 provides details of analysis of variance.
Note = Independent variable = unconfined compression strength.

correlation is between the strength and water content. The variations in strength and water content primarily reflect the different proportions of silt and clay in the stratified material. It is also important to note that all the samples that show low shear strength contain mostly clay with few or no silt layers. Considering only the samples of clay, there are a total of 16 samples the shear strengths of which range from 300–1,360 psf (14–65 kN/m^2), with an average of 900 psf (43 kN/m^2).

Stratification

To estimate the probable size of a given layer, the characteristics of the stratification must be known. Necessary characteristics were obtained from undisturbed tube samples and block samples taken from the embankment site and are described in the following paragraphs.

Transition Matrices.—The variations in soil stratification can be described by Markov chains (1,7,8,9). The lacustrine deposit at the site is composed of silt and clay layers of various thicknesses. A typical example of the stratification is shown in the cross-section in Fig. 4. A vertical line drawn across such a cross-section intersects silt and clay. A vertical transition matrix is used to describe the change in material type along the vertical line. In our study, transition counts were made every 0.1 in. (2.5 mm), which was chosen as the step length in the Markov chain. The vertical transition matrix obtained from examination of the block samples and tube samples is given in Appendix I.

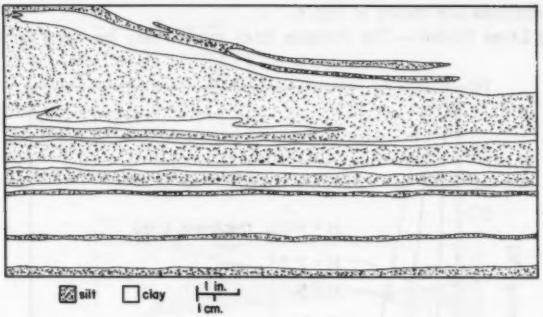

FIG. 4.—Cross-section of Cleveland Varved Clay

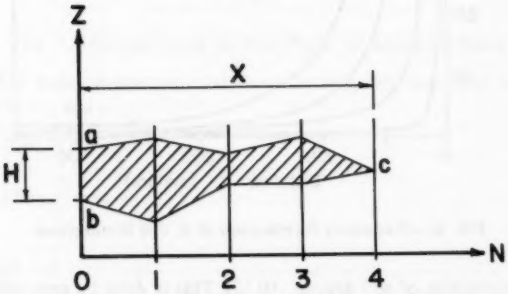

FIG. 5.—Random Walk Model of Soil Layer

Next, we consider the boundaries between silt and clay, shown in Fig. 5 as ac and bc. The undualtions in the boundaries is modeled by a horizontal transition matrix. In this matrix, the changes in the elevation of the boundary with each step, e.g. from 0 to 1, Fig. 5, are denoted by states, as listed in Appendix I. Each step in the horizontal direction covers a distance of 1 in. (2.5 mm). Block samples of the varved clay were taken and the changes in elevation of the boundaries were determined at regular intervals. From these, the horizontal transition matrix, in Appendix I, was obtained. Details of the

computations are given in Ref. 20. The horizontal transition matrix then may be used to generate soil profiles. For a clay layer with a known thickness, H, at $N = 0$ (Fig. 5), the horizontal transition martix is used to trace the paths of random walks beginning at a and b. These paths simulate, respectively, the upper and lower boundaries of the clay layer. The layer terminates at a distance, X (Point c), where the two paths meet. The procedures used to obtain the transition matrices and to generate the boundaries are described in detail (1,2).

Five hundred simulations each were used to obtain the distributions of width of clay layers with initial thicknesses of 1, 2, 4, and 6 in. (2.5, 5, 10, 15 mm). The distributions are shown in Fig. 6.

Poisson Lines Model.—The Poisson lines model may be used to simulate a

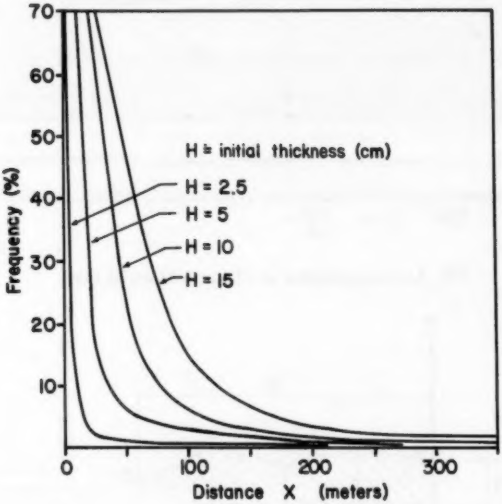

FIG. 6.—Frequency Distribution of X, 500 Simulations

vertical cross-section of soil deposit (10,15). This is done by generating random lines with density λ, on a plane. Convex polygons are formed by these lines. Next, the polygons are stretched by a stretching ratio:

$$E_u = \frac{1}{N} \sum_{i=1}^{N} \frac{\bar{W}_i}{\bar{T}_i} \quad \quad (1)$$

in which $\bar{W}_i$ = the mean width of each lithological unit within the deposit; and $\bar{T}_i$ = the mean thickness of each lithological unit within the deposit. The real plane and the stretched planes are shown in Figs. 7(*a*) and 7(*b*), respectively. Soil types are randomly assigned to the polygons based on Pi, the fraction of the soil mass that belongs to type *i*. This plane now represents a vertical

cross-section of the soil deposit. The geometry of the cross-section is represented by the elongation

$$E_s = \frac{W}{T} \quad \ldots\ldots\ldots\ldots\ldots\ldots\ldots\ldots\ldots\ldots\ldots\ldots\ldots\ldots\ldots\ldots\ldots\ldots\ldots\ldots\ldots\ldots (2)$$

in which W = width of the cross-section; and T = height of the cross-section.

A line, ab, drawn across the section shown in Fig 7(*b*), would intersect different materials at sample points spaced regularly at distance d apart. The frequency of transition from material i to material j between two sample points is denoted

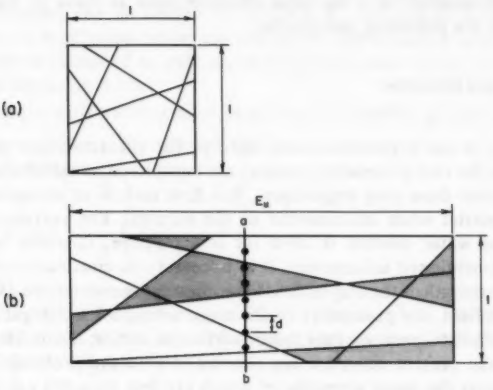

FIG. 7.—Poisson Lines: (*a*) Real Plane; (*b*) Stretched Plane

by n_{ij}. It has been shown (10) that the following relations hold between the parameters λ, P_i, and n_{ij}:

$$\lambda = d^* [\ln H - \ln (H - G)] \quad \ldots\ldots\ldots\ldots\ldots\ldots\ldots\ldots\ldots\ldots\ldots\ldots\ldots\ldots\ldots\ldots\ldots\ldots\ldots\ldots\ldots\ldots (3)$$

$$\text{in which} \quad d^* = \frac{d}{T}\frac{E_u}{E_s}; \quad \ldots\ldots\ldots\ldots\ldots\ldots\ldots\ldots\ldots\ldots\ldots\ldots\ldots\ldots\ldots\ldots\ldots\ldots\ldots\ldots\ldots\ldots (4)$$

$$H = \sum_{i=1}^{2} P_i (1 - P_i); \quad \ldots\ldots\ldots\ldots\ldots\ldots\ldots\ldots\ldots\ldots\ldots\ldots\ldots\ldots\ldots\ldots\ldots\ldots\ldots\ldots\ldots\ldots (5)$$

$$G = \frac{\sum_{i \neq j}^{2}}{\sum_{i=1}^{2} n_{ij} + \sum_{i \neq j}^{2} n_{ij}} \quad \ldots\ldots\ldots\ldots\ldots\ldots\ldots\ldots\ldots\ldots\ldots\ldots\ldots\ldots\ldots\ldots\ldots\ldots\ldots\ldots\ldots\ldots (6)$$

in which P_i and P_j = the prior probabilities that materials i and j will be found at any location.

In the present case, P_i and n_{ij} for the subsoil at the Cleveland site, were obtained from the borehole logs. The stratification revealed in the block samples

was used to estimate E_u by trial and error. Profiles of block samples were generated, using different value of E_u, and the vertical transition matrices for these profiles were determined. These were compared with the measured vertical transition matrix of the block samples. By means of hypothesis testing, the writers identified the generated cross-sections the transition matrices of which were identical with those of the block samples. The values of E_u for these cross-sections are all larger than 400. We find that $E_u > 400$ in general agrees with the distribution in width obtained by simulation (Fig. 6) which shows that E_u is of the order of 1,000 or larger for $T = 2$ in. (51 cm).

Since the soft material is composed primarily of clay (21), it is assumed that their dimensions have the same characteristics as those of the clay layers described in the preceding paragraphs.

Recognition and Detection

We return to our hypothetical case history. The characteristics of the deposit described in the two preceeding sections are considered as information available to the engineer from past experience. The first task is to recognize or detect the soft material when encountered in the borings. The correlation between strength and water content is used for this purpose. In order to make use of the aforementioned information, it is necessary to construct a model of the variation in strength of the clay layers. If we consider the variations as fluctuations of a random field, the probability of the mean strength $\bar{s} \leq 550$ psf (26 kN/m^2) along the horizontal portion of the failure surface in section AA or BB is extremely small. For the present case, we are concerned with the probable presence of soft clay layers the mean strengths of which are less than 550 psf (26 kN/m^2). Then, a more conservative model would be one that contains clay layers having different mean strengths. We assume that the samples with strengths between 300 and 850 psf (14 and 41 kN/m^2), the mean of which is 550 psf (26 kN/m^2), to represent the soft clay. All other soils are considered as the stiff material. The assumption is arbitrary or, more precisely, inductive (5), and it is important to note the subjective nature of the model. In a real problem, this represents the engineer's choice of an appropriate model for the failure mode based on his experience and judgment. After the model has been chosen, we proceed to the deductive process by which a material can be classified.

Decision Criterion.—In order to distinguish a soft material from a stiff material according to their water contents, a decision criterion is needed. Criteria frequently used in decision theory include the maximum likelihood criterion, Neyman-Pearson criterion, probability of error criterion, and Bayes risk criterion (11). In this study, the maximum likelihood criterion was employed because it is simple and does not involve the prior probability or the cost associated with decision making.

Suppose we have a single observation, z, which may be classified as belonging to class 1 or 2. Then, the decision statements are d_1: z is classified as belonging to 1; and d_2: z is classified as belonging to 2.

The likelihood function, $L(z|i)$ $(i = 1, 2)$ is defined as the probability that the random observation will take on a value, z, given that the state of nature is i. This probability is evaluated from a probability density function which

depends on certain parameters. Furthermore, the likelihood ratio is defined as

$$\Delta(z) = \frac{L(z|1)}{L(z|2)} \quad \ldots\ldots\ldots\ldots\ldots\ldots\ldots\ldots\ldots\ldots\ldots\ldots\ldots\ldots (7)$$

The maximum likelihood criterion states that if $\Delta(z) > 1$, choose d_1; if $\Delta(z) < 1$, choose d_2.

The water contents are taken to be normally distributed. The mean and standard deviation of water contents for the soft material are 30.6% and 1.9%, respectively; and those for the stiff material are 23.2% and 5.1%, respectively. Then the decision statements can be written as follows: d_1: the sample is classified as soft material (1) with mean water content 30.6% and standard deviation 1.9%; d_2: the sample is classified as stiff material (2) with mean water content 23.2% and standard deviation 5.1%.

Thus, a sample with water content equal to z is classified as soft clay if

$$\frac{L(z|1)}{L(z|2)} = \frac{(5.1)\exp\left[-\frac{1}{2}\left(\frac{z-30.6}{1.9}\right)^2\right]}{(1.9)\exp\left[-\frac{1}{2}\left(\frac{z-23.2}{5.1}\right)^2\right]} > 1 \quad \ldots\ldots\ldots\ldots\ldots\ldots (8)$$

This gives 27.5% as the dividing line between class 1 and class 2. Applying this decision criterion to the borings drilled before the slide, we identified the soil at elevation 610 ft (186 m) in Boring 2 and elevation 560 ft (168 m) in Borings WX-8, WX-10, and WX-11 as the soft material.

Inference: Probable Size of Soft Layer

Having identified the soft layer in the boring log and knowing the characteristics of stratification, the next question is: What are the sizes of the layers? Or, what fractions of the potential failure surfaces in sections AA, BB, and CC are composed of this material? Here we note again that the low strengths are attributed to the presence of thick layers of clay. Thus, the size of the soft layer can be treated as the size of clay layers with thickness exceeding some minimal value that will allow a low strength to be measured. Then the Poisson lines model may be used to derive a simple proximity rule.

Proximity Rule.—Proximity rules are based on the assumption that materials at locations close together are more likely to be of the same class than those at locations far apart. The probability that the material at a location is of class i, given that an observation at distance d from the location reveals material of class i, can be expressed as (4,15)

$$P[i|i(d)] = P_i + (1 - P_i)e^{-\lambda d} \quad \ldots\ldots\ldots\ldots\ldots\ldots\ldots\ldots\ldots\ldots (9)$$

in which P_i = prior probability that class i material is found; λ = parameter obtained from Poisson lines model, and

$$\sum_k P[k|i(d)] = 1.0 \quad \ldots\ldots\ldots\ldots\ldots\ldots\ldots\ldots\ldots\ldots\ldots\ldots\ldots\ldots (10)$$

in which k = different classes of material. For a two class problem

$$P[i|i(d)] + P[j|i(d)] = 1 \quad \ldots\ldots\ldots\ldots\ldots\ldots\ldots\ldots\ldots\ldots \quad (11)$$

in which i and j are classes. Eq. 9 shows that at a location next to the observation point ($d \to 0$), the conditional probability that the material is of the same class tends to 1.0. At a location far from the observation point ($d \to \infty$), the conditional probability tends to the prior probability that the material is of class i.

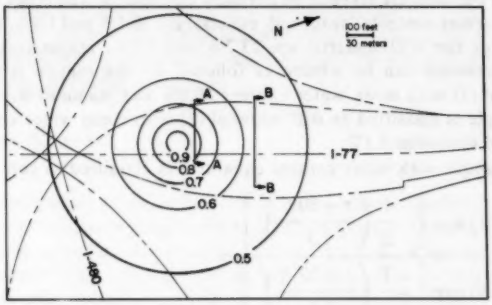

FIG. 8.—Probability Contours for Soft Layer near Elevation 610 ft (186 m) Constructed from Preliminary Information. Numbers Indicate Probabilities that Soft Layer may be Present

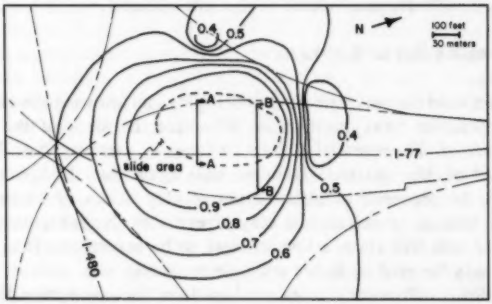

FIG. 9.—Probability Contours for Soft Layer near Elevation 610 ft (186 m) Constructed from Detailed Information Numbers Indicate Probabilities that Soft Layer may be Present

Probability Contours.—The proximity rule then is used to establish lines of equal probability that a certain material may exist. Such a probability contour map is based on the assumption that soil layers extend horizontally. Borehole locations are considered as observation points. At other locations, the unobserved points, the conditional probability that a material may exist depends on whether it is found at the observation points. By Bayes' theorem, the posterior probability

that the material is of class i is given by (4)

$$P_i' = \frac{P_i L(k|i)}{\sum_i P_i L(k|i)} = \frac{P_i \prod_{x=1}^{r} P[k|i(d)]}{\sum_i P_i \prod_{x=1}^{r} P[k|i(d)]} \quad \ldots\ldots\ldots\ldots\ldots\ldots\ldots\ldots (12)$$

in which P_i = prior probability that class i material exists; $L(k|i)$ = likelihood

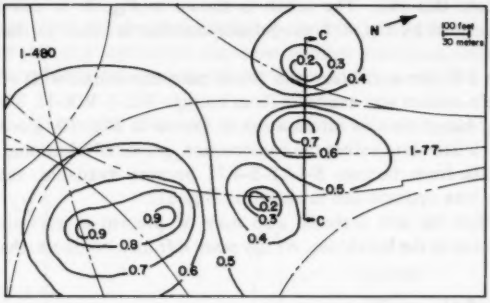

FIG. 10.—Probability Contours for Soft Layer near Elevation 560 ft (171 m) Constructed from Preliminary Information. Numbers Indicate Probabilities that Soft Layer may be Present

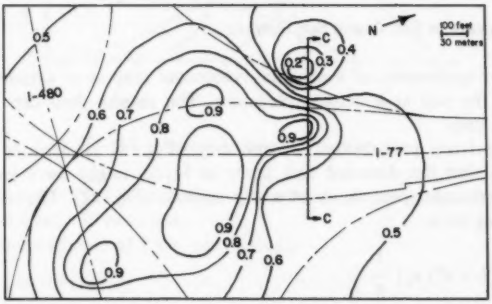

FIG. 11.—Probability Contours for Soft Layer near Elevation 650 ft (186 m) Constructed from Detailed Information. Numbers Indicate Probabilities that Soft Layer may be Present

that the material belongs to class k at an observation point if the material is of class i at an unexplored location; $P[k|i(d)]$ = conditional probability function that material is k at observation point x as defined by Eqs. 9–11; k = material type at observation point; $x = 1, 2, \ldots, r$; and r = total number of observation points. The necessary subsoil properties are P_i and λ, which includes the term

E_u. A value of E_u = 2,000 was chosen as a conservative estimate after consideration of the values of E_u given in the preceding section. The value of P_i was determined by noting the proportions of soft clay encountered in samples from the preliminary borings.

First, consider the soft layer near elevation 610 ft (186 m) at sections AA and BB. Boring 2 is the only source which provides preliminary information on this layer. The probability contours based on this information are shown in Fig. 8. The data from borings T-1-71–T-6-71, P-2-71–P-5-71, and S-1-71–S-4-71, which were made after the slide, were considered as detailed information and used to update this plot. The result is shown in Fig. 9. It can be seen that the region defined by the 90% probability contour is close to the actual slide area.

At section CC, the soft layer was found near elevation 560 ft (171 m). Prior to design, information was available from borings WX-7–WX-11. The probability contour map based on this information is shown in Fig. 10. Boring A, which was drilled at a later date before the construction, provided additional information. After the data from borings S-1-71–S-4-71 became available, the probability contour map was updated and is shown in Fig. 11.

We note that the soft material also may be present at elevations where it was not detected in the boreholes. At any point d from a borehole, that probability is

$$P[i|j(d)] = P_i(1 - e^{-2\lambda d}) \quad \ldots \quad (13)$$

The calculations are similar to those just described and are not repeated here. In this paper, the writers concentrate on the layers detected at elevation 610 and 560 ft (186 and 170 m) to illustrate the proposed method.

Average Strength of Soil Along Slip Surface

One major application of a probability contour map is to estimate the shear strength of the soil at a certain elevation. The results then can be used for stability analysis.

The preliminary probability contour map (Fig. 8) is used to obtain the probabilities that the detected soft layer or layers might have length $\ell > \ell_1$ along the horizontal portion ab of a slip surface (Fig. 12). The average shear strength along ab is

$$\bar{s} = [\ell s_1 + (L - \ell)\, s_2]\, \frac{1}{L} \quad \ldots \quad (14)$$

in which s = shear strength; the subscripts 1 and 2 refer to soft and stiff materials, respectively; and L = distance ab. Stability calculations have shown that the critical slip surface does not change appreciably with changes in ℓ. Thus, L may be taken as constant and

$$f_s(\bar{s}) = f_\ell\left(\frac{\bar{s} - s_2}{s_1 - s_2}\right) L\left(\frac{L}{s_1 - s_2}\right) \quad \ldots \quad (15)$$

If the strengths of the soft and stiff materials are taken to be equal to their mean values of 550 psf and 2,500 psf (25 and 120 KN/m^2), respectively, and

the variation in strength within the soft and stiff layers is ignored, then the probability of failure equals the probability that $\ell = L$. Then, $P_f = 0.64$, according to the probability contours in Fig. 7. To include the contributions of strength variations within layers, it is necessary to consider the joint distribution of ℓ and $\bar{s}$. Calculations using Eq. 22, Appendix II, gives $P_f = 0.67$. We see that the effect of strength variations is small and may be ignored in this case. Thus, the preliminary information can provide ample warning of possible failure. By similar calculations, the probability, $P[\bar{s} \leq 1{,}100 \text{ psf}]$ along the horizontal portion of the slip surface in section CC is about 0.40, which also suggests a high failure probability.

We note that these failure probabilities pertain only to the specific failure surfaces. Since soft clay layers also may exist at other elevations, other potential failure surfaces should be considered for a complete assessment of failure probability.

The overall objective of this soil exploration is to reduce the uncertainty

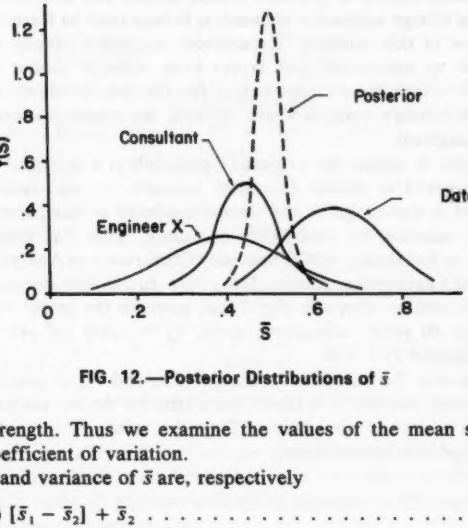

FIG. 12.—Posterior Distributions of $\bar{s}$

about the strength. Thus we examine the values of the mean strength along ab and its coefficient of variation.

The mean and variance of $\bar{s}$ are, respectively

$$E(\bar{s}) = E(f)\,[\bar{s}_1 - \bar{s}_2] + \bar{s}_2 \quad \text{(16)}$$

$$\text{Var}(\bar{s}) = \text{Var}\,[s_1 f + s_2 (1 - f)]$$

$$= [\bar{s}_1^2 + \bar{s}_2^2 + \tilde{s}_1^2 + \tilde{s}_2^2]\,\tilde{f}^2 + \bar{f}^2\,\tilde{s}_1^2 + (1 - \bar{f})^2\,\tilde{s}_2^2 \quad \text{(17)}$$

in which $f = \ell / L$; the bar and tilde over s_1, s_2, and f = the mean and standard deviation, respectively. If the strength variation within the soft and stiff layers is ignored as before, then $\tilde{s}_1$ and $\tilde{s}_2$ represents only the error due to inadequate sampling or

$$\tilde{s}_1 = \frac{\sigma_1}{\sqrt{n_1}} \quad \text{and} \quad \tilde{s}_2 = \frac{\sigma_2}{\sqrt{n_2}} \quad \text{(18)}$$

in which σ_1 and σ_2 = sample standard deviations; and n_1 and n_2 = number of samples.

For Section AA, the computed mean value, $E(\bar{s})$, and its coefficient of variation, V_s, are summarized in Table 2, (Two-class: Preliminary information). For comparison, we also show the values of $\bar{s}_1$ and $\bar{s}_2$, and the coefficients of variation obtained from $\bar{s}_1$ and $\bar{s}_2$ in Eq. 18 (Sample data: Preliminary information). The large difference in the values of V_s between Two-class: Preliminary information and sample data: Preliminary information indicates the important influence of the subsoil stratification in the evaluation of the preliminary information. When the detailed information becomes available, V_s for Two-class: Detailed information is naturally reduced, and approaches that of Sample data: Detailed information. Then, additional boreholes would not reduce the uncertainty below this level.

Professional Judgment

Since the identification of probable failure modes and the choice of subsoil models contain a large subjective element, it is important to learn the practicing engineer's view of this problem. Experienced engineers usually are aware of the risk posed by undetected soft layers even when it cannot be evaluated numerically. A safety factor, appropriate for the risk involved, is chosen on the basis of subjective opinion which reflects the engineer's experience and professional judgment.

As a first step to assess the subjective probability, a group of geotechnical engineers was asked to choose the shear strength, s_d, and factor of safety, F_{sd}, to be used in the design of the slope considered in this paper. They were also asked to estimate the probability of failure. This was done as part of the Workshop on Reliability, ASCE Specialty Conference on Analysis and Design in Geotechnical Engineering, Austin, Tex., 1974. In the first questionnaire, only the limited information shown in Fig. 2 was given to the group. A well-known consultant with 30 years' experience chose s_d = 1,000 psf (48 kN/m^2), F_{sd} = 1.5, and estimated $P_f = 0.01$.

We may consider the consultant's choice of s_d and F_{sd} to jointly reflect his overall uncertainty because it is likely that engineers do not assign quantitative values to each source of uncertainty. Then the safety factor with respect to the mean strength $\bar{s}$ is approximately

$$F_s = \frac{\bar{s}}{s_d} F_{sd} \quad (19)$$

Assuming that the safety factor has a normal distribution, the risk is

$$P_f = 1 - erf\left(\frac{F_s - 1}{\sigma_F}\right) \quad (20)$$

in which σ_F = standard deviation of F_s. If F_s is used in Eq. 20 with P_f = 0.01, we obtain the coefficient of variation, $V_F = 0.25$.

The most conservative reply, by Engineer X who had eight years of experience, consists of s_d = 1,000 psf (48 kN/m^2), $F_{sd} = 1.5$, and $P_f = 0.10$. Similar calculations were made and the results are shown in Table 2 as subjective probabilities.

In the second questionnaire, the group was given the detailed information (Fig. 3) obtained after extensive soil exploration. The well-known consultant chose s_d = 1,100 psf and 700 psf, (53 and 34 kN/m^2) for the varved clay and silty clay, respectively, F_{sd} = 1.5, and estimated P_f = 0.001. Engineer X chose s_d = 1,060 and 560 psf (51 and 26 kN/m^2) for the varved clay and silty clay, respectively, F_{sd} = 1.3, and estimated P_f = 0.10. Calculations similar to these were made and the results also are listed in Table 2.

We note that the design strengths and safety factors in the two responses are not very different and yet the two responses differ widely in the estimated P_f. However, when the results of the detailed exploration were made available, the consultant's P_f was significantly reduced. At the same time, Engineer X chose to reduce F_{sd} and design for the same P_f. Both indicate the engineers' reduced uncertainty and is reflected in the smaller values of V_F in Consultant: Detailed information and Engineer X: Detailed information, of Table 3. The

TABLE 2.—Shear Strength and Coefficients of Variation, Section AA and BB

(1)	Preliminary information (2)		Detailed information (3)		Posterior (4)	
			(*a*) Probability models			
Two-class	$E(\bar{s})$ = 1,000 psf (48 kN/m^2)	V_s = 0.51	$E(\bar{s})$ = 550 psf (26 kN/m^2)	V_s = 0.17		
Sample data	$\bar{s}_1$ = 550 psf (26 kN/m^2)	V_s = 0.27	$\bar{s}_1$ = 550 psf (26 kN/m^2)	V_{s1} = 0.17		
	$\bar{s}_2$ = 2,500 psf (120 kN/m^2)	V_{s2} = 0.14	$\bar{s}_2$ = 2,500 psf (120 kN/m^2)	V_{s2} = 0.08		
			(*b*) Subjective Probabilities			
Consultant	S_d = 1,000 psf (48 kN/m^2)	V_F = 0.25	S_d = 900 psf (43 kN/m^2)	V_F = 0.18	$\bar{s}$ = 1,000 psf (48 kN/m^2)	V_F = 0.06
	F_s = 1.5	P_f = 0.01	F_s = 1.5	P_f = 0.001		
Engineer X	S_d = 1,000 psf (48 kN/m^2)	V_F = 0.50	S_d = 820 psf (39 kN/m^2)	V_F = 0.40	$\bar{s}$ = 1,000 psf (48 kN/m^2)	V_F = 0.06
	F_s = 1.5	P_f = 0.10	F_s = 1.3	P_f = 0.10		

relative reductions in V_f are both smaller than that obtained by the probability model, (Two-class: Preliminary information and Two-class: Detailed information).

We can also study an engineer's changing opinions in the design of the slope by the use of Bayes' theorem (3).

$$f''(\alpha) = k\,L(\alpha)f'(\alpha) \quad \ldots \ldots \ldots \ldots \ldots \ldots \ldots \ldots \ldots \ldots \ldots \ldots \quad (21)$$

in which $f'(\alpha)$ and $f''(\alpha)$ = prior and posterior distributions, respectively; α = paramater of the distribution; $L(\alpha)$ = likelihood function of the data for a given value of α; and k = normalization factor. In the present case, the prior probability represents the engineer's choice and estimates after he was given the preliminary information (Consultant: Preliminary information, Table 2). The detailed information, which is the sample statistics of the test results from all the boreholes in the slide area, is the same as Case 2(b). By using Eq. 21 and the relationship for conjugate distribution (3), we obtained the posterior

distributions, the means and variances of which are given in column 3, Table 2. There is almost no difference between the two posterior distributions which is plotted in Fig. 12 as C. The engineers' opinions (Consultant: Detailed information and Engineer X: Detailed information, Table 3) also are shown in Fig. 12. We note again that both the consultant's and engineer X's subjective opinions are more conservative than the posterior distribution. The reductions in V_F are smaller than that obtained by Bayes' Theorem.

It is realized that answers to a short questionnaire cannot fully express engineers' opinions and judgment. Nevertheless, it is encouraging that the engineers' opinions qualitatively are in agreement with the model estimates. The larger coefficients of variation represented by the engineers' opinions are not surprising; the engineers may have in mind other uncertainties besides the failure mode considered in this analysis. While detailed comparison is unwarranted, the limited results suggest that quantitative measures of subjective probabilities can be obtained and incorporated in probability models. Research into the engineers' assessment of various uncertainties should be very rewarding, and the results should advance the adoption of probability concepts in practice.

Summary and Conclusions

Probability concepts are applied to the interpretation of soil exploration data at a site where failure in a weak layer is considered probable. The subsoil is modeled as a two-class material with soft clay layers included within a stiff clay. A hypothetical case history is constructed to illustrate the interpretation of the data obtained at different stages of the soil exploration program. The process consists of the following sequence: Detection and recognition of the soft material from limited information are based on the correlation between strength and index properties and a decision rule based on likelihood. In the next step, which represents inference, the proximity rule is used to obtain the probability that a soft layer exists at unexplored locations given that is has been detected or not detected at given explored locations. This probability then is used to obtain the probability distribution of shear strength and estimate the probability of failure.

The model of a two-class material addresses the problem of weak layers with unknown dimensions. It allows the engineer to assess the uncertainties at any stage of a exploration program and the reduction in the uncertainties as exploration progresses. The method is a useful tool but the engineer first must identify the failure mode and choose the subsoil model. This is an inductive process based largely on the engineer's judgment.

The approach used in this example is general and may be applied to other problems, such as those where the presence of a particular soil layer threatens the safety of the structure. The following summarizes the procedure to assess the risk caused by the suspected layer: (1) Calculate the dimension or dimensions of the layer that would result in a safety factor of 1; (2) use the proximity rule, Eq. 12 to calculate the probability that the layer may have the dimension or dimensions computed in step (1). This probability is equal to the failure probability. The parameters F_i and n_{ij} in Eqs. 1–6 may be evaluated from borehole records. It may be necessary to assume a value for E. A value between 100 and 500 would seem reasonable for sedimentary materials. To plan the soil

exploration program, the following additional steps should be taken; (3) determine the safety factor, or the controlling soil property such as mean shear strength, as a function of the dimension or dimensions of the layer; (4) use the proximity rule, Eq. 12, to calculate the probability distribution of the dimension or dimensions. This also gives the probability distribution of the safety factor or the soil property; (5) calculate the variance, or coefficient of variation, of the safety factor or the soil property; (6) repeat steps (3)–(5) as new data are obtained from boreholes. The progressive decrease of the variance with increasing data measures the reduction in uncertainty. Cost effectiveness requires that the cost of additional exploration be worth the reduction in uncertainty.

Acknowledgment

The writers are grateful to the National Science Foundation for the support of this research under its Grant ENG 76-20852, and to G. Baecher for his review and criticism of the manuscript. E. M. Ali provided valuable assistance with the calculations.

Appendix I.—Transition Matrices

Vertical transition probability matrix:

	clay	silt
clay	0.758	0.242
silt	0.219	0.781

States in horizontal transition matrix:

State	Change in elevation, in millimeters
1	less than −8.50
2	−8.50 to −6.25
3	−6.00 to −3.75
4	−3.50 to −1.25
5	−1.00 to 1.25
6	1.50 to 3.75
7	4.00 to 6.25
8	6.50 to 8.75
9	more than 8.75

Horizontal transition probability matrix:

0.0	0.750	0.0	0.0	0.250	0.0	0.0	0.0	0.0
0.0	0.238	0.286	0.095	0.048	0.095	0.095	0.048	0.095
0.0	0.043	0.130	0.261	0.304	0.174	0.087	0.0	0.0
0.012	0.074	0.012	0.247	0.506	0.099	0.025	0.025	0.0
0.0	0.001	0.002	0.038	0.876	0.063	0.013	0.005	0.003
0.0	0.007	0.059	0.078	0.320	0.431	0.065	0.026	0.013
0.0	0.029	0.086	0.086	0.114	0.314	0.171	0.143	0.057
0.0	−0.105	0.053	0.0	0.211	0.158	0.211	0.158	0.105
0.0	0.0	0.0	0.182	0.273	0.273	0.0	0.091	0.182

Appendix II.—Probability Density Function of Mean Strength

When $\bar{s}_1$ and $\bar{s}_2$ are random variables

$$f(\bar{s}|\ell) = \frac{1}{\sqrt{2\pi}\left[\left(\frac{\ell}{L}\right)^2 \bar{s}_1^2 + \left(1-\frac{\ell}{L}\right)^2 \bar{s}_2^2\right]^{1/2}}$$

$$\exp\left\{-\frac{\left[\bar{s} - \bar{s}_1\frac{\ell}{L} - \bar{s}_2\left(1-\frac{\ell}{L}\right)^2\right]}{2\left[\left(\frac{\ell}{L}\right)^2 \bar{s}_1^2 + \left(1-\frac{\ell}{L}\right)^2 \bar{s}_2^2\right]}\right\} \quad \ldots\ldots\ldots\ldots\ldots\ldots \quad (22a)$$

in which $f(\bar{s}\,\ell) = f(\bar{s}|\ell) f(\ell)$; $\ldots\ldots\ldots\ldots\ldots\ldots\ldots\ldots\ldots\ldots$ (22*b*)

and $f(\bar{s}) = \int f(\bar{s}|\ell) f(\ell)\, d\ell$ $\ldots\ldots\ldots\ldots\ldots\ldots\ldots\ldots\ldots\ldots$ (22*c*)

The function, $f(\ell)$, is obtained from the probability contour map and the integration is carried out numerically.

Appendix III.—References

1. Ali, E. M., "Stochastic Analysis of Seepage in Heterogeneous Soils," dissertation presented to Ohio State University, at Columbus, Ohio, in 1979, in partial fulfillment of the requirements for the degree of Doctor of Philosophy.
2. Ali, E. M., Wu, T. H., and Chang, N. Y., "Stochastic Model of Flow Through Stratified Soils," *Journal Geotechnical Engineering Division*, ASCE, Vol. 106, No. GT6, 1980, pp. 593–610.
3. Ang, A. H-S., and Tang, W. H., *Probability Concepts in Engineering Planning and Design*, John Wiley and Sons, New York, N.Y., 1975.
4. Baecher, G., "Site Exploration, A Probabilistic Approach," thesis presented to the Massachusetts Institute of Technology, at Cambridge, Mass., in 1972, in partial fulfillment of the requirements for the degree of Doctor of Philosophy.
5. Baecher, G., "Analyzing Exploration Strategies, Site Characterization and Exploration," C. H. Dowding, ed., ASCE, New York, N.Y., 1978, pp. 220–246.
6. Casagrande, A., "Role of the Calculated Risk in Earthwork and Foundation Engineering," *Journal of the Soil Mechanics and Foundation Engineering Division*, ASCE, Vol. 92, No. SM4, 1965, pp. 1–40.
7. Krumbein, W. C., "Fortran Computer Programs for Markov Chain Experiments in Geology," Computer Contribution 13, Kansas Geological Survey, Lawrence, Kans., 1967.
8. Krumbein, W. C., "Fortran IV Computer Program for Simulation of Transgression and Regression with Continuous Time Markov Models," Computer Contribution 26, Kansas Geological Survey, Lawrence, Kans., 1967.
9. Krumbein, W. C., and Dacey, M. F., "Markov Chains and Embedded Markov Chains in Geology," *Journal of the International Association of Mathematical Geology*, Vol. VI, 1969, pp. 79–96.
10. Lippmann, M. J., "Two-Dimensional Stochastic Model of Heterogeneous Geologic System," dissertation presented to the University of California, Berkeley, Calif., in 1974, in partial fulfillment of the requirements for the degree of Doctor of Philosophy.
11. Melsa, J. L., and Cohn, D. L., *Decision and Estimation Theory*, McGraw-Hill, Inc., New York, N.Y., 1978.
12. Morlá-Catalán, J., and Cornell, C. A., "Earth Slope Reliability by Level-Crossing Method," *Journal of the Geotechnical Engineering Division*, ASCE, Vol. 102, No. GT6, 1976, pp. 591–604.

13. Neter, J., and Wasserman, W., *Applied Linear Statistical Models,* Richard D. Irvin, Inc., Homewood, Ill., 1974.
14. Peck, R. B., "Where Has All the Judgement Gone?," *Canada Geotechnical Journal,* Vol. 17, 1980, pp. 584–590.
15. Switzer, P., "A Random Set Process in the Plane with Markovian Property," Annals of Mathematical Statistics, Vol. 36, 1965, pp. 1859–1863.
16. Tang, W. H., and Yucemen, M. S., "Probability-Based Short Term Design of Soil Slopes," *Canada Geotechnical Journal,* Vol. 13, 1976, pp. 201–215.
17. Terzaghi, K., "Relation between Soil Mechanics and Foundation Engineering," *Proceedings,* First International Conference on Soil Mechanics and Foundation Engineering, Cambridge, Mass., Vol. 3, 1936, pp. 13–18.
18. Vanmarcke, E. H., "Probabilistic Modeling of Soil Profiles," *Journal of the Geotechnical Engineering Division,* ASCE, Vol. 103, No. GT11, 1977, pp. 1227–1246.
19. Vanmarcke, E. H., "Reliability of Earth Slopes," *Journal of the Geotechnical Engineering Division,* ASCE, Vol. 103, No. GT11, 1977, pp. 1247–1266.
20. Wong, K., "A Probabilistic Approach to Subsoil Exploration," thesis presented to Ohio State University at Columbus, Ohio, in 1980, in partial fulfillment of the requirements for the degree of Master of Science.
21. Wu, T. H., Thayer, W. B., and Lin, S. S., "Stability of Embankment on Clay," *Journal of the Geotechnical Engineering Division,* ASCE, Vol. 101, No. GT9, 1975, pp. 913–932.

Appendix IV.—Notation

The following symbols are used in this paper:

d = distance between sampling points;
d_i = decision statements;
F_s = safety factor;
f = fraction of slip surface that passes through soft material;
L = total length of slip surface;
$L(z/i)$ = probability that of observing z, given state i;
ℓ = length of portion of slip surface that passes through soft material;
n_{ij} = frequency of transition from material i to material j;
P_i = probability that material i will be found;
s_i = shear strength of material i;
$\bar{s}$ = mean shear strength;
$\bar{s}$ = standard deviation of shear strength;
T = thickness of soil layer;
V = coefficient of variation;
W = width of soil layer;
z = observation;
λ = intensity of Poisson lines; and
σ = standard deviation.

LATERAL PILE RESPONSE DURING EARTHQUAKES

By Takaaki Kagawa[1] and Leland M. Kraft, Jr.,[2] Members, ASCE

INTRODUCTION

Liquefaction and pore pressure build-up in cohesionless soils around piles during earthquakes cause the natural frequencies of soil-pile systems to decrease, the vibration amplitudes of piles to increase, and, in extreme events, superstructures to collapse, due to large pile movements and the P-Δ effects (8). Adequate seismic design criteria for pile-supported structures in liquefiable sand deposits are needed to design piles that will provide a desired level of support. Proven analysis methods, however, are not readily available to predict the seismic performance of pile-supported structures in saturated sands.

A reliable prediction of pile behavior in saturated sands requires a model that can follow pore pressure build-up during earthquake-type irregular loadings, and a rational procedure to evaluate seismic soil-pile interactions effects.

This paper describes a nonlinear numerical method for soil-pile-structure interaction in saturated sands. The method combines a liquefaction model (21) with nonlinear, seismic p-y relationships. A concept to derive nonlinear seismic p-y relationships is based on our previous studies on the seismic p-y relationships for layered soil conditions with equivalent linear soil parameters (19,20). The general validity of the method was evaluated by analyzing shaking table test results on model soil-pile-structure systems by Maruyama (31). Although the method needs further confirmation, it represents state-of-the-art technology that can be used for practical problems to assess the potential effects of soil nonlinearity and pore pressure build-up on free-field soil response and seismic soil-pile-structure interaction.

OVERVIEW OF AVAILABLE METHODS

Soil-pile interaction can be studied using foundation spring methods (51), beam-on-Winkler foundation methods (1,2,7,20,27,34,37,39,40), elastic solutions (18,23,36,50), or finite element methods (3,20,25,44). Of these methods, the beam-on-Winkler foundation method is most suited to sophisticated design

[1]Engrg. Consultant, McClelland Engrs., Inc., Houston, Tex.
[2]Mgr., Special Projects Group, McClelland Engrs., Inc., Houston, Tex.

Note.—Discussion open until May 1, 1982. To extend the closing date one month, a written request must be filed with the Manager of Technical and Professional Publications, ASCE. Manuscript was submitted for review for possible publication on January 7, 1981. This paper is part of the Journal of the Geotechnical Engineering Division, Proceedings of the American Society of Civil Engineers, ©ASCE, Vol. 107, No. GT12, December, 1981. ISSN 0093-6405/81/0012-1713/$01.00.

analyses, as the method is economical and can incorporate complex nonlinear soil-pile interaction effects. Several researchers have used the beam-on-Winkler foundation method to study nonlinear aspects of seismic soil-pile interaction (1,7,34). These studies showed that the cyclic degradation of soil-pile stiffness, due to soil-pile interaction and free-field response, was important to the pile response.

Pile response from the beam-on-Winkler foundation method totally depends on assumed soil-pile springs. Well-established procedures to determine the soil-pile springs under seismic loading conditions in the nonlinear range, however, are not at present available. Most previous studies on nonlinear, seismic soil-pile interaction adopted the lateral load-deflection (p-y) relations obtained from a limited number of pile load tests for pile-head loading conditions (42).

To expand our understanding of dynamic soil-pile springs, the writers analytically studied the fundamental characteristics of soil-pile springs under dynamic loading conditions (18,19). These studies demonstrated that the soil-pile springs are affected by the relative stiffness of the pile and soil, pile diameter, pile-head fixity condition, and excitation frequency. Also, the soil-pile springs for seismic loading conditions can differ from those for pile-head loading conditions that simulate wave loadings. Most of these factors are not adequately accounted for in the p-y relations currently used. Therefore, a need exists to establish a procedure to determine rational, nonlinear p-y relations and to study nonlinear seismic soil-pile interaction.

Method of Analysis

Analytic Model.—A typical analytic model, based on the beam-on-Winkler foundation method for this study, is shown in Fig. 1. A pile-supported structure is idealized by a single-pile system. The superstructure is represented by a series of lumped masses, connected by beams, that possess lateral degrees-of-freedom only. Flexural rigidity of the beam right above the pile head may be adjusted to simulate rotational constraint at the pile cap. The pile is discretized into segments, and each pile segment is connected to free-field soil through discrete soil-pile elements (a spring and a dashpot) (Fig. 2). These discrete elements represent: (1) Spatial variation of soil properties; (2) nonlinear stress-strain behavior of soils; (3) pore pressure build-up in the free field and around a pile; and (4) three-dimensional soil-pile interaction.

Seismic excitation to the model is provided by free-field soil displacements. Free-field soil response is obtained in a separate analysis by a nonlinear site response method, SRANG, based on effective stresses coupled with pore pressure buildup (21).

Linear p-y Relationship.—For a pile in heterogeneous and linear elastic soil layers, Kagawa and Kraft (19) showed that the soil reaction, p, at some depth on a unit pile length can be approximated by

$$p = E_s \bar{\delta}_1 y + 2\rho_s B(V_p + V_s)\frac{dy}{dt} \quad \ldots\ldots\ldots\ldots\ldots\ldots\ldots\ldots (1)$$

in which E_s = effective Young's modulus of soil; $\bar{\delta}_1$ = the average soil-pile spring coefficient invariant with depth; y = the pile displacement relative to the free field; ρ_s = the mass density of soil; B = the equivalent width of

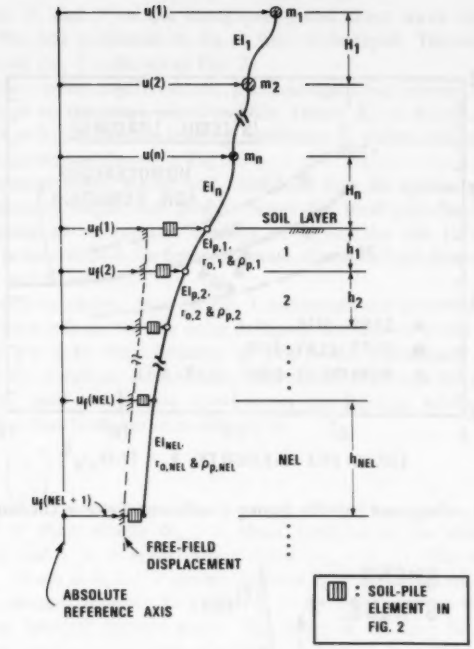

FIG. 1.—Analytic Model for Nonlinear Soil-Pile-Structure Interaction

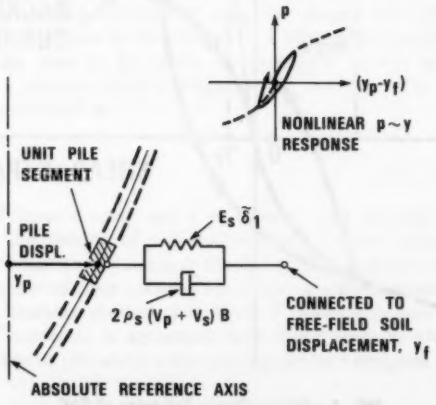

FIG. 2.—Analytic Model for Soil-Pile Element

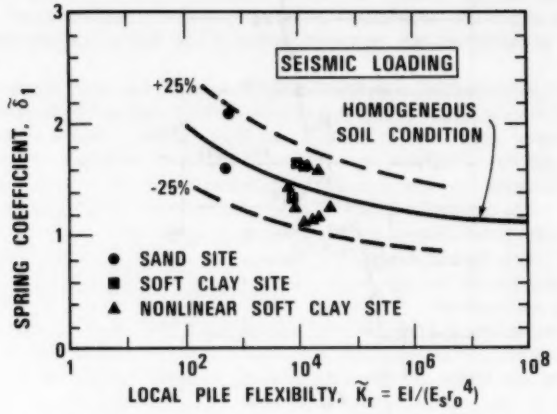

FIG. 3.—Proposed Soil-Pile Spring Coefficient, Seismic Loading

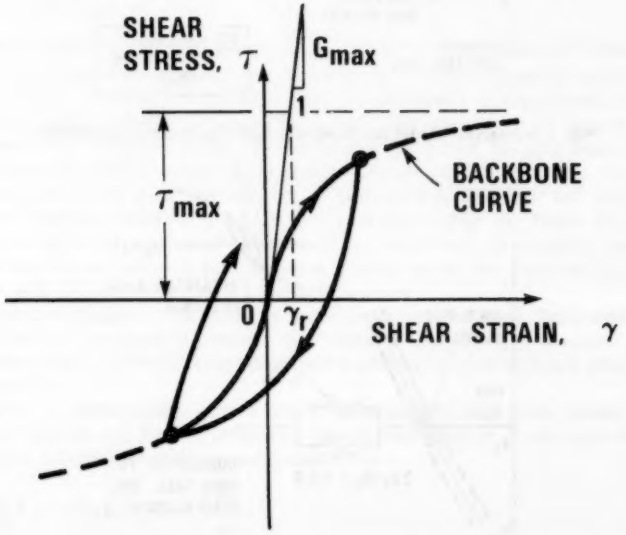

FIG. 4.—Stress-Strain Behavior of Soil

the pile; and V_p and V_s = the compression and shear wave velocities of the free-field. The soil properties in Eq. 1 vary with depth. The soil-pile element that represents Eq. 1 is shown in Fig. 2.

The soil-pile spring coefficient, $\bar{\delta}_1$, for homogeneous, elastic soil conditions, can be related to the local pile flexibility factor $\bar{K}_r = EI/(E_s r_o^4)$, as shown in Fig. 3. Since $\bar{\delta}_1$ depends on loading conditions, $\bar{\delta}_1$ values obtained for seismic loading conditions are shown in Fig. 3.

$\bar{\delta}_1$ for heterogeneous, elastic soil conditions may be approximated by those for homogeneous, elastic soil profiles when the local pile flexibility factor is evaluated using an appropriate average of E_s for the site (19). The detailed procedures to determine $\bar{\delta}_1$ for heterogeneous, elastic soil conditions are described by Kagawa and Kraft (19).

The velocity-dependent term in Eq. 1 represents the three-dimensional wave energy dissipation from the pile using dashpots that absorb plane P and S waves.

Nonlinear *p-y* with Pore Pressure in Free Field.—Nonlinear Response: To incorporate the nonlinear stress-strain behavior of soils into the *p-y* relationship in Eq. 1, we used a nonlinear stress-strain relationship, schematically shown in Fig. 4. The backbone curve is defined as

$$\tau = G_{max} F\left(\frac{\gamma}{\gamma_r}\right)\gamma \quad \text{. . . . . (2)}$$

in which τ = shear stress; G_{max} = shear modulus at low shear strain; γ = shear strain; and γ_r = reference shear strain (τ_{max}/G_{max}). The maximum shear stress, τ_{max}, is $\sin\bar{\phi}\cdot\bar{\sigma}_v/(1-\sin\phi)$, derived by considering the passive failure of the soil element adjacent to a pile. $\bar{\sigma}_v$ is the effective overburden pressure and $\bar{\phi}$ is the internal friction angle. The function, F, may be determined by conventional cyclic triaxial tests simulating the stress system around a pile and can be modeled by, for example, the hyperbolic model (10,24), the Ramberg-Osgood model (38,41,43), and the Martin-Davidenkov model (28). Unloading and reloading curves may be constructed using the Masing rule (32). High shear strain concentration occurs in the vicinity of a pile due to soil-pile interaction, and the soil strain used in Eq. 2 for the evaluation of soil stiffness around a pile must be a representative average of this variation. The average shear strain, γ, is approximated as

$$\gamma = \frac{(1+\nu)\,y}{(\bar{f}\,B)} \quad \text{. . . . . (3)}$$

in which ν = Poisson's ratio; and $\bar{f}$ = a factor that depends on the shape of loaded area, distribution of soil modulus, and relative stiffness of pile to soil, among other factors. To estimate the factor, $\bar{f}$, for typical offshore flexible piles, we used a closed-form solution for a pile in a homogeneous, elastic soil layer (18). Our analysis showed that factor $\bar{f}$ typically ranged from 2.0–3.0. This range of $\bar{f}$ values is in agreement with those used by Matlock (33) for the lateral response of pile under wave loading and by Skempton (48) for footing settlements.

Eq. 2 can be used with a Poisson's ratio to compute an average modulus, E_s. This modulus then can be combined with Eq. 1 to generate the dynamic *p-y* relationship in nonlinear soils, which is

$$p = p_1 + p_2 = 2(1+\nu)G_{max}F\left(\frac{\gamma}{\gamma_r}\right)\bar{\delta}_1 y + 2\rho_s B(V_p + V_s)\frac{dy}{dt} \quad \ldots\ldots\ldots (4)$$

This *p-y* relationship may vary along the pile length to account for vertical variations in the soil properties.

Pore Pressure Generation Model.—Soil-pile interaction is governed by the effective stress state of the soil in the immediate vicinity of the pile. The change in effective stress in the soil around the pile can differ from the change in the free-field. The change in total mean stress due to the lateral pressure, p, and the change in pore pressure, result in the change of the effective mean stress, $\Delta\bar{\sigma}_m$. The change in the normalized effective stress is

$$r = \frac{(\Delta u - \Delta\sigma_m)}{\bar{\sigma}_{v,o}} \quad \ldots\ldots\ldots (5)$$

in which $r = \Delta\bar{\sigma}_m/\bar{\sigma}_{v,o}$; $\bar{\sigma}_{v,o}$ = the initial effective overburden pressure; Δu = the induced excess pore pressure; and $\Delta\sigma_m$ = the change in total mean stress. The backbone curve in Eq. 2 can be modified, as shown in Eq. 6, to account for the change in effective stress:

$$\tau = (1-r)^{0.5} G_{max} F\left(\frac{\gamma}{\gamma_r}\right)\gamma \quad \ldots\ldots\ldots (6)$$

The change in $\Delta\sigma_m$ relative to Δu is considered small and is neglected. The degraded soil modulus in Eq. 6 then may be used in Eq. 1 to account for the soil nonlinearity effects on the *p-y* relationship.

Since the occurrence of the Niigata and Alaska earthquakes, considerable effort has been devoted to clarification of the fundamental mechanism of liquefaction (4,5,12,13,14,15,26,29,35,45,46,47,54,55,56). Although models are available to predict pore pressure response, the methods generally involve many parameters from various types of laboratory tests, and the basic rules to evaluate the pore pressure response against earthquake-type irregular loadings are not clearly defined in some models.

The model used here was simple and computationally efficient (21). According to the model, the pore pressure increase associated with a shear stress increase from τ_1 to τ_2 is represented as

$$\frac{\Delta u}{\bar{\sigma}_v} = \int_{(\tau_1/\bar{\sigma}_v)}^{(\tau_2/\bar{\sigma}_v)} \psi\, d\left(\frac{\tau}{\bar{\sigma}_v}\right) \quad \ldots\ldots\ldots (7)$$

in which Δu = pore pressure increase; τ = shear stress; and ψ = the potential function for pore pressure build-up that is determined for a given density of soil and a confining pressure. ψ is given as

$$\psi = \bar{A}\left[n(N) + f\left(\frac{u}{\bar{\sigma}_v}\right)\right]\left(\frac{\tau}{\bar{\sigma}_v}\right)^{\beta} \quad \ldots\ldots\ldots (8)$$

in which $\bar{A}$ and β = model parameters; $n(N)$ = the "memory function" that is affected only by the number of times the soil is sheared; and $f(u/\bar{\sigma}_v)$ = a function representing the change in the pore pressure generation capability of the soil caused by an increase in the pore pressure ratio, $u/\bar{\sigma}_v$.

All model parameters can be determined from conventional, cyclic, undrained simple shear or triaxial tests. The model requires only a limited number of laboratory tests and only a few model parameters. Eq. 7 can be numerically integrated to obtain pore pressure increases for irregular stress variations. Details of the model are presented elsewhere (21), but a typical comparison of measured and predicted pore pressure responses from the model is shown in Fig. 5.

In the field, drainage occurs to a certain extent, and the pore pressure redistributes with time. Seed, Martin, and Lysmer (45) studied the liquefaction characteristics of an idealized uniform sand deposit to determine the influence of drainage on the number of cycles to liquefaction. The study indicated that pore pressure dissipation had small effects on the pore pressure response for medium to fine sand deposits with the coefficient of permeability less than about 1.5×10^{-2} cm/s. Similar conclusions may be derived from the study by Finn, Lee, and Martin (5). For soil conditions with permeabilities higher than this value, the pore pressure build-up is appreciably affected by the dissipation effects, and the proposed method fails. Under these conditions, however, the

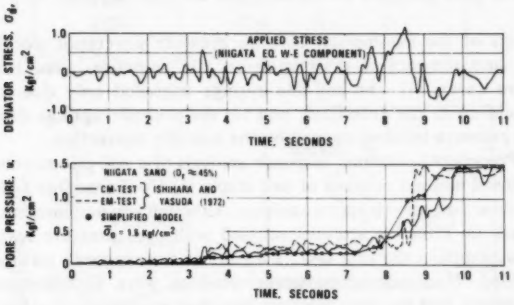

FIG. 5.—Measured and Predicted Pore Pressure for Niigata Sand and Irregular Loading, Niigata Earthquake W-E Component

pore pressure generated in the free-field and due to the soil-pile interaction dissipates rather quickly, and the impact of pore pressure build-up on pile response is expected to be small. The effects of pore pressure dissipation around a pile will be assessed in a later section, as this dissipation can be important to the pile response.

With Eq. 6, the relationship between p_1 and y reduces to

$$\frac{p_1}{2\bar{f}\,B\bar{\delta}_1} = (1-r)^{0.5}\, G_{\max}\, F(\gamma)\, \frac{(1+\nu)}{\bar{f}\,B}\, y \quad \ldots\ldots\ldots\ldots\ldots\ldots\ldots (9)$$

which represents a transformation between the p_1-y relationship and the stress-strain relationship of the soil. The soil-pile spring thus derived varies according to the nonlinear stress-strain properties of the soil.

Pore Pressure Build-up due to Soil-Pile Interaction.—During a seismic event, the soils in the vicinity of a pile may develop pore pressure in excess of that in the free-field, due solely to the soil-pile interaction. The pore pressure gradient

generated by the soil-pile interaction may be high, and rapid redistribution of the pore pressure may take place when the loading rate is slow and the permeability of the soil is high. Under these conditions, the pile response is mainly affected by the degradation of soil-pile springs due to the pore pressure build-up in the free field.

Martin, Lam, and Tsai (30) presented the results of radial dissipation of pore pressure in an idealized soil-pile system. According to their results, the rate of dissipation depends on the pile diameter, the permeability and compressibility of sand, and the loading rate. For typical values of the coefficient of compressibility (4.2×10^{-4} cm^2/N) and permeability (3×10^{-2} cm/s) for a well-drained sand, high pore pressure gradients around a pile still can be maintained for large diameter piles loaded at a period ranging from 3–7 sec. Thus, the effects of the pore pressure, developed due to the soil-pile interaction on pile response, cannot be neglected since they have the potential to impact pile response. The pore pressure generation due to the soil-pile interaction was obtained in our analytic model by assuming that the representative soil shear stress around a pile for the pore pressure assessment can be approximated by $p_1/(2\bar{f}B\bar{\delta}_1)$ in Eq. 9.

The effects of the assumption on pore pressure generation due to soil-pile interaction, and the rate of dissipation on pile response, were evaluated by studying two cases: (1) The soil-pile springs degraded only due to the pore pressure build-up in the free-field; and (2) the soil-pile springs degraded due to the pore pressure build-up caused by the soil-pile interaction.

Analysis Procedure.—Seismic response analysis of a soil-pile-structure system by the proposed method consists of two steps: (1) Nonlinear free-field analysis; and (2) nonlinear soil-pile-structure analysis. Although any nonlinear site response method based on effective stresses coupled with pore pressure response may be used to accomplish the first task, a nonlinear site response method SRANG was developed. Nonlinear stress-strain relations were approximated by the hyperbolic model, and the pore pressure response was obtained using the model presented by the writers (21).

With the computed free-field soil motion, a nonlinear soil-pile-structure interaction analysis is carried out in the time domain. At each time step, free-field soil response is read from a tape, and equations of motion of a soil-pile-structure system are established by assuming the appropriate soil-pile spring coefficient, $\bar{\delta}_1$. Since $\bar{\delta}_1$ depends on the deflected shape of the pile and the relative stiffness between the soil and pile, an iteration loop is provided to select an appropriate value of $\bar{\delta}_1$ for each time step. This iteration usually, however, is not required as $\bar{\delta}_1$ varies slowly with time and the time interval is small enough to follow this variation. After the equations of motion are solved, system properties such as soil constants, pore pressure around the pile, and the soil-pile spring coefficient are updated for the next time step. The procedure was automated into a computer program NONSPS. Time-step integration for the programs SRANG and NONSPS was performed by the unconditionally stable α-method (11).

Performance of Proposed Method

The proposed nonlinear seismic *p-y* relationships involve several simplifying assumptions to include the effect of soil nonlinearity and pore pressure build-up.

A basic assumption is related to the scaling relationship between p-y relations and stress-strain behavior of soil by the concept of average soil strain around a pile. Redistribution with time of the pore pressure generated by the soil-pile interaction is not incorporated into the relationships. The effects of these assumptions on pile response will be examined following.

Performance and validity of the proposed method should be tested using field observational data on seismic response of pile-supported structures. Avail-

TABLE 1.—p-y at Elastic and Plastic Ranges

Depth/B (1)	p/y at $y = 0$, in kilograms per square foot		p at $y = \infty$, in thousands of pounds per foot	
	Reference 42 (2)	Equation 9 (3)	Reference 42 (4)	Equation 9 (5)
1	432	1372	4.6	2.7
3	1296	2375	7.3	8.1
5	2160	3065	10.3	13.4
10	4320	4338	20.5	26.9

Note: 1 ksf = 47.8 kN/m^2; 1 kips/ft = 14.6 kN/m.

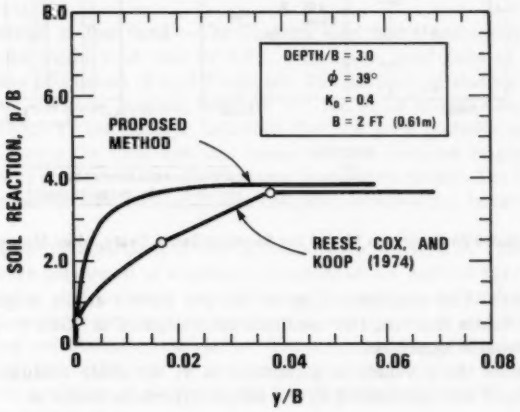

FIG. 6.—Predicted and Measured p-y Relations

able field data, however, are limited to seismic events of low intensity where the responses of pile-supported structures essentially were within the linear range. Thus, field data are not available to examine the performance of nonlinear seismic soil-pile-structure interaction methods. The proposed nonlinear p-y relations were first compared with the static p-y relations by Reese, Cox, and Koop (42), and the assumptions and performance of the seismic soil-pile interaction method presented herein were evaluated by comparing computed results with tests on a model soil-pile-structure system by Maruyama (31).

Evaluation of Nonlinear ***p-y***.—Nonlinear *p-y* relationships, using Eq. 9, were compared with those by Reese, Cox, and Koop (42). To make the comparison, the writers considered the test conditions at the Mustang Island (42): Earth pressure coefficient at rest of 0.4; angle of interal friction of 39°; coefficient of subgrade reaction of 125 pci (34,328 kN/m^3); effective unit soil weight of 66 pcf (10.5 kN/m^3); and pile diameter of 2 ft. The shear stress-strain relationships of the sand at the depth of the *p-y* evaluation were based on a maximum shear modulus, G_{max}, obtained from (10)

$$G_{max} = \frac{1{,}230\,(2.973 - e)^2\,(\bar{\sigma}_m)^{0.5}}{1 + e} \quad (10)$$

The void ratio of 0.66, used in Eq. 10, was estimated from the measured water content at the site. Using these parameters, we constructed *p-y* relationships. $\bar{f}$ was 2.5 and $\bar{\delta}_1$ was 1.2, which are typical values for piles in layered soil conditions, with soil modulus parabolically increasing with depth, loaded at

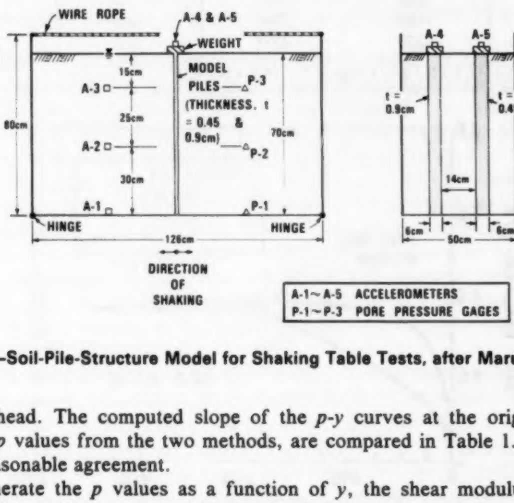

FIG. 7.—Soil-Pile-Structure Model for Shaking Table Tests, after Maruyama (31)

the pile head. The computed slope of the *p-y* curves at the origin, and the ultimate *p* values from the two methods, are compared in Table 1. The results are in reasonable agreement.

To generate the *p* values as a function of *y*, the shear modulus reduction curve in Eq. 9 was represented by the simple hyperbolic model as

$$F(\gamma) = \frac{\gamma}{\left[1 + \dfrac{G_{max}\,\gamma}{\tau_{max}}\right]} \quad (11)$$

The *p-y* relation of Eq. 9 is compared with that by Reese, Cox, and Koop (42) in Fig. 6 for a depth to pile diameter ratio of 3. Our *p-y* relation agrees reasonably well with that by Reese, Cox, and Koop (42) for small and large y/B values. Since the agreement for intermediate y/B values depends on the characteristics of the soil model used and easily can be improved by using a soil model that involves more parameters than the hyperbolic model in Eq.

11, we can conclude that Eq. 9 may be used to predict nonlinear *p-y* relationships. Further refinement of the results was not attempted here as more studies are needed to compare the performance of the proposed method in the light of field observational data. For this reason, the present study is based on the simple hyperbolic model in Eq. 11. Although the preceding comparisons are limited to the *p-y* relationship for pile-head loading conditions, the proposed *p-y* should also perform well for seismic loading conditions.

Shaking Table Tests on Model Soil-Pile Structure System.—The shaking table tests, which were carried out at the Ministry of Construction of Japan, were reported by Maruyama (31) and Hakuno, Iwasaki, and Tatsuoka (9). The steel piles of the model were 726 mm long, 60 mm wide and had a rectangular cross section. Two different thicknesses (9 and 4.5 mm) of model piles were used. Concentrated masses of 4.59 kgf for the 9 mm pile and 0.62 kgf for the 4.5 mm pile were attached at the top of the model piles.

The piles were placed in beds of pluvial deposited Toyoura sand placed at relative densities of between 20 and 50% in a 1,265 × 495 × 799 mm steel box supported on a shaking table. To eliminate the constraining effects of the side walls, they were designed to rotate freely with soil (Fig. 7).

Acceleration, pore pressure, and dynamic earth pressures were measured in the tests. Instrumentation lay-out for the tests is shown in Fig. 7. Acceleration pick-ups were equipped with light-weight stabilizers to maintain their positions during shaking.

Characteristics of Test Sand.—The Toyoura sand had a uniformity constant of 1.46, a maximum void ratio of 0.96, a minimum void ratio of 0.64, and a permeability coefficient of 0.0329 cm/sec. The duration of shaking was short and the pore pressure gradient was low for the small model. Our analysis, based on Darcy's flow theory, indicated that the pore pressure movements were small during the tests and that measured pore pressure responses were not affected by pore pressure redistributions in most test results. The hyperbolic stress-strain model was used to fit the estimated stress-strain behavior of the test sand.

Liquefaction characteristics of Toyoura sand were provided by Tatsuoka (52). The tests were performed at confining pressures of 0.5 and 1.0 kgf/cm^2, 50% relative density, and isotropic consolidation. The sand layers analyzed in this study had an average overburden pressure of 0.04 kgf/cm^2, 21 and 31% relative densities, and anisotropic consolidation. The test results by Tatsuoka (52) were modified for the difference in confining pressures, relative densities, and consolidation conditions to determine the liquefaction characteristics of the sand layers in the model tests.

Analysis of Model Test Results.—Analyses were made to predict the response of the model piles and to compare the predicted and measured responses. Although the real sand layer was three-dimensional, our analysis was made in two dimensions, and the friction between the soil and the walls parallel to the shaking direction was ignored. The rotating wall was simulated by a series of beam elements. The writers used the nonlinear plane-strain program NONPLS to compute the pore pressure response of the sand layer without the presence of the piles. Fig. 8 compares the computed and measured pore pressure responses for a typical case. Predicted pore pressure responses agree very well with test results.

Behavior of model piles in a saturated sand layer was then predicted using the free-field responses of the sand layer as input for the NONSPS analysis. The measured fundamental resonance frequency of the model piles was about 34 Hz before shaking. The soil-pile springs softened, and the measured fundamental resonance frequency of the soil-pile-structure system decreased with continued shaking to about 4 Hz, due to the pore pressure build-up in supporting soils. The frequency of the sinusoidal table input motion was 10 Hz. Therefore,

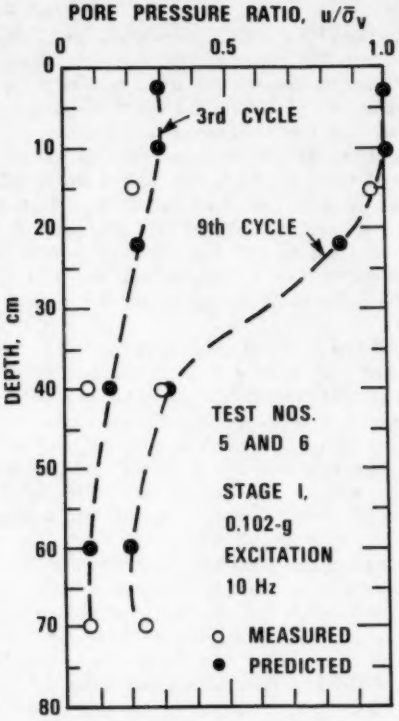

FIG. 8.—Measured and Predicted Pore Pressure Responses of Sand Layer

the model piles passed through the resonant conditions, and the soil-pile-structure system exhibited relatively large responses in the transient stage. The measured and predicted pile responses in Fig. 9 support this phenomenon. Our prediction is in good agreement with the measured data up to about three cycles at which the pile response is controlled by the elastic *p-y*. This indicates that our *p-y* relations at small *y* values are reasonable. Between three to seven cycles, however, the predicted pile response underestimated the measured results. This difference is consistent with that observed in the computed and measured resonance behavior

of the sand layer at about 10 Hz, and may be due to the possible existence of high frequency components in actual input table motions. After 7 cycles of loading, the upper one third of the sand layer liquefied and piles started to move with small constraint of soil motion. The predicted peak accelerations vary erratically after the sand layer starts to liquefy. The mean values of the histories, however, agree with the observed data. The fluctuation may be due to the lack of viscous damping to the pile provided by the liquefied sands in our analysis, and the comparison should be improved by incorporating this effect into our study.

The predicted model pile responses include the effects of pore pressure build-up in the free-field sand layer, and due to soil-pile interaction. As the upper portion of the free field was brought into liquefaction in a few cycles of loading, the pore pressure generated by the soil-pile interaction had only a small effect

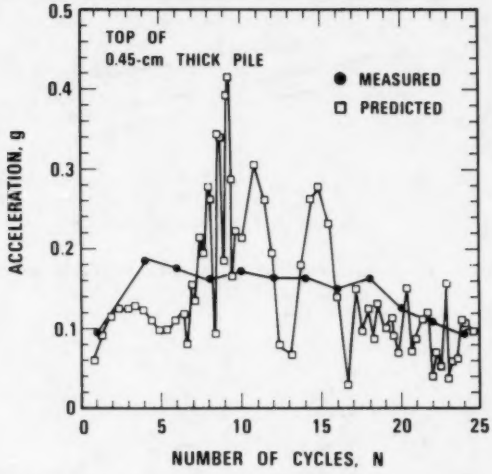

FIG. 9.—Measured and Predicted Pile Response in Liquefying Sand Layer

on the pile responses. This was confirmed by a separate analysis that included only the pore pressure build-up in the free field. Thus, the validity of the pore pressure model in the proposed soil-pile springs could not be assessed using the model test data. Pore pressure build-up in the soil around a pile, due to the soil-pile interaction, however can have a large effect on pile response, as demonstrated following. Further studies are needed to quantify this aspect of soil-pile interaction.

Significance of radiation damping on pile response was evaluated for cases with and without the damping term in Eq. 4. The radiation damping affected the pile response only in an early stage of loading.

Example Analysis

The seismic response of a typical 400 ft (122 m) water depth offshore structure

was computed with the proposed method to demonstrate the impact on pile response of pore pressure build-up in the soil around a pile. The structure was represented by a single vertical pile system the properties of which are given by Kagawa and Kraft (20). The soils at the site consist of a uniform sand depth of 400 ft (122 m). Three soil densities (D_r = 55%, 65%, and 75%) were used in the analysis. Shear moduli of the sand site were computed using the formula by Iwasaki, Tatsuoka, and Takagi (17). Liquefaction strengths of the sand used here are shown in Fig. 10. The soil motion at a depth of 400 ft (122 m) was based on the deconvoluted El Centro N-S component at a 200 ft (61 m) sand site with 85% relative density. The maximum acceleration of the base motion was 0.173 g, and the duration of shaking was 10.24 sec.

The writers first performed a nonlinear free-field analysis using the program

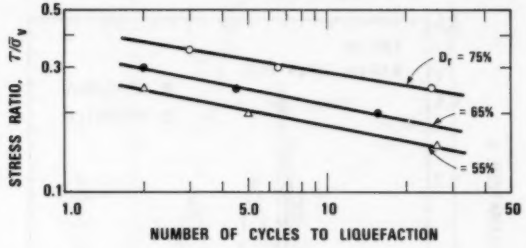

FIG. 10.—Liquefaction Strengths for Example Analysis

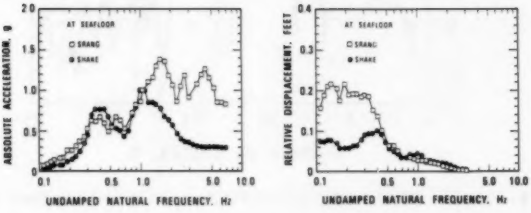

FIG. 11.—Response of Hypothetical Off-shore Sand Site (1 ft = 0.305 m)

SRANG. Fig. 11 represents the acceleration and displacement response spectra obtained from this analysis for the site with D_r = 55%. Large pore pressures developed only in the upper 15–20 ft (4.58–6.1 m). As pointed out by other investigators (6,28,49), nonlinear site response methods predict ample high frequency responses and large low frequency displacement responses, as compared with the equivalent linear method SHAKE. The results from a SHAKE analysis are also shown in Fig. 11. The difference in the high frequency response characteristics of the motions from the two methods has a relatively small impact on the response of the structure studied here with a natural frequency of 0.41 Hz. The difference in the displacement spectra at low frequencies, however, can have a large effect on the response of tall, flexible structures such as

offshore pile-supported structures in deep water.

The free-field motion obtained for the sand site was then used as input to a NONSPS analysis. Two separate NONSPS analyses were made, the first only considering the effect of pore pressure build-up in the free field, and the second also including the effect of pore pressure build-up around the pile due to soil-pile interaction.

If the pore pressure develops around the pile due to the soil-pile interaction, liquefaction may extend to about 15 to 22 pile-diameter depth, and large moment and shear can be transmitted to 10 to 25 pile-diameter depth. On the other hand, shear and moment profiles for the three soil densities were similar if the soil-pile springs only degraded due to the pore pressure build-up in the free-field. Thus, our analysis indicated that the pile response was affected more by the pore pressure build-up around the pile than by that in the free field. Fig. 12 shows a typical comparison for a 65% relative density between the shear and moment profiles for these two conditions. The pile shear is normalized by the weight of the superstructure and the pile moment is divided by the weight of the superstructure and the pile moment is divided by the weight

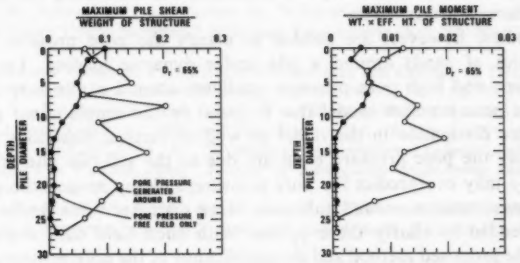

FIG. 12.—Effects of Pore Pressure around Pile on Pile Shear and Moment

times the effective height of the superstructure. The effective height was determined using the first mode vibration shape of the structure. The maximum shear and moment decrease rather rapidly with depth when the soil-pile springs degraded due solely to the pore pressure in the free-field. If the pore pressure develops around the pile due to the soil-pile interaction, the maximum shear along the pile does not occur at the same time, due to the progressive softening of the soil-pile springs. Therefore, the variation of the maximum pile shear is somewhat irregular. The same phenomenon is observed for the maximum pile moment.

Conclusions

The numerical method presented in this paper can be used to assess seismic response characteristics of off-shore as well as onshore pile-supported structures sited at saturated sand deposits. The primary feature of the proposed method is a consistent approach to determine nonlinear seismic *p-y* relationships. The pore pressure build-up effects in the free-field around a pile are included in

the proposed *p-y* relationships. The proposed method reproduced the static *p-y* relations under the pile-head loading condition by Reese, Cox, and Koop (42) with reasonable degree of agreement.

Performance and general validity of the method were examined through an analysis of shaking table tests on model soil-pile-structure systems. The pore pressure generation model in the proposed *p-y* could not be fully tested from this analysis, due to the lack of pore pressure measurement data in the vicinity of the model piles. General agreement between the predicted and measured pile responses during the liquefaction process, however, is encouraging. The proposed method provides a state-of-the-art technique to assess the potential impact of pore pressure build-up around a pile on pile response.

Using the proposed method, the writers analyzed seismic response characteristics of an idealized, off-shore, pile-supported structure at a sand site. Results indicated that the pile response can be significantly affected if pore pressure develops around a pile due to the soil-pile interaction. Shear and moment within a pile dramatically increased, due to the pore pressure build-up around the pile. The study identified the potential importance of the pore-pressure build-up around the pile, due to the soil-pile interaction, for evaluating the lateral pile responses during earthquakes.

More studies, however, are needed to clarify the pore pressure response characteristics of sands around a pile under dynamic loading. Large stress concentrations and high pore pressure gradients around a pile may invalidate a use of the pore pressure model that is based on the simple shear condition. Pore pressure dissipation in the radial as well as vertical directions along the pile can delay the pore pressure build-up, due to the soil-pile interaction. The proposed *p-y* may overpredict the pore pressure build-up around the pile. Pore pressure measurements around full-scale large diameter piles under dynamic loads are needed to clarify these points. With such field data available, the validity of the proposed method and the significance of the pore pressure build-up due to the soil-pile interaction on pile response can be fully examined.

Appendix I.—References

1. Arnold, P., Bea, R. G., Idriss, I. M., Reimer, R. B., Bebee, K. E., and Marshall, P. W., "A Study of Soil-Pile-Structure Systems in Severe Earthquakes," *Proceedings,* Offshore Technology Conference, Houston, Tex., Paper No. 2750, pp. 189–202.
2. Berger, E., Mahin, S. A., and Pyke, R., "Simplified Method for Evaluating Soil-Pile-Structure Interaction Effects," *Proceedings, Offshore Technology Conference,* Houston, Tex., Paper No. OTC 2954, pp. 589–598.
3. Blaney, G. W., Kausel, E., and Roesset, J. M., "Dynamic Stiffness of Piles, Numerical Methods in Geomechanics, C. S. Desai, ed., ASCE, New York, N.Y., Vol. 2, pp. 1001–1012.
4. Blazquez, R. M., Krizek, R. J., and Bazant, Z. P., "Site Factors Controlling Liquefaction," *Journal of the Geotechnical Engineering Division,* ASCE, Vol. 106, No. GT7, July, 1980, pp. 785–801.
5. Finn, W. D. L., Lee, K. W., and Martin, G. R., "An Effective Stress Model for Liquefaction," *Journal of the Geotechnical Engineering Division,* ASCE, Vol. 103, No. GT6, June, 1977, pp. 517–533.
6. Finn, W. D. L., Martin, G. R., and Lee, M. K. W., "Comparison of Dynamic Analyses for Saturated Sands," *Proceedings, ASCE Specialty Conference on Earthquake Engineering and Soil Dynamics,* Pasadena, Calif., pp. 472–491.
7. Finn, W. D. L., and Martin, G. R., "Aspects of Seismic Design of Pile-Supported

Offshore Platforms in Sand," *Soil Dynamics in the Marine Environment*, ASCE National Convention, Boston, Mass., Apr., 1979, (Preprint 3604).
8. Fukuoka, M., "Damage to Civil Engineering Structures," *Soils and Foundations*, Vol. 6, No. 2, 1979, pp. 45–52.
9. Hakuno, M., Iwasaki, T., and Tatsuoka, F., "Effects of Soil Liquefaction on Dynamic Behavior of Pile Foundations," *Proceedings, Specialty Session 10, 9th International Conference on Soil Mechanics and Foundation Engineering*, Tokyo, Japan, 1977, pp. 165–174.
10. Hardin, B. O. and Drnevich, V. P., "Shear Modulus and Damping in Soils: Design Equations and Curves," *Journal of the Soil Mechanics and Foundations Division*, ASCE, Vol. 98, No. SM7, 1972, pp. 667–692.
11. Hilber, H. M., Hughes, T. J. R., and Taylor, R. L., "Improved Numerical Dissipation for Time Integration Algorithms in Structural Dynamics," *Journal of Earthquake Engineering and Structural Dynamics*, Vol. 5, 1977, pp. 283–292.
12. Ishibashi, I., Sherif, M. A., and Tsuchiya, C., "Pore-Pressure Rise Mechanism and Soil Liquefaction," *Soils and Foundations*, Vol. 17, No. 2, 1977, pp. 17–27.
13. Ishihara, K., Iwamoto, S., Yasuda, S., and Takatsu, H., "Liquefaction of Anisotropically Consolidated Sand," *Proceedings, 9th International Conference on Soil Mechanics and Foundation Engineers*, Vol. 2, 1977, pp. 261–264.
14. Ishihara, K., Lysmer, J., Yasuda, S., and Hirao, H., "Prediction of Liquefaction in Sand Deposits during Earthquakes," *Soils and Foundations*, Vol. 16, No. 1, 1976, pp. 1–16.
15. Ishihara, K., Tatsuoka, F., and Yasuda, S., "Undrained Deformation and Liquefaction of Sand Under Cyclic Stresses," *Soils and Foundations*, Vol. 15, No. 1, 1975, pp. 29–44.
16. Iwasaki, T. and Tatsuoka, F., "Effects of Grain Size and Grading on Dynamic Shear Moduli of Sands," *Soils and Foundations*, Vol. 17, No. 3, 1977, pp. 19–35.
17. Iwasaki, T., Tatsuoka, F., and Takagi, Y., "Shear Moduli of Sands Under Cyclic Torsional Shear Loading," *Soils and Foundations*, Vol. 18, No. 1, 1978, pp. 39–56.
18. Kagawa, T., and Kraft, L. M., Jr., "Dynamic Characteristics of Lateral Load-Deflection Relationships of Flexible Piles," *Journal of Earthquake Engineering and Structural Dynamics*, Vol. 9, 1981, pp. 53–68.
19. Kagawa, T., and Kraft, L. M., Jr., "Lateral Load-Deflection Relationships of Piles Subjected to Dynamic Loadings," *Soils and Foundations*, Vol. 20, No. 4, 1980, pp. 19–36.
20. Kagawa, T. ,and Kraft, L. M., Jr., "Seismic *p-y* Responses of Flexible Piles," *Journal of the Geotechnical Engineering Division*, ASCE, Vol. 106, No. GT8, 1980, pp. 899–918.
21. Kagawa, T., and Kraft, L. M., Jr., "Modeling Liquefaction Process," submitted to *Journal of the Geotechnical Engineering Division*, ASCE, Vol. 107, No. GT12, 1981.
22. Kagawa, T., and Kraft, L. M., Jr., "Soil-Pile-Structure Interaction During an Earthquake," *Proceedings, Offshore Technology Conference*, Houston, Tex., 1980, Paper No. 3820, pp. 235–246.
23. Kobori, T., Minai, R., and Baba, K., "Dynamic Behavior of a Laterally Loaded Pile," *Proceedings, Specialty Session 10, 9th International Conference on Soil Mechanics and Foundation Engineering*, Tokyo, Japan, 1977, pp. 175–180.
24. Kondner, R. L., "Hyperbolic Stress-Strain Response; Cohesive Soils," *Journal of the Soil Mechanics and Foundations Division*, ASCE, Vol. 89, No. SM1, 1963, pp. 115–143.
25. Kuhlemeyer, R., "Static and Dynamic Lateral Loaded Floating Piles," *Journal of the Geotechnical Engineering Division*, ASCE, Vol. 105, No. GT2, 1979, pp. 289–304.
26. Liou, C. P., Streeter, V. L., and Richart, F. E., Jr., "Numerical Model for Liquefaction," *Journal of the Geotechnical Engineering Division*, ASCE, Vol. 103, No. GT6, 1977, pp. 589–606.
27. Liou, D. D. and Penzien, J., "Seismic Analysis of an Offshore Structure Supported on Pile Foundations," *Report No. EERC 77-25*, Earthquake Engineering Research Center, University of California, Berkeley, Calif., 1977.
28. Martin, P. P., "Non-Linear Methods for Dynamic Analysis of Ground Response," dissertation, presented to the University of California, at Berkeley, Calif., in 1975, in partial fulfillment of the requirements for the degree of Doctor of Philosophy.

29. Martin, G. R., Finn, W. D. L., and Seed, H. B., "Fundamentals of Liquefaction under Cyclic Loading," *Journal of the Geotechnical Engineering Division*, ASCE, Vol. 101, No. GT5, 1975, pp. 423–438.
30. Martin, G. R., Lam, I., and Tsai, C. F., "Pore-Pressure Dissipation During Offshore Cyclic Loading," *Journal of the Geotechnical Engineering Division*, ASCE, Vol. 106, No. GT9, 1980, pp. 981–996.
31. Maruyama, I., *Dynamic Behavior of Piles in Liquefiable Foundation Soils*, thesis, presented to Chuo University, at Tokyo, Japan, in 1977, in partial fulfillment of the requirements for the degree of Master of Science.
32. Masing, G., "Eigenspannungen und Verfestigung biem Messing," *Proceedings, 2nd International Congress of Applied Mechanics*, Switzerland, 1926, pp. 332–335.
33. Matlock, H., "Correlations for Design of Laterally Loaded Piles in Soft Clay," *Proceedings, 2nd Annual Offshore Technology Conference*, Houston, Tex., Vol. 1, 1970, pp. 577–588.
34. Matlock, H., Foo, S. H. C., and Bryant, L. M., "Simulation of Lateral Behavior Under Earthquake Motion," *Proceedings, Geotechnical Division Specialty Conference*, ASCE, Pasadena, Calif., June, 1978, pp. 600–619.
35. Mroz, Z., Noorix, V. A., and Zienkiewicz, O. C., "An Anisotropic Hardening Model for Soils and its Application to Cyclic Loading," *International Journal for Numerical and Analytical Methods in Geomechanics*, Vol. 2, 1978, pp. 203–221.
36. Nogami, T. and Novak, M., "Resistance of Soil to a Horizontally Vibrating Pile," *Journal of Earthquake Engineering and Structural Dynamics*, Vol. 5, 1977, pp. 249–261.
37. Ogata, N. and Kotsubo, S., "Seismic Force Effect on Pile Foundation," *Proceedings, Japan Earthquake Engineering Symposium*, Tokyo, Japan, 1966, (in Japanese).
38. Papadakis, C. N., Streeter, V. L., and Wylie, E. B., "Bedrock Motions Computed from Surface Seismograms," *Journal of the Geotechnical Engineering Division*, ASCE, Vol. 100, No. GT10, 1974, pp. 1091–1106.
39. Parmelee, R. A., Penzien, J., Sheffey, C. F., Seed, H. P., and Thiers, G. R., "Seismic Effect on Structures Supported on Piles Extending Through Deep Sensitive Clays," *Report* SESM 64-2, submitted to the California State Division of Highways, University of California, Berkeley, Calif., 1964.
40. Prakash, S. and Chandrasekaran, V., "Pile Foundations Under Dynamic Loads," *Symposium on Behavior of Earth and Earth Structures Subjected to Earthquakes and Other Dynamic Loads*, Roorkee, India, Vol. 1, Mar., 1973, pp. 165–173.
41. Ramberg, W., and Osgood, W. R., *Description of Stress-Strain Curves by Three Parameters*, Technical Note 902, NACA, National Advisory Committee for Aeronautics.
42. Reese, L. C., Cox, W. R., and Koop, F. D., "Analysis of Laterally Loaded Piles in Sand," *Proceedings*, Offshore Technology Conference, Houston, Tex., Paper No. OTC2080, 1974, pp. 473–484.
43. Richart, F. E., Jr., "Some Effects of Dynamic Soil Properties on Soil-Structure Interaction," *Journal of the Geotechnical Engineering Division*, ASCE, Vol. 101, No. GT12, 1976, pp. 1197–1240.
44. Roesset, J. M., and Angelides, D., "Dynamic Stiffness of Piles," *Numerical Methods in Offshore Piling*, Institute of Civil Engineers, London, England, 1979, Preprint.
45. Seed, H. B., Martin, P. P., and Lysmer, J., "Pore-Water Pressure Changes during Soil Liquefaction," *Journal of the Geotechnical Engineering Division*, ASCE, Vol. 102, No. GT4, 1976, pp. 323–346.
46. Sherif, M. A., Ishibashi, I., and Tsuchiya, C., "Pore-Pressure Prediction during Earthquake Loading," *Soils and Foundations*, Vol. 18, No. 4, 1978, pp. 19–30.
47. Shibata, T., Yukitomo, H., and Miyoshi, M., "Liquefaction Process of Sand during Cyclic Loading," *Soils and Foundations*, Vol. 12, No. 1, 1972, pp. 1–16.
48. Skempton, A. W., "The Bearing Capacity of Clays," *Building Research Congress*, Division 1, Part 3, 1951, pp. 180–189.
49. Streeter, V. L., Wylie, E. B., and Richart, F. E., Jr., "Soil Motion Computations by Characteristics Method," *Journal of the Geotechnical Engineering Division*, ASCE, Vol. 100, No. GT3, 1974, pp. 247–263.
50. Tajimi, H., "Dynamic Analysis of a Structure Embedded in an Elastic Stratum," *Proceedings, 4th World Conference on Earthquake Engineering*, Santiago, Chili, Vol. 3, 1969, pp. 54–69.

51. Tajimi, H., "Seismic Effects on Piles," *Proceedings, Specialty Session 10, 9th International Conference on Soil Mechanics and Foundation Engineering*, Tokyo, Japan, 1977, pp. 15–26.
52. Tatsuoka, F., (1980), private communication.
53. Tatsuoka, F., Iwasaki, T., and Takagi, Y., "Hysteretic Damping of Sands Under Cyclic Loading and its Relation to Shear Modulus," *Soils and Foundations*, Vol. 18, No. 2, 1978, pp. 25–40.
54. Yagi, N., "Volume Change and Excess Pore Pressure in Sands under Repeated Shear Stress," *Proceedings, Japan Society of Civil Engineers*, Vol. No. 275, 1978, pp. 79–90 (in Japanese).
55. Yoshimi, Y., and Oh-oka, H., "Influence of Degree of Shear Stress Reversal on the Liquefaction Potential of Saturated Sand," *Soils and Foundations*, Vol. 15, No. 3, 1975, pp. 27–40.
56. Zienkiewicz, O. C., Chang, C. T., and Hinton, E., "Non-Linear Seismic Response and Liquefaction," *International Journal for Numerical and Analytical Methods in Geomechanics*, Vol. 2, 1978, pp. 381–404.

Appendix II.—Notation

The following symbols are used in this paper:

$\bar{A}$ = model parameter;
B = effective width of pile;
e = void ratio;
E_s = Young's modulus of soil;
EI = flexural rigidity of pile;
$f(u/\bar{\sigma}_v)$ = pore pressure function;
$F(\gamma/\gamma_r)$ = shear modulus reduction function;
$\bar{f}$ = scaling factor between pile displacement and soil strain;
G_{max} = shear modulus at low strain;
K_o = earth pressure coefficient at rest;
$\bar{K}_r$ = local pile flexibility factor ($=EI/E_s r_o^4$);
$n(N)$ = memory function;
p = soil reaction on unit pile length;
r = pore pressure ratio ($= (\Delta u - \Delta\sigma_m)/\sigma_{v,o}$);
r_o = radius of pile;
V_p and V_s = compression and shear wave velocities of soil;
y = pile displacement relative to free field;
β = model parameter;
γ and γ_r = shear strain and reference shear strain;
$\bar{\delta}_1$ = average soil-pile spring coefficient;
ν = Poisson's ratio of soil;
ρ_s = mass density of soil;
$\bar{\sigma}_m$ = effective mean principal stress;
$\bar{\sigma}_v$ and $\sigma_{v,o}$ = effective vertical stress and initial effective vertical stress;
τ = shear stress;
ψ = potential function for pore pressure generation;
$\bar{\phi}$ = angle of internal friction;
Δu = pore pressure increase;
$\Delta\sigma_m$ = change in total mean stress; and
$\Delta\bar{\sigma}_m$ = change in effective mean stress.

TECHNICAL NOTES

Note.—Discussion open until May 1, 1982. To extend the closing date one month, a written request must be filed with the Editor of Technical and Professional Publications, ASCE. This paper is part of the Journal of the Geotechnical Engineering Division, Proceedings of the American Society of Civil Engineers, ©ASCE, Vol. 107, No. GT12, December, 1981.

Technical Notes

To provide a place within ASCE for publication of technical ideas that have not advanced, as yet, to the point where they warrant publication as a Proceedings paper in a *Journal*, the publication of Technical Notes was authorized by the Board of Direction on October 16–18, 1967, under the following guidelines:

1. An original manuscript and two copies are to be submitted to the Manager of Technical and Professional Publications, ASCE, 345 East 47th Street, New York, N.Y., 10017, along with a request by the author that it be considered as a Technical Note.
2. The two copies will be sent to an appropriate Technical Division or Council for review.
3. If the Division or Council approves the contribution for publication, it shall be returned to Society Headquarters with appropriate comments.
4. The technical publications staff will prepare the material for use in the earliest possible issue of the *Journal*, after proper coordination with the author.
5. Each Technical Note is not to exceed 4 pages in the *Journal*. As an approximation, each full manuscript page of text, tables, or figures is the equivalent of one-half a *Journal* page.
6. The Technical Notes will be grouped in a special section of each *Journal*.
7. Information retrieval abstracts and key words will be unnecessary for Technical Notes.
8. The final date on which a Discussion should reach the Society is given as a footnote with each Technical Note.
9. Technical Notes will not be included in *Transactions*.
10. Technical Notes will be included in ASCE's annual and cumulative subject and author indexes.

The manuscripts for Technical Notes must meet the following requirements:

1. Titles must have a length not exceeding 50 characters and spaces.
2. The author's full name, Society membership grade, and a footnote reference stating present employment must appear on the first page of the manuscript. Authors need not be Society members.
3. The manuscript is to be submitted as an original copy (with two duplicates) that is typed double-spaced on one side of 8-1/2-in. (220-mm) by 11-in. (280-mm) white bond paper.
4. All mathematics must be typewritten and special symbols must be properly identified. The letter symbols used must be defined where they first appear, in figures or text, and arranged alphabetically in an Appendix.—Notation.
5. Standard definitions and symbols must be used. Reference must be made to the lists published by the American National Standards Institute and to the *Authors' Guide to the Publications of ASCE*.
6. Tables must be typed double-spaced (an original ribbon copy and two duplicate copies) on one side of 8-1/2-in. (220-mm) by 11-in. (280-mm) paper. An explanation of each table must appear in the text.
7. Figures must be drawn in black ink on one side of 8-1/2-in. (220-mm) by 11-in. (280-mm) paper. Because figures will be reproduced with a width of between 3 in. (76 mm) to 4-1/2 in. (110 mm), the lettering must be large enough to be legible at this width. Photographs must be submitted as glossy prints. Explanations and descriptions must be made within the text for each figure.
8. References cited in text must be typed at the end of the Technical Note in alphabetical order in an Appendix.—References.
9. Dual units, i.e., U.S. Customary followed by SI (International System) units in parentheses, should be used throughout the paper.

SEISMIC DISPLACEMENT ANALYSIS OF EARTH DAMS

By Sarada K. Sarma,[1] M. ASCE

INTRODUCTION

In the limit equilibrium method of seismic design of earth dams, the computation of displacements during earthquakes play an important part. Since Newmark (1) presented his technique of a rigid block sliding on a plane surface, designers have tried to use it to compute the displacement of the crest during an earthquake. The sliding block technique gives displacements along a fictitious plane which is not properly defined. The definition given by Sarma (3) also is arbitrary.

There are only two kinds of surfaces along which a rigid body movement is possible. These are a plane and a circular arc. All other surfaces, such as a log spiral or a nonlinear one, cannot accommodate the rigid body mechanics of sliding. In the case of a plane surface, the sliding is purely translational; in the case of a circular arc, the sliding is purely rotational about the center of the circle. If rigid body movement is to be applied, then for all other surfaces an equivalent plane or a circular arc may be found.

Most limit equilibrium methods of stability analysis use circular arc slip surfaces, which provide a simple computational process to search for the critical surface. Therefore, displacements computed on the basis of rotation about the center of the circle are readily applicable.

Let us assume a rigid body on top of a circular arc slip surface ABC, shown in Fig. 1, which is being acted upon by an earthquake load KW in which K = a function of time. We also assume that sometime in the past a slide has been initiated, i.e. that $K(t)$ was greater than K_{co} in which K_{co} = the critical acceleration. Let G be the center of gravity of the body ABCA. O = the center of the circle with radius R. The forces acting on the body are its weight, W, the earthquake load, KW, the normal forces, N, and the shear forces, S. At the instant t, the center of gravity moves through an angle θ from G_o to G, in which G_o = the position of the center of gravity at the beginning of the movement.

We can write the equation of motion of the sliding body as

$$Wd \cos(\theta_o + \theta) + KWd \sin(\theta_o + \theta) - \Sigma SR = I\ddot{\theta} \quad \ldots\ldots\ldots\ldots\ldots (1)$$

in which I = the mass moment of inertia; and d = the distance of G from

[1] Lecturer, Civ. Engrg. Dept., Imperial College, London, England, SW7.

Note.—Discussion open until May 1, 1982. To extend the closing date one month, a written request must be filed with the Manager of Technical and Professional Publications, ASCE. Manuscript was submitted for review for possible publication on April 15, 1981. This paper is part of the Journal of the Geotechnical Engineering Division, Proceedings of the American Society of Civil Engineers, ©ASCE, Vol. 107, No. GT12, December 1981. ISSN 0093-6405/81/0012-1735/$01.00.

O. At this position of the sliding body, we can find a value K_c which satisfies

$$Wd \cos(\theta_o + \theta) + K_c Wd \sin(\theta_o + \theta) - \Sigma SR = 0 \quad \ldots\ldots\ldots\ldots\ldots (2)$$

In this equation, K_c may be a function of θ and t.

Combining Eqs. 1 and 2, we obtain

$$\ddot{\theta} = \alpha(K - K_c) \sin(\theta_o + \theta) \quad \ldots\ldots\ldots\ldots\ldots\ldots\ldots\ldots\ldots (3)$$

in which $$\alpha = \frac{Wd}{I} \quad \ldots\ldots\ldots\ldots\ldots\ldots\ldots\ldots\ldots\ldots\ldots (4)$$

The initial conditions are that

$$t = 0; \quad \theta = 0; \quad \dot{\theta} = 0 \quad \ldots\ldots\ldots\ldots\ldots\ldots\ldots\ldots\ldots\ldots (5)$$

We also can find a value of $K_c = K_{co}$, which was operative at the beginning of the slip at position G_o, which gives

$$Wd \cos\theta_o + K_{co} Wd \sin\theta_o - \Sigma S_o R = 0 \quad \ldots\ldots\ldots\ldots\ldots\ldots (6)$$

The value of K_{co} is the critical acceleration, computed from the stability analysis

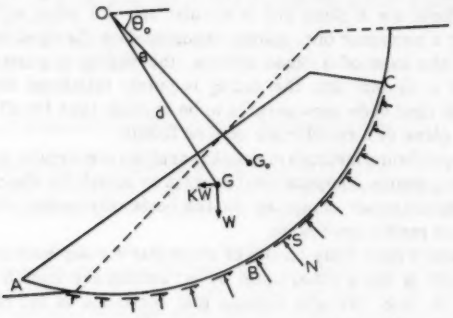

FIG. 1.—Rotational Sliding Surface

of slopes, Sarma (2). S_o = the shear stress on the slip surface at the beginning of the slip.

Assumption Case 1.—We assume that movement, θ, is small so that $K_c = K_{co}$, in which case Eq. 3 may be written as

$$\ddot{\theta} = \alpha(K - K_{co}) \sin(\theta_o + \theta) \quad \ldots\ldots\ldots\ldots\ldots\ldots\ldots\ldots\ldots (7)$$

Solution of Eq. 7 in a closed form, when K is a function of time, is not possible and numerical solutions may be devised. However, a special case of $K(t)$ may be studied.

If $K(t)$ represents a rectangular pulse so that

$$\left.\begin{aligned} K(t) &= K_m \quad \text{for} \quad 0 \le t \le T_o \\ &= 0 \quad \text{for} \quad t > T_o \end{aligned}\right\} \quad \ldots\ldots\ldots\ldots\ldots\ldots\ldots\ldots\ldots (8)$$

then, for small θ, Eq. 7 may be solved with initial conditions given by Eq. 5 to obtain

$$\theta_{max} = \frac{1}{2}\alpha(K_m - K_{co})\cdot\sin\theta_o\, T_o^2\left[\frac{K_m - K_{co}}{K_{co}}\cdot\frac{\sin\theta_o}{\sin\bar{\theta}_o} + 1\right] \quad \ldots\ldots\ldots (9)$$

in which $\bar{\theta}_o = \theta_o + \theta_{TO}$; and $\theta_{TO} = \theta$ at time T_o. Assuming that θ_{TO} is small so that $\sin\theta_o/\sin\bar{\theta}_o = 1$,

$$\theta_{max} = \frac{1}{2}\alpha\sin\theta_o K_m T_o^2\left(\frac{K_m}{K_{co}} - 1\right) \quad \ldots\ldots\ldots\ldots\ldots\ldots (10)$$

The displacement, x_m, along the arc of the circle is, therefore

$$x_m = R\theta_{max} = \frac{1}{2}R\alpha\sin\theta_o K_m T_o^2\left(\frac{K_m}{K_{co}} - 1\right) \quad \ldots\ldots\ldots\ldots\ldots (11)$$

$$\text{or} \quad \frac{x_m}{K_m g T_o^2} = \left(\frac{R\alpha\sin\theta_o}{g}\right)\frac{1}{2}\left(\frac{K_m}{K_{co}} - 1\right) \quad \ldots\ldots\ldots\ldots\ldots\ldots (12)$$

The solution in Eq. 12 is of the same form as was obtained for a sliding block on a plane surface (3), which is

$$\frac{1}{C}\frac{4x_m}{K_m g T^2} = \frac{1}{2}\left(\frac{K_m}{K_{co}} - 1\right) \quad \ldots\ldots\ldots\ldots\ldots\ldots\ldots\ldots (13)$$

$$\text{in which} \quad C = \frac{R\alpha\sin\theta_o}{g} = \frac{Rd}{r^2}\sin\theta_o; \quad \ldots\ldots\ldots\ldots\ldots\ldots (14)$$

$T = 2T_o$; and r = radius of gyration of the sliding body.

The value of Rd/r^2 for a simple geometry is shown in Fig. 2. This shows that C is approximately equal to $\sin\theta_o$ and, for all practical purposes, it will have a value between 0.5 and 1.

Looking back into the equation of motion, Eq. 7, we note that the same solution would have been arrived at if the assumption were made that for all practical purposes

$$\sin(\theta_o + \theta) = \sin\theta_o \quad \ldots\ldots\ldots\ldots\ldots\ldots\ldots\ldots\ldots (15)$$

With such an assumption, a statement may be made that displacements computed on the basis of a sliding block on a plane horizontal surface are approximately equal to the displacement along the arc of the circular sliding surface when the critical acceleration remains unchanged.

Assumption Case 2.—We assume that during sliding the shear stresses on the base of the sliding surface remain constant and are equal to those at the beginning of the slide. In this case, Eq. 2 will read

$$Wd\cos(\theta_o + \theta) + K_c W d\sin(\theta_o + \theta) - \Sigma S_o R = 0 \quad \ldots\ldots\ldots\ldots (16)$$

Using Eqs. 16 and 6 for small θ, so that $\sin(\theta_o + \theta) \simeq \sin\theta_o$, we obtain

$$K_c = K_{co} + \theta \quad \ldots\ldots\ldots\ldots\ldots\ldots\ldots\ldots\ldots\ldots (17)$$

Therefore, Eq. 3 becomes

$$\ddot{\theta} = \alpha(K - K_{co} - \theta)\sin\theta_o \quad (18)$$

Solution of Eq. 18 with initial conditions as given by Eq. 5 and for a rectangular pulse, as defined by Eq. 8, yields

$$\theta = (K_m - K_{co})[1 - \cos\sqrt{\alpha \sin\theta_o}\, t] \quad \text{for} \quad o \le t \le T_o \quad (19)$$

Eq. 19 shows that there are two possibilities. If the pulse duration,

$$T_o \ge \frac{\pi}{\sqrt{\alpha \sin\theta_o}} \quad (20)$$

then $\theta_{max} = 2(K_m - K_{co})$ (21)

which occurs during the pulse. If the duration, T_o, is small compared with Eq. 20

$$\theta_{max} = -K_{co} + \sqrt{K_{co}^2 + 2K_m\theta_{TO}} \quad (22)$$

in which θ_{TO} is given by Eq. 19 at $t = T_o$.

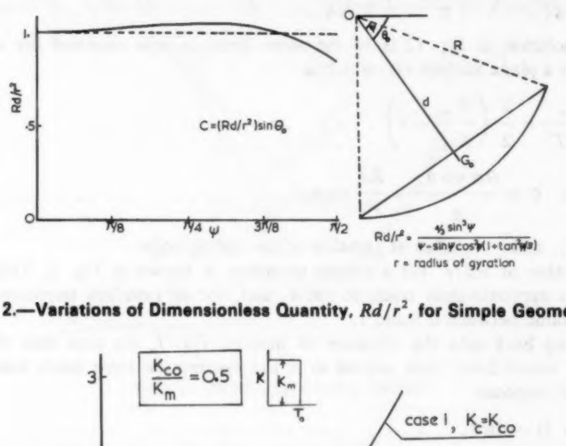

FIG. 2.—Variations of Dimensionless Quantity, Rd/r^2, for Simple Geometry

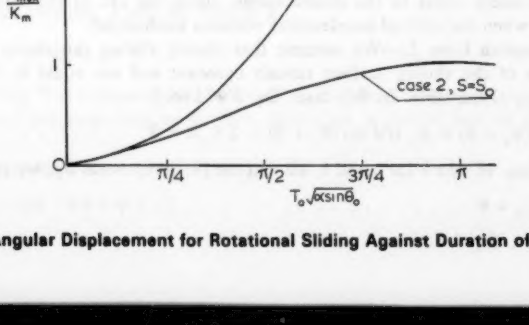

FIG. 3.—Angular Displacement for Rotational Sliding Against Duration of Pulse

This analysis shows that for rotating along a circular arc, if the shear strength along the slip surface remains constant, there is a maximum rotation $\theta_{max} = 2(K_m - K_{co})$ which cannot be exceeded. But this value in general is large and therefore is not of practical use. For example, for $(K_m - K_{co}) = 0.1$, and for a 50 m radius curve, the maximum possible displacement along the arc is $x_m = 10$ m, which is very large.

However, this also shows that even when the static factor of safety is equal to one, i.e. K_{co} = zero, an earthquake acceleration of 0.1 g will give a maximum displacement of 10 m instead of infinity, which will be obtained in the case of plane sliding surfaces or with circular surfaces when the critical acceleration remains constant. Fig. 3 shows a comparison of the displacements obtained in the two cases. This shows that for small angular displacements, the two cases give identical results. The case when the critical acceleration actually deteriorates with displacement is not included in this analysis.

Appendix.—References

1. Newmark, N. M., "Effects of Earthquakes on Dams and Embankments," *Geotechnique*, Vol. 15, No. 2, 1965, pp. 139–160.
2. Sarma, S. K., "Stability Analysis of Embankments and Slopes," *Geotechnique*, Vol. 23, No. 3, 1973, pp. 423–433.
3. Sarma, S. K., "Seismic Stability of Earth Dams and Embankments," *Geotechnique*, Vol. 25, No. 4, 1975, pp. 743–761.

DISCUSSION

Note.—This paper is part of the Journal of the Geotechnical Engineering Division, Proceedings of the American Society of Civil Engineers, ©ASCE, Vol. 107, No. GT12, December, 1981. ISSN 0093-6405/81/0012-1743/$01.00.

Discussions

Discussions may be submitted on any Proceedings paper or technical note published in any *Journal* or on any paper presented at any Specialty Conference or other meeting, the *Proceedings* of which have been published by ASCE. Discussion of a paper/technical note is open to anyone who has significant comments or questions regarding the content of the paper/technical note. Discussions are accepted for a period of 4 months following the date of publication of a paper/technical note and they should be sent to the Manager of Technical and Professional Publications, ASCE, 345 East 47th Street, New York, N.Y. 10017. The discussion period may be extended by a written request from a discusser.

The original and three copies of the Discussion should be submitted on 8-1/2-in. (220-mm) by 11-in. (280-mm) white bond paper, typed double-spaced with wide margins. The length of a Discussion is restricted to two *Journal* pages (about four typewritten double-spaced pages of manuscript including figures and tables); the editors will delete matter extraneous to the subject under discussion. If a Discussion is over two pages long it will be returned for shortening. All Discussions will be reviewed by the editors and the Division's or Council's Publications Committees. In some cases, Discussions will be returned to discussers for rewriting, or they may be encouraged to submit a paper or technical note rather than a Discussion.

Standards for Discussions are the same as those for Proceedings Papers. A Discussion is subject to rejection if it contains matter readily found elsewhere, advocates special interests, is carelessly prepared, controverts established fact, is purely speculative, introduces personalities, or is foreign to the purposes of the Society. All Discussions should be written in the third person, and the discusser should use the term "the writer" when referring to himself. The author of the original paper/technical note is referred to as "the author."

Discussions have a specific format. The title of the original paper/technical note appears at the top of the first page with a superscript that corresponds to a footnote indicating the month, year, author(s), and number of the original paper/technical note. The discusser's full name should be indicated below the title (see Discussions herein as an example) together with his ASCE membership grade (if applicable).

The discusser's title, company affiliation, and business address should appear on the first page of the manuscript, along with the *Proceedings* paper number of the original paper/technical note, the date and name of the *Journal* in which it appeared, and the original author's name.

Note that the discusser's identification footnote should follow consecutively from the original paper/technical note. If the paper/technical note under discussion contained footnote numbers 1 and 2, the first Discussion would begin with footnote 3, and subsequent Discussions would continue in sequence.

Figures supplied by the discusser should be designated by letters, starting with A. This also applies separately to tables and references. In referring to a figure, table, or reference that appeared in the original paper/technical note use the same number used in the original.

It is suggested that potential discussers request a copy of the *ASCE Authors' Guide to the Publications of ASCE* for more detailed information on preparation and submission of manuscripts.

Seismic Response of Cohesive Marine Soils[a]

Discussion by Tam J. Larkin,[4] A. M. ASCE

It is encouraging to see the growth and application of nonlinear analysis in seismic response studies and the authors are to be commended for their interesting and informative paper.

The question of low strain damping is a problem inherent in hysteretically damped nonlinear soil models, since at very small strains they predict elastic behavior and no attenuation of motion. For this reason, prediction of residual strains in soil masses is difficult when using such models. The inclusion of viscous damping in a linear model under steady state cyclic loading results in the maximum stress and maximum strain being nonconcurrent, which is at variance with experimental data. The inclusion of viscous damping in an Iwan model will result in a widening of the hysteresis loops in the midstrain range when harmonically cycled at a fixed amplitude.

Experimental work at the University of Auckland has been carried out to measure soil damping at strains down to 1×10^{-6} (15). A free vibration torsion test apparatus is employed using an almost friction free air bearing (16,17). The data is recorded and analyzed using an on-line computer for high resolution of low strain data and accurate post processing. This work established that energy dissipation is still occurring at strains of this magnitude. Equivalent viscous damping factors of about 2% have typically beeen measured. Fig. 14 shows some of the data gathered from a dynamic torsion test. It is important to note that this work does not prove the existence of viscous damping at low strains, but establishes that energy is absorbed during cyclic loading at very low strains (one microstrain).

One reason for using viscous damping is to reduce the "numerical noise," in the form of high frequency oscillations. It has been the writer's experience that such high frequency motion is often not a problem. This numerical noise usually occurs outside the frequency band of interest in cases involving high energy seismic events. This is likely to be the case for soft sites, since soil-structure interaction will increase the fundamental period of the structure being studied.

Degradation is an additional sophistication introduced to simulate the reduction in soil stiffness with strain history. A study of degradation in cohesive soils was undertaken by Bacchus (18), using cyclic triaxial test equipment. Similar results were obtained and a linear relationship was found between log σ_{oct} and log N. Using similar curve fitting procedures the results for a normally consolidated clay were expressed as

$$\sigma_{oct} = \sigma^{*}_{oct} (N + 1)^{-r} \quad \ldots \quad (1)$$

[a]September, 1980, by Chan-Feng Tsai, Ignatius Lam, and Geoffrey R. Martin (Proc. Paper 15708).

[4]Prof., Dept. of Civ. Engrg., Univ. of Auckland, Auckland, New Zealand.

in which σ_{oct} = the octahedral stress, initial value σ^*_{oct}; and r = a function of the strain amplitude.

The study used a series of tests with a variation in strain amplitude and measured excess pore pressures and the change in rheologic properties.

It has been the writers experience that degradation is not of great importance in seismic response studies, except in very soft soils in the near source region of a high magnitude earthquake. The numbers of cycles of loading reaching high strains, say 0.5%, is usually limited. Degradation is possibly an important feature in severe storm loading of off-shore structures where the number of cycles is of a different order of magnitude.

The transmitting boundary described by Joyner and Chen (3) is a significant advance in nonlinear methods. The writer has obtained similar results using this procedure, but note should be made that the methodology is based on the propagation of plane shear waves through an elastic medium. It assumes a constant shear wave velocity for the material below the transmitting boundary.

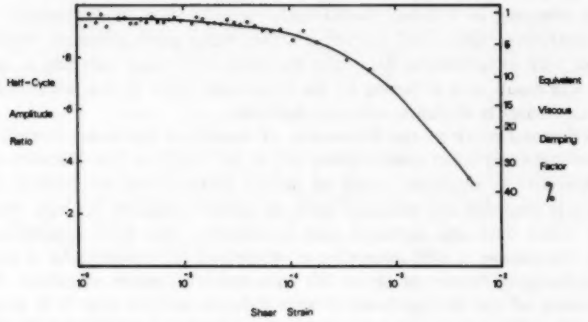

FIG. 14.—Variation of Damping with Shear Strain

This is not really the case in most seismic events of engineering significance, thus the procedure is an approximation in most cases.

Appendix—References

15. Mead, T. L., "Dynamic Soil Models," *Report No. 194*, School of Engineering, University of Auckland, Auckland, New Zealand, Mar., 1979.
16. Taylor, P. W., and Parton, I. M., "Dynamic Testing of Soils," *Proceedings of the 8th International Conference on Soil Mechanics and Foundation Engineering*, Vol. 1, 1973, p. 425.
17. Taylor, P. W., and Larkin, T. J., "Seismic Site Response of Nonlinear Soil Media," *Journal of the Geotechnical Engineering Division*, ASCE, Vol. 104, No. GT3, Proc. Paper 13597, Mar., 1978, pp. 369–383.
18. Bacchus, D. R., "Cyclic Deformation of a Clay," *Report No. 58*, School of Engineering, University of Auckland, Auckland, New Zealand, 1969.

Ground Control for Shallow Tunnels by Soil Grouting[a]

Discussion by Kurt M. Borchert[3] and Herbert Klapperich[4]

The suggestion of the paper appears to be helpful and applicable for practical purposes with respect to a suitable position of a grouted zone around tunnels and subways. For calculations with Finite-Element-Method the constitutive laws and their parameters are of essential importance with considerable influence, e.g., on the deformations (1).

This holds for soils and injections whereby the injections are always time dependent in two ways: (1) Dependency of the deformation on the onset of loading; and (2) the well-known creep. Both influences should be taken into consideration in calculating the soil grouting. In this way the factor mentioned in Table 2 can be increased as well as decreased in the case of a late respectively early onset of loading after the injection (2).

The creep deformations are also dependent on the onset of loading and are of the same magnitude as the initial deformations after excavation. For the design procedure the calculation of creep deformation is important especially before tunneling is performed and should be considered more strongly.

In the paper, the figures for design procedure were only determined by linear-elastic FE-calculations. It is of interest to know whether the stiffness at the onset of loading or decrease stiffness was used in order to consider the subsequent creep deformations directly.

For both assumptions it would be of interest for practical purposes in as far as the ratio of deformations after a certain duration of loading (even of one day) differ from the determined ones.

Appendix.—References

16. Müller-Kirchenbauer, H., "Spannungsverformungs-Verhalten von silikatinjizierten Böden unter Dauerlast," Baugrundtagung, Berlin, West Germany, 1978.
17. Richter, T., "Zum Einfluß der Fließregel bei der Berechnung eines Streifenfundamentes auf rolligem Boden mit der Methode der finiten Elemente," *Die Bautechnik*, No. 7, Berlin, West Germany, 1978.

[a]September, 1980, by D. Y. Tan and G. W. Clough (Proc. Paper 15716).
[3]Dipl.-Ing., Grundbauinstitut, Civ. Engrg. Dept., Technical Univ. of Berlin, Berlin, West Germany.
[4]Research Asst., Grundbauinstitut, Civ. Engrg. Dept., Tech. Univ. of Berlin, Berlin, West Germany.

1981 GT SUBJECT INDEX

Acoustic Detectors
Acoustic Emission Monitoring of Seepage, Robert M. Koerner, W. Martin McCabe and Luis F. Baldivieso, TN: GT4:Apr 81:521:16156

Acoustic Measurement
Acoustic Emission Monitoring of Seepage, Robert M. Koerner, W. Martin McCabe and Luis F. Baldivieso, TN: GT4:Apr 81:521:16156

Acoustic Surveillance
Sand Waves in Lower Cook Inlet, Alaska, Arshud A. Mahmood, Clarence J. Ehlers and Blase A. Cilweck, GT10:Oct 81:1293:16583

Allowable Settlement
Tolerable Settlement of Buildings, Harvey E. Wahls, GT11:Nov 81:1489:16628

Analog Models
Response of Circular Footings to Vertical Vibrations, Mysore V. Nagendra and Asuri Sridharan m116361, TN: GT7:July 81:989:16360

Anchored Bulkheads
Anchored Bulkheads: Horizontal and Sloping Anchors, Boris S. Browzin, GT5:May 81:629:16275

Anchors
Anchored Bulkheads: Horizontal and Sloping Anchors, Boris S. Browzin, GT5:May 81:629:16275

Anisotropic Soils
Anisotropic Strength of Cohesionless Sands, Masanobu Oda, GT9:Sept 81:1219:16491
Clay Anisotropy and Braced Wall Behavior, G. Wayne Clough and Lawrence A. Hansen, GT7:July 81:893:16391
Strength Anisotropy of Layered Soil System, M. Krishna Murthy, T. S. Nagaraj and A. Sridharan, TN: GT10:Oct 80:1143:15724

Anisotropy
Anisotropic Strength of Cohesionless Sands, Masanobu Oda, GT9:Sept 81:1219:16491
Clay Anisotropy and Braced Wall Behavior, G. Wayne Clough and Lawrence A. Hansen, GT7:July 81:893:16391

Aquatic Environment
Nitrogen-Cycle Model for Aquatic Systems: Analysis, Tavit O. Najarian and Jay L. Taft, GT12:Dec 81: 1141:16703

Archaeology
There Were Giants on the Earth in Those Days, George F. Sowers, GT4:Apr 81:383:16190

Axial Loads
Theoretical t-z Curves, Leland M. Kraft, Jr., Richard P. Ray and Takaaki Kagawa, GT11:Nov 81:1543: 16653

Base Loads
Repeated Loading on Single Piles in Sand, Sin-Fatt Chan and Thomas H. Hanna, GT2:Feb 80:171: 15222

Bearing Capacity
Compressibility and Bearing Capacity, Nabil F. Ismael and Aleksandar S. Vesic, GT12:Dec 81: 1677:16718
Cyclic Axial Response of Single File, Harry G. Poulos, GT1:Jan 81:41:15979
Experimental Study on Footings in Layered Soil, Adel M. Hanna, GT8:Aug 81:1113:16447
Foundations on Strong Sand Overlying Weak Sand, Adel M. Hanna, GT7:July 81:915:16367
New Design Correlations for Piles in Sand, Harry M. Coyle and Reno R. Castello, GT7:July 81:965: 16379
Stability of Loaded Footings on Reinforced Soil, Joe O. Akinmusuru and Jones A. Akinbolade, GT6: June 81:819:16320

Bedrock
Evaluating Pile Performance During Earthquakes, Issa S. Oweis, TN: GT5:May 81:678:16221

Benefit Cost Analysis
Dam Failure in Benefit/Cost Analysis, Gregory Baecher, Marie-Elisabeth Pate and Richard de Neufville, TN: GT1:Jan 80:101:15100

Bentonite
Soil-Bentonite Slurry Trench Cutoffs, David J. D'Appolonia, GT4:Apr 80:399:15372

Blasting
Construction Vibrations: State-of-the-Art, John F. Wiss, GT2:Feb 81:167:16030

Bond Stress
Caissons Socketed in Sound Mica Schist, Demetrious C. Koutsoftas, GT6:June 81:743:16288

Borehole Geophysics
Geotechnical Applications of Borehole Geophysics, James W. Crosby, III, Byron Konstantinidis and Paul Davis, GT10:Oct 81:1255:16585

Boreholes
Geotechnical Applications of Borehole Geophysics, James W. Crosby, III, Byron Konstantinidis and Paul Davis, GT10:Oct 81:1255:16585

Boundary Conditions
Finite Strain Consolidation: Test Conditions, Dobroslav Znidarcic and Robert L. Schiffman, TN: GT5:May 81:684:16221

Braced Excavation
Clay Anisotropy and Braced Wall Behavior, G. Wayne Clough and Lawrence A. Hansen, GT7:July 81:893:16391
Prediction of Movements for Braced Cuts in Clay, Abdulaziz I. Mana and G. Wayne Clough, GT6: June 81:759:16312

Braces
Clay Anisotropy and Braced Wall Behavior, G. Wayne Clough and Lawrence A. Hansen, GT7:July 81:893:16391

Breakwaters
Permanent Displacements Due to Cyclic Wave Loading, W. Allen Marr, Jr. and John T. Chrisitian, GT8:Aug 81:1129:16474

Buildings
Tolerable Settlement of Buildings, Harvey E. Wahls, GT11:Nov 81:1489:16628

Bulkheads
Anchored Bulkheads: Horizontal and Sloping Anchors, Boris S. Browzin, GT5:May 81:629:16275

Buried Cables
Coupled Heat and Water Flows Around Buried Cables, Omar N. Abdel-Hadi and James K. Mitchell, GT11:Nov 81:1461:16634

Caissons
Caissons Socketed in Sound Mica Schist, Demetrious C. Koutsoftas, GT6:June 81:743:16288
Deflection of Monopiles with Collar Caissons, Massimo Magni and Alex P. Michalopoulos, TN: GT5:May 81:667:16221

Calculations
Instrumentation Corrections to Wave Velocity Data, John R. Hall, Jr., John T. Christian, Eduardo Kausel and James L. Wolfgang, TN: GT10:Oct 81:1419:16530

Canals
Construction of Large Canal on Collapsing Soils, Paul C. Knodel, GT1:Jan 81:79:15992

Case Reports
Field Measurements of an Earth Support System, C. K. Shen, S. Bang, K. M. Romstad, L. Kulchin and J. S. DeNatale, GT12:Dec 81:1625:16734
Instability of Amuay Cliffside, T. William Lambe, Francisco Silva and W. Allen Marr, GT11:Nov 81:1505:16636
Settlement Comparison Used in Tank-Failure Study, Roy A. Bell and Jun Iwakiri, GT2:Feb 80:153:15219

Caves
Time-Dependant Behavior of Solution Caverns in Salt, Jameshid Ghaboussi, Afred J. Hendron, Jr. and Randall E. Ranken, GT10:Oct 81:1379:16597

Cellular Cofferdams
Cellular Cofferdam for Trident Drydock: Design, Max D. Sorota and Edward B. Kinner, GT12:Dec 81:1643:16758
Cellular Cofferdam for Trident Drydock: Performance, Max D. Sorota, Edward B. Kinner and Mark X. Haley, GT12:Dec 81:1657:16733

Cementation
Cemented Sands Under Static Loading, G. Wayne Clough, Nicholas Sitar, Robert C. Bachus and Nader Shafii Rad, GT6:June 81:799:16319

Centrifugation
Centrifuge Modeling of Coal Waste Embankments, Mosaid M. Al-Hussaini, Deborah J. Goodings, Andrew N. Schofield and Frank C. Townsend, GT4:Apr 81:481:16180
Drum Centrifuge Studies of Over Consolidated Slopes, Richard J. Fragaszy and James A. Cheney, GT7:July 81:843:16362
Offshore Gravity Structures: Analysis, Jean H. Prevost, Bernard Cuny, Thomas J.R. Hughes and Ronald F. Scott, GT2:Feb 81:143:16045
Offshore Gravity Structures: Centrifugal Modeling, Jean H. Prevost, Bernard Cuny and Ronald F. Scott, GT2:Feb 81:125:16044

Circular Footings
Foundations on Strong Sand Overlying Weak Sand, Adel M. Hanna, GT7:July 81:915:16367
Response of Circular Footings to Vertical Vibrations, Mysore V. Nagendra and Asuri Sridharan m116361, TN: GT7:Ju\; 81:989:16360

Clays
Clay Anisotropy and Braced Wall Behavior, G. Wayne Clough and Lawrence A. Hansen, GT7:July 81:893:16391
Computer Simulation of Creep of Clay, Roland Pusch and Paul Feltham, GT1:Jan 81:95:15998
Cone Penetration in Soil Profiling, Mohsen M. Baligh, Vitoon Vivatrat and Charles C. Ladd, GT4:Apr 80:447:15377
Drum Centrifuge Studies of Over Consolidated Slopes, Richard J. Fragaszy and James A. Cheney, GT7:July 81:843:16362
Finite Strain Consolidation: Test Conditions, Dobroslav Znidarcic and Robert L. Schiffman, TN: GT5:May 81:684:16221
Methodology for Foundations on Expansive Clays, Michael W. O'Neill and Nader Poormoayed, GT12:Dec 80:1345:15949
Prediction of Movements for Braced Cuts in Clay, Abdulaziz I. Mana and G. Wayne Clough, GT6:June 81:759:16312
Probabilistic Soil Exploration: Case History, Tien H. Wu and Kinfun Wong, GT12:Dec 81:1693:16764
Self-Boring Pressuremeter Study of San Francisco Bay Mud, G. Wayne Clough and Gordon M. Denby, GT1:Jan 80:45:15148
Strength Anisotropy of Layered Soil System, M. Krishna Murthy, T. S. Nagaraj and A. Sridharan, TN: GT10:Oct 80:1143:15724
Time-Dependent Deformation Behavior of Clays, Edward Kavazanjian, Jr. and James K. Mitchell, GT6:June 80:611:15488
Undrained Settlement of Plastic and Organic Clays, Roger Foott and Charles C. Ladd, GT8:Aug 81:1079:16421

Clay Soils
Deflection of Monopiles with Collar Caissons, Massimo Magni and Alex P. Michalopoulos, TN: GT5:May 81:667:16221
Friction Capacity of Piles Driven into Clay, Leland M. Kraft, John A. Focht, Jr. and Srinath F. Amerasinghe, GT11:Nov 81:1521:16663
Prediction of Swelling Potential for Natural Soils, Sudipta S. Bandyopadhyay, TN: GT5:May 81:658:16221

Clay Structure
Relationship of Electrical Dispersion to Soil Properties, Scott S. Smith and K. Arulanandan, GT5:May 81:591:16242

Cliffs
Instability of Amuay Cliffside, T. William Lambe, Francisco Silva and W. Allen Marr, GT11:Nov 81:1505:16636

Climatic Changes
Effect of Wetting and Drying on Shear Strength, Mehter Mohamed Allam and Asuri Sridharan, GT4:Apr 81:421:16178

Coal
Centrifuge Modeling of Coal Waste Embankments, Mosaid M. Al-Hussaini, Deborah J. Goodings, Andrew N. Schofield and Frank C. Townsend, GT4:Apr 81:481:16180

Coefficient of Earth Pressure
At-Rest Lateral Pressure of Peat Soils, Tuncer B. Edil and Abdulmohsin W. Dhowian, GT2:Feb 81:201:16063

Cohesionless Soils
Anisotropic Strength of Cohesionless Sands, Masanobu Oda, GT9:Sept 81:1219:16491
Dynamic Properties of Soils from In-Situ Tests, Shamsher Prakash and Vijay Kumar Puri, GT7:July 81:943:16366
New Design Correlations for Piles in Sand, Harry M. Coyle and Reno R. Castello, GT7:July 81:965:16379

Cohesive Soils
Anchored Bulkheads: Horizontal and Sloping Anchors, Boris S. Browzin, GT5:May 81:629:16275

Collapsible Soils
Construction of Large Canal on Collapsing Soils, Paul C. Knodel, GT1:Jan 81:79:15992
Design Considerations for Collapsible Soils, Samuel P. Clemence and Albert O. Finbarr, GT3:Mar 81: 305:16106

Collars
Deflection of Monopiles with Collar Caissons, Massimo Magni and Alex P. Michalopoulos, TN: GT5:May 81:667:16221

Compaction
Densification of Loose Deposits by Pounding, Robert G. Lukas, GT4:Apr 80:435:15376
Shear Strength of Rockfill, Nick Barton and Bjorn Kjaernsli, GT7:July 81:873:16374

Compaction (Soils)
Cellular Cofferdam for Trident Drydock: Performance, Max D. Sorota, Edward B. Kinner and Mark X. Haley, GT12:Dec 81:1657:16733

Complexity
Nitrogen-Cycle Model for Aquatic Systems: Analysis, Tavit O. Najarian and Jay L. Taft, GT12:Dec 81: 1141:16703

Compressibility (Soils)
Compressibility and Bearing Capacity, Nabil F. Ismael and Aleksandar S. Vesic, GT12:Dec 81: 1677:16718

Compressible Soils
Stresses in Soil around Vertical Compressible Piles, K. S. Sankaran, N. R. Krishnaswamy and B. K. Sharas Chandra, TN: GT1:Jan 81:107:15956

Compression Waves
Drilled-Shaft Integrity by Wave Propagation Method, Thomas M. Hearne, Jr., Kenneth H. Stokoe, II and Lyndon C. Reese, GT10:Oct 81:1327:16582

Computer Analysis
Coupled Heat and Water Flows Around Buried Cables, Omar N. Abdel-Hadi and James K. Mitchell, GT11:Nov 81:1461:16634
Laterally Loaded Pile Design, Robert L. Sogge, GT9: Sept 81:1179:16510

Computerized Simulation
Computer Simulation of Creep of Clay, Roland Pusch and Paul Feltham, GT1:Jan 81:95:15998

Computer Programs
Nonlinear Seismic Response of Soft Clay Sites, Ram D. Singh, Ricardo Debry, Earl H. Doyle and Izzat M. Idriss, GT9:Sept 81:1201:16493
Random Surface Generation in Stability Analysis, Ronald A. Siegel, William D. Kovacs and Charles W. Lovell, TN: GT7:July 81:996:16360

Computers
Laterally Loaded Pile Design, Robert L. Sogge, GT9: Sept 81:1179:16510

Cone Penetrometers
Cone Penetration in Soil Profiling, Mohsen M. Baligh, Vitoon Vivatrat and Charles C. Ladd, GT4: Apr 80:447:15377

Consolidation (Soils)
Hydroconsolidation Potential of Palouse Loess, Gary T. Lobdell, GT6:June 81:733:16309
Undrained Settlement of Plastic and Organic Clays, Roger Foott and Charles C. Ladd, GT8:Aug 81: 1079:16421

Consolidation Tests (Soils)
In-Situ Volume-Change Properties by Electro-Osmosis—Evaluation, James K. Mitchell and Sunirmal Banerjee, GT4:Apr 80:367:15371

Construction Equipment
Construction Vibrations: State-of-the-Art, John F. Wiss, GT2:Feb 81:167:16030

Construction Materials
Geotechnical Considerations for Construction in Saudi Arabia, Issa Oweis and John Bowman, GT3: Mar 81:319:16092

Construction Methods
There Were Giants on the Earth in Those Days, George F. Sowers, GT4:Apr 81:383:16190

Construction Planning
Geotechnical Considerations for Construction in Saudi Arabia, Issa Oweis and John Bowman, GT3: Mar 81:319:16092

Construction Procedure
Densification of Loose Deposits by Pounding, Robert G. Lukas, GT4:Apr 80:435:15376
Geotechnical Considerations for Construction in Saudi Arabia, Issa Oweis and John Bowman, GT3: Mar 81:319:16092
Ground Movements Caused by Braced Excavations, Thomas D. O'Rourke, GT9:Sept 81:1159:16511

Cores (Dams)
Cracking, Leakage, and Erosion of Earth Dam Materials, Erik I. Hjeldnes and Bhagwat V.K. Lavania, GT2:Feb 80:117:15220

Cracking
Cracking, Leakage, and Erosion of Earth Dam Materials, Erik I. Hjeldnes and Bhagwat V.K. Lavania, GT2:Feb 80:117:15220

Cracking (Fracturing)
Laboratory Study of Hydraulic Fracturing, Gary W. Jaworski, James M. Duncan and H. Bolton Seed, GT6:June 81:713:16287

Creep
Computer Simulation of Creep of Clay, Roland Pusch and Paul Feltham, GT1:Jan 81:95:15998
Time-Dependant Behavior of Solution Caverns in Salt, Jameshid Ghaboussi, Afred J. Hendron, Jr. and Randall E. Ranken, GT10:Oct 81:1379:16597
Undrained Settlement of Plastic and Organic Clays, Roger Foott and Charles C. Ladd, GT8:Aug 81: 1079:16421

Critical Depth
Pressuremeter Tests at Very Shallow Depth, Jean-Louis Briaud and Donald H. Shields, GT8:Aug 81: 1023:16416

Cycles
Cyclic Shear Resistance of Noncohesive Soils, Edward G. Prater, TN: GT1:Jan 80:111:15100

Cyclic Loads
Cyclic Axial Response of Single File, Harry G. Poulos, GT1:Jan 81:41:15979
Cyclic Strengths Compared for Two Sampling Techniques, Carlos Espana, Ronald C. Chaney and Dennis Duffy, GT5:May 81:563:16234
Dilation Angle and Liquefaction Potential, Yoginder P. Vaid, Peter M. Byrne and John M.O. Hughes, TN: GT7:July 81:1003:16360
Earthquake-Induced Liquefaction Near Lake Amatitlan, Guatemala, H. Bolton Seed, Ignacio Arango, Clarence K. Chan, Alberto Gomez-Masso and Rebecca Grant Ascoli, GT4:Apr 81:501:16212
Permanent Displacements Due to Cyclic Wave Loading, W. Allen Marr, Jr. and John T. Chrisitian, GT8:Aug 81:1129:16474

Pile Load Tests: Cyclic Loads and Varying Load Rates, Leland M. Kraft, William R. Cox and Edward A. Verner, GT1:Jan 81:1:16000
Soil Failure Modes in Undrained Cyclic Loading, Ernest T. Selig and Ching S. Chang, GT5:May 81: 539:16238

Cyclic Strength
Cyclic Strengths Compared for Two Sampling Techniques, Carlos Espana, Ronald C. Chaney and Dennis Duffy, GT5:May 81:563:16234

Dam Failure
Dam Failure in Benefit/Cost Analysis, Gregory Baecher, Marie-Elisabeth Pate and Richard de Neufville, TN: GT1:Jan 80:101:15100

Damping
Embedded Foundations Under Vertical Vibration, A. Sridharan, M. V. Nagendra and C. Chinnaswamy, TN: GT10:Oct 81:1429:16530

Dams
Laboratory Study of Hydraulic Fracturing, Gary W. Jaworski, James M. Duncan and H. Bolton Seed, GT6:June 81:713:16287

Dams (Earth)
Comparative Study of Dynamic Response of Earth Dam, Ahmed M. Abdel-Ghaffar and Ronald F. Scott, GT3:Mar 81:271:16097
Cracking, Leakage, and Erosion of Earth Dam Materials, Erik I. Hjeldnes and Bhagwat V.K. Lavania, GT2:Feb 80:117:15220
Dynamic FEM Model of Oroville Dam, John Vrymoed, GT8:Aug 81:1057:16464
Seepage From Freewater Above Impermeable Tailings, Lewis T. Isaacs and Bruce Hunt, GT11: Nov 81:1563:16652
Stability Analysis of Embankments and Slopes, Sarada K. Sarma, GT12:Dec 79:1511:15068
Vibration Tests of Full-Scale Earth Dam, Ahmed M. Abdel-Ghaffar and Ronald F. Scott, GT3:Mar 81: 241:16096

Dams (Rockfill)
Northfield Mountain Pumped Storage Project: Performance, William F. Swiger, Philip A. Wild and Thomas J. Lamb, GT6:June 80:673:15506

Decomposition
Ignition Test for Soil Organic-Content Measurement, Abdul-Amir W.N. Al-Kafaji and Orlando B. Andersland, GT4:Apr 81:465:16174

Deflection
Microgravity Surveys for Evaluation of Elevation Changes Due to Reservoir Impoundment, Dwain K. Butler, TN: GT3:Mar 81:355:16073

Deformation
Permanent Displacements Due to Cyclic Wave Loading, W. Allen Marr, Jr. and John T. Chrisitian, GT8:Aug 81:1129:16474
The Steady State of Deformation, Steve J. Poulos, GT5:May 81:553:16241
Stochastic FEM In Settlement Predictions, Gregory B. Beacher and Thomas S. Ingra, GT4:Apr 81:449: 16179
Time-Dependent Deformation Behavior of Clays, Edward Kavazanjian, Jr. and James K. Mitchell, GT6:June 80:611:15488
Undrained Settlement of Plastic and Organic Clays, Roger Foott and Charles C. Ladd, GT8:Aug 81: 1079:16421

Deformation Analysis
Strength and Deformability of Highly Fractured Rock, Jerome M. Raphael and Richard E. Goodman, GT11:Nov 79:1285:14988

Deposits
Statistical Analysis of Marine Clay Deposits, Hin Fatt Cheong and R. V. Subrahmanyam, TN: GT2: Feb 81:221:16009

Design
Design Considerations for Collapsible Soils, Samuel P. Clemence and Albert O. Finbarr, GT3:Mar 81: 305:16106

Design Criteria
Current USA Practices: Slurry Wall Specifications, Richard A. Millet and Jean-Yves Perez, GT8:Aug 81:1041:16458
New Design Correlations for Piles in Sand, Harry M. Coyle and Reno R. Castello, GT7:July 81:965: 16379

Design Practices
Design Considerations for Collapsible Soils, Samuel P. Clemence and Albert O. Finbarr, GT3:Mar 81: 305:16106

Dielectrics
Relationship of Electrical Dispersion to Soil Properties, Scott S. Smith and K. Arulanandan, GT5:May 81:591:16242

Displacements
Permanent Displacements Due to Cyclic Wave Loading, W. Allen Marr, Jr. and John T. Chrisitian, GT8:Aug 81:1129:16474

Dunes
Measurement of Porosity in Natural Sand Desposits, S. A. Denekamp and Y. Tsur-Lavie, GT4:Apr 81: 439:16173

Dynamic Characteristics
Comparative Study of Dynamic Response of Earth Dam, Ahmed M. Abdel-Ghaffar and Ronald F. Scott, GT3:Mar 81:271:16097
Vibration Tests of Full-Scale Earth Dam, Ahmed M. Abdel-Ghaffar and Ronald F. Scott, GT3:Mar 81: 241:16096

Dynamic Models
Dynamic FEM Model of Oroville Dam, John Vrymoed, GT8:Aug 81:1057:16464

Dynamic Properties
Dynamic Properties of Soils from In-Situ Tests, Shamsher Prakash and Vijay Kumar Puri, GT7:July 81:943:16366
Field and Laboratory Determination of Soil Moduli, William F. Marcuson, III and Joseph R. Curro, Jr., GT10:Oct 81:1269:16591

Dynamic Response
Comparative Study of Dynamic Response of Earth Dam, Ahmed M. Abdel-Ghaffar and Ronald F. Scott, GT3:Mar 81:271:16097
Nonlinear Lateral Dynamic Stiffness of Piles, Demosthenes C. Angelides and Jose M. Roesset, GT11:Nov 81:1443:16635

Dynamics
Construction Vibrations: State-of-the-Art, John F. Wiss, GT2:Feb 81:167:16030
Nonlinear Lateral Dynamic Stiffness of Piles, Demosthenes C. Angelides and Jose M. Roesset, GT11:Nov 81:1443:16635

Dynamic Stability
Vibration Tests of Full-Scale Earth Dam, Ahmed M. Abdel-Ghaffar and Ronald F. Scott, GT3:Mar 81: 241:16096

Dynamic Tests
Comparative Study of Dynamic Response of Earth Dam, Ahmed M. Abdel-Ghaffar and Ronald F. Scott, GT3:Mar 81:271:16097

Strength and Deformability of Highly Fractured Rock, Jerome M. Raphael and Richard E. Goodman, GT11:Nov 79:1285:14988

Earth Dam Performance
Line of Seepage in Earth Dams on Inclined Ledge, Yang H. Huang, TN: GT5:May 81:662:16221

Earth Dams
Dynamic FEM Model of Oroville Dam, John Vrymoed, GT8:Aug 81:1057:16464
Line of Seepage in Earth Dams on Inclined Ledge, Yang H. Huang, TN: GT5:May 81:662:16221
Longitudinal Vibrations of Embankment Dams, George Gazetas, GT1:Jan 81:21:15980
Seismic Displacement Analysis of Earth Dams, Sarada K. Sarma, TN: GT12:Dec 81:1735:16688

Earth Dam Seepage
Line of Seepage in Earth Dams on Inclined Ledge, Yang H. Huang, TN: GT5:May 81:662:16221

Earthfill
Densification of Loose Deposits by Pounding, Robert G. Lukas, GT4:Apr 80:435:15376

Earth Pressure
In Situ Tests by Flat Dilatometer, Silvano Marchetti, GT3:Mar 80:299:15290
Laterally Loaded Pile Design, Robert L. Sogge, GT9: Sept 81:1179:16510
Principal Stress Rotation: A Missing Parameter, J. Robin F. Arthur, Ken S. Chua, Treve Dunstan and Juan I. Rodriguez del C., GT4:Apr 80:419:15375

Earthquake Damage
Seismic Displacement Analysis of Earth Dams, Sarada K. Sarma, TN: GT12:Dec 81:1735:16688

Earthquake Engineering
Evaluating Pile Performance During Earthquakes, Issa S. Oweis, TN: GT5:May 81:678:16221

Earthquakes
Dynamic FEM Model of Oroville Dam, John Vrymoed, GT8:Aug 81:1057:16464
Earthquake-Induced Liquefaction Near Lake Amatitlan, Guatemala, H. Bolton Seed, Ignacio Arango, Clarence K. Chan, Alberto Gomez-Masso and Rebecca Grant Ascoli, GT4:Apr 81:501:16212
Evaluating Pile Performance During Earthquakes, Issa S. Oweis, TN: GT5:May 81:678:16221
Lateral Pile Response During Earthquakes, Takaaki Kagawa and Leland M. Kraft, Jr., GT12:Dec 81: 1713:16735
Liquefaction Analysis for Multidirectional Shaking, Jamshid Ghaboussi and S. Umit Dikmen, GT5:May 81:605:16243
Longitudinal Vibrations of Embankment Dams, George Gazetas, GT1:Jan 81:21:15980
Probabilistic Evaluation of Loads, Wilson H. Tang, GT3:Mar 81:287:16100
Stability Analysis of Embankments and Slopes, Sarada K. Sarma, GT12:Dec 79:1511:15068
Statistical Study of Uniform Cycles in Earthquakes, Achintya Haldar and Wilson H. Tang, GT5:May 81:577:16239

Earth Tides
Microgravity Surveys for Evaluation of Elevation Changes Due to Reservoir Impoundment, Dwain K. Butler, TN: GT3:Mar 81:355:16073

Elasticity
Laboratory Tests on Model Piled Raft Foundations, Terence J. Wiesner and Peter T. Brown, GT7:July 80:767:15576

Electrical Properties
Relationship of Electrical Dispersion to Soil Properties, Scott S. Smith and K. Arulanandan, GT5:May 81:591:16242

Electroosmosis
In-Situ Volume-Change Properties by Electro-Osmosis—Evaluation, James K. Mitchell and Sunirmal Banerjee, GT4:Apr 80:367:15371

Elevation
Microgravity Surveys for Evaluation of Elevation Changes Due to Reservoir Impoundment, Dwain K. Butler, TN: GT3:Mar 81:355:16073

Embankments
Centrifuge Modeling of Coal Waste Embankments, Mosaid M. Al-Hussaini, Deborah J. Goodings, Andrew N. Schofield and Frank C. Townsend, GT4:Apr 81:481:16180
Longitudinal Vibrations of Embankment Dams, George Gazetas, GT1:Jan 81:21:15980

Energy
Computer Simulation of Creep of Clay, Roland Pusch and Paul Feltham, GT1:Jan 81:95:15998

Energy Bands
Computer Simulation of Creep of Clay, Roland Pusch and Paul Feltham, GT1:Jan 81:95:15998

Equilibrium
Extreme-Value Problems of Limiting Equilibrium, Michael Garber and Rafael Baker, GT10:Oct 79: 1155:14901

Erosion
Cracking, Leakage, and Erosion of Earth Dam Materials, Erik I. Hjeldnes and Bhagwat V.K. Lavania, GT2:Feb 80:117:15220

Estimates
Shear Strength of Rockfill, Nick Barton and Bjorn Kjaernsli, GT7:July 81:873:16374

Estimating Equations
Optimal Estimators for Soil Properties, Gregory B. Baecher, TN: GT5:May 81:649:16221

Excavation
Field Measurements of an Earth Support System, C. K. Shen, S. Bang, K. M. Romstad, L. Kulchin and J. S. DeNatale, GT12:Dec 81:1625:16734
Ground Movement Analysis of Earth Support System, C. K. Shen, S. Bang and L. R. Herrmann, GT12:Dec 81:1609:16732
Ground Movements Caused by Braced Excavations, Thomas D. O'Rourke, GT9:Sept 81:1159:16511
Prediction of Movements for Braced Cuts in Clay, Abdulaziz I. Mana and G. Wayne Clough, GT6: June 81:759:16312

Excitation
Embedded Foundations Under Vertical Vibration, A. Sridharan, M. V. Nagendra and C. Chinnaswamy, TN: GT10:Oct 81:1429:16530
Response of Circular Footings to Vertical Vibrations, Mysore V. Nagendra and Asuri Sridharan m116361, TN: GT7:July 81:989:16360

Expansion
Methodology fo, Foundations on Expansive Clays, Michael W. O'Neill and Nader Poormoayed, GT12: Dec 80:1345:15949

Expansive Soils
Prediction of Swelling Potential for Natural Soils, Sudipta S. Bandyopadhyay, TN: GT5:May 81:658: 16221
Soil Stabilization with Preheater Fines, Sudipta S. Bandyopadhyay, TN: GT5:May 81:654:16221

Fabrics
Anisotropic Strength of Cohesionless Sands, Masanobu Oda, GT9:Sept 81:1219:16491
Geotextile-Reinforced Unpaved Road Design, Jean-Pierre Giroud and Laure Noiray, GT9:Sept 81: 1233:16489

Facilities
Safety of a Constructed Facility: Geotechnical Aspects, T. William Lambe, W. Allen Marr and Franciso Silva, GT3:Mar 81:339:16107

Failure
Anchored Bulkheads: Horizontal and Sloping Anchors, Boris S. Browzin, GT5:May 81:629:16275
Extreme-Value Problems of Limiting Equilibrium, Michael Garber and Rafael Baker, GT10:Oct 79: 1155:14901
Rock Joints: Roughness-Shear Strength Relationship, Ralf Peek, TN: GT5:May 81:672:16221
Settlement Comparison Used in Tank-Failure Study, Roy A. Bell and Jun Iwakiri, GT2:Feb 80:153: 15219
Shear Strength of Rockfill, Nick Barton and Bjorn Kjaernsli, GT7:July 81:873:16374

Failure Surfaces
Random Surface Generation in Stability Analysis, Ronald A. Siegel, William D. Kovacs and Charles W. Lovell, TN: GT7:July 81:996:16360

Field Data
Dilation Angle and Liquefaction Potential, Yoginder P. Vaid, Peter M. Byrne and John M.O. Hughes, TN: GT7:July 81:1003:16360
Prediction of Movements for Braced Cuts in Clay, Abdulaziz I. Mana and G. Wayne Clough, GT6: June 81:759:16312

Field Tests
Coupled Heat and Water Flows Around Buried Cables, Omar N. Abdel-Hadi and James K. Mitchell, GT11:Nov 81:1461:16634
Dynamic Properties of Soils from In-Situ Tests, Shamsher Prakash and Vijay Kumar Puri, GT7:July 81:943:16366
In Situ Tests by Flat Dilatometer, Silvano Marchetti, GT3:Mar 80:299:15290
Instrumentation Corrections to Wave Velocity Data, John R. Hall, Jr., John T. Christian, Eduardo Kausel and James L. Wolfgang, TN: GT10:Oct 81: 1419:16530
Northfield Mountain Pumped Storage Project: Performance, William F. Swiger, Philip A. Wild and Thomas J. Lamb, GT6:June 80:673:15506

Filters
Instrumentation Corrections to Wave Velocity Data, John R. Hall, Jr., John T. Christian, Eduardo Kausel and James L. Wolfgang, TN: GT10:Oct 81: 1419:16530

Fines
Soil Stabilization with Preheater Fines, Sudipta S. Bandyopadhyay, TN: GT5:May 81:654:16221

Fine-Textured Soils
Relationship of Electrical Dispersion to Soil Properties, Scott S. Smith and K. Arulanandan, GT5:May 81:591:16242

Finite Element Method
Ground Control for Shallow Tunnels by Soil Grouting, David Y. Tan and G. Wayne Clough, GT9:Sept 80:1037:15716
Permanent Displacements Due to Cyclic Wave Loading, W. Allen Marr, Jr. and John T. Chrisitian, GT8:Aug 81:1129:16474
Response of Buried Structures to Traveling Waves, Richard N. Nwang and John Lysmer, GT2:Feb 81: 183:16052
Stochastic FEM In Settlement Predictions, Gregory B. Beacher and Thomas S. Ingra, GT4:Apr 81:449: 16179

Finite Elements
Dynamic FEM Model of Oroville Dam, John Vrymoed, GT8:Aug 81:1057:16464
Time-Dependant Behavior of Solution Caverns in Salt, Jameshid Ghaboussi, Afred J. Hendron, Jr. and Randall E. Ranken, GT10:Oct 81:1379:16597

Floods
Hydroconsolidation Potential of Palouse Loess, Gary T. Lobdell, GT6:June 81:733:16309

Flow Characteristics
The Steady State of Deformation, Steve J. Poulos, GT5:May 81:553:16241

Fluid Flow
Acoustic Emission Monitoring of Seepage, Robert M. Koerner, W. Martin McCabe and Luis F. Baldivieso, TN: GT4:Apr 81:521:16156

Footings
Stability of Loaded Footings on Reinforced Soil, Joe O. Akinmusuru and Jones A. Akinbolade, GT6: June 81:819:16320
Stochastic FEM In Settlement Predictions, Gregory B. Beacher and Thomas S. Ingra, GT4:Apr 81:449: 16179

Foundation Construction
Miami Limestone Foundation Design and Construction, Thomas J. Kaderabek and Richard T. Reynolds, GT7:July 81:859:16377

Foundation Design
Design Considerations for Collapsible Soils, Samuel P. Clemence and Albert O. Finbarr, GT3:Mar 81: 305:16106
Miami Limestone Foundation Design and Construction, Thomas J. Kaderabek and Richard T. Reynolds, GT7:July 81:859:16377

Foundation Investigations
Foundations on Strong Sand Overlying Weak Sand, Adel M. Hanna, GT7:July 81:915:16367

Foundations
Compressibility and Bearing Capacity, Nabil F. Ismael and Aleksandar S. Vesic, GT12:Dec 81: 1677:16718
Embedded Anchor Response to uplift Loading, Andreas Andreadis, Roger C. Harvey and Eldon Burley, GT1:Jan 81:59:15985
Embedded Foundations Under Vertical Vibration, A. Sridharan, M. V. Nagendra and C. Chinnaswamy, TN: GT10:Oct 81:1429:16530
Ground Movements Caused by Braced Excavations, Thomas D. O'Rourke, GT9:Sept 81:1159:16511
Hydroconsolidation Potential of Palouse Loess, Gary T. Lobdell, GT6:June 81:733:16309
Laterally Loaded Pile Design, Robert L. Sogge, GT9: Sept 81:1179:16510
Nonlinear Lateral Dynamic Stiffness of Piles, Demosthenes C. Angelides and Jose M. Roesset, GT11:Nov 81:1443:16635
Optimal Estimators for Soil Properties, Gregory B. Baecher, TN: GT5:May 81:649:16221
Prediction of Swelling Potential for Natural Soils, Sudipta S. Bandyopadhyay, TN: GT5:May 81:658: 16221
Resorcinolic Grout for Injecting Sandy Foundations, Arvind V. Shroff and Dhananjay L. Shah, TN: GT10:Oct 80:1153:15724
Stochastic FEM In Settlement Predictions, Gregory B. Beacher and Thomas S. Ingra, GT4:Apr 81:449: 16179

Foundation Stability Analysis
Field and Laboratory Determination of Soil Moduli, William F. Marcuson, III and Joseph R. Curro, Jr., GT10:Oct 81:1269:16591
Response of Circular Footings to Vertical Vibrations, Mysore V. Nagendra and Asuri Sridharan m116361, TN: GT7:July 81:989:16360

Foundation Vibrations
Response of Circular Footings to Vertical Vibrations, Mysore V. Nagendra and Asuri Sridharan m116361, TN: GT7:July 81:989:16360

Fractures (Geology)
Permeability and Piping in Fractured Rocks, Richard E. Goodman and Panchanatham N. Sundaram, GT5:May 80:485:15433

Frequencies
Relationship of Electrical Dispersion to Soil Properties, Scott S. Smith and K. Arulanandan, GT5:May 81:591:16242

Friction
Repeated Loading on Single Piles in Sand, Sin-Fatt Chan and Thomas H. Hanna, GT2:Feb 80:171:15222
Shear Strength of Rockfill, Nick Barton and Bjorn Kjaernsli, GT7:July 81:873:16374

Friction Resistance
Friction Capacity of Piles Driven into Clay, Leland M. Kraft, John A. Focht, Jr. and Srinath F. Amerasinghe, GT11:Nov 81:1521:16663

Geodetic Surveys
Microgravity Surveys for Evaluation of Elevation Changes Due to Reservoir Impoundment, Dwain K. Butler, TN: GT3:Mar 81:355:16073

Geological Surveys
Geotechnical Considerations for Construction in Saudi Arabia, Issa Oweis and John Bowman, GT3:Mar 81:319:16092
Sand Waves in Lower Cook Inlet, Alaska, Arshud A. Mahmood, Clarence J. Ehlers and Blase A. Cilweck, GT10:Oct 81:1293:16583

Geophysical Logging
Geotechnical Applications of Borehole Geophysics, James W. Crosby, III, Byron Konstantinidis and Paul Davis, GT10:Oct 81:1255:16585

Geophysical Surveys
Sand Waves in Lower Cook Inlet, Alaska, Arshud A. Mahmood, Clarence J. Ehlers and Blase A. Cilweck, GT10:Oct 81:1293:16583

Geotechnical Engineering
Geotechnical Considerations for Construction in Saudi Arabia, Issa Oweis and John Bowman, GT3:Mar 81:319:16092
Offshore Gravity Structures: Analysis, Jean H. Prevost, Bernard Cuny, Thomas J.R. Hughes and Ronald F. Scott, GT2:Feb 81:143:16045
Offshore Gravity Structures: Centrifugal Modeling, Jean H. Prevost, Bernard Cuny and Ronald F. Scott, GT2:Feb 81:125:16044
Safety of a Constructed Facility: Geotechnical Aspects, T. William Lambe, W. Allen Marr and Franciso Silva, GT3:Mar 81:339:16107
There Were Giants on the Earth in Those Days, George F. Sowers, GT4:Apr 81:383:16190

Geotextiles
Geotextile-Reinforced Unpaved Road Design, Jean-Pierre Giroud and Laure Noiray, GT9:Sept 81:1233:16489

Granular Materials
Particle Contacts in Discrete Materials, Dimitri Athanasiou-Grivas and Milton E. Harr, TN: GT5:May 80:559:15432

Gravity
Microgravity Surveys for Evaluation of Elevation Changes Due to Reservoir Impoundment, Dwain K. Butler, TN: GT3:Mar 81:355:16073

Gravity Studies
Microgravity Surveys for Evaluation of Elevation Changes Due to Reservoir Impoundment, Dwain K. Butler, TN: GT3:Mar 81:355:16073

Ground Motion
Field Measurements of an Earth Support System, C. K. Shen, S. Bang, K. M. Romstad, L. Kulchin and J. S. DeNatale, GT12:Dec 81:1625:16734

Ground Water
Microgravity Surveys for Evaluation of Elevation Changes Due to Reservoir Impoundment, Dwain K. Butler, TN: GT3:Mar 81:355:16073

Grout
Resorcinolic Grout for Injecting Sandy Foundations, Arvind V. Shroff and Dhananjay L. Shah, TN: GT10:Oct 80:1153:15724

Grouting
Ground Control for Shallow Tunnels by Soil Grouting, David Y. Tan and G. Wayne Clough, GT9:Sept 80:1037:15716
Northfield Mountain Pumped Storage Project: Performance, William F. Swiger, Philip A. Wild and Thomas J. Lamb, GT6:June 80:673:15506
Resorcinolic Grout for Injecting Sandy Foundations, Arvind V. Shroff and Dhananjay L. Shah, TN: GT10:Oct 80:1153:15724

Hardening
Measurement of Porosity in Natural Sand Desposits, S. A. Denekamp and Y. Tsur-Lavie, GT4:Apr 81:439:16173

Heat Transfer
Coupled Heat and Water Flows Around Buried Cables, Omar N. Abdel-Hadi and James K. Mitchell, GT11:Nov 81:1461:16634

Heterogeneity
Relationship of Electrical Dispersion to Soil Properties, Scott S. Smith and K. Arulanandan, GT5:May 81:591:16242

Historic Sites
There Were Giants on the Earth in Those Days, George F. Sowers, GT4:Apr 81:383:16190

History
Dam Failure in Benefit/Cost Analysis, Gregory Baecher, Marie-Elisabeth Pate and Richard de Neufville, TN: GT1:Jan 80:101:15100
There Were Giants on the Earth in Those Days, George F. Sowers, GT4:Apr 81:383:16190

Hydraulic Fracturing
Laboratory Study of Hydraulic Fracturing, Gary W. Jaworski, James M. Duncan and H. Bolton Seed, GT6:June 81:713:16287

Ignition Tests
Ignition Test for Soil Organic-Content Measurement, Abdul-Amir W.N. Al-Kafaji and Orlando B. Andersland, GT4:Apr 81:465:16174

Impact
Densification of Loose Deposits by Pounding, Robert G. Lukas, GT4:Apr 80:435:15376

Impact Forces
Soil-Steel Structure Response to Live Loads, Baidar Bakht, GT6:June 81:779:16316

Impoundment
Microgravity Surveys for Evaluation of Elevation Changes Due to Reservoir Impoundment, Dwain K. Butler, TN: GT3:Mar 81:355:16073

Impregnation
Measurement of Porosity in Natural Sand Desposits, S. A. Denekamp and Y. Tsur-Lavie, GT4:Apr 81:439:16173

In Situ Tests
Cone Penetration in Soil Profiling, Mohsen M. Baligh, Vitoon Vivatrat and Charles C. Ladd, GT4:Apr 80:447:15377

In-Situ Volume-Change Properties by Electro-Osmosis—Evaluation, James K. Mitchell and Sunirmal Banerjee, GT4:Apr 80:367:15371

Instrumentation
Geotechnical Applications of Borehole Geophysics, James W. Crosby, III, Byron Konstantinidis and Paul Davis, GT10:Oct 81:1255:16585
Instrumentation Corrections to Wave Velocity Data, John R. Hall, Jr., John T. Christian, Eduardo Kausel and James L. Wolfgang, TN: GT10:Oct 81: 1419:16530

Internal Pressure
Time-Dependant Behavior of Solution Caverns in Salt, Jameshid Ghaboussi, Afred J. Hendron, Jr. and Randall E. Ranken, GT10:Oct 81:1379:16597

Joints (Geology)
Rock Joints: Roughness-Shear Strength Relationship, Ralf Peek, TN: GT5:May 81:672:16221

Laboratory Tests
Dilation Angle and Liquefaction Potential, Yoginder P. Vaid, Peter M. Byrne and John M.O. Hughes, TN: GT7:July 81:1003:16360
Instability of Amuay Cliffside, T. William Lambe, Francisco Silva and W. Allen Marr, GT11:Nov 81: 1505:16636
Seismic Techniques in the Laboratory, Richard D. Woods and Robert Henke, GT10:Oct 81:1309: 16599

Landslides
Instability of Amuay Cliffside, T. William Lambe, Francisco Silva and W. Allen Marr, GT11:Nov 81: 1505:16636
Stability Analysis of Embankments and Slopes, Sarada K. Sarma, GT12:Dec 79:1511:15068

Lateral Displacement Effect
Ground Movement Analysis of Earth Support System, C. K. Shen, S. Bang and L. R. Herrmann, GT12:Dec 81:1609:16732

Lateral Loads (Piles)
Deflection of Monopiles with Collar Caissons, Massimo Magni and Alex P. Michalopoulos, TN: GT5:May 81:667:16221
Nonlinear Lateral Dynamic Stiffness of Piles, Demosthenes C. Angelides and Jose M. Roesset, GT11:Nov 81:1443:16635

Lateral Pressure
At-Rest Lateral Pressure of Peat Soils, Tuncer B. Edil and Abdulmohsin W. Dhowian, GT2:Feb 81: 201:16063
In Situ Tests by Flat Dilatometer, Silvano Marchetti, GT3:Mar 80:299:15290
Total Lateral Surcharge Pressure Due to Strip Load, Ramon Jarquio, TN: GT10:Oct 81:1424:16530

Layered Soils
Experimental Study on Footings in Layered Soil, Adel M. Hanna, GT8:Aug 81:1113:16447
Foundations on Strong Sand Overlying Weak Sand, Adel M. Hanna, GT7:July 81:915:16367
Liquefaction Analysis for Multidirectional Shaking, Jamshid Ghaboussi and S. Umit Dikmen, GT5:May 81:605:16243
Strength Anisotropy of Layered Soil System, M. Krishna Murthy, T. S. Nagaraj and A. Sridharan, TN: GT10:Oct 80:1143:15724

Leakage
Cracking, Leakage, and Erosion of Earth Dam Materials, Erik I. Hjeldnes and Bhagwat V.K. Lavania, GT2:Feb 80:117:15220

Lighting Tests
Rock Joints: Roughness-Shear Strength Relationship, Ralf Peek, TN: GT5:May 81:672:16221

Limestone
Miami Limestone Foundation Design and Construction, Thomas J. Kaderabek and Richard T. Reynolds, GT7:July 81:859:16377

Limit Analysis
Limit Plasticity Approach to Slope Stability Program, Ryszard J. Izbicki, TN: GT2:Feb 81:228:16009

Limit Design Method
Stability Analysis of Embankments and Slopes, Sarada K. Sarma, GT12:Dec 79:1511:15068

Limiting Factors
Extreme-Value Problems of Limiting Equilibrium, Michael Garber and Rafael Baker, GT10:Oct 79: 1155:14901

Liquefaction
Cyclic Strengths Compared for Two Sampling Techniques, Carlos Espana, Ronald C. Chaney and Dennis Duffy, GT5:May 81:563:16234
Dilation Angle and Liquefaction Potential, Yoginder P. Vaid, Peter M. Byrne and John M.O. Hughes, TN: GT7:July 81:1003:16360
Earthquake-Induced Liquefaction Near Lake Amatitlan, Guatemala, H. Bolton Seed, Ignacio Arango, Clarence K. Chan, Alberto Gomez-Masso and Rebecca Grant Ascoli, GT4:Apr 81:501:16212
Lateral Pile Response During Earthquakes, Takaaki Kagawa and Leland M. Kraft, Jr., GT12:Dec 81: 1713:16735
Liquefaction Analysis for Multidirectional Shaking, Jamshid Ghaboussi and S. Umit Dikmen, GT5:May 81:605:16243
Modeling the Liquefaction Process, Takaaki Kagawa and Leland M. Kraft, Jr., GT12:Dec 81:1593:16709
Probabilistic Evaluation of Loads, Wilson H. Tang, GT3:Mar 81:287:16100
Static Shear and Liquefaction Potential, Yoginder P. Vaid and W. D. Liam Finn, GT10:Oct 79:1233: 14909
Statistical Analysis of Sand Liquefaction, Michael N. Fardis and Daniele Veneziano, GT10:Oct 81:1361: 16604
Statistical Study of Uniform Cycles in Earthquakes, Achintya Haldar and Wilson H. Tang, GT5:May 81:577:16239

Live Loads
Soil-Steel Structure Response to Live Loads, Baidar Bakht, GT6:June 81:779:16316

Load Distribution
Caissons Socketed in Sound Mica Schist, Demetrious C. Koutsoftas, GT6:June 81:743:16288

Loading Rate
Pile Load Tests: Cyclic Loads and Varying Load Rates, Leland M. Kraft, William R. Cox and Edward A. Verner, GT1:Jan 81:1:16000

Loads (Forces)
Ground Movements Caused by Braced Excavations, Thomas D. O'Rourke, GT9:Sept 81:1159:16511

Loess
Hydroconsolidation Potential of Palouse Loess, Gary T. Lobdell, GT6:June 81:733:16309

Machine Foundation
Embedded Foundations Under Vertical Vibration, A. Sridharan, M. V. Nagendra and C. Chinnaswamy, TN: GT10:Oct 81:1429:16530

Marine Clays
Statistical Analysis of Marine Clay Deposits, Hin Fatt Cheong and R. V. Subrahmanyam, TN: GT2: Feb 81:221:16009

Marine Engineering
Sand Waves in Lower Cook Inlet, Alaska, Arshud A. Mahmood, Clarence J. Ehlers and Blase A. Cilweck, GT10:Oct 81:1293:16583

Measuring Instruments
Self-Boring Pressuremeter Study of San Francisco Bay Mud, G. Wayne Clough and Gordon M. Denby, GT1:Jan 80:45:15148

Mica
Caissons Socketed in Sound Mica Schist, Demetrious C. Koutsoftas, GT6:June 81:743:16288

Microstructure
Computer Simulation of Creep of Clay, Roland Pusch and Paul Feltham, GT1:Jan 81:95:15998

Miniaturization
Geotechnical Applications of Borehole Geophysics, James W. Crosby, III, Byron Konstantinidis and Paul Davis, GT10:Oct 81:1255:16585

Mining
Seepage From Freewater Above Impermeable Tailings, Lewis T. Isaacs and Bruce Hunt, GT11: Nov 81:1563:16652

Models
Laboratory Tests on Model Piled Raft Foundations, Terence J. Wiesner and Peter T. Brown, GT7:July 80:767:15576
Nitrogen-Cycle Model for Aquatic Systems: Analysis, Tavit O. Najarian and Jay L. Taft, GT12:Dec 81: 1141:16703

Model Tests
Compressibility and Bearing Capacity, Nabil F. Ismael and Aleksandar S. Vesic, GT12:Dec 81: 1677:16718

Modulus of Deformation
Pressuremeter Tests at Very Shallow Depth, Jean-Louis Briaud and Donald H. Shields, GT8:Aug 81: 1023:16416

Monitoring
Acoustic Emission Monitoring of Seepage, Robert M. Koerner, W. Martin McCabe and Luis F. Baldivieso, TN: GT4:Apr 81:521:16156

Mud Displacement
Deflection of Monopiles with Collar Caissons, Massimo Magni and Alex P. Michalopoulos, TN: GT5:May 81:667:16221

Nitrogen Cycle
Nitrogen-Cycle Model for Aquatic Systems: Analysis, Tavit O. Najarian and Jay L. Taft, GT12:Dec 81: 1141:16703

Noncohesive Soils
Cyclic Shear Resistance of Noncohesive Soils, Edward G. Prater, TN: GT1:Jan 80:111:15100

Nondestructive Tests
Drilled-Shaft Integrity by Wave Propagation Method, Thomas M. Hearne, Jr., Kenneth H. Stokoe, II and Lyndon C. Reese, GT10:Oct 81:1327:16582

Ocean Bottom
Sand Waves in Lower Cook Inlet, Alaska, Arshud A. Mahmood, Clarence J. Ehlers and Blase A. Cilweck, GT10:Oct 81:1293:16583

Ocean Engineering
Embedded Anchor Response to uplift Loading, Andreas Andreadis, Roger C. Harvey and Eldon Burley, GT1:Jan 81:59:15985

Odometers
In Situ Tests by Flat Dilatometer, Silvano Marchetti, GT3:Mar 80:299:15290

Offshore Structures
Cyclic Axial Response of Single File, Harry G. Poulos, GT1:Jan 81:41:15979
Lateral Pile Response During Earthquakes, Takaaki Kagawa and Leland M. Kraft, Jr., GT12:Dec 81: 1713:16735
Offshore Gravity Structures: Analysis, Jean H. Prevost, Bernard Cuny, Thomas J.R. Hughes and Ronald F. Scott, GT2:Feb 81:143:16045
Permanent Displacements Due to Cyclic Wave Loading, W. Allen Marr, Jr. and John T. Chrisitian, GT8:Aug 81:1129:16474
Principal Stress Rotation: A Missing Parameter, J. Robin F. Arthur, Ken S. Chua, Treve Dunstan and Juan I. Rodriguez del C., GT4:Apr 80:419:15375

Organic Soils
Ignition Test for Soil Organic-Content Measurement, Abdul-Amir W.N. Al-Kafaji and Orlando B. Andersland, GT4:Apr 81:465:16174

Overconsolidation
Drum Centrifuge Studies of Over Consolidated Slopes, Richard J. Fragaszy and James A. Cheney, GT7:July 81:843:16362
In Situ Tests by Flat Dilatometer, Silvano Marchetti, GT3:Mar 80:299:15290

Particles
Particle Contacts in Discrete Materials, Dimitri Athanasiou-Grivas and Milton E. Harr, TN: GT5: May 80:559:15432

Pavement Design
Pressuremeter Tests at Very Shallow Depth, Jean-Louis Briaud and Donald H. Shields, GT8:Aug 81: 1023:16416

Pavements
Pressuremeter Tests at Very Shallow Depth, Jean-Louis Briaud and Donald H. Shields, GT8:Aug 81: 1023:16416

Peat
At-Rest Lateral Pressure of Peat Soils, Tuncer B. Edil and Abdulmohsin W. Dhowian, GT2:Feb 81: 201:16063

Peat Bog
Road on Peat: Observations and Design, Edward T. Hanrahan and Martin G. Rogers, GT10:Oct 81: 1403:16588

Penetration
Friction Capacity of Piles Driven into Clay, Leland M. Kraft, John A. Focht, Jr. and Srinath F. Amerasinghe, GT11:Nov 81:1521:16663

Permeability
Permeability and Piping in Fractured Rocks, Richard E. Goodman and Panchanatham N. Sundaram, GT5:May 80:485:15433
Soil-Bentonite Slurry Trench Cutoffs, David J. D'Appolonia, GT4:Apr 80:399:15372

Permeability (Soils)
Finite Strain Consolidation: Test Conditions, Dobroslav Znidarcic and Robert L. Schiffman, TN: GT5:May 81:684:16221
Relationship of Electrical Dispersion to Soil Properties, Scott S. Smith and K. Arulanandan, GT5:May 81:591:16242

Phreatic Water
Line of Seepage in Earth Dams on Inclined Ledge, Yang H. Huang, TN: GT5:May 81:662:16221

Piers
Methodology for Foundations on Expansive Clays, Michael W. O'Neill and Nader Poormoayed, GT12: Dec 80:1345:15949

Pile Driving
Construction Vibrations: State-of-the-Art, John F. Wiss, GT2:Feb 81:167:16030

Pile-Driving Formulas
New Design Correlations for Piles in Sand, Harry M. Coyle and Reno R. Castello, GT7:July 81:965: 16379

Pile Foundation Design
New Design Correlations for Piles in Sand, Harry M. Coyle and Reno R. Castello, GT7:July 81:965: 16379

Pile Foundation Performance
Evaluating Pile Performance During Earthquakes, Issa S. Oweis, TN: GT5:May 81:678:16221

Pile Friction
Friction Capacity of Piles Driven into Clay, Leland M. Kraft, John A. Focht, Jr. and Srinath F. Amerasinghe, GT11:Nov 81:1521:16663

Pile Loading Tests
Piles Subjected to Torsion, M. F. Randolph, GT8: Aug 81:1095:16424

Pile Load Tests (Cyclic Loading)
Pile Load Tests: Cyclic Loads and Varying Load Rates, Leland M. Kraft, William R. Cox and Edward A. Verner, GT1:Jan 81:1:16000

Piles
Laboratory Tests on Model Piled Raft Foundations, Terence J. Wiesner and Peter T. Brown, GT7:July 80:767:15576
Laterally Loaded Pile Design, Robert L. Sogge, GT9: Sept 81:1179:16510
Repeated Loading on Single Piles in Sand, Sin-Fatt Chan and Thomas H. Hanna, GT2:Feb 80:171: 15222
Stresses in Soil around Vertical Compressible Piles, K. S. Sankaran, N. R. Krishnaswamy and B. K. Sharas Chandra, TN: GT1:Jan 81:107:15956

Piles (Foundations)
Piles Subjected to Torsion, M. F. Randolph, GT8: Aug 81:1095:16424

Pile Settlement
Cyclic Axial Response of Single File, Harry G. Poulos, GT1:Jan 81:41:15979
Theoretical t-z Curves, Leland M. Kraft, Jr., Richard P. Ray and Takaaki Kagawa, GT11:Nov 81:1543: 16653

Pipelines
Response of Buried Structures to Traveling Waves, Richard N. Nwang and John Lysmer, GT2:Feb 81: 183:16052

Piping (Erosion)
Permeability and Piping in Fractured Rocks, Richard E. Goodman and Panchanatham N. Sundaram, GT5:May 80:485:15433

Pneumatic Tired Rollers
Construction of Large Canal on Collapsing Soils, Paul C. Knodel, GT1:Jan 81:79:15992

Pondweeds
Construction of Large Canal on Collapsing Soils, Paul C. Knodel, GT1:Jan 81:79:15992

Pore Water Pressure
Cone Penetration in Soil Profiling, Mohsen M. Baligh, Vitoon Vivatrat and Charles C. Ladd, GT4: Apr 80:447:15377
Lateral Pile Response During Earthquakes, Takaaki Kagawa and Leland M. Kraft, Jr., GT12:Dec 81: 1713:16735
Modeling the Liquefaction Process, Takaaki Kagawa and Leland M. Kraft, Jr., GT12:Dec 81:1593:16709

Porosity
Measurement of Porosity in Natural Sand Desposits, S. A. Denekamp and Y. Tsur-Lavie, GT4:Apr 81: 439:16173

Portland Cements
Soil Stabilization with Preheater Fines, Sudipta S. Bandyopadhyay, TN: GT5:May 81:654:16221

Predicting
Theoretical t-z Curves, Leland M. Kraft, Jr., Richard P. Ray and Takaaki Kagawa, GT11:Nov 81:1543: 16653

Preheating
Soil Stabilization with Preheater Fines, Sudipta S. Bandyopadhyay, TN: GT5:May 81:654:16221

Pressure
Self-Boring Pressuremeter Study of San Francisco Bay Mud, G. Wayne Clough and Gordon M. Denby, GT1:Jan 80:45:15148

Pressure Measurement
Pressuremeter Tests at Very Shallow Depth, Jean-Louis Briaud and Donald H. Shields, GT8:Aug 81: 1023:16416

Probability Theory
Probabilistic Evaluation of Loads, Wilson H. Tang, GT3:Mar 81:287:16100
Stochastic FEM In Settlement Predictions, Gregory B. Beacher and Thomas S. Ingra, GT4:Apr 81:449: 16179

Pumped Storage
Northfield Mountain Pumped Storage Project: Performance, William F. Swiger, Philip A. Wild and Thomas J. Lamb, GT6:June 80:673:15506

Rayleigh Waves
Seismic Techniques in the Laboratory, Richard D. Woods and Robert Henke, GT10:Oct 81:1309: 16599

Reinforced Earth
Field Measurements of an Earth Support System, C. K. Shen, S. Bang, K. M. Romstad, L. Kulchin and J. S. DeNatale, GT12:Dec 81:1625:16734
Ground Movement Analysis of Earth Support System, C. K. Shen, S. Bang and L. R. Herrmann, GT12:Dec 81:1609:16732
Stability of Loaded Footings on Reinforced Soil, Joe O. Akinmusuru and Jones A. Akinbolade, GT6: June 81:819:16320

Reinforced Roads
Geotextile-Reinforced Unpaved Road Design, Jean-Pierre Giroud and Laure Noiray, GT9:Sept 81: 1233:16489

Relative Density
Estimation of SPT-N and Relative Density, Michael A. Fardis and Daniele Veneziano, GT10:Oct 81: 1345:16590
Measurement of Porosity in Natural Sand Desposits, S. A. Denekamp and Y. Tsur-Lavie, GT4:Apr 81: 439:16173

Repeated Loading
Repeated Loading on Single Piles in Sand, Sin-Fatt Chan and Thomas H. Hanna, GT2:Feb 80:171: 15222

Reservoirs
Microgravity Surveys for Evaluation of Elevation Changes Due to Reservoir Impoundment, Dwain K. Butler, TN: GT3:Mar 81:355:16073

Residual Shear Strength
The Steady State of Deformation, Steve J. Poulos, GT5:May 81:553:16241

Residual Stress
New Design Correlations for Piles in Sand, Harry M. Coyle and Reno R. Castello, GT7:July 81:965: 16379

Responses
Theoretical t-z Curves, Leland M. Kraft, Jr., Richard P. Ray and Takaaki Kagawa, GT11:Nov 81:1543: 16653

Retaining Walls
Total Lateral Surcharge Pressure Due to Strip Load, Ramon Jarquio, TN: GT10:Oct 81:1424:16530

Rheology
Road on Peat: Observations and Design, Edward T. Hanrahan and Martin G. Rogers, GT10:Oct 81: 1403:16588

Road Construction
Road on Peat: Observations and Design, Edward T. Hanrahan and Martin G. Rogers, GT10:Oct 81: 1403:16588

Road Design
Geotextile-Reinforced Unpaved Road Design, Jean-Pierre Giroud and Laure Noiray, GT9:Sept 81: 1233:16489
Road on Peat: Observations and Design, Edward T. Hanrahan and Martin G. Rogers, GT10:Oct 81: 1403:16588

Rock Analysis
Miami Limestone Foundation Design and Construction, Thomas J. Kaderabek and Richard T. Reynolds, GT7:July 81:859:16377

Rockfill Dam Design
Shear Strength of Rockfill, Nick Barton and Bjorn Kjaernsli, GT7:July 81:873:16374

Rock Mechanics
Northfield Mountain Pumped Storage Project: Performance, William F. Swiger, Philip A. Wild and Thomas J. Lamb, GT6:June 80:673:15506
Strength and Deformability of Highly Fractured Rock, Jerome M. Raphael and Richard E. Goodman, GT11:Nov 79:1285:14988

Rock Properties
Strength and Deformability of Highly Fractured Rock, Jerome M. Raphael and Richard E. Goodman, GT11:Nov 79:1285:14988

Rock Salt
Time-Dependant Behavior of Solution Caverns in Salt, Jameshid Ghaboussi, Afred J. Hendron, Jr. and Randall E. Ranken, GT10:Oct 81:1379:16597

Rock Strength
Strength and Deformability of Highly Fractured Rock, Jerome M. Raphael and Richard E. Goodman, GT11:Nov 79:1285:14988

Rock Tests
Miami Limestone Foundation Design and Construction, Thomas J. Kaderabek and Richard T. Reynolds, GT7:July 81:859:16377

Roughness
Rock Joints: Roughness-Shear Strength Relationship, Ralf Peek, TN: GT5:May 81:672:16221

Safety
Safety of a Constructed Facility: Geotechnical Aspects, T. William Lambe, W. Allen Marr and Franciso Silva, GT3:Mar 81:339:16107

Safety Engineering
Safety of a Constructed Facility: Geotechnical Aspects, T. William Lambe, W. Allen Marr and Franciso Silva, GT3:Mar 81:339:16107

Safety Factor
Limit Plasticity Approach to Slope Stability Program, Ryszard J. Izbicki, TN: GT2:Feb 81:228:16009
Line of Seepage in Earth Dams on Inclined Ledge, Yang H. Huang, TN: GT5:May 81:662:16221
Random Surface Generation in Stability Analysis, Ronald A. Siegel, William D. Kovacs and Charles W. Lovell, TN: GT7:July 81:996:16360

Salt Domes
Time-Dependant Behavior of Solution Caverns in Salt, Jameshid Ghaboussi, Afred J. Hendron, Jr. and Randall E. Ranken, GT10:Oct 81:1379:16597

Sampling
Cyclic Strengths Compared for Two Sampling Techniques, Carlos Espana, Ronald C. Chaney and Dennis Duffy, GT5:May 81:563:16234

Sand
Dilation Angle and Liquefaction Potential, Yoginder P. Vaid, Peter M. Byrne and John M.O. Hughes, TN: GT7:July 81:1003:16360
Earthquake-Induced Liquefaction Near Lake Amatitlan, Guatemala, H. Bolton Seed, Ignacio Arango, Clarence K. Chan, Alberto Gomez-Masso and Rebecca Grant Ascoli, GT4:Apr 81:501:16212
Measurement of Porosity in Natural Sand Desposits, S. A. Denekamp and Y. Tsur-Lavie, GT4:Apr 81: 439:16173
New Design Correlations for Piles in Sand, Harry M. Coyle and Reno R. Castello, GT7:July 81:965: 16379
Soil Failure Modes in Undrained Cyclic Loading, Ernest T. Selig and Ching S. Chang, GT5:May 81: 539:16238
Stability of Loaded Footings on Reinforced Soil, Joe O. Akinmusuru and Jones A. Akinbolade, GT6: June 81:819:16320

Sands
Anisotropic Strength of Cohesionless Sands, Masanobu Oda, GT9:Sept 81:1219:16491
Cemented Sands Under Static Loading, G. Wayne Clough, Nicholas Sitar, Robert C. Bachus and Nader Shafii Rad, GT6:June 81:799:16319
Compressibility and Bearing Capacity, Nabil F. Ismael and Aleksandar S. Vesic, GT12:Dec 81: 1677:16718
Cyclic Strengths Compared for Two Sampling Techniques, Carlos Espana, Ronald C. Chaney and Dennis Duffy, GT5:May 81:563:16234
Estimation of SPT-N and Relative Density, Michael A. Fardis and Daniele Veneziano, GT10:Oct 81: 1345:16590
Lateral Pile Response During Earthquakes, Takaaki Kagawa and Leland M. Kraft, Jr., GT12:Dec 81: 1713:16735
Modeling the Liquefaction Process, Takaaki Kagawa and Leland M. Kraft, Jr., GT12:Dec 81:1593:16709
Permanent Displacements Due to Cyclic Wave Loading, W. Allen Marr, Jr. and John T. Chrisitian, GT8:Aug 81:1129:16474
Principal Stress Rotation: A Missing Parameter, J. Robin F. Arthur, Ken S. Chua, Treve Dunstan and Juan I. Rodriguez del C., GT4:Apr 80:419:15375
Resorcinolic Grout for Injecting Sandy Foundations, Arvind V. Shroff and Dhananjay L. Shah, TN: GT10:Oct 80:1153:15724
Static Shear and Liquefaction Potential, Yoginder P. Vaid and W. D. Liam Finn, GT10:Oct 79:1233: 14909
Statistical Analysis of Sand Liquefaction, Michael N. Fardis and Daniele Veneziano, GT10:Oct 81:1361: 16604

Sand Waves
Sand Waves in Lower Cook Inlet, Alaska, Arshud A. Mahmood, Clarence J. Ehlers and Blase A. Cilweck, GT10:Oct 81:1293:16583

Sandy Soils
Earthquake-Induced Liquefaction Near Lake Amatitlan, Guatemala, H. Bolton Seed, Ignacio Arango, Clarence K. Chan, Alberto Gomez-Masso and Rebecca Grant Ascoli, GT4:Apr 81:501:16212
Statistical Analysis of Sand Liquefaction, Michael N. Fardis and Daniele Veneziano, GT10:Oct 81:1361: 16604

Saudi Arabia
Geotechnical Considerations for Construction in Saudi Arabia, Issa Oweis and John Bowman, GT3: Mar 81:319:16092

Seepage
Acoustic Emission Monitoring of Seepage, Robert M. Koerner, W. Martin McCabe and Luis F. Baldivieso, TN: GT4:Apr 81:521:16156
Centrifuge Modeling of Coal Waste Embankments, Mosaid M. Al-Hussaini, Deborah J. Goodings, Andrew N. Schofield and Frank C. Townsend, GT4:Apr 81:481:16180
Line of Seepage in Earth Dams on Inclined Ledge, Yang H. Huang, TN: GT5:May 81:662:16221
Seepage From Freewater Above Impermeable Tailings, Lewis T. Isaacs and Bruce Hunt, GT11: Nov 81:1563:16652

Seepage Control
Soil-Bentonite Slurry Trench Cutoffs, David J. D'Appolonia, GT4:Apr 80:399:15372

Seepage Theory
Acoustic Emission Monitoring of Seepage, Robert M. Koerner, W. Martin McCabe and Luis F. Baldivieso, TN: GT4:Apr 81:521:16156

Seismic Design
Response of Buried Structures to Traveling Waves, Richard N. Nwang and John Lysmer, GT2:Feb 81: 183:16052
Seismic Displacement Analysis of Earth Dams, Sarada K. Sarma, TN: GT12:Dec 81:1735:16688

Seismic Stability
Nonlinear Seismic Response of Soft Clay Sites, Ram D. Singh, Ricardo Debry, Earl H. Doyle and Izzat M. Idriss, GT9:Sept 81:1201:16493
Seismic Displacement Analysis of Earth Dams, Sarada K. Sarma, TN: GT12:Dec 81:1735:16688

Seismic Tests
Seismic Techniques in the Laboratory, Richard D. Woods and Robert Henke, GT10:Oct 81:1309: 16599

Seismic Waves
Instrumentation Corrections to Wave Velocity Data, John R. Hall, Jr., John T. Christian, Eduardo Kausel and James L. Wolfgang, TN: GT10:Oct 81: 1419:16530

Seismographs
Instrumentation Corrections to Wave Velocity Data, John R. Hall, Jr., John T. Christian, Eduardo Kausel and James L. Wolfgang, TN: GT10:Oct 81: 1419:16530

Sensitivity
Nitrogen-Cycle Model for Aquatic Systems: Analysis, Tavit O. Najarian and Jay L. Taft, GT12:Dec 81: 1141:16703

Settlement (Structural)
Laboratory Tests on Model Piled Raft Foundations, Terence J. Wiesner and Peter T. Brown, GT7:July 80:767:15576
Settlement Comparison Used in Tank-Failure Study, Roy A. Bell and Jun Iwakiri, GT2:Feb 80:153: 15219
Stochastic FEM In Settlement Predictions, Gregory B. Beacher and Thomas S. Ingra, GT4:Apr 81:449: 16179
Tolerable Settlement of Buildings, Harvey E. Wahls, GT11:Nov 81:1489:16628

Settlement Analysis
Undrained Settlement of Plastic and Organic Clays, Roger Foott and Charles C. Ladd, GT8:Aug 81: 1079:16421

Shadows
Rock Joints: Roughness-Shear Strength Relationship, Ralf Peek, TN: GT5:May 81:672:16221

Shafts
Drilled-Shaft Integrity by Wave Propagation Method, Thomas M. Hearne, Jr., Kenneth H. Stokoe, II and Lyndon C. Reese, GT10:Oct 81:1327:16582
Repeated Loading on Single Piles in Sand, Sin-Fatt Chan and Thomas H. Hanna, GT2:Feb 80:171: 15222

Shaking
Liquefaction Analysis for Multidirectional Shaking, Jamshid Ghaboussi and S. Umit Dikmen, GT5:May 81:605:16243

Shallow Foundations
Experimental Study on Footings in Layered Soil, Adel M. Hanna, GT8:Aug 81:1113:16447
Miami Limestone Foundation Design and Construction, Thomas J. Kaderabek and Richard T. Reynolds, GT7:July 81:859:16377

Shearing
Slip Circles and Critical Shear Planes, Eric Spencer, GT7:July 81:929:16369

Shear Modulus
Field and Laboratory Determination of Soil Moduli, William F. Marcuson, III and Joseph R. Curro, Jr., GT10:Oct 81:1269:16591
Seismic Techniques in the Laboratory, Richard D. Woods and Robert Henke, GT10:Oct 81:1309: 16599
Undrained Settlement of Plastic and Organic Clays, Roger Foott and Charles C. Ladd, GT8:Aug 81: 1079:16421

Shear Planes
Slip Circles and Critical Shear Planes, Eric Spencer, GT7:July 81:929:16369

Shear Resistance
Cyclic Shear Resistance of Noncohesive Soils, Edward G. Prater, TN: GT1:Jan 80:111:15100

Shear Strain
Cyclic Axial Response of Single File, Harry G. Poulos, GT1:Jan 81:41:15979
Evaluating Pile Performance During Earthquakes, Issa S. Oweis, TN: GT5:May 81:678:16221

Shear Strength
Effect of Wetting and Drying on Shear Strength, Mehter Mohamed Allam and Asuri Sridharan, GT4:Apr 81:421:16178
Shear Strength of Rockfill, Nick Barton and Bjorn Kjaernsli, GT7:July 81:873:16374

Shear Strength (Rock)
Rock Joints: Roughness-Shear Strength Relationship, Ralf Peek, TN: GT5:May 81:672:16221

Shear Strength (Soils)
Clay Anisotropy and Braced Wall Behavior, G. Wayne Clough and Lawrence A. Hansen, GT7:July 81:893:16391
Probabilistic Soil Exploration: Case History, Tien H. Wu and Kinfun Wong, GT12:Dec 81:1693:16764

Shear Stress
Evaluating Pile Performance During Earthquakes, Issa S. Oweis, TN: GT5:May 81:678:16221
Modeling the Liquefaction Process, Takaaki Kagawa and Leland M. Kraft, Jr., GT12:Dec 81:1593:16709

Shear Tests
Dilation Angle and Liquefaction Potential, Yoginder P. Vaid, Peter M. Byrne and John M.O. Hughes, TN: GT7:July 81:1003:16360
Principal Stress Rotation: A Missing Parameter, J. Robin F. Arthur, Ken S. Chua, Treve Dunstan and Juan I. Rodriguez del C., GT4:Apr 80:419:15375

Shear Strength of Rockfill, Nick Barton and Bjorn Kjaernsli, GT7:July 81:873:16374
Statistical Analysis of Sand Liquefaction, Michael N. Fardis and Daniele Veneziano, GT10:Oct 81:1361:16604

Shrinkage
Methodology for Foundations on Expansive Clays, Michael W. O'Neill and Nader Poormoayed, GT12:Dec 80:1345:15949

Simple Shear Tests
Static Shear and Liquefaction Potential, Yoginder P. Vaid and W. D. Liam Finn, GT10:Oct 79:1233:14909

Sinkage
Anchored Bulkheads: Horizontal and Sloping Anchors, Boris S. Browzin, GT5:May 81:629:16275

Site Evaluation
Nonlinear Seismic Response of Soft Clay Sites, Ram D. Singh, Ricardo Debry, Earl H. Doyle and Izzat M. Idriss, GT9:Sept 81:1201:16493

Site Preparation (Construction)
Densification of Loose Deposits by Pounding, Robert G. Lukas, GT4:Apr 80:435:15376

Slabs
Methodology for Foundations on Expansive Clays, Michael W. O'Neill and Nader Poormoayed, GT12:Dec 80:1345:15949

Slipping
Extreme-Value Problems of Limiting Equilibrium, Michael Garber and Rafael Baker, GT10:Oct 79:1155:14901

Slopes
Limit Plasticity Approach to Slope Stability Program, Ryszard J. Izbicki, TN: GT2:Feb 81:228:16009

Slope Stability
Centrifuge Modeling of Coal Waste Embankments, Mosaid M. Al-Hussaini, Deborah J. Goodings, Andrew N. Schofield and Frank C. Townsend, GT4:Apr 81:481:16180
Drum Centrifuge Studies of Over Consolidated Slopes, Richard J. Fragaszy and James A. Cheney, GT7:July 81:843:16362
Extreme-Value Problems of Limiting Equilibrium, Michael Garber and Rafael Baker, GT10:Oct 79:1155:14901
Random Surface Generation in Stability Analysis, Ronald A. Siegel, William D. Kovacs and Charles W. Lovell, TN: GT7:July 81:996:16360
Slip Circles and Critical Shear Planes, Eric Spencer, GT7:July 81:929:16369
Stability Analysis of Embankments and Slopes, Sarada K. Sarma, GT12:Dec 79:1511:15068

Slope Stability Analysis
Random Surface Generation in Stability Analysis, Ronald A. Siegel, William D. Kovacs and Charles W. Lovell, TN: GT7:July 81:996:16360
Slip Circles and Critical Shear Planes, Eric Spencer, GT7:July 81:929:16369

Slurry Excavation
Current USA Practices: Slurry Wall Specifications, Richard A. Millet and Jean-Yves Perez, GT8:Aug 81:1041:16458

Slurry Trenches
Current USA Practices: Slurry Wall Specifications, Richard A. Millet and Jean-Yves Perez, GT8:Aug 81:1041:16458
Soil-Bentonite Slurry Trench Cutoffs, David J. D'Appolonia, GT4:Apr 80:399:15372

Sociological Factors
There Were Giants on the Earth in Those Days, George F. Sowers, GT4:Apr 81:383:16190

Soft Soils
Nonlinear Seismic Response of Soft Clay Sites, Ram D. Singh, Ricardo Debry, Earl H. Doyle and Izzat M. Idriss, GT9:Sept 81:1201:16493
Self-Boring Pressuremeter Study of San Francisco Bay Mud, G. Wayne Clough and Gordon M. Denby, GT1:Jan 80:45:15148

Soil Analysis
Optimal Estimators for Soil Properties, Gregory B. Baecher, TN: GT5:May 81:649:16221

Soil Cement
Relationship of Electrical Dispersion to Soil Properties, Scott S. Smith and K. Arulanandan, GT5:May 81:591:16242

Soil Compression Tests
At-Rest Lateral Pressure of Peat Soils, Tuncer B. Edil and Abdulmohsin W. Dhowian, GT2:Feb 81:201:16063

Soil Consolidation Tests
Hydroconsolidation Potential of Palouse Loess, Gary T. Lobdell, GT6:June 81:733:16309

Soil Density
Estimation of SPT-N and Relative Density, Michael A. Fardis and Daniele Veneziano, GT10:Oct 81:1345:16590

Soil Dynamics
Dynamic Properties of Soils from In-Situ Tests, Shamsher Prakash and Vijay Kumar Puri, GT7:July 81:943:16366
Ignition Test for Soil Organic-Content Measurement, Abdul-Amir W.N. Al-Kafaji and Orlando B. Andersland, GT4:Apr 81:465:16174
Liquefaction Analysis for Multidirectional Shaking, Jamshid Ghaboussi and S. Umit Dikmen, GT5:May 81:605:16243
Prediction of Swelling Potential for Natural Soils, Sudipta S. Bandyopadhyay, TN: GT5:May 81:658:16221
Seismic Techniques in the Laboratory, Richard D. Woods and Robert Henke, GT10:Oct 81:1309:16599
Soil Failure Modes in Undrained Cyclic Loading, Ernest T. Selig and Ching S. Chang, GT5:May 81:539:16238
Undrained Settlement of Plastic and Organic Clays, Roger Foott and Charles C. Ladd, GT8:Aug 81:1079:16421

Soil Engineering
Relationship of Electrical Dispersion to Soil Properties, Scott S. Smith and K. Arulanandan, GT5:May 81:591:16242

Soil Investigations
Cone Penetration in Soil Profiling, Mohsen M. Baligh, Vitoon Vivatrat and Charles C. Ladd, GT4:Apr 80:447:15377
Probabilistic Soil Exploration: Case History, Tien H. Wu and Kinfun Wong, GT12:Dec 81:1693:16764

Soil Liquefaction
Static Shear and Liquefaction Potential, Yoginder P. Vaid and W. D. Liam Finn, GT10:Oct 79:1233:14909

Soil Mechanics
Cemented Sands Under Static Loading, G. Wayne Clough, Nicholas Sitar, Robert C. Bachus and Nader Shafii Rad, GT6:June 81:799:16319
Effect of Wetting and Drying on Shear Strength, Mehter Mohamed Allam and Asuri Sridharan, GT4:Apr 81:421:16178
Embedded Anchor Response to uplift Loading, Andreas Andreadis, Roger C. Harvey and Eldon Burley, GT1:Jan 81:59:15985
Experimental Study on Footings in Layered Soil, Adel M. Hanna, GT8:Aug 81:1113:16447

Geotechnical Considerations for Construction in Saudi Arabia, Issa Oweis and John Bowman, GT3: Mar 81:319:16092
Ignition Test for Soil Organic-Content Measurement, Abdul-Amir W.N. Al-Kafaji and Orlando B. Andersland, GT4:Apr 81:465:16174
Laterally Loaded Pile Design, Robert L. Sogge, GT9: Sept 81:1179:16510
Seepage From Freewater Above Impermeable Tailings, Lewis T. Isaacs and Bruce Hunt, GT11: Nov 81:1563:16652
Slip Circles and Critical Shear Planes, Eric Spencer, GT7:July 81:929:16369
Soil-Steel Structure Response to Live Loads, Baidar Bakht, GT6:June 81:779:16316

Soil Moisture
Coupled Heat and Water Flows Around Buried Cables, Omar N. Abdel-Hadi and James K. Mitchell, GT11:Nov 81:1461:16634

Soil Profiles
Optimal Estimators for Soil Properties, Gregory B. Baecher, TN: GT5:May 81:649:16221

Soil Properties
Cyclic Shear Resistance of Noncohesive Soils, Edward G. Prater, TN: GT1:Jan 80:111:15100
Cyclic Strengths Compared for Two Sampling Techniques, Carlos Espana, Ronald C. Chaney and Dennis Duffy, GT5:May 81:563:16234
In Situ Tests by Flat Dilatometer, Silvano Marchetti, GT3:Mar 80:299:15290
Nonlinear Lateral Dynamic Stiffness of Piles, Demosthenes C. Angelides and Jose M. Roesset, GT11:Nov 81:1443:16635

Soils
Pile Load Tests: Cyclic Loads and Varying Load Rates, Leland M. Kraft, William R. Cox and Edward A. Verner, GT1:Jan 81:1:16000

Soil Stability
Cemented Sands Under Static Loading, G. Wayne Clough, Nicholas Sitar, Robert C. Bachus and Nader Shafii Rad, GT6:June 81:799:16319
Hydroconsolidation Potential of Palouse Loess, Gary T. Lobdell, GT6:June 81:733:16309
Prediction of Movements for Braced Cuts in Clay, Abdulaziz I. Mana and G. Wayne Clough, GT6: June 81:759:16312
Slip Circles and Critical Shear Planes, Eric Spencer, GT7:July 81:929:16369
Stability of Loaded Footings on Reinforced Soil, Joe O. Akinmusuru and Jones A. Akinbolade, GT6: June 81:819:16320

Soil Stabilization
Soil Stabilization with Preheater Fines, Sudipta S. Bandyopadhyay, TN: GT5:May 81:654:16221

Soil Stratification
Probabilistic Soil Exploration: Case History, Tien H. Wu and Kinfun Wong, GT12:Dec 81:1693:16764

Soil Strength
Deflection of Monopiles with Collar Caissons, Massimo Magni and Alex P. Michalopoulos, TN: GT5:May 81:667:16221

Soil Stresses
Field and Laboratory Determination of Soil Moduli, William F. Marcuson, III and Joseph R. Curro, Jr., GT10:Oct 81:1269:16591

Soil-Structure Interaction
Dynamic Properties of Soils from In-Situ Tests, Shamsher Prakash and Vijay Kumar Puri, GT7:July 81:943:16366
Ground Movements Caused by Braced Excavations, Thomas D. O'Rourke, GT9:Sept 81:1159:16511
Nonlinear Lateral Dynamic Stiffness of Piles, Demosthenes C. Angelides and Jose M. Roesset, GT11:Nov 81:1443:16635
Response of Buried Structures to Traveling Waves, Richard N. Nwang and John Lysmer, GT2:Feb 81: 183:16052

Soil Swelling
Prediction of Swelling Potential for Natural Soils, Sudipta S. Bandyopadhyay, TN: GT5:May 81:658: 16221
Soil Stabilization with Preheater Fines, Sudipta S. Bandyopadhyay, TN: GT5:May 81:654:16221

Soil Tests
Dynamic Properties of Soils from In-Situ Tests, Shamsher Prakash and Vijay Kumar Puri, GT7:July 81:943:16366
Soil Failure Modes in Undrained Cyclic Loading, Ernest T. Selig and Ching S. Chang, GT5:May 81: 539:16238

Soil Tests (Laboratory)
Laboratory Study of Hydraulic Fracturing, Gary W. Jaworski, James M. Duncan and H. Bolton Seed, GT6:June 81:713:16287
Prediction of Swelling Potential for Natural Soils, Sudipta S. Bandyopadhyay, TN: GT5:May 81:658: 16221
Soil Stabilization with Preheater Fines, Sudipta S. Bandyopadhyay, TN: GT5:May 81:654:16221

Specifications
Current USA Practices: Slurry Wall Specifications, Richard A. Millet and Jean-Yves Perez, GT8:Aug 81:1041:16458

Stability
Anchored Bulkheads: Horizontal and Sloping Anchors, Boris S. Browzin, GT5:May 81:629:16275
Limit Plasticity Approach to Slope Stability Program, Ryszard J. Izbicki, TN: GT2:Feb 81:228:16009
Safety of a Constructed Facility: Geotechnical Aspects, T. William Lambe, W. Allen Marr and Franciso Silva, GT3:Mar 81:339:16107

Stability Analysis
Instability of Amuay Cliffside, T. William Lambe, Francisco Silva and W. Allen Marr, GT11:Nov 81: 1505:16636
Random Surface Generation in Stability Analysis, Ronald A. Siegel, William D. Kovacs and Charles W. Lovell, TN: GT7:July 81:996:16360
Total Lateral Surcharge Pressure Due to Strip Load, Ramon Jarquio, TN: GT10:Oct 81:1424:16530

Stabilization
Ground Control for Shallow Tunnels by Soil Grouting, David Y. Tan and G. Wayne Clough, GT9:Sept 80:1037:15716

Standard Penetration Tests
Estimation of SPT-N and Relative Density, Michael A. Fardis and Daniele Veneziano, GT10:Oct 81: 1345:16590

Static Loads
Cemented Sands Under Static Loading, G. Wayne Clough, Nicholas Sitar, Robert C. Bachus and Nader Shafii Rad, GT6:June 81:799:16319

Statistical Analysis
Finite Strain Consolidation: Test Conditions, Dobroslav Znidarcic and Robert L. Schiffman, TN: GT5:May 81:684:16221
Optimal Estimators for Soil Properties, Gregory B. Baecher, TN: GT5:May 81:649:16221
Probabilistic Evaluation of Loads, Wilson H. Tang, GT3:Mar 81:287:16100
Statistical Analysis of Marine Clay Deposits, Hin Fatt Cheong and R. V. Subrahmanyam, TN: GT2: Feb 81:221:16009
Statistical Study of Uniform Cycles in Earthquakes, Achintya Haldar and Wilson H. Tang, GT5:May 81:577:16239

Steady State
The Steady State of Deformation, Steve J. Poulos, GT5:May 81:553:16241

Steel Piles
Pile Load Tests: Cyclic Loads and Varying Load Rates, Leland M. Kraft, William R. Cox and Edward A. Verner, GT1:Jan 81:1:16000

Steel Sheet Piles
Cellular Cofferdam for Trident Drydock: Design, Max D. Sorota and Edward B. Kinner, GT12:Dec 81:1643:16758
Cellular Cofferdam for Trident Drydock: Performance, Max D. Sorota, Edward B. Kinner and Mark X. Haley, GT12:Dec 81:1657:16733

Steel Structures
Soil-Steel Structure Response to Live Loads, Baidar Bakht, GT6:June 81:779:16316

Stiffness Tests
Dynamic Properties of Soils from In-Situ Tests, Shamsher Prakash and Vijay Kumar Puri, GT7:July 81:943:16366

Storms
Permanent Displacements Due to Cyclic Wave Loading, W. Allen Marr, Jr. and John T. Chrisitian, GT8:Aug 81:1129:16474

Strain
Finite Strain Consolidation: Test Conditions, Dobroslav Znidarcic and Robert L. Schiffman, TN: GT5:May 81:684:16221

Strains
Shear Strength of Rockfill, Nick Barton and Bjorn Kjaernsli, GT7:July 81:873:16374

Stratification
Cone Penetration in Soil Profiling, Mohsen M. Baligh, Vitoon Vivatrat and Charles C. Ladd, GT4: Apr 80:447:15377

Strength
Effect of Wetting and Drying on Shear Strength, Mehter Mohamed Allam and Asuri Sridharan, GT4:Apr 81:421:16178

Stress
Time-Dependant Behavior of Solution Caverns in Salt, Jameshid Ghaboussi, Afred J. Hendron, Jr. and Randall E. Ranken, GT10:Oct 81:1379:16597

Stress Cycle
Statistical Study of Uniform Cycles in Earthquakes, Achintya Haldar and Wilson H. Tang, GT5:May 81:577:16239

Stresses
Stresses in Soil around Vertical Compressible Piles, K. S. Sankaran, N. R. Krishnaswamy and B. K. Sharas Chandra, TN: GT1:Jan 81:107:15956

Stress Strain Relations
The Steady State of Deformation, Steve J. Poulos, GT5:May 81:553:16241

Structural Analysis
Drilled-Shaft Integrity by Wave Propagation Method, Thomas M. Hearne, Jr., Kenneth H. Stokoe, II and Lyndon C. Reese, GT10:Oct 81:1327:16582
Total Lateral Surcharge Pressure Due to Strip Load, Ramon Jarquio, TN: GT10:Oct 81:1424:16530

Structural Design
Cellular Cofferdam for Trident Drydock: Design, Max D. Sorota and Edward B. Kinner, GT12:Dec 81:1643:16758
Ground Control for Shallow Tunnels by Soil Grouting, David Y. Tan and G. Wayne Clough, GT9:Sept 80:1037:15716

Subsidence
Construction of Large Canal on Collapsing Soils, Paul C. Knodel, GT1:Jan 81:79:15992
Hydroconsolidation Potential of Palouse Loess, Gary T. Lobdell, GT6:June 81:733:16309
Tolerable Settlement of Buildings, Harvey E. Wahls, GT11:Nov 81:1489:16628

Subsoil
Foundations on Strong Sand Overlying Weak Sand, Adel M. Hanna, GT7:July 81:915:16367

Surcharge
Total Lateral Surcharge Pressure Due to Strip Load, Ramon Jarquio, TN: GT10:Oct 81:1424:16530

Surveying
Microgravity Surveys for Evaluation of Elevation Changes Due to Reservoir Impoundment, Dwain K. Butler, TN: GT3:Mar 81:355:16073

Swelling
Relationship of Electrical Dispersion to Soil Properties, Scott S. Smith and K. Arulanandan, GT5:May 81:591:16242

Tanks (Containers)
Settlement Comparison Used in Tank-Failure Study, Roy A. Bell and Jun Iwakiri, GT2:Feb 80:153: 15219

Temperature Gradients
Coupled Heat and Water Flows Around Buried Cables, Omar N. Abdel-Hadi and James K. Mitchell, GT11:Nov 81:1461:16634

Tensile Stress
Laboratory Study of Hydraulic Fracturing, Gary W. Jaworski, James M. Duncan and H. Bolton Seed, GT6:June 81:713:16287

Tests
Finite Strain Consolidation: Test Conditions, Dobroslav Znidarcic and Robert L. Schiffman, TN: GT5:May 81:684:16221
Soil-Steel Structure Response to Live Loads, Baidar Bakht, GT6:June 81:779:16316

Textiles
Geotextile-Reinforced Unpaved Road Design, Jean-Pierre Giroud and Laure Noiray, GT9:Sept 81: 1233:16489

Thrust
Soil-Steel Structure Response to Live Loads, Baidar Bakht, GT6:June 81:779:16316

Tiltmeters
Northfield Mountain Pumped Storage Project: Performance, William F. Swiger, Philip A. Wild and Thomas J. Lamb, GT6:June 80:673:15506

Time Dependence
Time-Dependent Deformation Behavior of Clays, Edward Kavazanjian, Jr. and James K. Mitchell, GT6:June 80:611:15488

Time Factors
Effect of Wetting and Drying on Shear Strength, Mehter Mohamed Allam and Asuri Sridharan, GT4:Apr 81:421:16178
Road on Peat: Observations and Design, Edward T. Hanrahan and Martin G. Rogers, GT10:Oct 81: 1403:16588
Statistical Study of Uniform Cycles in Earthquakes, Achintya Haldar and Wilson H. Tang, GT5:May 81:577:16239

Torsion
Piles Subjected to Torsion, M. F. Randolph, GT8: Aug 81:1095:16424

Triaxial Compression
Strength and Deformability of Highly Fractured Rock, Jerome M. Raphael and Richard E. Goodman, GT11:Nov 79:1285:14988

Triaxial Tests
Dilation Angle and Liquefaction Potential, Yoginder P. Vaid, Peter M. Byrne and John M.O. Hughes, TN: GT7:July 81:1003:16360
Effect of Wetting and Drying on Shear Strength, Mehter Mohamed Allam and Asuri Sridharan, GT4:Apr 81:421:16178
Particle Contacts in Discrete Materials, Dimitri Athanasiou-Grivas and Milton E. Harr, TN: GT5: May 80:559:15432
Shear Strength of Rockfill, Nick Barton and Bjorn Kjaernsli, GT7:July 81:873:16374
Soil Failure Modes in Undrained Cyclic Loading, Ernest T. Selig and Ching S. Chang, GT5:May 81: 539:16238

Tunnel Linings
Ground Control for Shallow Tunnels by Soil Grouting, David Y. Tan and G. Wayne Clough, GT9:Sept 80:1037:15716

Tunnels
Response of Buried Structures to Traveling Waves, Richard N. Nwang and John Lysmer, GT2:Feb 81: 183:16052

Unconsolidated Soils
Pile Load Tests: Cyclic Loads and Varying Load Rates, Leland M. Kraft, William R. Cox and Edward A. Verner, GT1:Jan 81:1:16000

Unpaved Roads
Geotextile-Reinforced Unpaved Road Design, Jean-Pierre Giroud and Laure Noiray, GT9:Sept 81: 1233:16489

Velocity
Seismic Techniques in the Laboratory, Richard D. Woods and Robert Henke, GT10:Oct 81:1309: 16599

Vertical Alinement
Ground Movement Analysis of Earth Support System, C. K. Shen, S. Bang and L. R. Herrmann, GT12:Dec 81:1609:16732

Vertical Oscillations
Response of Circular Footings to Vertical Vibrations, Mysore V. Nagendra and Asuri Sridharan m116361, TN: GT7:July 81:989:16360

Vibration
Construction Vibrations: State-of-the-Art, John F. Wiss, GT2:Feb 81:167:16030
Embedded Foundations Under Vertical Vibration, A. Sridharan, M. V. Nagendra and C. Chinnaswamy, TN: GT10:Oct 81:1429:16530
Statistical Study of Uniform Cycles in Earthquakes, Achintya Haldar and Wilson H. Tang, GT5:May 81:577:16239

Vibration Measurement
Vibration Tests of Full-Scale Earth Dam, Ahmed M. Abdel-Ghaffar and Ronald F. Scott, GT3:Mar 81: 241:16096

Vibration Response
Nonlinear Seismic Response of Soft Clay Sites, Ram D. Singh, Ricardo Debry, Earl H. Doyle and Izzat M. Idriss, GT9:Sept 81:1201:16493
Response of Circular Footings to Vertical Vibrations, Mysore V. Nagendra and Asuri Sridharan m116361, TN: GT7:July 81:989:16360

Vibration Tests
Comparative Study of Dynamic Response of Earth Dam, Ahmed M. Abdel-Ghaffar and Ronald F. Scott, GT3:Mar 81:271:16097
Vibration Tests of Full-Scale Earth Dam, Ahmed M. Abdel-Ghaffar and Ronald F. Scott, GT3:Mar 81: 241:16096

Walls
Clay Anisotropy and Braced Wall Behavior, G. Wayne Clough and Lawrence A. Hansen, GT7:July 81:893:16391

Washington
Hydroconsolidation Potential of Palouse Loess, Gary T. Lobdell, GT6:June 81:733:16309

Wastes
Centrifuge Modeling of Coal Waste Embankments, Mosaid M. Al-Hussaini, Deborah J. Goodings, Andrew N. Schofield and Frank C. Townsend, GT4:Apr 81:481:16180

Water Flow
Acoustic Emission Monitoring of Seepage, Robert M. Koerner, W. Martin McCabe and Luis F. Baldivieso, TN: GT4:Apr 81:521:16156

Wave Propagation
Drilled-Shaft Integrity by Wave Propagation Method, Thomas M. Hearne, Jr., Kenneth H. Stokoe, II and Lyndon C. Reese, GT10:Oct 81:1327:16582

Wave Velocity
Instrumentation Corrections to Wave Velocity Data, John R. Hall, Jr., John T. Christian, Eduardo Kausel and James L. Wolfgang, TN: GT10:Oct 81: 1419:16530

Wye Branches
Cellular Cofferdam for Trident Drydock: Design, Max D. Sorota and Edward B. Kinner, GT12:Dec 81:1643:16758

Youngs Modulus
Field and Laboratory Determination of Soil Moduli, William F. Marcuson, III and Joseph R. Curro, Jr., GT10:Oct 81:1269:16591

1981 GT NAME INDEX

Abdel-Ghaffar, Ahmed M.
Comparative Study of Dynamic Response of Earth Dam, with Ronald F. Scott, GT3:Mar 81:271:16097
Vibration Tests of Full-Scale Earth Dam, with Ronald F. Scott, GT3:Mar 81:241:16096

Abdel-Hadi, Omar N.
Coupled Heat and Water Flows Around Buried Cables, with James K. Mitchell, GT11:Nov 81:1461:16634

Akinbolade, Jones A.
See Joe O. Akinmusuru, GT6:June 81:819:16320

Akinmusuru, Joe O.
Stability of Loaded Footings on Reinforced Soil, with Jones A. Akinbolade, GT6:June 81:819:16320
Dsc, GT8:Aug 81:1153:16408, of "Laboratory Tests on Model Piled Raft Foundations", GT7:July 80:767:15576

Al-Hussaini, Mosaid M.
Centrifuge Modeling of Coal Waste Embankments, with Deborah J. Goodings, Andrew N. Schofield and Frank C. Townsend, GT4:Apr 81:481:16180

Al-Kafaji, Abdul-Amir W.N.
Ignition Test for Soil Organic-Content Measurement, with Orlando B. Andersland, GT4:Apr 81:465:16174

Allam, Mehter Mohamed
Effect of Wetting and Drying on Shear Strength, with Asuri Sridharan, GT4:Apr 81:421:16178

Amerasinghe, Srinath F.
See Leland M. Kraft, GT11:Nov 81:1521:16663

Andersland, Orlando B.
See Abdul-Amir W.N. Al-Kafaji, GT4:Apr 81:465:16174

Anderson, Thomas C.
Dsc, with Robert G. Lukas, GT3:Mar 81:372:16066, of "Self-Boring Pressuremeter Study of San Francisco Bay Mud", GT1:Jan 80:45:15148

Andreadis, Andreas
Embedded Anchor Response to uplift Loading, with Roger C. Harvey and Eldon Burley, GT1:Jan 81:59:15985

Angelides, Demosthenes C.
Nonlinear Lateral Dynamic Stiffness of Piles, with Jose M. Roesset, GT11:Nov 81:1443:16635

Arango, Ignacio
See H. Bolton Seed, GT4:Apr 81:501:16212

Arthur, J. Robin F.
Principal Stress Rotation: A Missing Parameter, with Ken S. Chua, Treve Dunstan and Juan I. Rodriguez del C., GT4:Apr 80:419:15375
Dsc: Atonio Gens, Matthew Symes and David Hight, GT5:May 81:702:16216; David M. Wood, GT5:May 81:704:16216
Clo: Keng S. Chua, Treve Dunstan and Juan I. Rodriguez del C., GT5:May 81:707:16216
TR:145:709

Arulanandan, K.
See Scott S. Smith, GT5:May 81:591:16242

Ascoli, Rebecca Grant
See H. Bolton Seed, GT4:Apr 81:501:16212

Athanasiou-Grivas, Dimitri
Particle Contacts in Discrete Materials, with Milton E. Harr, TN: GT5:May 80:559:15432
Dsc: Roland Gourves, TN: GT10:Oct 81:1437:16525; Robert D. Holtz, TN: GT10:Oct 81:1437:16525
Clo: TN: GT10:Oct 81:1440:16525

Bachus, Robert C.
See G. Wayne Clough, GT6:June 81:799:16319

Baecher, Gregory
Dam Failure in Benefit/Cost Analysis, with Marie-Elisabeth Pate and Richard de Neufville, TN: GT1:Jan 80:101:15100
Dsc: Francis G. McLean, TN: GT4:Apr 81:529:16150; Ralph B. Peck, TN: GT4:Apr 81:531:16150
Clo: TN: GT4:Apr 81:532:16150

Baecher, Gregory B.
Optimal Estimators for Soil Properties, TN: GT5:May 81:649:16221

Baker, Rafael
See Michael Garber, GT10:Oct 79:1155:14901

Bakht, Baidar
Soil-Steel Structure Response to Live Loads, GT6:June 81:779:16316

Baldivieso, Luis F.
See Robert M. Koerner, TN: GT4:Apr 81:521:16156

Baligh, Mohsen M.
Cone Penetration in Soil Profiling, with Vitoon Vivatrat and Charles C. Ladd, GT4:Apr 80:447:15377
Dsc: Marius Roy, GT11:Nov 81:1583:16614
TR:145:714

Bandyopadhyay, Sudipta S.
Prediction of Swelling Potential for Natural Soils, TN: GT5:May 81:658:16221
Soil Stabilization with Preheater Fines, TN: GT5:May 81:654:16221

Banerjee, Sunirmal
See James K. Mitchell, GT4:Apr 80:367:15371

Bang, S.
See C. K. Shen, GT12:Dec 81:1609:16732
See C. K. Shen, GT12:Dec 81:1625:16734

Barron, Reginald A.
Dsc, GT1:Jan 81:115:15952, of "Extreme-Value Problems of Limiting Equilibrium", GT10:Oct 79:1155:14901
Dsc, GT7:July 81:1012:16356, of "Permeability and Piping in Fractured Rocks", GT5:May 80:485:15433

Barton, Nick
Shear Strength of Rockfill, with Bjorn Kjaernsli, GT7:July 81:873:16374

Beacher, Gregory B.
Stochastic FEM In Settlement Predictions, with Thomas S. Ingra, GT4:Apr 81:449:16179

Bell, Roy A.
Settlement Comparison Used in Tank-Failure Study, with Jun Iwakiri, GT2:Feb 80:153:15219
Dsc: Robert E. Bigham, GT3:Mar 81:377:16066
Clo: GT3:Mar 81:379:16066
TR:145:656

Bigham, Robert E.
Dsc, GT3:Mar 81:377:16066, of "Settlement Comparison Used in Tank-Failure Study", GT2:Feb 80:153:15219

Borchert, Kurt K.
Dsc, with Herbert Klapperich, GT12:Dec 81:1745 s0ASCE:16683, of "Ground Control for Shallow Tunnels by Soil Grouting", GT9:Sept 80:1037: 15716

Bowman, John
See Issa Oweis, GT3:Mar 81:319:16092

Briaud, Jean-Louis
Pressuremeter Tests at Very Shallow Depth, with Donald H. Shields, GT8:Aug 81:1023:16416

Brown, Peter T.
See Terence J. Wiesner, GT7:July 80:767:15576

Browzin, Boris S.
Anchored Bulkheads: Horizontal and Sloping Anchors, GT5:May 81:629:16275

Burley, Eldon
Dsc, with Roger C. Harvey, Bhas Kar Nath and Lawrence A. Wood, GT8:Aug 81:1155:16408, of "Laboratory Tests on Model Piled Raft Foundations", GT7:July 80:767:15576
See Andreas Andreadis, GT1:Jan 81:59:15985

Butler, Dwain K.
Microgravity Surveys for Evaluation of Elevation Changes Due to Reservoir Impoundment, TN: GT3:Mar 81:355:16073

Byrne, Peter M.
See Yoginder P. Vaid, TN: GT7:July 81:1003:16360

Castello, Reno R.
See Harry M. Coyle, GT7:July 81:965:16379

Castillo, E.
See A. Luceno, GT1:Jan 81:118:15952

Chan, Clarence K.
See H. Bolton Seed, GT4:Apr 81:501:16212

Chan, Sin-Fatt
Repeated Loading on Single Piles in Sand, with Thomas H. Hanna, GT2:Feb 80:171:15222
Dsc: N. K. Jain and Gopal Ranjan, GT3:Mar 81: 380:16066
Clo: GT3:Mar 81:380:16066
TR:145:671

Chaney, Ronald C.
See Carlos Espana, GT5:May 81:563:16234

Chang, Ching S.
See Ernest T. Selig, GT5:May 81:539:16238

Cheney, James A.
See Richard J. Fragaszy, GT7:July 81:843:16362

Cheong, Hin Fatt
Statistical Analysis of Marine Clay Deposits, with R. V. Subrahmanyam, TN: GT2:Feb 81:221:16009

Chinnaswamy, C.
See A. Sridharan, TN: GT10:Oct 81:1429:16530

Chowdhury, Robin N.
Dsc, GT5:May 81:691:16216, of "Stability Analysis of Embankments and Slopes", GT12:Dec 79:1511: 15068

Chrisitian, John T.
See W. Allen Marr, Jr., GT8:Aug 81:1129:16474

Christian, John T.
See John R. Hall, Jr., TN: GT10:Oct 81:1419:16530

Chua, Ken S.
See J. Robin F. Arthur, GT4:Apr 80:419:15375

Chugh, Ashok K.
Dsc, GT5:May 81:693:16216, of "Stability Analysis of Embankments and Slopes", GT12:Dec 79:1511: 15068

Cilweck, Blase A.
See Arshud A. Mahmood, GT10:Oct 81:1293:16583

Clemence, Samuel P.
Design Considerations for Collapsible Soils, with Albert O. Finbarr, GT3:Mar 81:305:16106

Clough, G. Wayne
Cemented Sands Under Static Loading, with Nicholas Sitar, Robert C. Bachus and Nader Shafii Rad, GT6:June 81:799:16319
Clay Anisotropy and Braced Wall Behavior, with Lawrence A. Hansen, GT7:July 81:893:16391
Self-Boring Pressuremeter Study of San Francisco Bay Mud, with Gordon M. Denby, GT1:Jan 80:45: 15148
Dsc: Thomas C. Anderson and Robert G. Lukas, GT3:Mar 81:372:16066; J. C.P. Dalton, GT3: Mar 81:374:16066
Clo: GT3:Mar 81:375:16066
TR:145:647
See David Y. Tan, GT9:Sept 80:1037:15716
See Abdulaziz I. Mana, GT6:June 81:759:16312

Cox, William R.
See Leland M. Kraft, GT1:Jan 81:1:16000

Coyle, Harry M.
New Design Correlations for Piles in Sand, with Reno R. Castello, GT7:July 81:965:16379

Crosby, James W., III
Geotechnical Applications of Borehole Geophysics, with Byron Konstantinidis and Paul Davis, GT10: Oct 81:1255:16585

Cuny, Bernard
See Jean H. Prevost, GT2:Feb 81:125:16044
See Jean H. Prevost, GT2:Feb 81:143:16045

Curro, Joseph R., Jr.
See William F. Marcuson, III, GT10:Oct 81:1269: 16591

Dalton, J. C.P.
Dsc, GT3:Mar 81:374:16066, of "Self-Boring Pressuremeter Study of San Francisco Bay Mud", GT1:Jan 80:45:15148

D'Appolonia, David J.
Soil-Bentonite Slurry Trench Cutoffs, GT4:Apr 80: 399:15372
Dsc: S. A. Jefferis, GT11:Nov 81:1581:16614
TR:145:705

Davis, Paul
See James W. Crosby, III, GT10:Oct 81:1255:16585

Debry, Ricardo
See Ram D. Singh, GT9:Sept 81:1201:16493

DeNatale, J. S.
See C. K. Shen, GT12:Dec 81:1625:16734

Denby, Gordon M.
See G. Wayne Clough, GT1:Jan 80:45:15148

Denekamp, S. A.
Measurement of Porosity in Natural Sand Desposits, with Y. Tsur-Lavie, GT4:Apr 81:439:16173

de Neufville, Richard
See Gregory Baecher, TN: GT1:Jan 80:101:15100

Dhowian, Abdulmohsin W.
See Tuncer B. Edil, GT2:Feb 81:201:16063

Dikmen, S. Umit
See Jamshid Ghaboussi, GT5:May 81:605:16243

Doyle, Earl H.
See Ram D. Singh, GT9:Sept 81:1201:16493

Duffy, Dennis
See Carlos Espana, GT5:May 81:563:16234

Duncan, James M.
See Gary W. Jaworski, GT6:June 81:713:16287

Dunstan, Treve
See J. Robin F. Arthur, GT4:Apr 80:419:15375

Edil, Tuncer B.
At-Rest Lateral Pressure of Peat Soils, with Abdulmohsin W. Dhowian, GT2:Feb 81:201:16063

Ehlers, Clarence J.
See Arshud A. Mahmood, GT10:Oct 81:1293:16583

Espana, Carlos
Cyclic Strengths Compared for Two Sampling Techniques, with Ronald C. Chaney and Dennis Duffy, GT5:May 81:563:16234

Fardis, Michael A.
Estimation of SPT-N and Relative Density, with Daniele Veneziano, GT10:Oct 81:1345:16590

Fardis, Michael N.
Statistical Analysis of Sand Liquefaction, with Daniele Veneziano, GT10:Oct 81:1361:16604

Feltham, Paul
See Roland Pusch, GT1:Jan 81:95:15998

Fetzer, Claude A.
Dsc, GT7:July 81:1011:16356, of "Permeability and Piping in Fractured Rocks", GT5:May 80:485:15433
Dsc, GT7:July 81:1020:16356, of "Northfield Mountain Pumped Storage Project: Performance", GT6:June 80:673:15506

Finbarr, Albert O.
See Samuel P. Clemence, GT3:Mar 81:305:16106

Finn, W. D. Liam
See Yoginder P. Vaid, GT10:Oct 79:1233:14909

Focht, John A., Jr.
See Leland M. Kraft, GT11:Nov 81:1521:16663

Foott, Roger
Undrained Settlement of Plastic and Organic Clays, with Charles C. Ladd, GT8:Aug 81:1079:16421

Fragaszy, Richard J.
Drum Centrifuge Studies of Over Consolidated Slopes, with James A. Cheney, GT7:July 81:843:16362

Garber, Michael
Extreme-Value Problems of Limiting Equilibrium, with Rafael Baker, GT10:Oct 79:1155:14901
Dsc: Reginald A. Barron, GT1:Jan 81:115:15952; Ryszard J. Izbicki, GT1:Jan 81:116:15952; A. Luceno and E. Castillo, GT1:Jan 81:118:15952
Clo: GT1:Jan 81:121:15952
TR:145:532

Gazetas, George
Longitudinal Vibrations of Embankment Dams, GT1:Jan 81:21:15980

Gens, Atonio
Dsc, with Matthew Symes and David Hight, GT5:May 81:702:16216, of "Principal Stress Rotation: A Missing Parameter", GT4:Apr 80:419:15375

Ghaboussi, Jameshid
Time-Dependant Behavior of Solution Caverns in Salt, with Afred J. Hendron, Jr. and Randall E. Ranken, GT10:Oct 81:1379:16597

Ghaboussi, Jamshid
Liquefaction Analysis for Multidirectional Shaking, with S. Umit Dikmen, GT5:May 81:605:16243

Giroud, Jean-Pierre
Geotextile-Reinforced Unpaved Road Design, with Laure Noiray, GT9:Sept 81:1233:16489

Gomez-Masso, Alberto
See H. Bolton Seed, GT4:Apr 81:501:16212

Goodings, Deborah J.
See Mosaid M. Al-Hussaini, GT4:Apr 81:481:16180

Goodman, Richard E.
Permeability and Piping in Fractured Rocks, with Panchanatham N. Sundaram, GT5:May 80:485:15433
Dsc: Claude A. Fetzer, GT7:July 81:1011:16356; Reginald A. Barron, GT7:July 81:1012:16356
Clo: GT7:July 81:1013:16356
TR:145:717
See Jerome M. Raphael, GT11:Nov 79:1285:14988

Gourves, Roland
Dsc, TN: GT10:Oct 81:1437:16525, of "Particle Contacts in Discrete Materials", TN: GT5:May 80:559:15432

Haldar, Achintya
Statistical Study of Uniform Cycles in Earthquakes, with Wilson H. Tang, GT5:May 81:577:16239

Haley, Mark X.
See Max D. Sorota, GT12:Dec 81:1657:16733

Hall, John R., Jr.
Instrumentation Corrections to Wave Velocity Data, with John T. Christian, Eduardo Kausel and James L. Wolfgang, TN: GT10:Oct 81:1419:16530

Hanna, Adel M.
Experimental Study on Footings in Layered Soil, GT8:Aug 81:1113:16447
Foundations on Strong Sand Overlying Weak Sand, GT7:July 81:915:16367

Hanna, Thomas H.
See Sin-Fatt Chan, GT2:Feb 80:171:15222

Hanrahan, E. T.
Dsc, GT7:July 81:1014:16356, of "Time-Dependent Deformation Behavior of Clays", GT6:June 80:611:15488

Hanrahan, Edward T.
Road on Peat: Observations and Design, with Martin G. Rogers, GT10:Oct 81:1403:16588

Hansen, Lawrence A.
See G. Wayne Clough, GT7:July 81:893:16391

Harr, Milton E.
See Dimitri Athanasiou-Grivas, TN: GT5:May 80:559:15432

Harvey, Roger C.
See Andreas Andreadis, GT1:Jan 81:59:15985
See Eldon Burley, GT8:Aug 81:1155:16408

Hearne, Thomas M., Jr.
Drilled-Shaft Integrity by Wave Propagation Method, with Kenneth H. Stokoe, II and Lyndon C. Reese, GT10:Oct 81:1327:16582

Hendron, Alfred J., Jr.
See Jameshid Ghaboussi, GT10:Oct 81:1379:16597

Henke, Robert
See Richard D. Woods, GT10:Oct 81:1309:16599

Herrmann, L. R.
See C. K. Shen, GT12:Dec 81:1609:16732

Hight, David
See Atonio Gens, GT5:May 81:702:16216

Hjeldnes, Erik I.
Cracking, Leakage, and Erosion of Earth Dam Materials, with Bhagwat V.K. Lavania, GT2:Feb 80:117:15220
Dsc: Marvin R. Pyles, GT4:Apr 81:533:16150
Clo: GT4:Apr 81:535:16150
TR:145:661

Holtz, Robert D.
Dsc, TN: GT10:Oct 81:1437:16525, of "Particle Contacts in Discrete Materials", TN: GT5:May 80:559:15432

Huang, Yang H.
Line of Seepage in Earth Dams on Inclined Ledge, TN: GT5:May 81:662:16221

Hughes, John M.O.
See Yoginder P. Vaid, TN: GT7:July 81:1003:16360

Hughes, Thomas J.R.
See Jean H. Prevost, GT2:Feb 81:143:16045

Hunt, Bruce
See Lewis T. Isaacs, GT11:Nov 81:1563:16652

Idriss, Izzat M.
See Ram D. Singh, GT9:Sept 81:1201:16493

Ingra, Thomas S.
See Gregory B. Beacher, GT4:Apr 81:449:16179

Isaacs, Lewis T.
Seepage From Freewater Above Impermeable Tailings, with Bruce Hunt, GT11:Nov 81:1563:16652

Ismael, Nabil F.
Compressibility and Bearing Capacity, with Aleksandar S. Vesic, GT12:Dec 81:1677:16718

Iwakiri, Jun
See Roy A. Bell, GT2:Feb 80:153:15219

Izbicki, Ryszard J.
Limit Plasticity Approach to Slope Stability Program, TN: GT2:Feb 81:228:16009
Dsc, GT1:Jan 81:116:15952, of "Extreme-Value Problems of Limiting Equilibrium", GT10:Oct 79:1155:14901

Jain, N. K.
Dsc, with Gopal Ranjan, GT3:Mar 81:380:16066, of "Repeated Loading on Single Piles in Sand", GT2:Feb 80:171:15222

James, Anthony Noel
Dsc, TN: GT11:Nov 81:1588:16614, of "Resorcinolic Grout for Injecting Sandy Foundations", TN: GT10:Oct 80:1153:15724

Jarquio, Ramon
Total Lateral Surcharge Pressure Due to Strip Load, TN: GT10:Oct 81:1424:16530

Jaworski, Gary W.
Laboratory Study of Hydraulic Fracturing, with James M. Duncan and H. Bolton Seed, GT6:June 81:713:16287

Jefferis, S. A.
Dsc, GT11:Nov 81:1581:16614, of "Soil-Bentonite Slurry Trench Cutoffs", GT4:Apr 80:399:15372

Johnston, Ian W.
Dsc, GT6:June 81:837:16281, of "In-Situ Volume-Change Properties by Electro-Osmosis—Evaluation", GT4:Apr 80:367:15371

Kaderabek, Thomas J.
Miami Limestone Foundation Design and Construction, with Richard T. Reynolds, GT7:July 81:859:16377

Kagawa, Takaaki
Lateral Pile Response During Earthquakes, with Leland M. Kraft, Jr., GT12:Dec 81:1713:16735
Modeling the Liquefaction Process, with Leland M. Kraft, Jr., GT12:Dec 81:1593:16709
See Leland M. Kraft, Jr., GT11:Nov 81:1543:16653

Kausel, Eduardo
See John R. Hall, Jr., TN: GT10:Oct 81:1419:16530

Kavazanjian, Edward, Jr.
Time-Dependent Deformation Behavior of Clays, with James K. Mitchell, GT6:June 80:611:15488
Dsc: E. T. Hanrahan, GT7:July 81:1014:16356
Clo: GT7:July 81:1018:16356
TR:145:726

Kessler, Erwin
Dsc, GT5:May 81:709:16216, of "Densification of Loose Deposits by Pounding", GT4:Apr 80:435:15376

Kinner, Edward B.
See Max D. Sorota, GT12:Dec 81:1643:16758
See Max D. Sorota, GT12:Dec 81:1657:16733

Kjaernsli, Bjorn
See Nick Barton, GT7:July 81:873:16374

Klapperich, Herbert
See Kurt K. Borchert, GT12:Dec 81:1745 s0ASCE: 16683

Knodel, Paul C.
Construction of Large Canal on Collapsing Soils, GT1:Jan 81:79:15992

Koerner, Robert M.
Acoustic Emission Monitoring of Seepage, with W. Martin McCabe and Luis F. Baldivieso, TN: GT4: Apr 81:521:16156

Konstantinidis, Byron
See James W. Crosby, III, GT10:Oct 81:1255:16585

Koutsoftas, Demetrious C.
Caissons Socketed in Sound Mica Schist, GT6:June 81:743:16288

Kovacs, William D.
See Ronald A. Siegel, TN: GT7:July 81:996:16360

Kraft, Leland M.
Friction Capacity of Piles Driven into Clay, with John A. Focht, Jr. and Srinath F. Amerasinghe, GT11:Nov 81:1521:16663
Pile Load Tests: Cyclic Loads and Varying Load Rates, with William R. Cox and Edward A. Verner, GT1:Jan 81:1:16000

Kraft, Leland M., Jr.
Theoretical t-z Curves, with Richard P. Ray and Takaaki Kagawa, GT11:Nov 81:1543:16653
See Takaaki Kagawa, GT12:Dec 81:1593:16709
See Takaaki Kagawa, GT12:Dec 81:1713:16735

Krishnaswamy, N. R.
See K. S. Sankaran, TN: GT1:Jan 81:107:15956

Kulchin, L.
See C. K. Shen, GT12:Dec 81:1625:16734

Ladd, Charles C.
See Mohsen M. Baligh, GT4:Apr 80:447:15377
See Roger Foott, GT8:Aug 81:1079:16421

Lamb, Thomas J.
See William F. Swiger, GT6:June 80:673:15506

Lambe, T. William
Instability of Amuay Cliffside, with Francisco Silva and W. Allen Marr, GT11:Nov 81:1505:16636
Safety of a Constructed Facility: Geotechnical Aspects, with W. Allen Marr and Franciso Silva, GT3:Mar 81:339:16107

Lavania, Bhagwat V.K.
See Erik I. Hjeldnes, GT2:Feb 80:117:15220

Lobdell, Gary T.
Hydroconsolidation Potential of Palouse Loess, GT6: June 81:733:16309

Lovell, Charles W.
See Ronald A. Siegel, TN: GT7:July 81:996:16360

Luceno, A.
Dsc, with E. Castillo, GT1:Jan 81:118:15952, of "Extreme-Value Problems of Limiting Equilibrium", GT10:Oct 79:1155:14901

Lukas, Robert G.
Densification of Loose Deposits by Pounding, GT4: Apr 80:435:15376
Dsc: Erwin Kessler, GT5:May 81:709:16216
Clo: GT5:May 81:709:16216
TR:145:710
See Thomas C. Anderson, GT3:Mar 81:372:16066

Lysmer, John
See Richard N. Nwang, GT2:Feb 81:183:16052

Magni, Massimo
Deflection of Monopiles with Collar Caissons, with Alex P. Michalopoulos, TN: GT5:May 81:667: 16221

Mahmood, Arshud A.
Sand Waves in Lower Cook Inlet, Alaska, with Clarence J. Ehlers and Blase A. Cilweck, GT10:Oct 81:1293:16583

Mana, Abdulaziz I.
Prediction of Movements for Braced Cuts in Clay, with G. Wayne Clough, GT6:June 81:759:16312

Marchetti, Silvano
In Situ Tests by Flat Dilatometer, GT3:Mar 80:299: 15290
Dsc: John H. Schmertmann, GT6:June 81:831: 16281
Clo: GT6:June 81:832:16281
TR:145:693

Marcuson, William F., III
Field and Laboratory Determination of Soil Moduli, with Joseph R. Curro, Jr., GT10:Oct 81:1269:16591

Marr, W. Allen
See T. William Lambe, GT3:Mar 81:339:16107
See T. William Lambe, GT11:Nov 81:1505:16636

Marr, W. Allen, Jr.
Permanent Displacements Due to Cyclic Wave Loading, with John T. Chrisitian, GT8:Aug 81: 1129:16474

McCabe, W. Martin
See Robert M. Koerner, TN: GT4:Apr 81:521:16156

McLean, Francis G.
Dsc, TN: GT4:Apr 81:529:16150, of "Dam Failure in Benefit/Cost Analysis", TN: GT1:Jan 80:101:15100

Michalopoulos, Alex P.
See Massimo Magni, TN: GT5:May 81:667:16221

Millet, Richard A.
Current USA Practices: Slurry Wall Specifications, with Jean-Yves Perez, GT8:Aug 81:1041:16458

Mitchell, James K.
In-Situ Volume-Change Properties by Electro-Osmosis—Evaluation, with Sunirmal Banerjee, GT4:Apr 80:367:15371
Dsc: Ian W. Johnston, GT6:June 81:837:16281
Clo: GT6:June 81:840:16281
TR:145:703
See Edward Kavazanjian, Jr., GT6:June 80:611:15488
See Omar N. Abdel-Hadi, GT11:Nov 81:1461:16634

Moriwaki, Yoshiharu
Dsc, with Maurice S. Power, TN: GT3:Mar 81:367: 16066, of "Cyclic Shear Resistance of Noncohesive Soils", TN: GT1:Jan 80:111:15100

Murthy, M. Krishna
Strength Anisotropy of Layered Soil System, with T. S. Nagaraj and A. Sridharan, TN: GT10:Oct 80: 1143:15724
Errata: TN: GT11:Nov 81:1591:16614

Nagaraj, T. S.
See M. Krishna Murthy, TN: GT10:Oct 80:1143: 15724

Nagendra, M. V.
See A. Sridharan, TN: GT10:Oct 81:1429:16530

Nagendra, Mysore V.
Response of Circular Footings to Vertical Vibrations, with Asuri Sridharan m116361, TN: GT7:July 81:989:16360

Najarian, Tavit O.
Nitrogen-Cycle Model for Aquatic Systems: Analysis, with Jay L. Taft, GT12:Dec 81:1141:16703

Nath, Bhas Kar
See Eldon Burley, GT8:Aug 81:1155:16408

Noiray, Laure
See Jean-Pierre Giroud, GT9:Sept 81:1233:16489

Nwang, Richard N.
Response of Buried Structures to Traveling Waves, with John Lysmer, GT2:Feb 81:183:16052

Oda, Masanobu
Anisotropic Strength of Cohesionless Sands, GT9:Sept 81:1219:16491

O'Neill, Michael W.
Methodology for Foundations on Expansive Clays, with Nader Poormoayed, GT12:Dec 80:1345:15949
Errata: GT5:May 81:711:16216

O'Rourke, Thomas D.
Ground Movements Caused by Braced Excavations, GT9:Sept 81:1159:16511

Oweis, Issa
Geotechnical Considerations for Construction in Saudi Arabia, with John Bowman, GT3:Mar 81:319:16092

Oweis, Issa S.
Evaluating Pile Performance During Earthquakes, TN: GT5:May 81:678:16221

Pate, Marie-Elisabeth
See Gregory Baecher, TN: GT1:Jan 80:101:15100

Peck, Ralph B.
Dsc, TN: GT4:Apr 81:531:16150, of "Dam Failure in Benefit/Cost Analysis", TN: GT1:Jan 80:101:15100

Peek, Ralf
Rock Joints: Roughness-Shear Strength Relationship, TN: GT5:May 81:672:16221

Perez, Jean-Yves
See Richard A. Millet, GT8:Aug 81:1041:16458

Poormoayed, Nader
See Michael W. O'Neill, GT12:Dec 80:1345:15949

Poulos, Harry G.
Cyclic Axial Response of Single File, GT1:Jan 81:41:15979

Poulos, Steve J.
The Steady State of Deformation, GT5:May 81:553:16241

Power, Maurice S.
See Yoshiharu Moriwaki, TN: GT3:Mar 81:367:16066

Prakash, Shamsher
Dynamic Properties of Soils from In-Situ Tests, with Vijay Kumar Puri, GT7:July 81:943:16366

Prater, Edward G.
Cyclic Shear Resistance of Noncohesive Soils, TN: GT1:Jan 80:111:15100
Dsc: Yoshiharu Moriwaki and Maurice S. Power, TN: GT3:Mar 81:367:16066
Clo: TN: GT3:Mar 81:370:16066

Prevost, Jean H.
Offshore Gravity Structures: Analysis, with Bernard Cuny, Thomas J.R. Hughes and Ronald F. Scott, GT2:Feb 81:143:16045
Offshore Gravity Structures: Centrifugal Modeling, with Bernard Cuny and Ronald F. Scott, GT2:Feb 81:125:16044

Puri, Vijay Kumar
See Shamsher Prakash, GT7:July 81:943:16366

Pusch, Roland
Computer Simulation of Creep of Clay, with Paul Feltham, GT1:Jan 81:95:15998

Pyles, Marvin R.
Dsc, GT4:Apr 81:533:16150, of "Cracking, Leakage, and Erosion of Earth Dam Materials", GT2:Feb 80:117:15220

Rad, Nader Shafii
See G. Wayne Clough, GT6:June 81:799:16319

Randolph, M. F.
Piles Subjected to Torsion, GT8:Aug 81:1095:16424

Ranjan, Gopal
See N. K. Jain, GT3:Mar 81:380:16066

Ranken, Randall E.
See Jameshid Ghaboussi, GT10:Oct 81:1379:16597

Raphael, Jerome M.
Strength and Deformability of Highly Fractured Rock, with Richard E. Goodman, GT11:Nov 79:1285:14988
Dsc: J. Laginha Serafim, GT3:Mar 81:365:16066
Clo: GT3:Mar 81:366:16066
TR:145:570

Ray, Richard P.
See Leland M. Kraft, Jr., GT11:Nov 81:1543:16653

Reese, Lyndon C.
See Thomas M. Hearne, Jr., GT10:Oct 81:1327:16582

Reynolds, Richard T.
See Thomas J. Kaderabek, GT7:July 81:859:16377

Rodriguez del C., Juan I.
See J. Robin F. Arthur, GT4:Apr 80:419:15375

Roesset, Jose M.
See Demosthenes C. Angelides, GT11:Nov 81:1443:16635

Rogers, Martin G.
See Edward T. Hanrahan, GT10:Oct 81:1403:16588

Romstad, K. M.
See C. K. Shen, GT12:Dec 81:1625:16734

Roy, Marius
Dsc, GT11:Nov 81:1583:16614, of "Cone Penetration in Soil Profiling", GT4:Apr 80:447:15377

Sankaran, K. S.
Stresses in Soil around Vertical Compressible Piles, with N. R. Krishnaswamy and B. K. Sharas Chandra, TN: GT1:Jan 81:107:15956

Sarma, Sarada K.
Seismic Displacement Analysis of Earth Dams, TN: GT12:Dec 81:1735:16688
Stability Analysis of Embankments and Slopes, GT12:Dec 79:1511:15068
Dsc: Robin N. Chowdhury, GT5:May 81:691: 16216; Ashok K. Chugh, GT5:May 81:693: 16216
Clo: GT5:May 81:697:16216
TR:145:625

Schiffman, Robert L.
See Dobroslav Znidarcic, TN: GT5:May 81:684: 16221

Schmertmann, John H.
Dsc, GT6:June 81:831:16281, of "In Situ Tests by Flat Dilatometer", GT3:Mar 80:299:15290

Schofield, Andrew N.
See Mosaid M. Al-Hussaini, GT4:Apr 81:481:16180

Scott, Ronald F.
See Jean H. Prevost, GT2:Feb 81:125:16044
See Jean H. Prevost, GT2:Feb 81:143:16045
See Ahmed M. Abdel-Ghaffar, GT3:Mar 81:241: 16096
See Ahmed M. Abdel-Ghaffar, GT3:Mar 81:271: 16097

Seed, H. Bolton
Earthquake-Induced Liquefaction Near Lake Amatitlan, Guatemala, with Ignacio Arango, Clarence K. Chan, Alberto Gomez-Masso and Rebecca Grant Ascoli, GT4:Apr 81:501:16212
See Gary W. Jaworski, GT6:June 81:713:16287

Selig, Ernest T.
Soil Failure Modes in Undrained Cyclic Loading, with Ching S. Chang, GT5:May 81:539:16238

Serafim, J. Laginha
Dsc, GT3:Mar 81:365:16066, of "Strength and Deformability of Highly Fractured Rock", GT11: Nov 79:1285:14988

Shah, Dhananjay L.
See Arvind V. Shroff, TN: GT10:Oct 80:1153:15724

Sharas Chandra, B. K.
See K. S. Sankaran, TN: GT1:Jan 81:107:15956

Shen, C. K.
Field Measurements of an Earth Support System, with S. Bang, K. M. Romstad, L. Kulchin and J. S. DeNatale, GT12:Dec 81:1625:16734
Ground Movement Analysis of Earth Support System, with S. Bang and L. R. Herrmann, GT12: Dec 81:1609:16732

Shields, Donald H.
See Jean-Louis Briaud, GT8:Aug 81:1023:16416

Shroff, Arvind V.
Resorcinolic Grout for Injecting Sandy Foundations, with Dhananjay L. Shah, TN: GT10:Oct 80:1153: 15724
Dsc: Anthony Noel James, TN: GT11:Nov 81: 1588:16614
Clo: TN: GT11:Nov 81:1590:16614

Siegel, Ronald A.
Random Surface Generation in Stability Analysis, with William D. Kovacs and Charles W. Lovell, TN: GT7:July 81:996:16360

Silva, Francisco
See T. William Lambe, GT11:Nov 81:1505:16636

Silva, Franciso
See T. William Lambe, GT3:Mar 81:339:16107

Singh, Ram D.
Nonlinear Seismic Response of Soft Clay Sites, with Ricardo Debry, Earl H. Doyle and Izzat M. Idriss, GT9:Sept 81:1201:16493

Sitar, Nicholas
See G. Wayne Clough, GT6:June 81:799:16319

Smith, Scott S.
Relationship of Electrical Dispersion to Soil Properties, with K. Arulanandan, GT5:May 81:591: 16242

Sogge, Robert L.
Laterally Loaded Pile Design, GT9:Sept 81:1179: 16510

Sorota, Max D.
Cellular Cofferdam for Trident Drydock: Design, with Edward B. Kinner, GT12:Dec 81:1643:16758
Cellular Cofferdam for Trident Drydock: Performance, with Edward B. Kinner and Mark X. Haley, GT12:Dec 81:1657:16733

Sowers, George F.
There Were Giants on the Earth in Those Days, GT4:Apr 81:383:16190

Spencer, Eric
Slip Circles and Critical Shear Planes, GT7:July 81: 929:16369

Sridharan, A.
Embedded Foundations Under Vertical Vibration, with M. V. Nagendra and C. Chinnaswamy, TN: GT10:Oct 81:1429:16530
See M. Krishna Murthy, TN: GT10:Oct 80:1143: 15724

Sridharan, Asuri
See Mehter Mohamed Allam, GT4:Apr 81:421:16178

Sridharan m116361, Asuri
See Mysore V. Nagendra, TN: GT7:July 81:989: 16360

Stokoe, Kenneth H., II
See Thomas M. Hearne, Jr., GT10:Oct 81:1327: 16582

Subrahmanyam, R. V.
See Hin Fatt Cheong, TN: GT2:Feb 81:221:16009

Sundaram, Panchanatham N.
See Richard E. Goodman, GT5:May 80:485:15433

Swiger, William F.
Northfield Mountain Pumped Storage Project: Performance, with Philip A. Wild and Thomas J. Lamb, GT6:June 80:673:15506
Dsc: Claude A. Fetzer, GT7:July 81:1020:16356
Clo: GT7:July 81:1021:16356
TR:145:731

Symes, Matthew
See Atonio Gens, GT5:May 81:702:16216

Taft, Jay L.
See Tavit O. Najarian, GT12:Dec 81:1141:16703

Tan, David Y.
Ground Control for Shallow Tunnels by Soil Grouting, with G. Wayne Clough, GT9:Sept 80: 1037:15716

Dsc: Kurt K. Borchert and Herbert Klapperich, GT12:Dec 81:1745 s0ASCE:16683

Tang, Wilson H.
Probabilistic Evaluation of Loads, GT3:Mar 81:287:16100
See Achintya Haldar, GT5:May 81:577:16239

Tokimatsu, Kohji
See Yoshiaki Yoshimi, GT2:Feb 81:237:16003

Townsend, Frank C.
See Mosaid M. Al-Hussaini, GT4:Apr 81:481:16180

Tsur-Lavie, Y.
See S. A. Denekamp, GT4:Apr 81:439:16173

Vaid, Yoginder P.
Dilation Angle and Liquefaction Potential, with Peter M. Byrne and John M.O. Hughes, TN: GT7:July 81:1003:16360
Static Shear and Liquefaction Potential, with W. D. Liam Finn, GT10:Oct 79:1233:14909
Dsc: Yoshiaki Yoshimi and Kohji Tokimatsu, GT2:Feb 81:237:16003
TR:145:555

Veneziano, Daniele
See Michael A. Fardis, GT10:Oct 81:1345:16590
See Michael N. Fardis, GT10:Oct 81:1361:16604

Verner, Edward A.
See Leland M. Kraft, GT1:Jan 81:1:16000

Vesic, Aleksandar S.
See Nabil F. Ismael, GT12:Dec 81:1677:16718

Vivatrat, Vitoon
See Mohsen M. Baligh, GT4:Apr 80:447:15377

Vrymoed, John
Dynamic FEM Model of Oroville Dam, GT8:Aug 81:1057:16464

Wahls, Harvey E.
Tolerable Settlement of Buildings, GT11:Nov 81:1489:16628

Wiesner, Terence J.
Laboratory Tests on Model Piled Raft Foundations, with Peter T. Brown, GT7:July 80:767:15576
Dsc: Joe O. Akinmusuru, GT8:Aug 81:1153:16408; Eldon Burley, Roger C. Harvey, Bhas Kar Nath and Lawrence A. Wood, GT8:Aug 81:1155:16408
Clo: GT8:Aug 81:1157:16408

Wild, Philip A.
See William F. Swiger, GT6:June 80:673:15506

Wiss, John F.
Construction Vibrations: State-of-the-Art, GT2:Feb 81:167:16030

Wolfgang, James L.
See John R. Hall, Jr., TN: GT10:Oct 81:1419:16530

Wong, Kinfun
See Tien H. Wu, GT12:Dec 81:1693:16764

Wood, David M.
Dsc, GT5:May 81:704:16216, of "Principal Stress Rotation: A Missing Parameter", GT4:Apr 80:419:15375

Wood, Lawrence A.
See Eldon Burley, GT8:Aug 81:1155:16408

Woods, Richard D.
Seismic Techniques in the Laboratory, with Robert Henke, GT10:Oct 81:1309:16599

Wu, Tien H.
Probabilistic Soil Exploration: Case History, with Kinfun Wong, GT12:Dec 81:1693:16764

Yoshimi, Yoshiaki
Dsc, with Kohji Tokimatsu, GT2:Feb 81:237:16003, of "Static Shear and Liquefaction Potential", GT10:Oct 79:1233:14909

Znidarcic, Dobroslav
Finite Strain Consolidation: Test Conditions, with Robert L. Schiffman, TN: GT5:May 81:684:16221